DEVELOPMENT OF AN ENGINEERING, ECONOMIC & ENVIRONMENTAL DESIGN TOOL FOR PLANETARY SCALE SUSTAINABLE POWER SYSTEMS

A Dissertation

by

HUSSEIN MOHAMMAD KHALAF AL-MASRI

Submitted to the Office of Graduate and Professional Studies of
Texas A&M University
in partial fulfillment of the requirements for the degree of

DOCTOR OF PHILOSOPHY

Chair of Committee,	Mehrdad (Mark) Ehsani
Committee Members,	Chanan Singh
	Laszlo B. Kish
	Ramesh Talreja
Head of Department,	Miroslav Begovic

December 2016

Major Subject: Electrical Engineering

ABSTRACT

There are plenty of fossil fuels for hundreds of years. The importance of moving toward sustainable energy stems from global climate change and the need to provide access to affordable energy to all of humanity. The way forward is to help the developing world that dominates the future emissions (90% solution) with "clean" energy, rather than reducing the emissions for the developed world to make it clean (10% solution). The 90% solution has to be done consistent with appropriate technologies, sound business plan, and market economy. The ultimate goal of information presented in this dissertation is to satisfy a country's national load demand by establishing multiple utility grid connections to various geographic locations of high wind or solar energy resources. This is done by building a new optimization design tool which investigates the engineering, economic feasibility and the environmental impacts. This tool is applied in Jordan as a case validation. This is done using single figure of merit (SFOM) optimizations. A mathematical modeling is developed for each component, and the optimal configuration is determined for each city. The annual system cost of energy (ASCE) is optimized to be 32.57% less than the grid energy price, and the CO_2 emissions are reduced by 80.13%. These are excellent indications for the economic feasibility and the environmental benefits of the designed system. The levelized cost of energy (LCOE), total net present cost (TNPC), renewable penetration (RP) and annual emission indicator (AEI) are 0.058212 $/kWh, $8.713857 billion, 59.49817% and 4.576 Megatonne/year respectively. Multi-figure of merits (MFOM) optimization cases based on a non-sorting genetic algorithm

(NSGA) are investigated such as: AEI vs. ASCE, AEI vs. LCOE, AEI vs. RP and (RP, LCOE, AEI). The MFOM optimization results are either 2D or 3D Pareto frontier, where exists various competitive non-dominant solutions. The sweet spot selection (triple-S) procedure is proposed to help select the sweet spot in the two figure of merits Pareto frontier in order to have both environmental and feasible solutions. This design tool will be versatile enough for the application to any on-grid renewable power system worldwide. It will be made available on the internet as a public service of Texas A&M University Renewable Energy Program at the Power Electronics and Motor Drives Laboratory of the Electrical Engineering Department.

DEDICATION

To

My Father; Abu Tariq, My Mother; Um Tariq,

My Wife; Wala'a, My Brother; Tariq and My Sisters; Hala and Roa'a

ACKNOWLEDGEMENTS

I would like to express my utmost gratitude to Dr. M. Ehsani for his support, guidance, and words of wisdom throughout the course of my graduate studies. I also would like to convey my appreciation to the faculty and staff of the Electrical Engineering Department at Texas A&M University for their support and dedication to my education. Finally, thanks to my mother and my father for their encouragement and to my wife for her patience and love.

NOMENCLATURE

AIT	Artificial intelligence techniques
GA	Genetic algorithm
NSGA	Non-dominated sorting genetic algorithm
FOM	Figure of merit
ASCE	Annual system cost of energy in $/kWh
RP	Renewable penetration in %
AEI	Annual CO_2 emission indicator in MegatonneCO_2/year
EF	CO_2 emission factor in kgCO_2/kWh
LOA	Level of autonomy in %
MFOM	Multi-figure of merits
EEPY	Energy extracted per year
GHG	Greenhouse gases
ICC	Initial capital cost in $
GOC	Grid operational cost in $
HOMER	Hybrid optimization multiple energy resources
PV	Photo-voltaic
WT	Wind turbine
ICM	Improved cubic model of the WT
HWPVG	Hybrid wind-photovoltaic on-grid system
EC	Energy center

ERC	The Jordanian energy & minerals regulatory commission
JRSS	Jordanian royal scientific society
NCC	National control center
NEPCO	National electric power company
PVGIS	Photovoltaic geographical information system
SCADA	Supervisory control and data acquisition
PDF	Probability distribution frequency
ECWS	Energy curve of wind speeds
C_p	WT power coefficient
SPDC-Betz	Shaft power distribution curve at Betz limit
P_{SWT}	Single WT output power in kW
GR	Global solar radiation in kW/m^2
N_{WT}	Number of wind turbines
N_{PV}	Number of PV panels
W_{SP}	Wind sharing percent
S_{SP}	PV sharing percent
A_{PV}	Area of a single PV panel in m^2
CC	Capital cost
RC	Replacement cost
OMC	Operation and maintenance cost
SC	Salvage cost
LCOE or COE	Levelized cost of energy in $/kWh

TNPC or NPC	Total net present cost in $
TAC	Total annualized cost
JD	Jordanian Dinar. It is the main currency in Jordan (1$~0.7JD).
CRF	Capital recovery factor in %
i	Interest rate in %
f	Inflation rate in %
N	Number of years
AC	Alternative current
WP	Wind farm penetration
WFP	Wind farm production
OST	Optimal system type
v_{ci} or $v_{cut_{in}}$	Cut-in wind speed value in m/sec
v_{co} or $v_{cut_{out}}$	Cut-out wind speed value in m/sec
v_{rated}or v_r	Rated wind speed value in m/sec
$P_R$or $P_{r_{WT}}$	Rated power of the WT
A_{WT}	Single WT swept area in m^2
a.s.l	Above sea level
ρ	Air density in kg/m^3
ρ_o	The air density at sea level (1.225 kg/m^3)
DF	Discount factor
T	Temperature in Kelvin in K
t	Temperature in °C

T_o	Temperature at sea level in Kelvin (288K)
H	Altitude a.s.l in m
L	Temperature lapse rate (0.0065 °C /m)
P_o	Standard pressure at sea level (101325.0 Pa)
g	Acceleration due to gravity (9.80665m/sec^2)
M	Molecular weight of dry air (0.0289644 kg/mol)
R	The ideal gas constant (8.31432 N·m /(mol·K))
K_g	The specific gas constant For Air (287 J/kg K)
p	The atmospheric pressure In hPa, (1 hPa = 100 Pa)
RH	Relative humidity in %
v	Wind speed at the hub height in m/sec
H_{WT} or H_h	WT hub height in m
D_R or RD	Rotor diameter of a WT in m
H_a	Anemometer height in m
v_a	Wind speed at H_a in m/sec
α	Wind power law coefficient
$E_{out_{wind}}$	Output energy from a WT in kWh
$P_{out_{wind}}$	Output power from a WT in kW
G_I	Global radiation incident on the surface of the PV in kW/m^2
TC_p	Maximum power temperature coefficient in %/°C
T_c	Module cell temperature in °C
$T_{ambient}$	Ambient temperature in °C

T_{NOCT}	Nominal operating cell temperature in °C at (800 W/m^2, 20°C)
STC	Standard testing conditions (25 °C and 1000 W/m^2).
$Prated_{PV}$ or $P_{r_{PV}}$	Rated power of a PV module at STC in Watt
$\frac{G_I}{Radiation_{STC}}$	Normalized de-rated radiation.
$E_{out_{PV}}$	Output energy from a PV module in kWh
$P_{out_{PV}}$	Output power from a PV module in kW
η_{inv}	Inverter efficiency in %
L_{PV}	Length of the PV panel in m
W_{PV}	Width of the PV panel in m
V_{mp}	Voltage at maximum power point in V
I_{mp}	Current at maximum power point in A
V_{oc}	Open circuit voltage in V
I_{SC}	Short circuit current in A
FF	Fill factor in %
n	How many times has component replaced during the project life
$t_{project}$	Project life time in years
$t_{component}$	Component life time in years
$t_{remaining}$	Remaining life time of a component in years

TABLE OF CONTENTS

Page

ABSTRACT ii

DEDICATION iv

ACKNOWLEDGEMENTS v

NOMENCLATURE vi

TABLE OF CONTENTS xi

LIST OF FIGURES xvi

LIST OF TABLES xxii

1. INTRODUCTION 1

- 1.1 Engineering and socio-economic aspects of sustainable energy 6
  - 1.1.1 Motivations for renewables & current perspectives 8
  - 1.1.2 Sustainable energy metrics & requirements 10
- 1.2 Importance of renewables when the oil prices fall down 10
- 1.3 Emissions 11
- 1.4 PV module characteristics & Solar Path Finder (SPF) 13
  - 1.4.1 Characteristics of the PV module with fixed insolation 17
  - 1.4.2 Characteristics of the PV module with fixed temperature 20
  - 1.4.3 SPF to reduce shading 23
- 1.5 Wind Turbine (WT) characteristics 26
  - 1.5.1 Characteristics of the WT at sea level 26
  - 1.5.2 WT control strategies 28
    - 1.5.2.1 Pitch-regulated WT control strategy 28
    - 1.5.2.2 Stall-regulated WT control strategy 30

2. LITERATURE REVIEW 32

3. SINGLE POINT GRID CONNECTION INVESTIGATION USING MODIFIED HOMER ..... 53.

- 3.1 Single point connection data set (SPCDS) 54
  - 3.1.1 Analysis of city data 55

3.1.2 Selection of WT & PV module 57
3.1.3 Estimated cost & life time for each element 60
3.1.4 Sizing of system elements 61
3.1.4.1 First method using Matlab 61
3.1.4.2 Second method using HOMER 63
3.1.5 Detailed results of the HOMER optimal system 65
3.1.5.1 Discounted cash flow 65
3.1.5.2 Production and consumption of electrical energy 66
3.1.5.3 Output of GE1.5sle wind farm & CS6X PV array 68
3.1.6 Sensitivity analysis 70
3.1.6.1 Interest and inflation rates 70
3.1.6.2 Exponent of wind power law 72
3.1.6.3 Average daily load demand 73
3.1.6.4 Oil price 74
3.1.6.5 Natural gas price 76
3.2 Summary 78

4. MULTI-POINT GRID CONNECTION DATA ACQUISITION AND PREPARATION 79

4.1 Jordan hourly load profile in 2014 79
4.1.1 Average daily load profile in Jordan in 2014 80
4.1.2 Seasonal load profile in Jordan in 2014 81
4.2 Load in workweek and weekend days in Jordan in 2014 82
4.3 Multi-point grid connection data (MPGCD) 83
4.4 Wind speeds 84
4.5 Wind speeds probability distribution frequency (PDF) curve 86
4.6 Solar radiation 88
4.7 Solar insolation probability distribution frequency (PDF) curve 90
4.8 Multi-point system component costs 92
4.8.1 Current market price of the renewable components 92
4.8.2 Current price of dealing with the grid in Jordan 94

5. MATHMATICAL MODELING, INVESTIGATION AND A DEVELOPED OPTIMIZATION DESIGN TOOL 96

5.1 Accurate WT annual energy computation by advanced modeling 98
5.1.1 Linear model 98
5.1.2 Quadratic model 99
5.1.3 1st Cubic model 99
5.1.4 2nd Cubic model 99
5.1.4.1 Air density modeling 100
5.A. ρ as a function of the elevation a.s.l 101
5.B. ρ as a function of pressure and the elevation 102

5.C. ρ as a function of temperature and the elevation 102
5.D. ρ as another function of temperature and the elevation . 103
5.E. ρ as a function of temperature, pressure and humidity ... 103
5.1.4.2 Wind power coefficient 104
5.1.4.3 WT hub height 105
5.1.5 Investigation of WT modeling 105
5.1.6 Investigation of air density modeling 108
5.1.6.1 Effect of city elevation (a.s.l) 108
5.1.6.2 Effect of temperature variation 112
5.1.7 Investigation of 10 WTs 114
5.1.8 Section summary 117
5.2 Impact of WT modeling on a hybrid renewable energy system 118
5.2.1 Investigation of the linear model 119
5.2.2 Investigation of the quadratic model 120
5.2.3 Investigation of the 1st cubic model 121
5.2.4 Discussion on the simplified WT models 121
5.2.5 Impact of air density modeling on a hybrid renewable system ... 122
5.2.5.1 Investigation of city elevation 123
5.2.5.2 Investigation of temperature model 124
5.2.5.3 An ICM vs. a simple linear model 126
5.2.5.4 Section Summary 126
5.3 Impact of WT Modeling on a wind energy system 128
5.3.1 Impact of straightforward WT models on a system level 128
5.3.1.1 Impact of the WT linear model on a system level 128
5.3.1.2 Impact of the WT quadratic model on a system level 129
5.3.1.3 Impact of the WT straightforward cubic model on a system level 129
5.3.1.4 Discussion on the accuracy of the straightforward WT models 129
5.3.2 Impact of air density modeling on a wind system 130
5.3.2.1 Impacts of elevation a.s.l on a system level 131
5.3.2.2 Impacts of air temperature on a system level 133
5.3.2.3 An ICM compared with a linear straightforward model ... 134
5.3.2.4 Section Summary 135
5.4 Modeling of the PV module 136
5.4.1 Incident radiation, temperature & PV output energy in Ma'an ... 137
5.4.2 Investigation of 10 PVs 140
5.5 Utility grid model 142
5.6 Footprint of renewable energy generation 143
5.6.1 Footprint of wind farm 144
5.6.2 Footprint of PV array 145
5.7 System performance indicators 146
5.7.1 The ASCE & the LCOE 146
5.7.2 Salvage & replacement costs 149

5.7.3 Clarification example 150
5.7.3.1 1st case: Single WT/ignoring SC & RC 151
5.7.3.2 2nd case: Single WT/including SC & RC 153
5.7.3.3 3rd case: System/single unit each/including SC&RC 156
5.7.4 Annual CO_2 emission indicator (AEI) 158
5.7.5 Level of autonomy (LOA) 158
5.7.6 Renewable penetration (RP) 160

6. OVERVIEW OF GENETIC ALGORITHMS 161

6.1 Motivations of the AIT to optimize hybrid renewable systems 161
6.2 The GA operators for a single FOM 162
6.3 Non-dominated sorting genetic algorithm (NSGA) 163

7. PERFORMANCE RESULTS AND DISCUSSION 165

7.1 Introduction and tailoring needed information 165
7.2 Filling order of the candidate cities 167
7.3 Single FOM solution to satisfy the national load 168
7.4 Multi-Point solutions using the GA & NSGA 171
7.5 Discussion on the GA single FOM solutions 173
7.6 MFOM solutions using the NSGA 174
7.6.1 Results – 2D Pareto Frontier 175
7.6.1.1 Pareto Front – CO_2 emissions vs. ASCE 175
7.6.1.2 Pareto Front – CO_2 emissions vs. LCOE 176
7.6.1.3 Pareto Front – CO_2 emissions vs. RP 177
7.6.1.4 Sweet spot selection (triple-S) procedure 178
7.6.2 Results – 3D Pareto Frontier 180

8. CONCLUSIONS AND FUTURE WORKS 182

8.1 Conclusions 182
8.2 Future works 184

REFERENCES 185

APPENDIX A 196

APPENDIX B 197

APPENDIX C 198

APPENDIX D 199

APPENDIX E 200

APPENDIX F 201

APPENDIX G 202

APPENDIX H 203

APPENDIX I 204

APPENDIX J 205

APPENDIX K 206

LIST OF FIGURES

FIGURE		Page
1.1	World energy consumption 1965-2035	1
1.2	World energy consumption by fuel in 2014	2
1.3	Hybrid wind-PV grid connected system	6
1.4	CO_2 emissions for developing (90%) and developed (10%) countries	9
1.5	Global GHG emissions	12
1.6	PV effect and construction	13
1.7	CS6X-310 polycrystalline PV panel	14
1.8	SIMULINK to gain output characteristics of (CS6X-310) PV module	16
1.9	I-V output characteristics of (CS6X-310) PV module	17
1.10	P-V output characteristics of (CS6X-310) PV module	17
1.11	I-V characteristics at constant insolation and variable temperature	18
1.12	P-V characteristics at constant insolation and variable temperature	18
1.13	Effect of temperature on an open circuit voltage	19
1.14	Effect of temperature on maximum power point	20
1.15	I-V characteristics at constant temperature and variable insolation	20
1.16	P-V characteristics at constant temperature and variable insolation	21
1.17	Effect of solar insolation on short circuit current	21
1.18	Effect of solar insolation on maximum power point	22
1.19	Sun position	23

1.20 Solar site assessment for LOCATION 1 using Panorama SPF chart..... 24

1.21 Solar site assessment for LOCATION 2 using Panorama SPF chart..... 26

1.22 V90-1.8MW wind power simplified curve 27

1.23 Pitch-regulated (solid line) and stall-regulated (dashed line)..... 28

1.24 Power vs. time for GE-1.5 MW 29

1.25 WT power curve for GE-1.5 MW 29

1.26 WT power curve for BWC Excel-S..... 30

1.27 Power vs. time for BWC Excel-S WT..... 31

2.1 Wind-PV-fuel cell on-grid hybrid system..... 36

2.2 A hybrid wind-PV-diesel system 38

2.3 Hybrid wind-PV-battery standalone system..... 40

2.4 A flowchart to describe the system in Fig. 2.3..... 41

2.5 A hybrid wind-PV-diesel-battery system..... 44

2.6 Standalone hybrid wind-diesel system..... 47

3.1 Annual wind speed for the SPCDS in Jordan 54

3.2 Annual solar radiation for the SPCDS in Jordan..... 55

3.3 Monthly average wind speed values for Ibrahimyya 56

3.4 Histogram PDF curve for the wind speed time series data 57

3.5 PDF & ECWS curves..... 57

3.6 SPDC-Betz (shaft power distribution curve at Betz limit)..... 58

3.7 Output power characteristics of the GE1.5sle-77 wind turbine 59

3.8 Ibrahimyya load profile 61
3.9 Ibrahimyya global radiation 62
3.10 GE1.5sle-77 output power 62
3.11 Hybrid wind/PV system compared with other configurations 65
3.12 Monthly average electrical production 67
3.13 GE1.5sle-77 wind farm output 69
3.14 CS6X-310 PV array output 69
3.15 Sensitivity of the interest rate on the OST 70
3.16 Sensitivity of the inflation rate on the OST 71
3.17 Sensitivity of α if the rotor is below the anemometer 72
3.18 Sensitivity of α if the rotor is at the anemometer 72
3.19 Sensitivity of α if the rotor is above the anemometer 73
3.20 Sensitivity of load demand variation on COE & NPC 74
3.21 Sensitivity of oil price on COE & NPC 75
3.22 Sensitivity of oil price on energy purchased & sold to grid 75
3.23 Sensitivity of NG on the COE & NPC 77
3.24 Sensitivity of NG on energy purchased & sold to grid 77
4.1 Yearly load profile in Jordan in 2014 79
4.2 Average daily load demand in Jordan in 2014 80
4.3 Monthly load profile in Jordan in 2014 81
4.4 Annual wind speed for most recent candidate sites in Jordan 85
4.5 Monthly average wind speed after averaging the MPGCD in Jordan 86

4.6 Histogram PDF curve for the wind speed time series data 86

4.7 Histogram PDF hourly curve for the wind speed time series data..... 87

4.8 Annual average solar irradiation for the MPGCD in Jordan 88

4.9 Monthly average solar radiation after averaging the MPGCD in Jordan... 90

4.10 Insolation PDF after averaging the MPGCD in Jordan..... 90

4.11 Hourly insolation after averaging the MPGCD in Jordan..... 91

5.1 Alteration of the optimum power curve due to air density variation 100

5.2 Power coefficient & WT output power curve 104

5.3 Simplified models for a single V90-1.8MW WT installed in Maan-LH site 106

5.4 Simplified models for a single GE-1.5sle WT installed in Ibrahimyya city 107

5.5 Effect of elevation on V90-1.8MW WT 2nd cubic model characteristics .. 109

5.6 Alteration of the WT power curve due to air density variation..... 110

5.7 Effect of the city elevation on the WT power curve 111

5.8 Alteration of WT power curve due to temperature variation 112

5.9 Effect of temperature on the WT power curve..... 113

5.10 Ten WTs output characteristics using the ICM..... 116

5.11 Ibrahimyya load yearly profile in 2015..... 119

5.12 Energy purchased difference from the grid for the elevation model..... 123

5.13 Energy purchased difference from the grid for the temperature model 125

5.14 Wind on-grid energy system 128

5.15 Grid energy purchased difference: city elevation vs. reference models 132
5.16 Grid energy purchased difference: Temperature vs. reference models..... 134
5.17 Global hourly incident radiation in Maan-LH..... 137
5.18 Global hourly basis average temperature in Jordan 138
5.19 PV output energy from a single PV panel installed in Maan-LH 139
5.20 Typical layout spacing of a wind farm..... 144
5.21 Typical layout spacing of a PV array 145
5.22 NCF for V90-1.8MW WT with ignoring RC & SC..... 151
5.23 DCF for V90-1.8MW WT with ignoring RC & SC..... 153
5.24 NCF for V90-1.8MW WT with including SC & RC 153
5.25 DCF for V90-1.8MW WT with including SC & RC 156
5.26 NCF for the entire system with a single unit each 157
5.27 DCF for the entire system with a single unit each 157
6.1 GA operators for a single FOM..... 162
6.2 NSGA operators for a MFOM 164
7.1 Wind & PV candidate cities in Jordan 166
7.2 GA optimization of ASCE as the FOM 168
7.3 Genealogy of individual children..... 169
7.4 Instantaneous energy purchased from grid..... 170
7.5 Pareto points – CO_2 emissions vs. ASCE 175
7.6 Pareto points – CO_2 emissions vs. LCOE 176
7.7 Pareto points – CO_2 emissions vs. RP..... 177

7.8 Triple-S procedure for the Pareto Front of Fig. 7.5..... 178

7.9 Triple-S Procedure for the Pareto Front of Fig. 7.6 179

7.10 Triple-S Procedure for the Pareto Front of Fig. 7.7 180

7.11 Pareto Front – (RP, LCOE, CO_2 emissions) 181

LIST OF TABLES

TABLE		Page
1.1	Sustainable energy requirements	10
1.2	Specifications of (CS6X-310) PV panel	14
1.3	Shading experiment site information	24
1.4	Percent of solar energy that can reach LOCATION 1 (%)	25
1.5	Percent of solar energy that can reach LOCATION 2 (%)	25
2.1	Cost comparison for 3 combinations of wind or PV	33
2.2	Various points of comparisons for distributed and central PV types	34
2.3	Advantages and disadvantages of distributed PV systems	35
2.4	Cost comparison for the system described in Fig. 2.1	37
2.5	Cost for each component in Fig. 2.2	39
2.6	Cost for each component in Fig. 2.3	42
2.7	Cost for each component for the proposed system in Makka	46
2.8	Cost for each component in the wind-diesel hybrid system in Fig. 2.6	48
2.9	Sensitivity parameters to get optimization results	48
2.10	Sensitivity variables tested for the system in Fig. 2.6	49
3.1	Ibrahimyya load profile summary	56
3.2	Specifications of GE1.5sle-77 WT	59
3.3	STC parameters	60
3.4	Estimated cost and life time for components of single point connection	61

3.5 Sizing results for the 1st method 63
3.6 Optimal size system main screen HOMER results 64
3.7 Only PV panels/grid system main screen HOMER results 64
3.8 Only WTs/grid system main screen HOMER results 64
3.9 Discounted cash flow 66
3.10 Production elements 67
3.11 Consumption elements 67
3.12 GE1.5sle-77 wind farm output 68
3.13 CS6X-310 PV array output 69
3.14 PV and wind's allocation with load sensitivity variation 74
4.1 Monthly average weekdays load in GW for Jordan in 2014 82
4.2 Monthly average weekends load in GW for Jordan in 2014 83
4.3 Coordinates and site altitude for each candidate site in Jordan 84
4.4 Wind speed in m/sec for the candidate sites in Jordan 85
4.5 Monthly average irradiation in $kWh/m^2/day$ for the MPGCD in Jordan 89
4.6 Hybrid wind/PV system component costs MPGCD in Jordan 93
4.7 Sale price to the AC grid in Jordan 95
4.8 Passing cost with the AC grid in Jordan 95
4.9 Grid cost for renewable hybrid resources 95
5.1 Specifications considered for two WTs 106
5.2 EEPY from a single WT unit in Maan-LH and Ibrahimyya cities 107
5.3 Relationship between city elevation and the air density 109

5.4 Wind energy from a single V90-1.8MW in Maan-LH, at T_{min}=8.18°C, at T_{max}=26.72°C, model C 112
5.5 Temperature effect on a single GE1.5sle installed in Ibrahimyya 113
5.6 Ten large-scale WTs 115
5.7 Alteration of WT curve of all model types due to ρ variation using model A 116
5.8 Optimal size system results for a WT modeled using the linear model 120
5.9 Optimal size system results for a WT modeled using the quadratic model 120
5.10 Optimal size system results for a WT modeled using the 1st cubic model 121
5.11 Optimal size system results for a WT modeled at sea level 122
5.12 Optimal size system for a WT modeled using equation 5.4 & equation 5.16 124
5.13 Optimal size system for a WT modeled using equation 5.4 & Equation 5.12 124
5.14 System results for the linear modeled wind farm 128
5.15 System results for the quadratic modeled wind farm 129
5.16 System results for the straightforward cubic modeled wind farm 129
5.17 Wind only system results for a WT modeled at sea level 131
5.18 Wind only system results for a WT ICM a.s.l 131
5.19 Wind only system results for a WT ICM at T_{max} 133

5.20 Specifications considered for (VBHN240SA11) PV panel 138
5.21 Ten PVs 140
5.22 EEPY and the FF from a single PV model..... 141
5.23 Results of a single (VBHN240SA11) PV module installed in each site.... 141
5.24 Trial and error grid model results for only WTs (GE-1.5sle) test..... 142
5.25 Trial and error grid model results for only PVs (VBHN240SA11) test..... 143
5.26 Geographical available area for the candidate cities in Jordan 144
5.27 NCF & DCF for a single V90-1.8MW WT during the project life time.... 152
5.28 NCF for a single V90-1.8MW WT during the project lifetime..... 154
5.29 DCF for a single V90-1.8MW WT during the project life time..... 155
7.1 Multi-point connection candidate cities information needed 166
7.2 EEPY per unit ("GE-1.5sle" WT & "VBHN240SA11" PV module) installed in each candidate city..... 167
7.3 Arranging MPGCD cities based on the highest wind EEPY 167
7.4 Arranging MPGCD cities based on the highest solar EEPY 168
7.5 Specifications for the selected WT for the multi-point investigation 170
7.6 Specifications for the selected PV panel for the multi-point investigation 170
7.7 The optimized hybrid wind/PV system to satisfy the national load of Jordan 171
7.8 OST for each location in the multi-point connection..... 172
7.9 Optimized WT value of: Sharing percent, dedicated and occupied area

for each candidate city..... 172

7.10 Optimized PV value of: Sharing percent, dedicated and occupied area for each candidate city..... 173

1. INTRODUCTION*

Electrical energy is considered as an integral part of our daily life. It is useful and crucial in all sectors of modern societies. The world population has tripled in one lifetime, and is expected by the UN to rise to 9.2 billion by 2050 before stabilizing. Energy demand is rising rapidly. The world's electrical power demand is around 15 TW [1]. The world energy consumption will grow by 32% between 2015 and 2035 as shown in Fig. 1.1 [2].

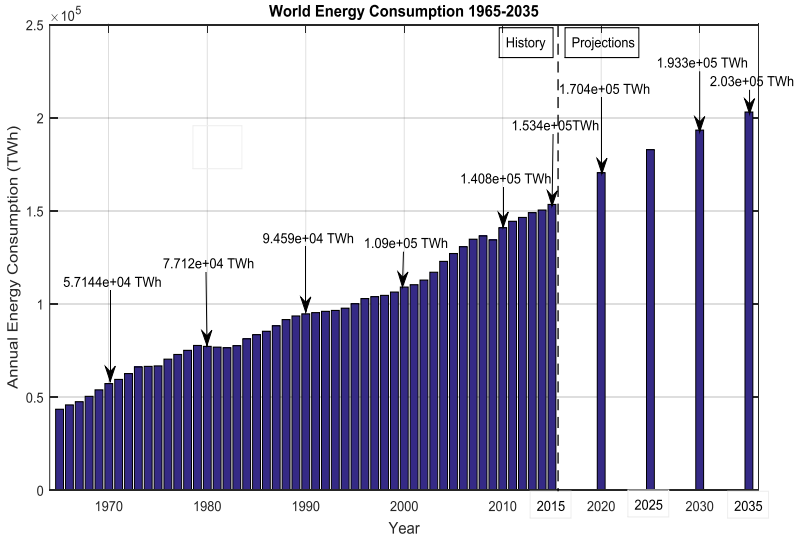

Fig. 1.1 World energy consumption 1965-2035

The world energy consumption by fuel in 2014 is shown in Fig. 1.2 for a total annual energy of 150357.292 TWh. Fig. 1.2 shows the high dependence on fossil fuel

* Part of this section is reprinted with permission from Hussein M. K. Al-Masri and M. Ehsani, "Engineering and Socio-Economic Aspects of Sustainable Energy," IEEE Global Humanitarian Technology Conference, October, 2016, © 2016 IEEE and H. M. Al-Masri and M. Ehsani, "Feasibility Investigation of a Hybrid On-Grid Wind Photovoltaic Retrofitting System," IEEE Transactions on Industry Applications, May-June, 2016, © 2016 IEEE and H. Al-Masri and M. Ehsani, "Feasibility Investigation of A Hybrid On-Grid Wind Photovoltaic Retrofitting System," IEEE Industry Applications Society Annual Meeting, October, 2015, © 2015 IEEE and N. Pandiarajan and R. Muthu, "Mathematical Modeling of Photovoltaic Module With Simulink,", 1st International Conference on Electrical Energy Systems, January, 2011, © 2011 IEEE and Hussein Al-Masri, Ahmad Abu-Elrub, Walaa R. Ayyad and Mark Ehsani, "On The PV Module Characteristics", 23rd International Symposium on Power Electronics, Electrical Drives, Automation and Motion, June, 2016, © 2016 IEEE and H. Al-Masri, F. Alhuwaishel, F. Alismail, S. Sabeeh and H. Kanakri, "Investigation of MPPT For PV Applications by Mathematical Model," 15th IEEE International Conference on Environment and Electrical Engineering (EEEIC), June, 2015, © 2015 IEEE.

resources (oil, natural gas and coal) which constitute 87% from the total energy consumed worldwide [2]. This is because our industrial economy was built on abundant energy, mostly from fossil fuel. Globally, around 87% of our total energy is produced by fossil fuels [3]. The supply seems to be shrinking. The fossil fuel resources will get depleted in the next few decades.

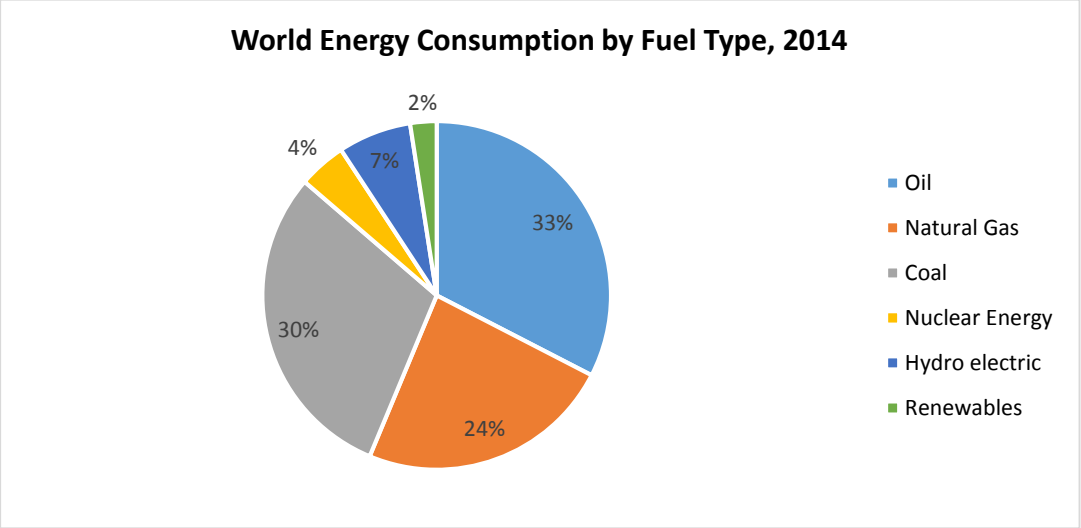

Fig. 1.2 World energy consumption by fuel in 2014

GHG emissions mainly, produced by CO_2, are the result of burning fossil fuels. The GHG concentrations have reached their highest level in human history. Therefore, it is the time to look for renewable energy alternatives.

Wind energy is one of the eminent renewable energy resources on the planet. It is the result of the uneven heating of the earth's surface [4]. The wind energy resource is available all the time by free. It is ecological and inexhaustible. It has helped the human beings in the ancient time by propelling ships and driving WTs to grind grain and pump water. People show an interest in wind energy, especially when an embargo placed by

Arabic nations in 1973 on oil exports. After that, people realize that the world's oil supplies should be replaced by alternatives such as wind energy [5]. These days, it is technically possible to extract 20 TW from wind power [1], which is four-third the world's electrical power demand. During the last ten years there has been a tremendous growth in the wind installed capacity [6]. The global installed wind power capacity reaches 432.419 GW in 2015 [7]. On the other hand, the sun produces a vast amount of energy every day, which is enough to satisfy the energy needs worldwide. However, there are challenges in harvesting this source free energy in efficient and feasible devices and materials [8]. A PV array employs PV modules composed of a number of PV cells to supply usable solar power. PV module is the device where solar energy gets converted to electric energy. This device mechanism is called Photovoltaics, which means "light-electricity". There is a tremendous growth in the PV capacity in the recent years. The PV installed capacity has been quadrupled in the past four years. The global installed PV capacity is 180 GW at the end of 2014 [9].

Nowadays, it is technically possible to extract 70 TW from solar and wind power [1], which is around five times the world's power demand. The U.S. Energy Information Administration (EIA) estimates a projection of 15% of world energy consumption by 2040 that comes from renewable energy resources (biofuels, biomass, geothermal, hydropower, solar, and wind). EIA estimates that about 21% of world energy production was from renewable energy in 2011, with a projection for approximately 25% in 2040 [10]. The renewable energy resources are considered as abundant, ecological, economical, omnipresent and publicly acceptable compared with fossil fuel resources. The solar and

wind energies are the most promising ones for human beings. On an annual basis, wind and solar are highly complementary, but on a daily basis they are only somewhat complementary [11]. Because of the inherent nature of these two resources, the electrical power generation is complementary. Therefore, the hybrid wind/PV power system has higher reliability to deliver continuous power than either individual resources[12]. Therefore, it is recommended to have them both in a hybrid combination in an on-grid or standalone system to satisfy a given load profile. However, an optimization algorithm is highly recommended to determine the best configuration to satisfy a given load.

In Jordan as one of the non-oil producing countries, and most of fuel needs are imported. It is one of the highest worldwide in dependency on foreign energy resources. Actually, 96% of the Jordan's energy needs coming from imported natural gas and oil. This constitutes financial burden on the Jordanian national economy as well as consuming a big amount of the gross domestic product (GDP). This motivated decision makers in Jordan to plan investments of $15 billion in renewable energy and nuclear energy [13]. Therefore, great efforts and considerable researches are being done on renewable energy. Exploitation of renewable energy resources such as wind and solar energy as environmentally friendly sources is highly encouraged.

The feasibility investigation of the renewable energy system is very important step in order to fully utilization of renewable energy resources. The hybrid system, as a multiple energy resources, is considered as a complex problem, which needs to be studied and analyzed extensively. In [14], the authors mentioned 19 software tools that have been discussed and used in the literature, such as HOMER and iHOGA. HOMER was found to

be the most used tool among others [14]. But, in our study it is found that HOMER can only be used to solve the problem for only one location at a time by making an economic decision for a single site with its own data. Thereby, HOMER has been used to study the feasibility for only one city in Jordan called Ibrahimyya. The data in our study have been collected for six candidate sites with high potential of wind and solar energies. As a matter of fact, the main goal in our study is to investigate the feasibility of wind/PV systems designed in different high potential cities to satisfy the national load of Jordan. Thereby, a new optimization design tool is built that can find the optimal solution in case of multi-potential areas and to satisfy the national load for the country which includes these areas. Then, in our problem, an investigation will be established on large-scale renewable wind and/or PV systems. Feasibility performance factors or indicators will be considered to decide what is the most cost effective and economical choice. The ASCE is considered as the FOM to be optimized using the GA. Other indicators are modeled such as LCOE, AEI and RP. In some cases, grid-connected renewable energy systems do not usually have batteries. This will reduce the renewable system overall cost. The usage of battery banks is not accepted environmentally, geographically and economically because of their high weights, bulky size, high costs, limited life cycles and chemical pollutions [12]. Thereby, it is better to apply renewable energy system connected to the AC bus directly. In this case, excess energy after satisfying the load is sent back to the grid. Moreover, unsatisfied load will be supplied from the grid, once the renewable energy is insufficient [15].

For simplicity, a single point connection to the utility grid is investigated at the beginning. This is considered as an excellent step to understand all the aspects behind the

multi-point grid connection problem. So, a hybrid wind-PV on-grid (HWPVG) (See Fig. 1.3) retrofitting system is considered for economic investigation in Jordan.

To satisfy the national load in Jordan for example, since it is a non-oil producing country, and many cities are of high potential of wind speed and solar radiation, so the hybrid system is highly reliable and recommended in some cities. Other cities are potentially suitable to install wind farms or PV arrays configurations. Some cities are of high potential of wind and/or PV will not be used to install renewables because the national load has been already satisfied. So, the unused cities may be used in the future once the load is increased.

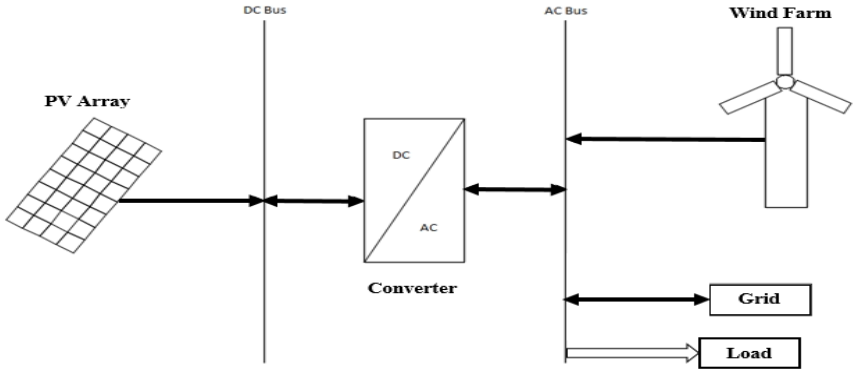

Fig. 1.3 Hybrid wind-PV grid connected system

1.1 Engineering and socio-economic aspects of sustainable energy

Our paper in [16] has been accepted and presented out of the work in this section. The ideas that we discussed in this dissertation are based on the fact that there is plenty of fossil fuels for hundreds of years. Worldwide, the urgency of sustainable energy comes from global warming or greenhouse effects, and equitable access to energy for all humanity. The developing world is the sector that will dominate the growth of greenhouse

gas emissions in the coming decades. The developed world should provide technologies for the developing world (90%) that are green and are appropriate for their development, which is the key to reduce carbon emissions, rather than making the developed world clean (10% solution).

There are numerous examples of technologies that can be considered as an outcome of this study. First, locally appropriate renewable on-grid power systems. The renewable energy resources of different types are of high potential in many locations around the world. For example, Jordan is blessed with the abundance of both solar and wind energy resources. Thereby, many studies are being done to investigate the feasibility for the application of on-grid wind/PV retrofitting systems in Jordan. Moreover, Saudi Arabia, an oil producing country, is of high potential of solar energy, where several research projects are being conducted to maximize national revenue due the solar plants, connected to the Saudi utility grid, displacing the fossil fuel plants. Furthermore, Panama is rich in water resources. Approximately, half of Panama's electrical energy comes from hydro-generation. So, several promising projects are being done to hybridize hydro with wind power generation in order to decrease Panama's dependence on fossil fuel. This also reduces the emissions of the GHG in Panama. Further, the application of renewable low cost island power systems for the developing world is being studied. The development of power infrastructure to provide electrical energy to these rural areas must begin sustainably. By starting off sustainably and emissions-free, these energy systems will set the precedent by not contributing to global warming and is consistent with the inevitable transition from fossil fuels. Further, inexpensive EV products for the developing world are

the best use of this technology. Gasoline automobiles are convenient for people because of the reasonable refilling rate, no residue, and their long driving distance. Therefore, in order to change the way we travel toward the electric vehicles (EVs), various challenges should be overcome such as the energy density, cost, and recharging time. However, the EVs may very well be appropriate for the developing 90 % world who have no need of long range personal cars.

The most effective contribution that the developed countries can make to the reduction of greenhouse gas emissions is improving their energy efficiency. For example, the commercial aircraft kerosene consumption per passenger miles has been reduced by 50% since 1960. Similar or more energy savings can be achieved through technology improvement in vehicles, lighting, manufacturing, etc. This sets the long term priorities for the technology development for the 10% of the world population that consumes most of the world energy today.

1.1.1 Motivations for renewables & current perspectives

A vast majority of the world population (~90%) is still economically developing and in need of more energy (China, India, Asia, Africa, etc.), causing the fastest growth in world energy consumption in history. This will easily overwhelm any energy and greenhouse gas (GHG) emissions savings from improved efficiency and going “green” in the 10% developed world. This situation is further aggravated by the complicated relationship between the fossil fuel use in the developed world and the developing world. This is because fossil fuels are fungible, i.e. if the developed world does not use it, its price will go down and the developing world will use it much faster to develop. Furthermore,

because of the very high-energy usage, which depends greatly on fossil fuel energy resources, it can be concluded that the 90% dominates future emissions by the year 2040 as shown in Fig. 1.4. Therefore, CO_2 reduction in the developed countries is not an effective motivation for renewable energy development [17].

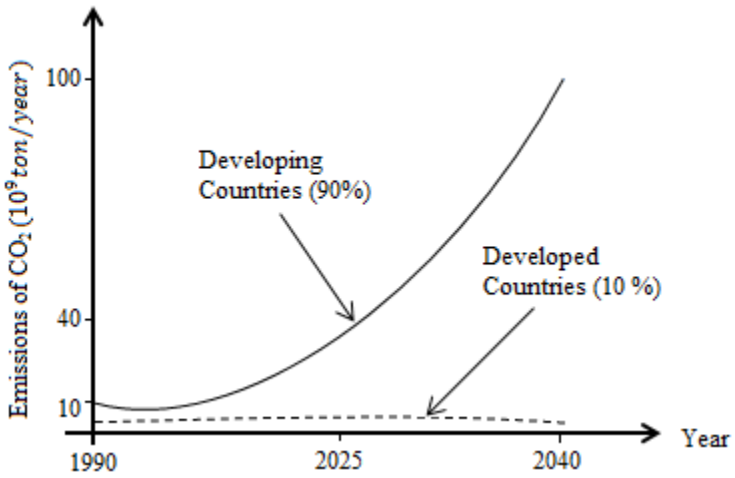

Fig. 1.4 CO_2 emissions for developing (90%) and developed (10%) countries [17]

In other words, the only logical solution, to the world fossil fuel emissions problem, is for the developed world to solve the problem of carbon emission associated with the growth in the developing world. The developed world must produce technologies for the developing world that are green and are appropriate for their development. Affordable developing world access to "green" energy is the key to reduction of carbon emissions. Appropriate technologies must be developed for the emerging nations to conserve energy and move rapidly from coal to lower-carbon power sources, including bio energy, natural gas, solar, wind, and nuclear. Of course, we must also continue to develop better products for the developed world that are more efficient.

1.1.2 Sustainable energy metrics & requirements

Equitable world access to energy is a reliable motivation for sustainable energy. Table 1.1 summarizes the requirements that should be clarified to acknowledge the importance of sustainable energy resources.

Table 1.1 Sustainable energy requirements

Terminology	Definition
Adequate	No energy limits on economic development and prosperity.
Ecological	Environmentally acceptable
Economical	Reasonable capital & production cost, market compatible.
Realizable	Starting with the present infrastructure, smooth transition to future technologies.
Global	Producible in the United States and elsewhere, eliminating international “haves and have-nots”.
Publicly Acceptable	Compatible with the public sense of risk, aesthetics, ethics, etc.
Unifying	Compatible with the sense of world economic equity and world community.
Robust	Not prone to technical failures, not maintenance intensive, no single-point failures.
Secure	Not concentrated, volatile, vulnerable to terrorism.

1.2 Importance of renewables when the oil prices fall down

Falling of oil prices starting from June, 2014 has mainly three consequences: Financial deficits in the oil industries worldwide, investments in the conventional fossil fuel resources have been reduced and the problem of the unemployment has been increased by decommissioning thousands of labors in oil companies. In this case, investors are looking for renewable energy resources as the best alternatives because they felt frustrated of the financial loss they had in their oil-based projects. Those investors got the benefits and the recommendations came out from global humanitarian conferences such

as the World Climate Conference (WCC) held in Paris in late 2015. WCC aims to strengthen the global response to the threat of climate change by holding the increase in the global average temperature (GAT) well below 2^{o}C above pre-industrial levels, and continue working to limit the GAT increase to 1.5^{o}C above pre-industrial levels [18]. Also, the WCC in Paris had the goal that the developed countries will annually provide $100 billion to the developing countries in order to implement renewable energy projects that will definitely help minimize the risk of climate change [18], which is considered as an excellent opportunity for investors in both private and public sectors. In this case, it can be foreseen that the global use of sustainable energy resources will be increased in the near future as alternatives to the depletable fossil fuels conventional resources.

1.3 Emissions

Burning of fossil fuel resources (oil, coal and natural gases) causes pollution by the emission of detrimental gases, such as SO_2, CO, NO_X, HC, and CO_2, which will destroy the ecological system. For instance, SO_2 and NO_X cause acid rain. Many agreements have been signed to help the countries worldwide mitigate the GHG emissions such as Kyoto Protocol. It is a binding agreement signed in Tokyo, Japan in 1997 by industrialized countries to lower the overall emissions from six GHG (CO_2, CH_4, N_2O, SF_6, HFCs, and PFCs) [19]. In Copenhagen accord, they endorse Kyoto protocol by mitigating global emissions, and maintain the global temperature increase below 2^{o}C [20]. The United States environmental protection agency (EPA) states in a global scale that (GHG) shown in Fig. 1.5 emitted and caused by human activities [21].

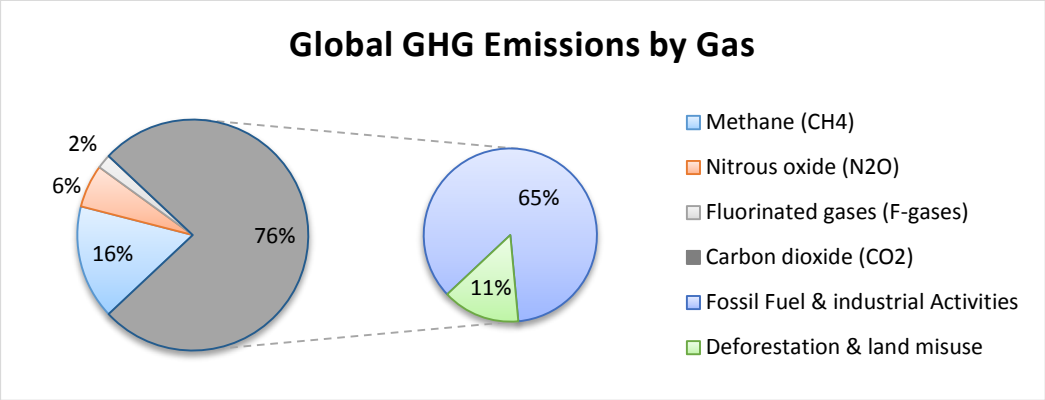

Fig. 1.5 Global GHG emissions

Sulfur dioxide (SO_2) and Oxides of nitrogen (NO_X) cause environmental problems as a result of the electrical energy produced by the conventional utility power plants. Numerous models have been used to model the emission function of the conventional power generation [22, 23]. The emission function ψ (in kg/hour) is a quadratic model for both (SO_2) and (NO_X) emissions as shown in Equation 1.1. Where P_{grid} is the power produced from the grid conventional power plants.

$$\psi(P_{grid}) = \alpha + \beta P_{grid} + \gamma P_{grid}^2 \quad (1.1)$$

The (α, β *and* γ) values are the emission coefficients. They have been calculated for an equivalent thermal plant as discussed in [22].

Fig. 1.5 shows that the impact on the ecological system comes mainly from Carbon Dioxide (CO_2) which constitutes 76% of the global GHG. Moreover, 65% is the result of the fossil fuel and industrial activities, and 11% is the result of the deforestation and land misuse. Global warming is just one more reason to address the energy challenge urgently. Global warming problem that is mainly caused by CO_2, where the solar heat in the atmosphere will be trapped leading to a phenomenon called the greenhouse effect [3]. To

compute the amount of CO_2 produced per kWh when generating electricity with fossil fuels, the CO_2 emission factor (EF) (in $kgCO_2/kWh$) is measured in many countries to determine the amount of the CO_2 in their regions. This helps develop energy plans to protect from climate change in the atmosphere. In this dissertation, the CO_2 will be used and formulated as an AEI which is measured in Megatonne CO_2 per year.

1.4 PV module characteristics & Solar Path Finder (SPF)

When the PV arrays are exposed to the solar insolation; the semi-conducting material will absorb the photons of the sun light and release the electrons. The electron will be moved from the valence to the conduction band forming a buildup of voltage between the terminals. For the goal of mechanical protection the PV module is provided with cover glass and an applied transparent adhesive. To enhance the ability of absorbing more radiation; the modules in a PV array are enhanced with an anti-reflection coating [24]. Fig. 1.6 shows a front cross-section for a PV module.

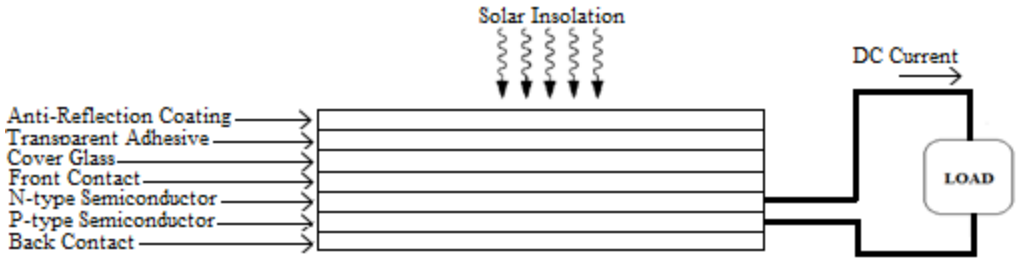

Fig. 1.6 PV effect and construction

A CS6X-310 module has been selected for the time being as an example in order to investigate the characteristics of the PV module. The specifications of the PV panel is measured under standard test conditions (STC) with irradiance of $1000W/m^2$, spectrum

AM 1.5 and cell temperature of 25°C (See Table 1.2). In addition, Fig. 1.7 shows that polycrystalline PV cells look exactly rectangular with no rounded edges.

Table 1.2 Specifications of (CS6X-310) PV panel

$P_{nominal}$ (W)	V_{oc} (V)	I_{sc} (A)	V_{mp} (V)	I_{mp} (A)	η (%)	A_{PV} (m^2)	Weight (kg)	Cell Type	FF (%)
310	44.9	9.08	36.4	8.52	16.16	1.9188	22	Polycrystalline	76.07

Fig. 1.7 CS6X-310 polycrystalline PV panel

MATLAB/SIMULINK is used to build the Canadian Solar (CS6X-310) PV module output characteristics, i.e. both I-V and P-V curves [25, 26]. SIMULINK model of Fig. 1.8 results in the output characteristics of (CS6X-310) PV module (Output current and power versus voltage, See Fig. 1.9 and Fig. 1.10). Model set of equations for the PV module are shown below [27].

$$I_{ph} = [I_{scr} + K_i\,(T\ - 298)] * \frac{\lambda}{1000} \tag{1.2}$$

$$I_{rs} = \frac{I_{scr}}{e^{\left(\frac{qV_{OC}}{N_s KAT}\right)} - 1} \tag{1.3}$$

$$I_o = I_{rs} \times \left(\frac{T}{T_r}\right)^3 \times e^{\left(\frac{qE_{go}}{BK}\left[\frac{1}{T_r} - \frac{1}{T}\right]\right)} \tag{1.4}$$

$$I_{PV} = N_P \times I_{ph} - N_P \times I_o \times \left[e^{\left\{\frac{q\times(V_{PV} + I_{PV}\times R_S)}{N_S KAT}\right\}} - 1\right] \tag{1.5}$$

Where [27, 28]:

$I_{ph} =$ The light generated current in amps.

$I_{scr} = 2.55\text{A} =$ The PV module short-circuit current at 25^{o}C and 1000 $watt/m^2$.

$I_{rs} =$ Module reverse saturation current in amps.

$K_i = 0.0017\text{A}/^{o}\text{C} =$The short-circuit current temperature co-efficient at I_{scr}.

$T =$ The PV panel operating temperature in Kelvin.

$\lambda =$ The PV module radiation in $watt/m^2$.

$q = 1.6 \times 10^{-19}C =$ Absolute value of electron charge.

$E_{go} = 1.1$ eV = The band gap energy for silicon.

$A = B = 1.6 =$ The ideality factor, a number between 1 and 2, usually increases with the current.

$K = 1.3805 \times 10^{-23}J/K =$ Boltzmann's constant.

$T_r =$ 298 K = The reference temperature.

$I_{PV} =$ PV module output current in amps.

$N_P =$ The number of cells connected in parallel.

$I_o =$ The dark saturation current in amps, or the diode leakage current in the absence of light. Note that, I_o increases with temperature. So, it will have a very low value for high quality materials.

$V_{PV} =$ PV module output voltage in volts.

$R_s =$ The series resistance of a PV module.

$N_s =$ The number of cells connected in series.

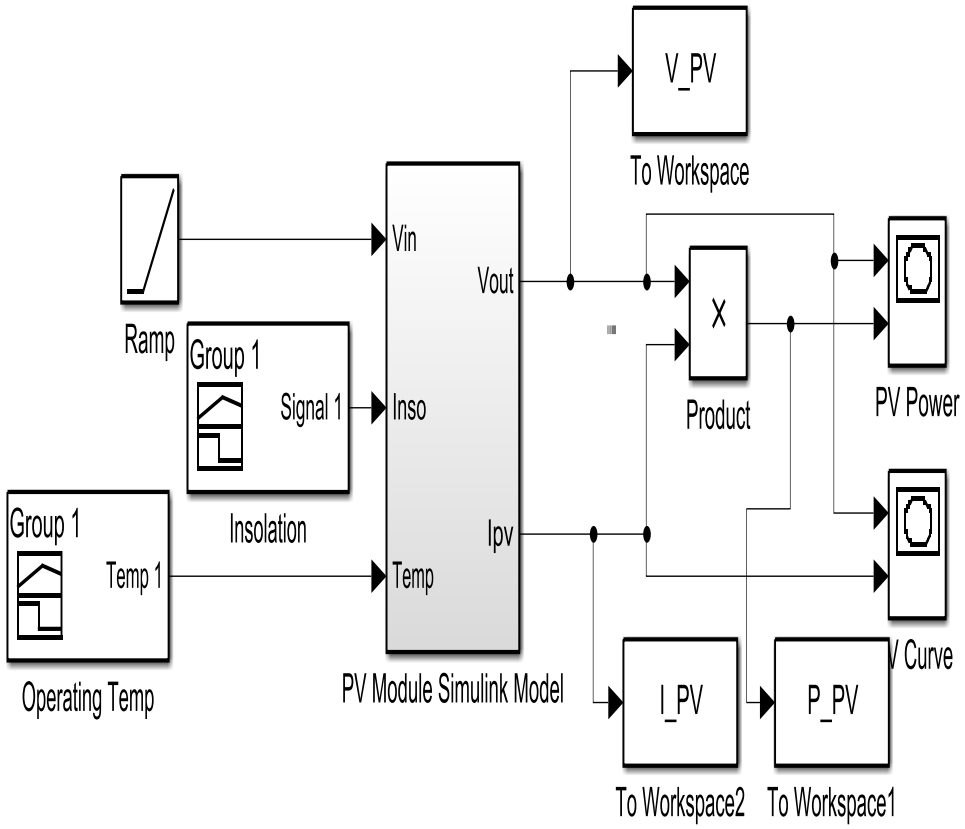

Fig. 1.8 SIMULINK to gain output characteristics of (CS6X-310) PV module

Note that, in Fig. 1.8, opening the mask of "PV Module Simulink Model" will show the application of Equations (1.2-1.5). Furthermore, the manufacturer data for the Canadian solar (CS6X-310) PV module shown in Table 1.2 are inserted to this model in addition to the STC values of both insolation ($1000 watt/m^2$) and ambient temperature of (25^oC). Afterwards, two outputs are gained from this model, i.e. the PV current, PV voltage, and the multiplication of both in order to get the PV power. After that, those outputs are sent to the workspace as arrays in order to have both Fig. 1.9 and Fig. 1.10 which are exactly the same as what is provided by the Canadian Solar manufacturer for (CS6X-310) PV module.

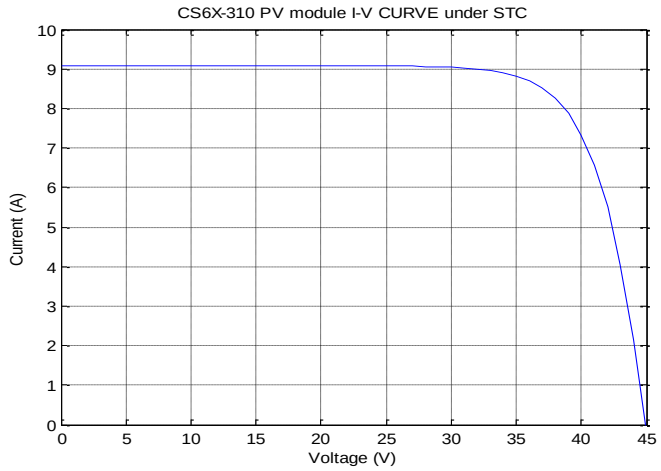

Fig. 1.9 I-V output characteristics of (CS6X-310) PV module

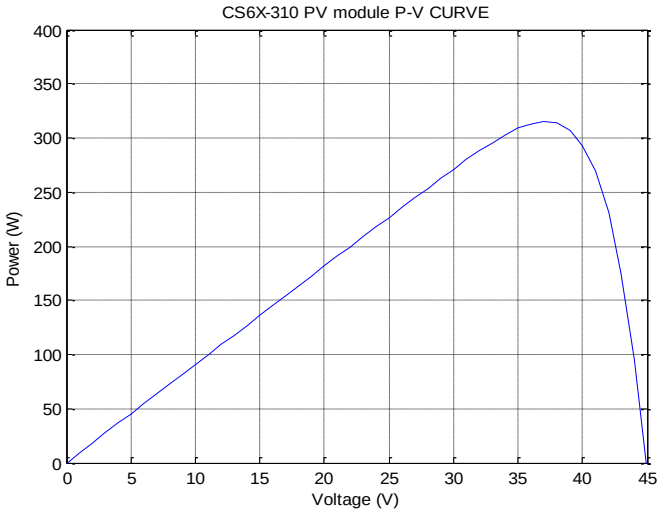

Fig. 1.10 P-V output characteristics of (CS6X-310) PV module

1.4.1 Characteristics of the PV module with fixed insolation

PV renewable energy systems are rarely operated under (STC). Throughout the day, there are various variable conditions happened to solar insolation and temperature. Thereby, the output of a PV module varies. This would make changes to the characteristics of the PV module. In order to understand the characteristics of the PV modules (i.e. I-V

& PV Characteristics), we should investigate how the solar radiation and cell temperature affect those characteristics. Note that, the rating of the PV module is given under STC when the temperature is $25^{o}C$. But, what happens to the PV characteristics when the temperature increases or decreases. Fig. 1.11 and Fig. 1.12 show that as the temperature increases the open circuit voltage and output power decrease, this would reduce the lifetime and performance of the (CS6X-310) PV module[29].

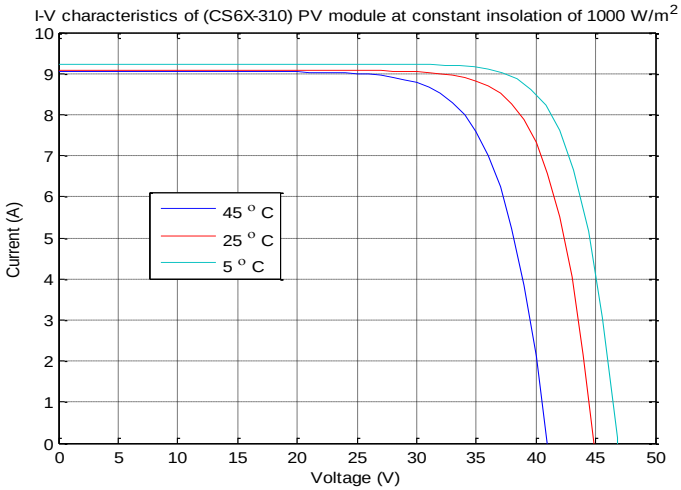

Fig. 1.11 I-V characteristics at constant insolation and variable temperature

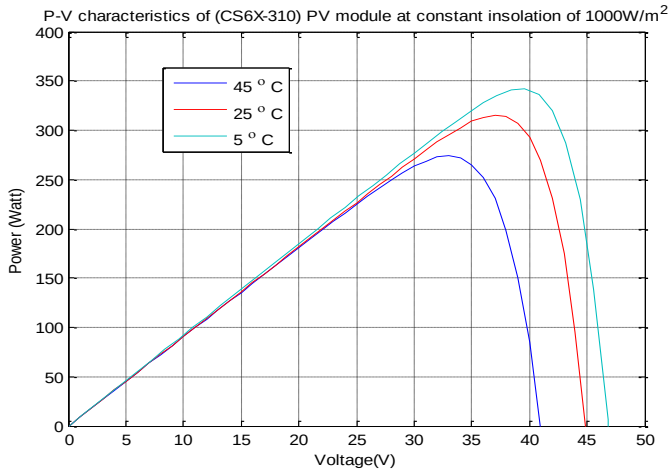

Fig. 1.12 P-V characteristics at constant insolation and variable temperature

Thereby, different cooling systems are investigated in order to overcome the temperature increasing. Most of semiconductor devices including the PV cells are sensitive to temperature variations [30]. Fig. 1.13 shows that as the temperature of the PV module increases, the the open circuit voltage decreases. Also, it shows that the relathionship is a linear with negative slope as Equation 1.6 shows.

$$Voc = -0.15T + 48.05 \quad (1.6)$$

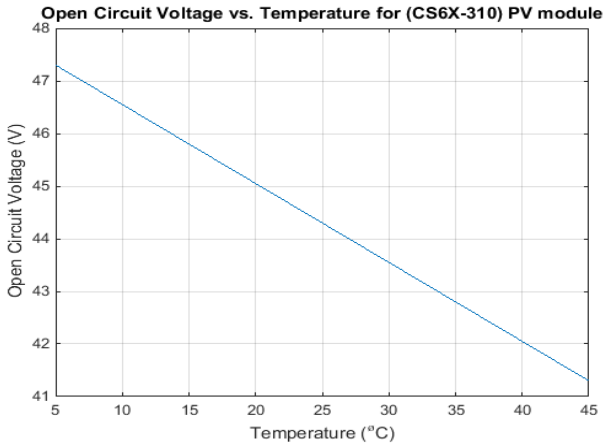

Fig.1.13 Effect of temperature on an open circuit voltage

This decaying line describes the first order effect of the cell temprature on Voc. Temperature increasing is considered as a bad electrical effect on the PV cell performance. So, in many cases various cooling techniques are used to overcome the temperature increasing. Another considered electrical effect on the PV module performance is the effect of temperature on the maximum power point gained from the PV module as shown in Fig. 1.14. It shows that it is also a decreasing line with a negative slope as Equation 1.7 shows.

$$Pmax = -1.693T + 352.6 \quad (1.7)$$

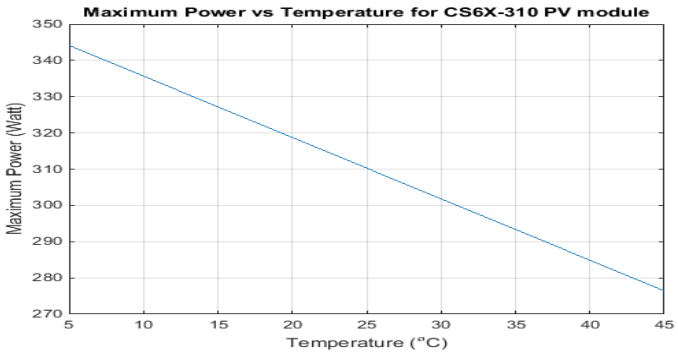

Fig. 1.14 Effect of temperature on maximum power point

The temperature increasing results in a lower maximum power point for the PV module. Also here, temperature increasing is considered as a bad electrical effect on the PV cell performance.

1.4.2 Characteristics of the PV module with fixed temperature

Changing the solar irradiation also affects the I-V and P-V characteristics of the PV module. Note that the rating of the PV module is given under STC where the radiation is 1kW/m^2 . But, what happens to the PV characteristics when the insolation increases or decreases. Fig. 1.15 and Fig. 1.16 show that as the solar insolation increases the short circuit current and the maximum power increase respectively.

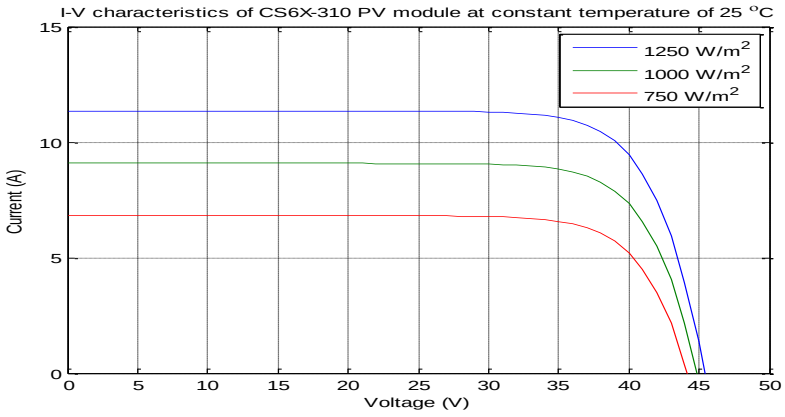

Fig. 1.15 I-V characteristics at constant temperature and variable insolation

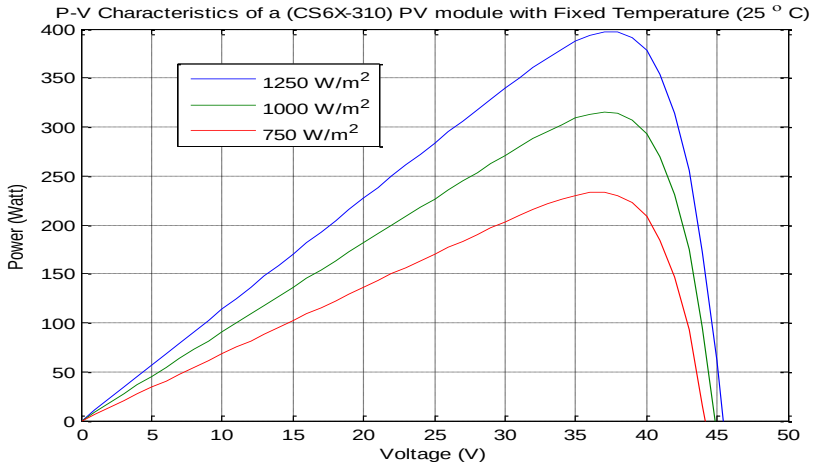

Fig. 1.16 P-V characteristics at constant temperature and variable insolation

The solar insolation or the light intensity is defined in some resources as the number of Suns [31], i.e. one sun means 1kW/m^2. Fig. 1.17 & Fig. 1.18 show that increasing in solar irradiation of the PV module, increases both the short circuit current and maximum power. Also, those figures show that the relathionship is a linear upward line as Equation 1.8 & 1.9 show below.

$$Isc = 0.00908 * GR - 4.487 \times 10^{-15} \quad (1.8)$$

$$Pmax = 0.3286 * GR - 13.3 \quad (1.9)$$

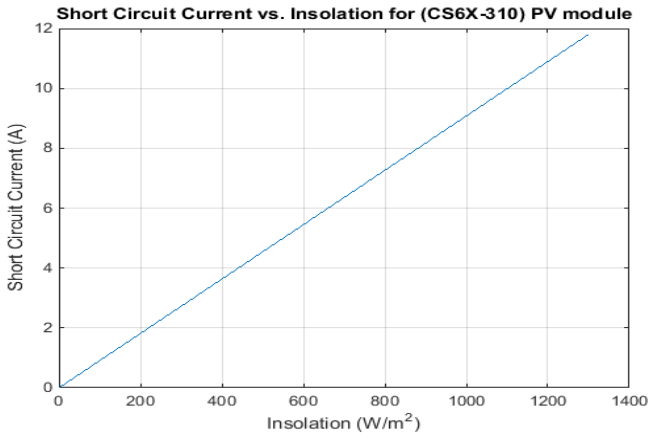

Fig. 1.17 Effect of solar insolation on short circuit current

Equations 1.12&1.13 describe the first order effect of the irradiance on *Isc* and *Pmax*. Radiation increasing is considered as a desired electrical effect on the PV cell performance. So, in many cases various tracking techniques are considered to exploit high percentage of the solar insolation.

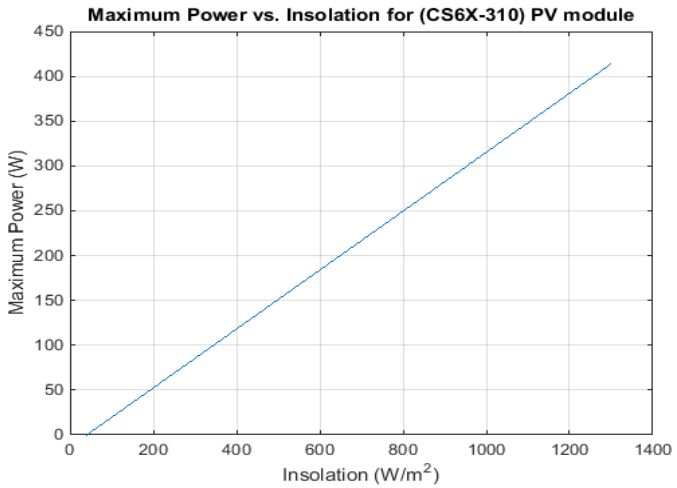

Fig. 1.18 Effect of solar insolation on maximum power point

In order to see which affects more on a PV module, i.e. the temperature or the solar insolation. Equations 1.10&1.11 are used. They represent a comparison factor for the temperature (C_{FT}), and a comparison factor for the solar insolation C_{FSI}:

$$C_{FT} = \left| \frac{P_{(\max value)} - P_{(\min value)}}{\frac{T_{max} - T_{min}}{T_{STC}}} \right| \tag{1.10}$$

$$C_{FSI} = \left| \frac{P_{(\max value)} - P_{(\min value)}}{\frac{SI_{max} - SI_{min}}{SI_{STC}}} \right| \tag{1.11}$$

After the application of these two equations on the data of the (CS6X-310) PV module, it is shown that solar insolation affects the PV module more than temperature. Since $C_{FT} = 102.6875 Watt$ and $C_{FSI} = 328.6 Watt$.

1.4.3 SPF to reduce shading

SPF is a non-electronic tool that is used to determine the shading for any site. Thereby, it is very useful device prior the application of a PV arrays. SPF helps determine the shaded portion for a randomly selected point. So, it is one of valuable tools to correctly select an appropriate location for PV installations with no or very little amount of shading. Furthermore, SPF is used to determine the sun position (See Fig. 1.19), i.e to measure the elevation (altitude) angle which is the angle between the two green lines, note that the Zenith is referred to the sky. Also, SPF is used to measure the compass (azimuth) angle, which is the angle between the two red lines.

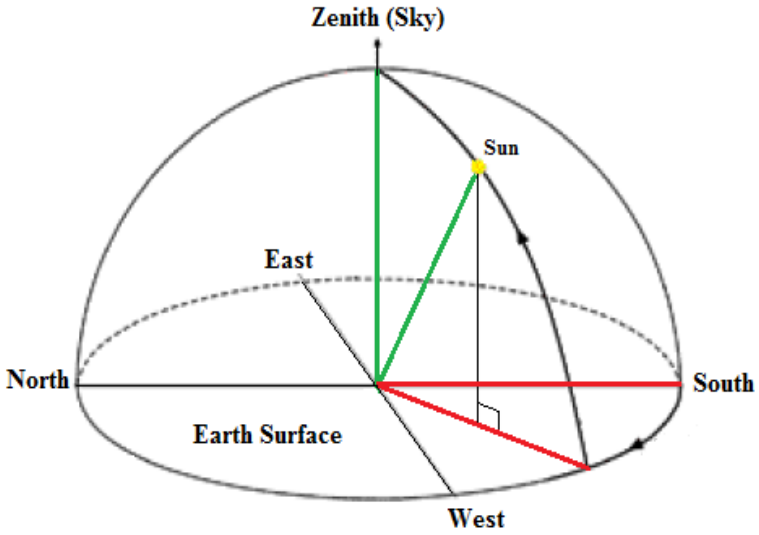

Fig. 1.19 Sun position

For example, two locations at Texas A&M University, USA, have been tested in order to select the one with lower shading in order to increase the percentage of incoming solar radiation for a PV installation. The conditions and measurements are taken under some conditions given in Table 1.3.

Table 1.3 Shading experiment site information

Location	Texas A&M University (Near Wisenbaker Building)
Longitude	-96.3344068^{o}
Latitude	30.627977^{o}
Date	September 10, 2014
Time	9:15 a.m.
Temperature (F)	92^{o}

At this point, the SPF is used to evaluate the available solar insolation over a year's period for the given site in Table 1.3 to see the impact of shading. In this experiment, the SPF has been placed in the backyard of the Wisenbaker building at Texas A&M University. At the selected point there was a shading from Wisenbaker, Zachry and adjacent buildings for the time less than 9 a.m. and the time more than 4p.m as shown in Fig. 1.20, which shows a picture for the panorama of LOCATION 1. So, in this case PV application is useful between 9 a.m. and 4p.m. A solar assessment is performed by calculating the percent of shaded energy, and the percent of solar energy that reaches LOCATION 1 (See Fig. 1.20 and Table 1.4).

Fig. 1.20 Solar site assessment for LOCATION 1 using Panorama SPF chart

Table 1.4 Percent of solar energy that can reach LOCATION 1 (%)

Month	#'s Shaded	Total #'s	Shaded regions (%)	Unshaded regions (%)
Jan	13	100	13	87
Feb	16	94	17.02128	82.97872
Mar	23	96	23.95833	76.04167
Apr	29	98	29.59184	70.40816
May	30	94	31.91489	68.08511
Jun	36	101	35.64356	64.35644
Jul	36	101	35.64356	64.35644
Aug	27	96	28.125	71.875
Sep	23	90	25.55556	74.44444
Oct	16	96	16.66667	83.33333
Nov	16	113	14.15929	85.84071
Dec	15	89	16.85393	83.14607

Moreover, this device has been used to test another location. Fig. 1.21 below shows a picture for the panorama of LOCATION 2. A solar assessment is performed by calculating the percent of shaded energy, and the percent of solar energy that reaches LOCATION 2 (See Fig. 1.21 and Table 1.5).

Table 1.5 Percent of solar energy that can reach LOCATION 2 (%)

Month	#'s Shaded	Total #'s	Shaded regions (%)	Unshaded regions (%)
Jan	9	99	9.090909	90.90909
Feb	6	100	6	94
Mar	6	103	5.825243	94.17476
Apr	6	103	5.825243	94.17476
May	8	104	7.692308	92.30769
Jun	4	104	3.846154	96.15385
Jul	5	104	4.807692	95.19231
Aug	6	103	5.825243	94.17476
Sep	6	103	5.825243	94.17476
Oct	5	99	5.050505	94.94949
Nov	9	90	10	90
Dec	14	100	14	86

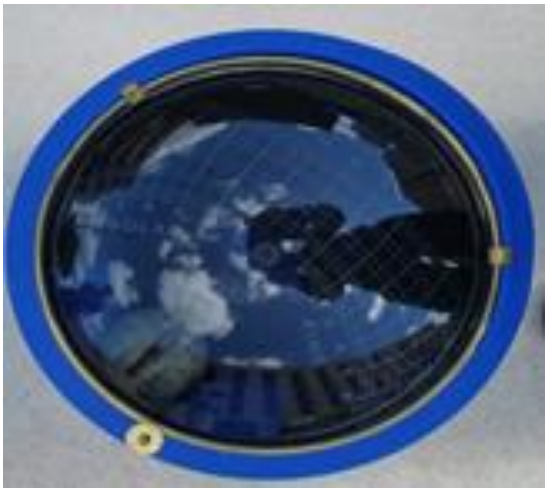

Fig. 1.21 Solar site assessment for LOCATION 2 using Panorama SPF chart

In conclusion, application of PV modules in LOCATION 2 is recommended since the annual percentage (93.02%) of solar energy that can reach LOCATION 2 is higher than the corresponding percentage (75.99%) of solar energy that can reach LOCATION 1 for all months throughout the year. As the aforementioned two SPF cases show that it is very important to reduce shading to help exploit the solar radiation. Thereby, in this dissertation the rectangular area of the PV array will be computed to reduce self-shading as discussed in Section 5.6.2.

1.5 Wind Turbine (WT) characteristics

1.5.1 Characteristics of the WT at sea level

The WT power curve depends on manufacturer data or more detailed data about the models. In the literature, many simplified WT models have been used to model the part between the cut-in and rated wind speeds, which includes linear, quadratic or cubic models. The WT models will be explained in details in Section 5.1. At this point, a V90-1.8MW turbine has been selected as an example to investigate a simplified characteristics

of the WT. MATLAB code described by the flow chart in APPENDIX A is used to represent V90-1.8MW turbine characteristics (Output power in MW versus Wind speed in m/s, See Fig. 1.22) referring to the system of Equations of (1.12).

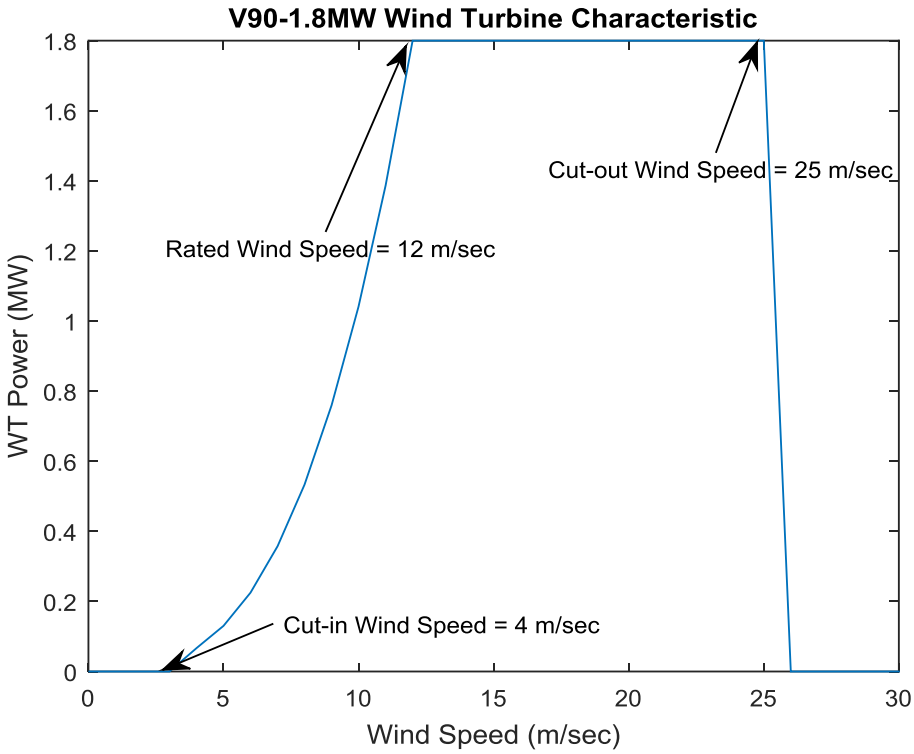

Fig. 1.22 V90-1.8MW wind power simplified curve

$$P_{WT} = \begin{cases} 0 & , \quad v < v_{cut_{in}} \\ \frac{1}{2}\rho A_{WT} v^3 Cp & , \quad v_{cut_{in}} \le v \le v_{rated} \\ P_{rated} & , \quad v_{rated} \le v \le v_{cut_{out}} \\ 0 & , \quad v > v_{cut_{out}} \end{cases} \tag{1.12}$$

Where: ρ is the air density at sea level (1.225kg/m^3), A_{WT} is the swept area in m^2, $v_{rated}, v_{cut_{in}}, v_{cut_{out}}$ are the rated, cut-in, cut-out wind speed values respectively, P_{rated} is the rated power of the WT and Cp is the power coefficient.

1.5.2 WT control strategies

Note that, the output power is expected not to be flat in most WT types. The first justification for this behavior, that the maximum power should not be flat unless the instantaneous wind speed exceeds the rated value when the WT cannot generate more than its rated value. This phenomenon is called wind shedding. However, this behavior could be explained by examining the control strategies applied in a WT. There are two main control strategies (Pitch-regulated and Stall-regulated) that are used to protect the WT by withstanding the stormy wind speed values before reaching the cut out value when the braking system is activated to turn off the WT, See Fig. 1.23.

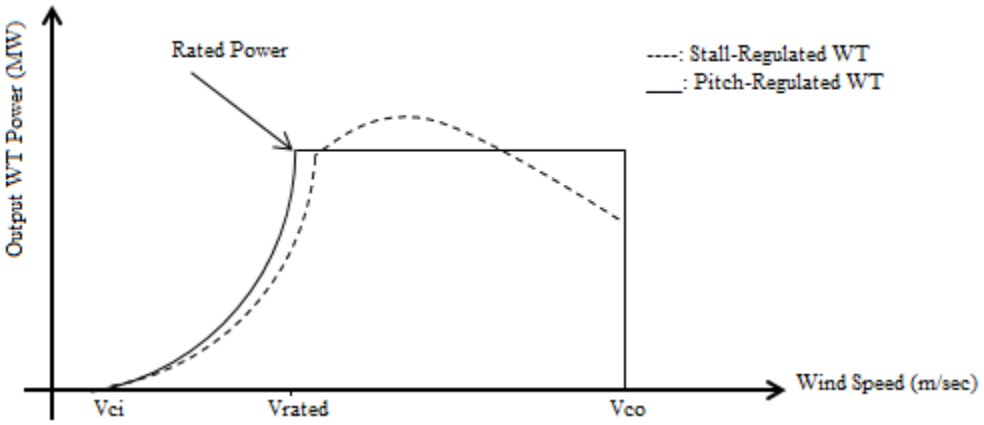

Fig. 1.23 Pitch-regulated (solid line) and stall-regulated (dashed line)

1.5.2.1 Pitch-regulated WT control strategy

Pitch control strategy that uses an active control which will change the pitch angle. In other words, this strategy will turn the WT blade around its own axis. As a results there are two cases: the rotational speed above the rated value will be decreased, and the blades will pitch for the purpose of slowing down the turbine till reaching the rated value. On the

other hand, if the rotational wind speed is less than the rated value, then the blade will pitch to speed-up the WT till reaching the rated value. In this case, it is expected to see a cut-off at a value less than or greater than the rated value. For instance, Fig. 1.24 shows the instantaneous power for GE-1.5MW WT. It shows a lot of cutoff, which is the result of the pitch control strategy that makes this WT characteristics as shown in Fig. 1.25.

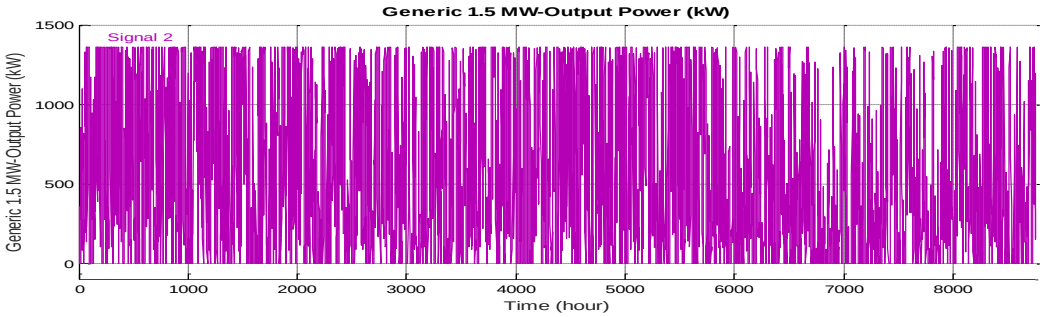

Fig. 1.24 Power vs. time for GE-1.5 MW

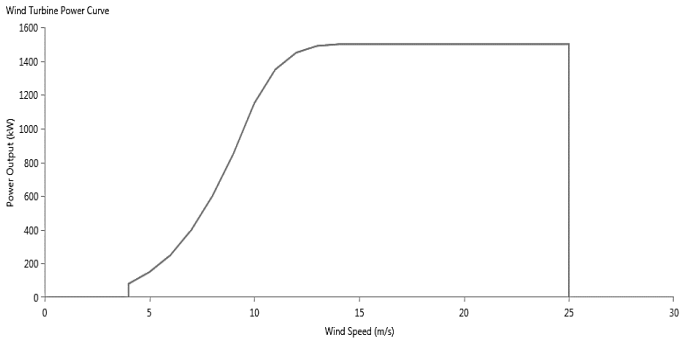

Fig. 1.25 WT power curve for GE-1.5 MW

Afterwards, investigation of the hourly wind speed values shows that 469 values (5.35%) are between the rated wind speed (14 m/sec) and the cut-out value (25m/sec). In this case, the pitch regulated system will be activated to slow down the WT to make a cutoff at the rated value. In addition, there are 6889 hourly wind speed values (78.64%) are between the cut-in wind speed (3.5 m/sec) and the rated value (14m/sec). In this case,

the pitch regulated system will be activated to speed up the WT to make a cutoff at the rated value. In sum, in the pitch regulated control strategy wind turbines (WTs), it is expected to see a high percentage (83.99%) of cut-off values in the power vs. time curve (See Fig. 1.24).

1.5.2.2 Stall-regulated WT control strategy

In the stall-regulated control strategy for WTs, the blades are designed and stalled to decrease the output power when the wind speed exceeds a specified value (usually slightly greater than the rated value). Thereby, this type of control strategy is not able to keep a constant power in high wind speed values. For example, the WT power curve in Fig. 1.26 is for BWC Excel-S WT. It shows that it has a stall regulated control strategy. In other words, the stall-regulated strategy will not be activated for BWC Excel-S WT for values less than the rated value (13.5m/sec), and it will be activated for a set value of (16 m/sec) higher than the rated value. As shown in Fig. 1.26 this strategy will start slowing down the turbine at 16m/sec, and continue decreasing the output power passing below the rated power value till reaching the cut-out wind speed value (25m/sec) when the WT will be turned off using the braking system.

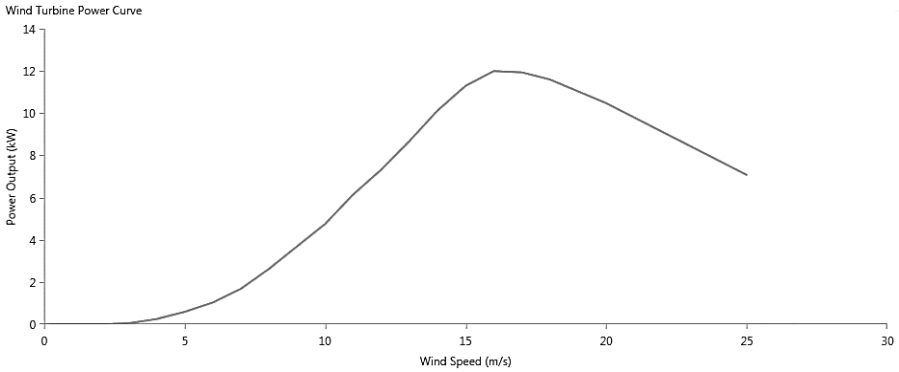

Fig. 1.26 WT power curve for BWC Excel-S

At this point, investigation of the hourly wind speed values shows that 8095 values (92.41%) are between the cut-in wind speed (2 m/sec) and the set value (16m/sec). In this case, the stall regulated system will not be activated, and there will be no cutoff (with 92.41%) before the set value of wind speed. In addition, there are 198 hourly wind speed values (2.26%) are between the set wind speed (16 m/sec) and the cut-out value (25m/sec). In this case, the stall regulated system will be activated to slow down the WT to make a cutoff at the set value (16m/sec), and the power will continue decreasing till reach the cut-out value. In sum, in the stall regulated control strategy WTs, it is expected to see a high percentage (92.41%) with no cut-off values in the power vs. time curve (See Fig. 1.27).

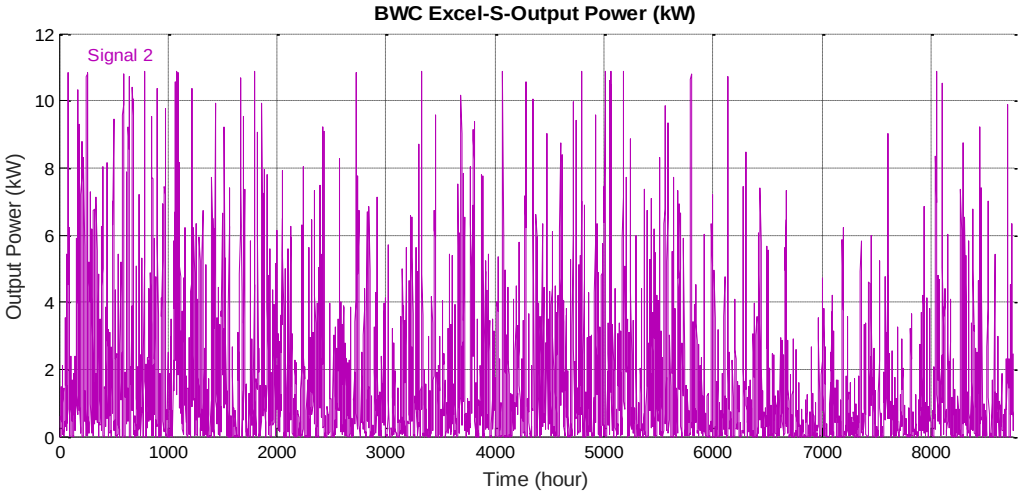

Fig. 1.27 Power vs. time for BWC Excel-S WT

2. LITERATURE REVIEW

This section will cover a literature review of what has been done regarding renewable energy resources and especially techno-economic studies performed by researchers before. This overview of renewable energy systems will be presented along with state of the art topologies being researched. Our research was motivated by the topics covered in this section.

In today's society the need for renewable energy sources is in high demand. Over the past few years technological advances have been made in wind power systems, photovoltaics, fuel cells, and hydroelectric power systems, just to name a few. With these advances come the question of how to take the correct decision, whether they are feasible, environmental or not. Thereby, a growing need for techno-economic and environmental investigations have become interesting topics in renewable energy studies.

The following literature survey consists of various papers that are related to the wind/PV renewable energy systems:

A. M. AL-ASHWAL and I. S. MOGHRAM [32] presented a paper to determine the optimal combination (PV only, wind only or hybrid wind/PV) in terms of cost comparison. At the beginning, this paper said that the availability of both wind and PV is often in contrast. So, is it better to combine them as a hybrid system? To answer this question, a village in Yaman consists of 20 houses is considered as the load. The average daily energy demand for the whole village is estimated to be 75 kWh per day which is around 3kW per day. Note that, in Table 2.1 the capacity for the PV module and WT are 50W and 1kW respectively.

Table 2.1 Cost comparison for 3 combinations of wind or PV

Component	#	Capacity	Cost ($/W)	Total Cost
Wind	10	10kW	2	20,000$
PV	300	15kW	4	60,000$
PV+Wind	30_PV+9_Wind	1.5kW_PV+9kW_Wind	/	24,000$

Table 2.1 shows that the capacity of the three combinations ranges between 10kW to 15 kW which is around 3 to 5 times the average daily power demand for the whole village. The only interpretation for this assumption is that the author considered the point where the load is maximum. But, the load is a function of time, and it is better to consider the average value of 3kW in order to minimize the total cost of any combination shown in Table 2.1. In sum, for this paper two notes are concluded. First, as the sharing percent of the wind power increases (or the sharing percent of the PV power decreases) the total cost decreases. Second, as the sharing percent of the PV power increases (or the sharing percent of the wind power decreases) the loss of load risk decreases. So as a result, it is better to combine wind and PV systems in order to have a reliable and feasible system.

Maya Chaudhari [33] presented a report with various points of comparisons (See Table 2.2) for distributed and central PV types. This report classifies the distributed PV systems as residential type (1kW to 4kW), and commercial type (2kW to 1MW). Regarding the central PV, in general it is greater than 100 kW. But, the majority is greater than 1MW.

Table 2.2 Various points of comparisons for distributed and central PV types

Points of comparison	Distributed PV		Centralized PV	
Siting issues and land requirement	Advantages	Disadvantages	Advantages	Disadvantages
	Customer sited. So, no land costs.	Shading of PV panels reduces the system output.	There is no shading.	Extending transmission lines to a remote location costs too much.
Roof Warrantees	Disadvantages (No mentioned advantages)		Advantages only (No mentioned Disadvantages)	
	Building owners require roof warrantees, because the weight added to the roof may cause damage.		There is no need of roof warranty.	
Operation & Maintenance (OMC) costs	• 14$/kW/year for residential buildings. • 12$/kW/year for commercial buildings.		• The tracking system contains moving parts. Thereby, OMC cost would be higher than the distributed type. • 28-55$/kW/year including the OMC of the tracking system.	
Cell Performance	Advantages only (No mentioned Disadvantages)		Disadvantages (No mentioned advantages)	
	There is often a small gap between the PV installation and the rooftop that allows for air circulation to reduce heat build-up. As a result, the cell performance will be improved.		PV cells will be operating at higher temperatures and therefore may reduce the cell performance.	

The Authors in [34] presented a paper mainly discusses the distributed type or the Building Integrated PV system (BIPV). The number of BIPV is increasing as new types of solar cells are developed, See Table 2.3.

Table 2.3 Advantages and disadvantages of distributed PV systems

Advantages	Disadvantages
• The energy is consumed in the same place of generation.	• The orientations and inclination is almost never the optimal one.
• There is no need of land.	• Difficult module working conditions (such as: shadows, reflections,…etc) causes mismatching. This will reduce the extracted energy. The solution for this problem is the use of DC-DC converter with maximum power point tracker (MPPT). • Individual reliability goes down.

B. Türkay and A. Y. Telli. [35] presented a paper that makes an economic analysis of a grid-connected hybrid energy systems. The main scope of this paper is to make a feasibility study for various structures of renewable energy systems that will satisfy the load. Thereby, each component of the hybrid system should be evaluated economically. HOMER program is used to analyze the feasibility of the hybrid systems. The system in Fig. 2.1 shows the configuration suggested in the paper. The excess energy from wind and PV is converted to Hydrogen using Electrolyzer (ELC), then it is stored in a Hydrogen tanks, which could be converted to electrical power using Fuel Cells (FC) in case of peak load requirements. HOMER makes a yearly simulation for each renewable structure and decides if it is feasible, can or cannot satisfy the load. This software requires three main inputs. First of all, the load profile which is expected to be satisfied by the designed system. The paper assumes that the load is 239kW peak and 627 kWh/day.

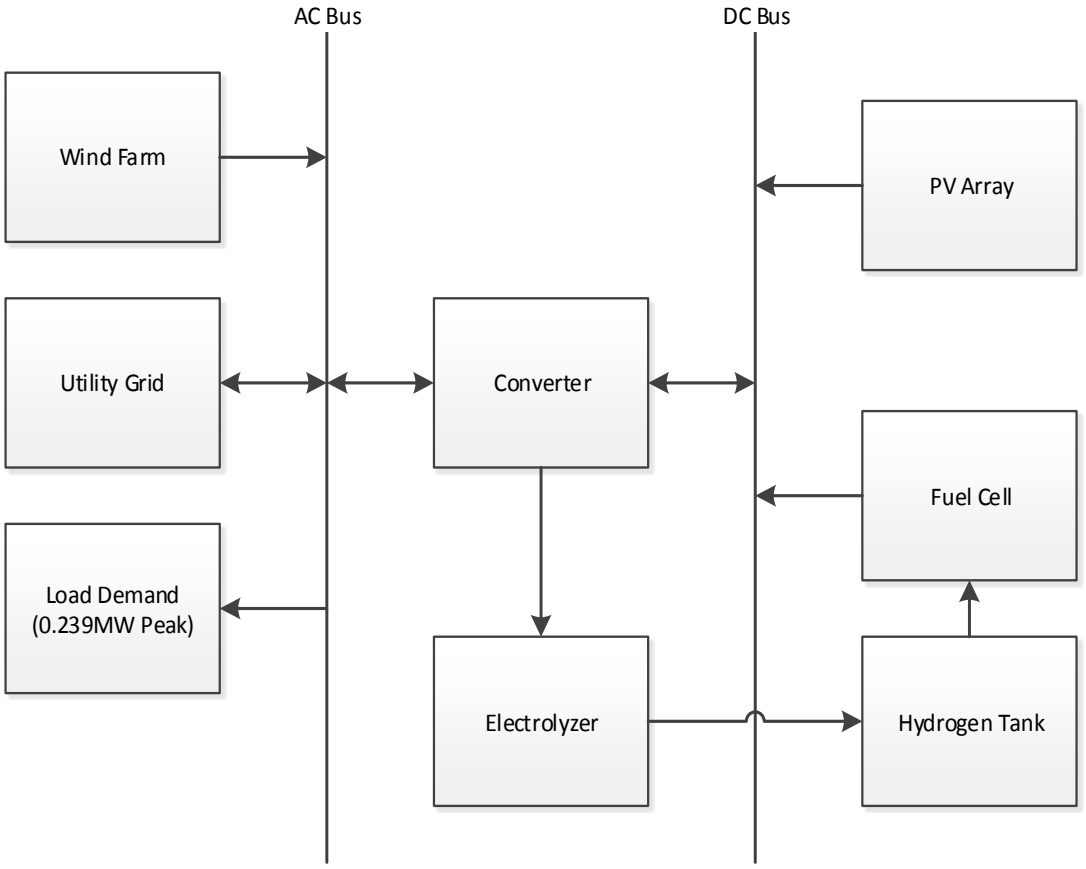

Fig. 2.1 Wind-PV-fuel cell on-grid hybrid system [35]

Second input is the cost for each component, which is shown in Table 2.4. Third input is the weather conditions which are represented by solar radiation with an average annual value of 4.186kWh/m^2, and by the wind speed with an average annual value of 3.762 m/sec. Now, running the simulation for one structure of 40 kW PV, 20 kW FC and ELC, respectively; 30 kW converter, 100 kg HT, and the grid connection. The total system cost was 789,300$ and COE is 0.307$/kWh. The contribution of sources to the network load was 25% (24% PV array and 1% fuel cell); and the grid provided as much as 75% of the load [35].

Table 2.4 Cost comparison for the system described in Fig. 2.1 [35]

Cost Type / Component	CC	OMC	RC
Wind Turbine (D_R=13m, H_{WT}=26m)	78,000$	No Info.	No Info.
PV	5000$/kWh	No Info.	No Info.
Electrolyzer	3128$/kwh	50%*Capital Cost	5%*Capital Cost
FC	5000$/kwh	0.1$/hour	No Info.
HT (3.2kg)	2288$	9$/year	195$
Converter (inverter, Rectifier and charge controller)	1000$	100$/kwh	1000$

Note that, numerous effects are studied in this paper. First, the effect of decreasing the component cost to 50% is investigated. As a results, the capital cost, system cost and the energy cost will be reduced. Second, the effect of capacity shortage (CS) is tested between 0% and 4%. This means that some of load will be unsaved during the year. In other words, no need to size the component for extreme cases. Simulation results shows that an increase in CS, the system cost conversely decreased and the cost of energy values fell from $.307/kWh to $0.108/kWh. In the final analysis, the study indicates that grid-connected hybrid systems including grid, PV, and hydrogen systems have been the most feasible solution in view of the monthly average solar radiation intensity and wind energy capacity of the region and today's equipment costs. The LCOE for this hybrid configuration is $0.307/kWh. It has been observed that cost factor of renewable energy system equipment and changes in capacity shortage fraction lead to remarkable differences in the OST and energy generation cost [35].

Shafiqur Rehman, Md. Mahbub Alam, J.P. Meyer and Luai M. Al-Hadhrami [36] presented a paper to design a wind-PV-diesel hybrid power system with a competitive cost for a village in Saudi Arabia. Note that, this village is currently powered by 8 diesel generators with 1.12MW each. HOMER helps finds the optimal configuration, which reduces the number of diesel generators into five units as shown in Fig. 2.2.

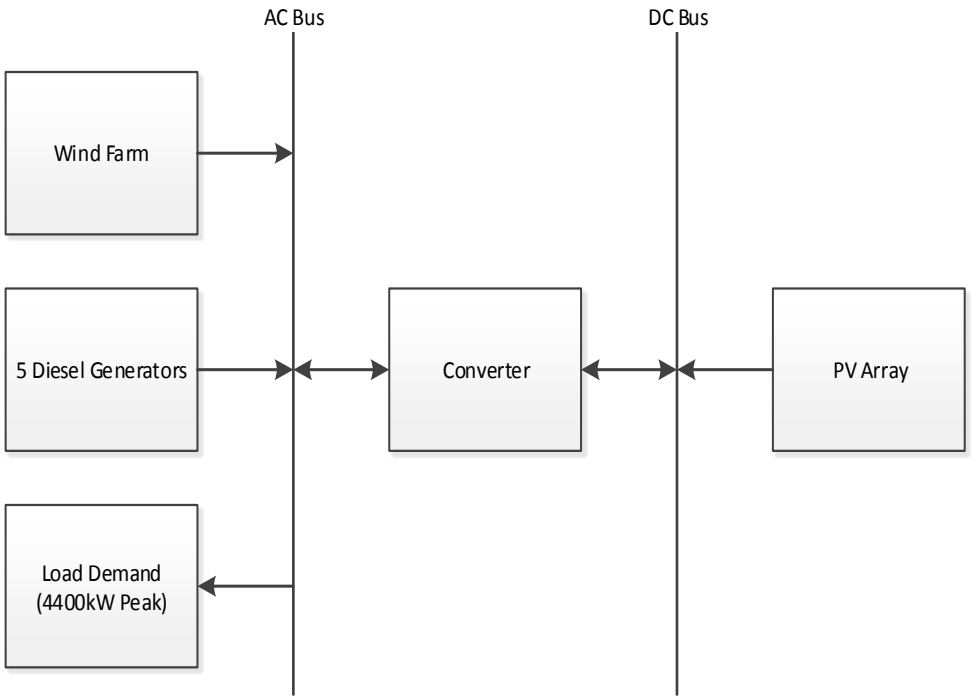

Fig. 2.2 A hybrid wind-PV-Diesel system [36]

The main input data include the hourly mean wind speed, hourly solar radiation, load data, technical specifications and the cost of each component in the system shown in Fig. 2.2. First of all, the load profile, which is expected to be satisfied by the designed system, is inserted as diurnal variation during all months of the year. The peak value of

the load recorded was 4.4 MW. Second input is the cost for each component, which is shown in the Table 2.5.

Table 2.5 Cost for each component in Fig. 2.2 [36]

Info. / Component	Life Time	Scenarios	CC	OMC	RC
Wind Turbine	20 years	4 scenarios (MW): 0, 0.6, 0.6*2, 0.6*3	1,000,000$	12,000$	800,000$
PV	20 years	2 scenarios (MW): 0, 1	3500$/kW	25$/kW/year	3500$/kW
Diesel Generator	20,000 hours	5 Generators, each (MW): 0, 1.12	1521$	0.012$/hour	1521$
Converter	15 years	2 scenarios (MW): 0, 0.5	900$	0	900$

Thirdly, weather conditions which are represented by the wind speed and solar radiation. The annual average wind speed is 5.85m/sec. The annual average global solar radiation is 5.75 kWh/m^2/day. Based on these inputs, a total of 276,480 runs were made. HOMER suggested an optimal wind-PV-diesel hybrid power system for the village with three WTs each of 0.6 MW (26% wind penetration), 1MW PV array (9% solar penetration); 5 diesel generators with rated power of 1.12MW each, and 0.5 MW power converter. The suggested optimal hybrid power system has a LCOE of 0.212 $/kWh. The proposed wind-PV-diesel hybrid power system with 35% renewable energy penetration could avoid addition of around 5000 ton of GHG. Whereas, the diesel only power system

was found to be the uneconomical power systems (LCOE is 0.232 $/kWh) even at a diesel price of 0.2 $/L. The LCOE for diesel only system at same diesel price was 9.4% more than the hybrid wind-PV-diesel system [36].

Tao Ma, Hongxing Yang, Lin LuKing [37] performed a paper based on a research project for a small remote island in Hong Kong. The paper focuses on investigating the feasibility of utilizing solar and wind energies to meet the electricity requirements for this remote island with using battery storage. HOMER software is employed to do the simulations and perform the techno-economic evaluation. The authors studied the effects of sizing (PV and wind) on the system's reliability and economic performance. Afterwards, they did a sensitivity analysis on the load and renewable energy resources to evaluate the robustness and the viability of the proposed hybrid system. Most remote areas suffer from energy shortage, brownout or even blackout. Fortunately, remote areas are usually rich of renewable energy resources such as wind and solar. Fig. 2.3 shows the system suggested system configuration and energy flow [37].

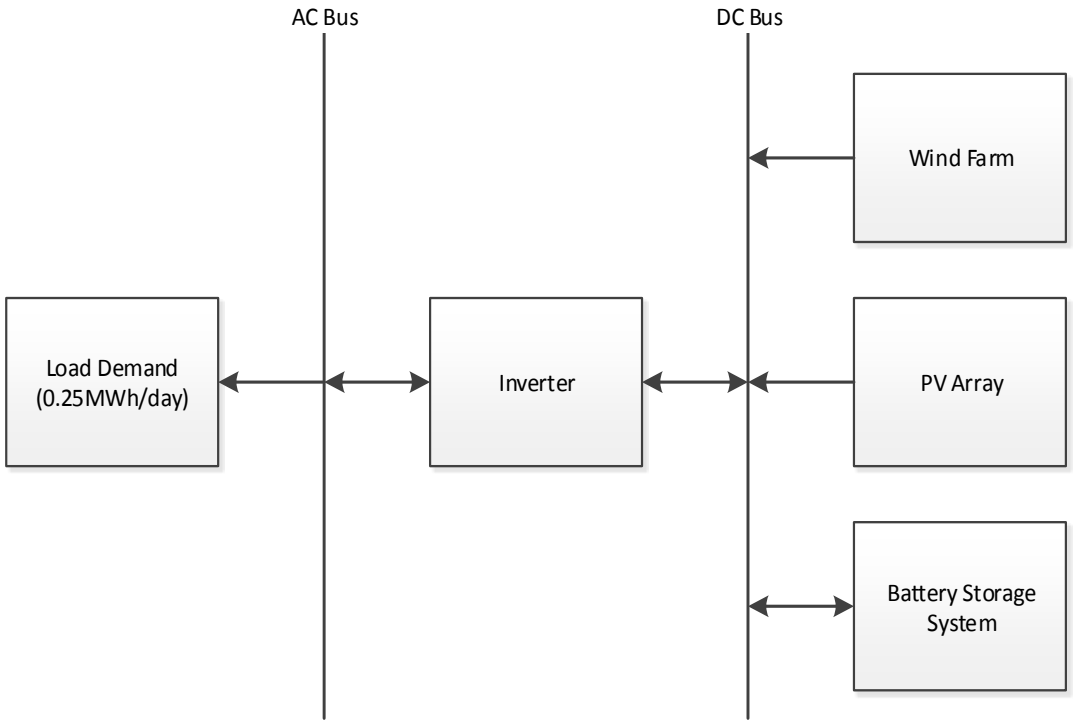

Fig. 2.3 Hybrid wind-PV-battery standalone system [37]

The system mainly consists of PV array, WTs, battery bank, and an inverter. The authors used a DC WT in order to have not concern about the frequency, and to gain maximum power output. The DC output power from the PV array and WT are converted into AC by the inverter to supply the load, while available excess energy is fed into the battery bank. When it is fully charged, the surplus energy is dumped. Note that, it is better not to include a dump load that cost a lot of money, since the PV or wind circuit could be opened out using a switch once the battery is fully charged. In this case, the economic goal of the study will be enhanced. The battery bank releases power to the load when the renewable energy output is unavailable or is insufficient to supply the load. Another way to describe the system is a flowchart shown in Fig. 2.4 [37].

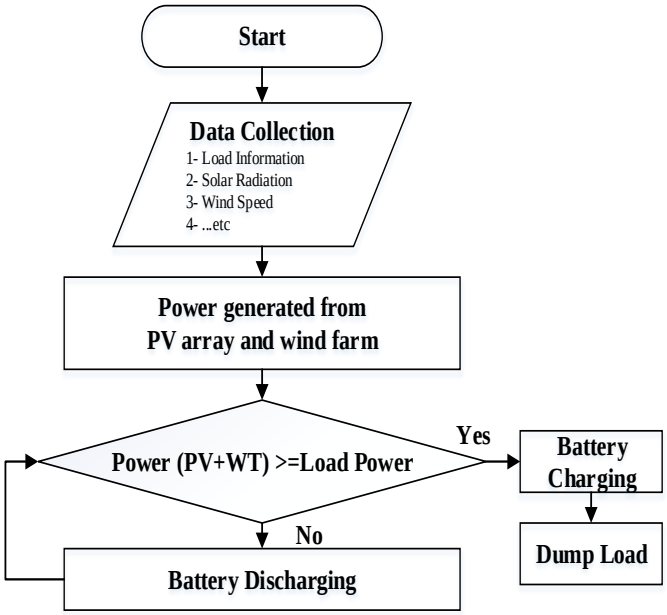

Fig. 2.4 A flowchart to describe the system in Fig. 2.3 [37]

The manufacturer gave information including the cost for each component, which is shown in Table 2.6.

Table 2.6 Cost for each component in Fig. 2.3 [37]

	WT	PV	Battery
Type	Proven 11 (known as kW6)	Suntech	Hoppecke
Life Time	20 years	25 years	10,196 kW h
Info.	Rated Power: 5.2kW Hub height: 15m	Rated Power: 210W Efficiency: 14.3%	Nominal capacity: 3000 Ah Nominal voltage: 2 V
CC	$27,658	2$/Wp	$1644/unit
OMC	$500/year	Assumed zero	$ 10/year
RC	$27,658	2$/Wp	/

The battery (in Table 2.6) has a roundtrip efficiency of 86%. It indicates the quantity of electricity which can be recovered as a percentage of the electricity used to charge and discharge the device. The main inputs to the program are the daily base load on this island was estimated at 250 kWh/day. The solar radiation and wind speed data are collected for this island in Hong Kong. As a matter of fact, the summer provides a good solar energy resource but poor wind, while the winter has a crosscurrent. In other words, it is the complement nature. The energy output of the PV generator (kWh) was calculated based equation 2.1, where: $Radiation_{STC}$ =1kW/m^2 and f_{PV}=80% [37].

$$E_{out_{PV}}(kWh) = f_{PV} \times Prated_{PV}(kW) \times \frac{G_I\ (kWh/m^2)}{Radiation_{STC}(kW/m^2)} \quad (2.1)$$

In the final analysis, this study showed that the island's existing diesel generator could be fully replaced by a 100% hybrid wind PV system. The optimal system includes 691 units PV module units (145 kW), 2 WT units (10.4kW), 144 battery bank units (706 kWh) and 6 converter units (30 kW). The results shows that 84% of the load was covered by the PV energy and 16% by wind energy. The levelized cost of energy (COE) is $0.595/kWh, which is a practical and cost effective compared with diesel generator for this remote island. Another important issue investigated by the author is the sensitivity analysis for various aspects. First, the effect of changing the battery number and PV capacity on the total NPC. Results shows that there is an inverse relationship between the PV capacity and the # of batteries. Second, another factor was to study the effect of changing the number of wind turbines. As the number of WTs increases, the battery bank and PV capacities can be reduced but the NPC will also be increased [37].

Ahmed Helal, Rasha El-Mohr, and Hussien Eldosouki [38] presented a paper to build an off-grid hybrid system in Egypt. This paper describes design, simulation and feasibility study of a PV-wind-battery and diesel hybrid system for electrification of a remote village in Egypt. HOMER is used for simulation of the proposed system and for components sizing optimization. In renewable energy analysis, it is required to minimize NPC or COE in order to have an economic and efficient system. The NPC is mathematically calculated using TAC, and the capital recovery factor (CRF). CRF is used to determine the current price value using the future price value and the real interest rate. In this case, a decision could be performed today. Also, this value is related to the price depreciation and the time value of the money. Fig. 2.5 below shows the configuration of the suggested hybrid system in this paper.

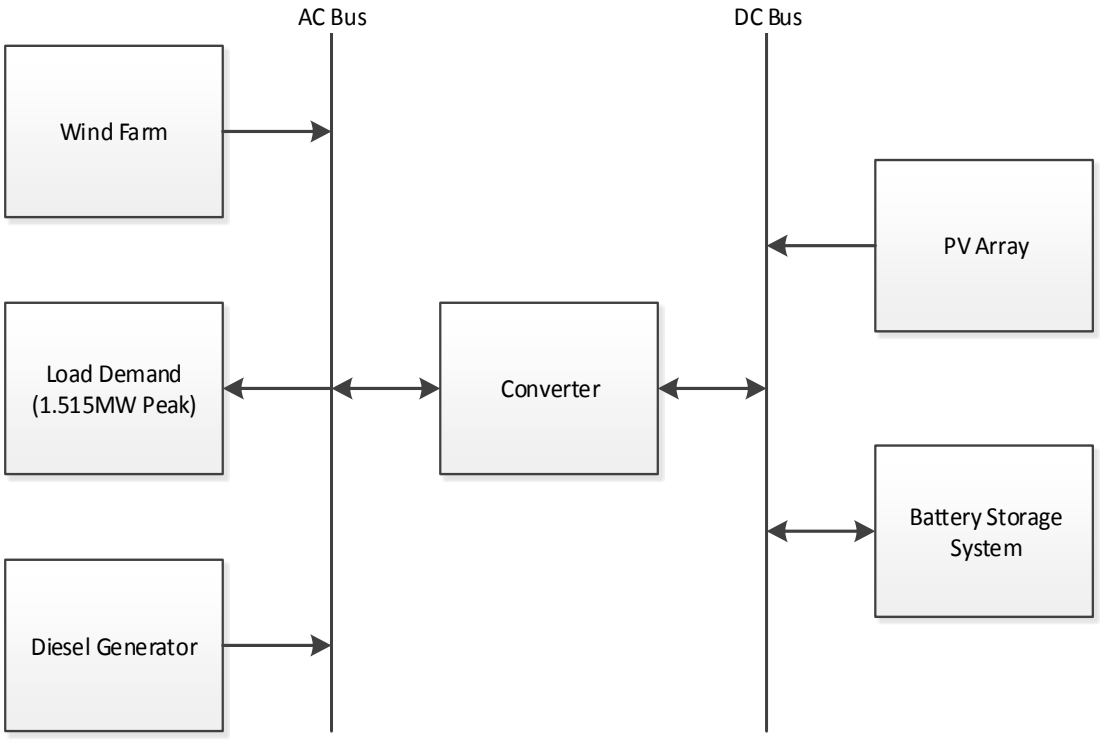

Fig. 2.5 A hybrid wind-PV-diesel-battery system [38]

The load demand for this remote village is 1.515MW peak. The annual average solar radiation is equal to 5.37kWh/m^2/day. The monthly average wind speed ranges between 4.4 m/sec and 5.6 m/sec. To find the optimal system and make sensitivity analysis, the authors assumed 8 PV cases, 11 Wind cases, 7 diesel generator cases, 11 battery cases and 11 inverter cases. In sum, 74,536 combinations are simulated in HOMER. Then, for each component, CC, OMC and RC are inserted. In this paper three configuration were investigated: diesel generators only, PV/diesel, and PV/WT/diesel generators. HOMER shows the hybrid PV/WT/diesel system is the optimal configuration, which has the minimum TNPC. The LCOE is 0.17$/kWh, and NPC is 14,518,144$. The shares of PV, wind and diesel generator are 79%, 7% and 14% respectively [38].

Makbul A.M. Ramli, Ayong Hiendro, Khaled Sedraoui and Ssennoga Twaha [15] used HOMER to analyze the optimal PV and inverter sizes for a grid-connected PV system in Makkah, Saudi Arabia. Most power is generated in Saudi Arabia, an oil-exporting country, using diesel with a cost of around 10 cents/liter, which may be cheaper than PV systems. Note that, the use of PV energy in this case could be justified by increasing oil exports, since there will be a reduction in oil consumption. Also, it will reduce the CO_2 emissions which is mainly the reason of the GHG. In some cases, on-grid PV systems do not usually have battery storage. The difference between price of buying electricity from the grid and that of selling to the grid is important in sizing the grid-connected PV system. The load of Makka is found to be 2.2 GW peak which is around the Jordanian average load demand. In HOMER the solar resource could be described by the solar radiation data or by the clearness index (which is the ratio of the global radiation striking the earth

surface divided by the extraterrestrial radiation hitting the surface of the atmosphere. It has a value of around 0.8 in the clearest conditions to near zero in overcast conditions [39]). The solar radiation in Makka has an average of 5.94 kWh/m^2/day.

The buying prices for renewable energy during off-peak hours, shoulder hours and peak hours are assumed to be 1.6 cents/kWh, 2.7 cents/kWh and 4 cents/kWh respectively. Also, in this paper the battery backup is excluded for economic reasons. Note that, this will reduce the cost of the whole system by 40% to 50% depending on the battery type used. The PV and inverter cost data is provided in Table 2.7. In large scale applications, central inverters are commonly used that offer easy installation and high efficiency [40].

Table 2.7 Cost for each component for the proposed system in Makka

Info. / Component	Life Time	Info.	CC	OMC	RC
Inverter	10 years	Efficiency: 90%	$ 27,658	$500/year	$ 27,658
PV	20 years	De-rating Factor: 90%	2.5$/W	$10/year	2$/W

Simulation results in this paper shows that the excess electricity, as a function of the PV size, starts to appear after satisfying the load of 2.2 GW. On the other hand, there is a linear relationship for the NPC with the PV size, but after the load is met, there will be an exponential behavior. Moreover, there is an inverse relationship between the PV production and the grid supply when plotting both of them versus the PV size.

Furthermore, there is an inverse relationship between the inverter size and the excess electricity. Note that, there is no excess electricity once the size is 2.2GW. Regarding the environmental benefit, results show as the PV size increases the CO_2 emissions decreases. A grid emission factor (GEF) as an environmental indicator is found by measuring the CO_2 emissions per plant in the grid system [41]. In this case, for a GF of 0.99kg/kWh, the AEI 8,066,000 tonnes/year for the PV size of 2.2 GW. On the other hand, as the inverter size increases, the CO_2 emissions decreases till be vanished at 2.2GW. This is because increasing the inverter size beyond the PV size of 2.2GW has no effect on the power from PV or from the utility grid [15]. In sum, the authors considered two configurations to do the economic analysis. First, an equal size of 2.2GW (which is equal to the peal load) for both PV and inverter. Second, a PV size of 2.2 GW and an inverter size of 1.5GW. Results show that the equal size configuration has a PV penetration of 33% to the total electricity production. This configuration has zero unmet load and no excess electricity. Moreover, the CO_2 emissions are lower than the 2^{nd} configuration. As a result, the equal size configuration is better to be applied to the grid-connected PV system in Makkah.

S. Rehman, I.M. El-Amin, F. Ahmad, S.M. Shaahid, A.M. Al-Shehri, J.M. Bakhashwain, A. Shash Makbul, A.M. Ramli, Ayong Hiendro, Khaled Sedraoui and Ssennoga Twaha [42] presented a paper to study the feasibility for a wind energy retrofitting on an existing off-grid diesel generator that supplies a load for village in Saudi Arabia as shown in Fig. 2.6.

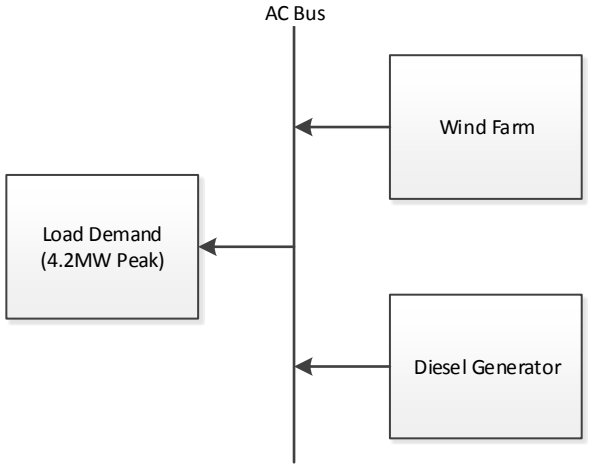

Fig. 2.6 Standalone hybrid wind-diesel system

HOMER shows that the diesel Hybrid system becomes more feasible in Saudi Arabia when the wind speed is 6m/sec or more and the fuel price is 10 cents/L or more. The peak load of this village is 4.231 MW. Currently, there are 6 diesel generating units (1.12MW each) in order to supply the load. Note that, most of the people moved to nearby cities. So, right now 3 or 4 diesel units are enough to satisfy a load of 4.2MW peak. The author assumed that we have 3 diesel generating units plus WTs with the information shown in Table 2.8 [42].

Table 2.8 Cost for each component in the wind-diesel hybrid system in Fig 2.6 [42]

	Type	Info.	CC	OMC	RC
Diesel Generator	Cummins	*Rated Power:* 1.12 MW	180,000$	3.01 $/hour	$ 120,000
Wind Turbine	DeWind	$P_{r_{WT}}$=0.6 MW H_{WT}=60m D_R=48m	575,000$	13,000$/year	400,000$

Table 2.9 Sensitivity parameters to get optimization results [42]

Wind Speed	4.95 m/sec
Maximum annual capacity shortage (MACS)	0%
Minimum Wind Energy Penetration (MWEP)	0%
Fuel Price	10 cents/L

Note that, the fuel cost obtained locally, including the transportation cost, was 0.102 $/L. The authors got optimization results for a sensitivity parameters shown in the Table 2.9. HOMER showed that the most feasible configuration is the 3 diesel generators. The TNPC and the LCOE are 11 million$ and 4.4 cents/kWh. Note that, this is simply due to the very low cost of fuel in Saudi Arabia. However, at 7m/sec the hybrid system with 7 WTs and 3 diesel generators was found to be the most feasible. In this case a 51% of wind penetration was achieved with a LCOE of 4.1 cents/kWh and TNPC of 10,158,187$. The HOMER software simulates all system configurations in a search space for each sensitivity variable shown in Table 2.10 [42].

Table 2.10 Sensitivity variables tested for the system in Fig 2.6 [42]

sensitivity variable	Cases	Number of cases
Wind Speed	(4, 4.95, 6, 7 and 8)m/s	5
Diesel Price	(0.025, 0.05, 0.075, 0.1, 0.125 and 0.15) $/L	6
wind energy operating reserve	(0, 10, 20 and 30%)	4
Maximum annual capacity shortage	(0, 3, 5, 7 and 10%)	5
minimum renewable energy fraction	(0, 5, 10, 15, 20 and 25%)	6
Total Number of Cases		3600

The sensitivity results are performed in two cases terms of wind speed and diesel price. First, for a maximum annual capacity shortage (MACS) of 0%, results show for a wind speed of 5 m/sec and less, the most feasible is the diesel only configuration. But, for a wind speed of 6 m/sec and more, and a fuel price of 10 cents/L and more the hybrid wind diesel will be the feasible one. The LCOE for this system is 4.41 cents/kWh. Second, for a MACS of 3%, results show for a wind speed of 5 m/sec and less, the most feasible is the diesel only configuration. Regarding the hybrid wind diesel system, it is feasible when the wind speed is more than 6m/sec, and fuel price is greater than 10 cents/L. In conclusions, this paper investigates the feasibility of penetrating a standalone diesel system with WTs. The optimal system is determined using a sensitivity analysis which finds the optimal system type which varies based on the wind speed and fuel price [42].

In [43], the authors sized an energy storage system (ESS) by maximizing the cost or benefit for the DG owners and the utility taking into account the amount of the curtailed wind energy that is equal to the increase of WT production beyond a specific limit in order not to violate system constraints. However, they linearly modeled the WT without considering the effect of other parameters such as the air density, which can affect the wind EEPY, and hence the size of EES will be influenced, and may be different than what the authors obtained in this paper.

In [44], we performed a feasibility investigation and a sensitivity analysis on a hybrid wind-PV on-grid system. We used a built-in WT model without considering other

parameters such as the weather conditions, which can affect the sizing results we got, and thus influencing the economic outcomes obtained.

In [45], the authors proposed a data driven methodology to virtually model the WT. They selected the output WT power and rotor speed parameters for modeling.

In [46], the authors model the output power from a WT by solving a multi-objective optimization problem using a Neural Network as one of the artificial intelligence techniques which can mitigate any error in the wind speed that results in a big error in the output WT power due to the cubic relationship.

In [20], the authors performed an economic study on a standalone hybrid wind/PV/diesel system. They started by clustering the states of the load demand, wind generators and PV panels. Then, the number of states will be much smaller than 8760 of the chronological data, which therefore reduces greatly the computational time. Then, those state numbers will be used in the Markov model to establish models for load, wind and PV. Then, those Markov models will be embedded into the GA to have the optimal size for each component in the system. The authors shows that total cost, fuel cost, loss of load probability, CO_2 and computational time are smaller than results obtained on a chronological based solution.

In [47], the authors use the hourly data for the whole year for a house in Okinawa, Japan. Then, they used GA to minimize the objective function of the total cost which includes initial cost as well as OMC costs. The authors did kind of approximations which will affect the system component sizing. For instance, in the WT modeling, they assumed a linear behavior between the cut-in and the rated wind speeds, which is simple but not

practically precise. However, the optimal configuration of renewable generating systems was obtained where total cost is more reasonable using GA.

In [48], the authors performed an optimization process on a stand-alone hybrid wind-solar system with a backup battery banks. The objective functions were the total annualized cost (TAC) as well as the loss of power supply probability (LPSP). The decision variables are the number of PV panels, the number of WTs, the number of batteries, slope angle of the PV panel and the WT installation height. The objective is to find the best compromise between TAC and LPSP. The results shows as the LPSP decreases the TAC increases. For a 1% desired LPSP the TAC of the hybrid wind-PV system is 10,600$ which is less than 11,145$ for the PV only and 16,889$ for the wind only configuration.

In [49], the authors optimizes an off-grid hybrid wind-photovoltaic with the aid of the GA. The decision variables are the optimal number as well as the type of the units for both wind and PV. GA attains the global optimum configuration for a system supplies a household. The cost of the hybrid system is less than the cost for the PV only and the wind only configurations

Most of the literature studies, to solve hybrid systems renewable energy problems, have some drawbacks. First, they did not precisely model system components, which will have a big difference in the annual energy extracted from a single unit as well as the whole system sizing. Second, some papers suggest changing linearly the decision variables to have suboptimal solution, but this will take long time and effort and may result in falling in one of the local minima solutions.

3. SINGLE POINT GRID CONNECTION INVESTIGATION USING MODIFIED HOMER*

At the outset, it is worthy to mention here that a conference paper [44] as well as an IEEE transaction paper [50] have been published out of our work in this section

For simplicity in this dissertation, this section investigates a single point connection to the utility grid of Jordan. This is considered as an excellent step to understand all the aspects behind the multi-point grid connection problem whose solutions are the ultimate goal out from this dissertation.

In a review paper in [14], it has been mentioned lots of software tools to solve a single point connection problem, such as HOMER and iHOGA. HOMER was found to be the most usable compared with others [14]. HOMER is used in this section to investigate the feasibility for only one city in Jordan called Ibrahimyya.

HOMER stands for Hybrid Optimization Model for Electric Renewables. In other resources, it has been mentioned that HOMER stands for Hybrid Optimization Multiple Energy Resources. It was created by the US National Renewable Energy Laboratory (NREL) in 1993 [51, 52]. It can be used for grid-tied PV systems and complicated off-grid systems and other types of generators [53]. So, HOMER can be used for one or more energy resources. This tool can analyze either on-grid or off-grid. These resources could be renewables such as wind and PV or conventional resource. Selection of energy resources depends on the potential of natural or fossil fuel resources. Some locations have

* Part of this section is reprinted with permission from H. M. Al-Masri and M. Ehsani, "Feasibility Investigation of a Hybrid On-Grid Wind Photovoltaic Retrofitting System," IEEE Transactions on Industry Applications, May-June, 2016, © 2016 IEEE and H. Al-Masri and M. Ehsani, "Feasibility Investigation of A Hybrid On-Grid Wind Photovoltaic Retrofitting System," IEEE Industry Applications Society Annual Meeting, October, 2015, © 2015 IEEE.

only high potential of solar radiation, so it is recommended to have only PV arrays. While some places have high potential of many natural or fossil fuel resources which recommends to have hybrid system of a mix of these resources. HOMER allows the user to input an hourly power consumption profile and match renewable energy generation to the required load. This is allows a user to analyze micro-grid potential, peak renewables penetration, ratio of renewable sources to total energy [51]. Additionally, HOMER's sensitivity analysis algorithms allow the user to evaluate the economic and technical feasibility of a large number of technology options and to account for uncertainty in technology costs, energy resource availability, and other variables [51].

3.1 Single point connection data set (SPCDS)

The site of the hybrid wind-PV system to investigate the single point grid connection is considered based on environmental aspects of the SPCDS in Jordan. The monthly averages wind speed data for the SPCDS in Jordan (wind speed & solar radiation) are obtained from the Energy Center (EC) which is located in the Jordanian Royal Scientific Society (JRSS). Note that, those values are taken at 50 m height. Fig. 3.1 shows the annual average wind speed in m/sec for the SPCDS in Jordan.

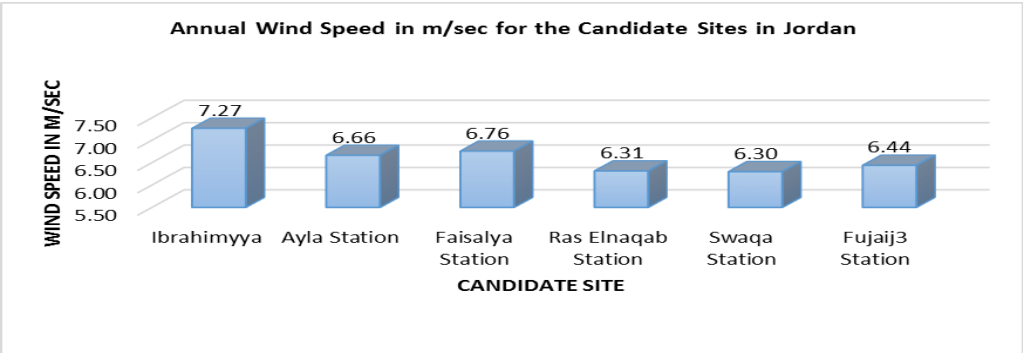

Fig. 3.1 Annual wind speed for the SPCDS in Jordan

The main input for PV energy is the solar radiation. The EC provides the monthly average solar insolation data for the SPCDS in Jordan from the Photovoltaic Geographical Information System (PVGIS), See Fig. 3.2.

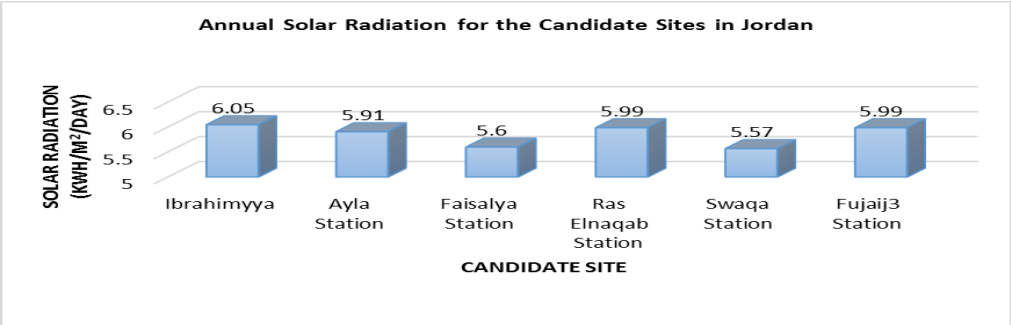

Fig. 3.2. Annual solar radiation for the SPCDS in Jordan

Both Fig. 3.1 and Fig. 3.2 show that Ibrahimyya site (32.43645° N 35.82970° E), as an interesting case in the SPCDS in Jordan, has highest annual average wind speed of 7.27 m/sec, and highest annual average solar radiation of 6.05 kWh/m^2/day. Thereby, it is interesting to apply a hybrid wind-PV system at Ibrahimyya city.

3.1.1 Analysis of city data

Ibrahimyya load profile is obtained from the National Control Center (NCC) of the National Electric Power Company (NEPCO) which is responsible for transmission of electrical power in Jordan. Note that, the load data is gained using the supervisory control and data Acquisition (SCADA) system every 60 minutes a day for the whole year of 2014. Note that, the load data are gained as electrical current measured values at 33kV bus voltage and a power factor of 88%. Afterwards, the data are converted to electrical power values using Equation 3.1.

$$P = \sqrt{3}\, VI\, cos\theta \qquad (3.1)$$

On the other hand, HOMER program requires two types of data set each with 288 entries, which are load of weekdays and load of weekends. Note that, in Jordan and most of the Arab countries the situation is different. The workweek starts from Sunday through Thursday, and the weekend days are Fridays and Saturdays. Now, using Microsoft Excel, an averaging is performed for Ibrahimyya load of weekdays and weekends. Afterwards, HOMER summarizes Ibrahimyya load data in Table 3.1.

Table 3.1 Ibrahimyya load profile summary

Average (MWh/day)	150.27
Average (MW)	6.26
Peak (MW)	10.85
Load Factor (%)	58

Fig. 3.3 shows the monthly average wind speed values in m/sec for Ibrahimyya. Note that, the rated wind speed is a good parameter for selecting the WT. This is because if the generator rated speed is chosen to be low, the site loses too much of the energy in the higher wind speed intervals. If the generator rated speed is too high, the turbine will seldom operate at low capacity and the capital cost will be high [54].

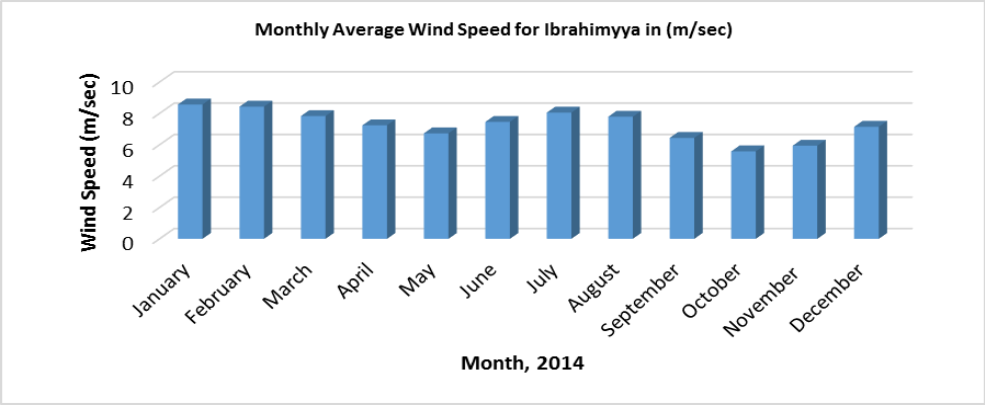

Fig. 3.3 Monthly average wind speed values for Ibrahimyya

3.1.2 Selection of WT & PV module

A Histogram curve for the wind speed time series data has been built (See Fig. 3.4) to express the probability distribution frequency (PDF), which provides the percentage frequency for the wind speed range from zero to the cut-out value.

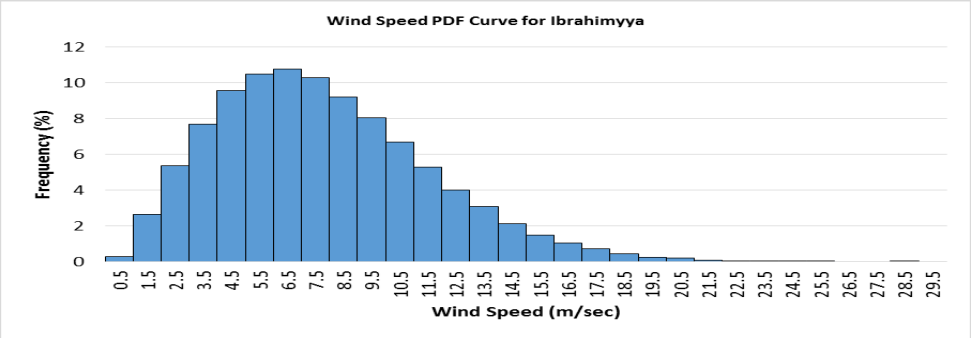

Fig. 3.4 Histogram PDF curve for the wind speed time series data

Now, the PDF curve is used to build the Energy Curve of Wind Speeds (ECWS). Afterwards, the PDF and ECWS will be used to find the power available in wind in Ibrahimyya city. Thereby, the cubic value is taken for all wind speeds in the PDF curve and multiply it by the corresponding time value to get the ECWS curve. Fig. 3.5 shows both PDF as well as ECWS curves.

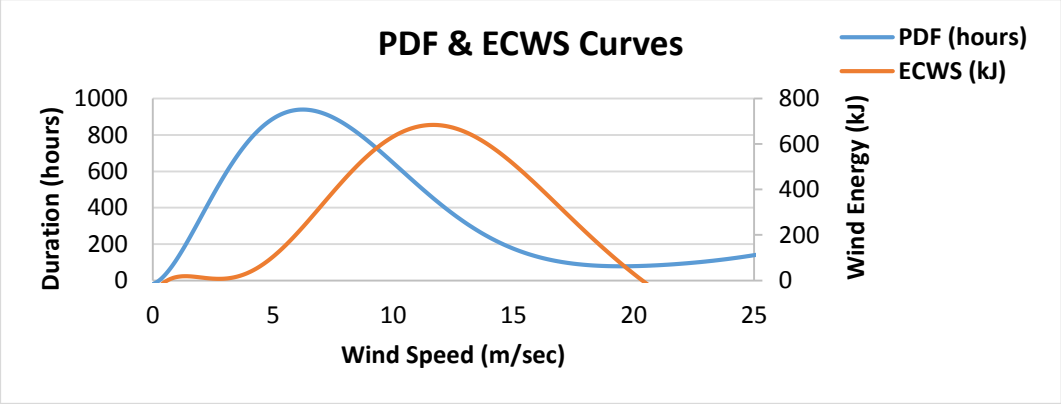

Fig. 3.5 PDF & ECWS curves

After that, the power in the wind is found using a Matlab curve fitting after dividing the ECWS to the PDF functions to get the function in Equation 3.2.

$$P_{in\,wind} = 1.127\sin(0.08229v + 1.569) + 1.225\sin(0.281v + 3.552) + 0.3322sin(0.5957v + 4.54) \quad (3.2)$$

In order to find the shaft power from WT, the power in wind in Equation 3.2 should be multiplied by the power coefficient (*Cp*), which is defined as the ratio of the shaft power produced by WT to the total power available in the wind. So, the best coefficient to take is the Betz limit. Albert Betz was a German physicist who calculated that no WT could convert more than 59.3% of the kinetic energy of the wind into mechanical energy turning a rotor [55]. At this point, the power available in the wind is multiplied by the Betz limit (59%) in order to find the proportion max shaft power in Watt/m^2 produced by WT. Fig. 3.6 shows the proportion of maximum power at Betz limit. The peak value of SPDC-Betz corresponds to 14.9 m/sec.

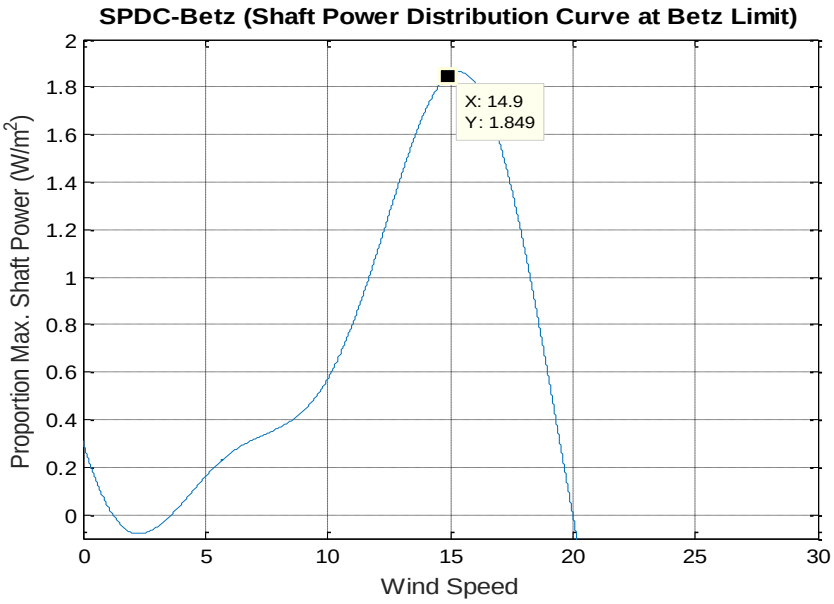

Fig. 3.6 SPDC-Betz (shaft power distribution curve at Betz limit)

A (GE1.5sle-77) WT has been selected, since it has a rated wind speed around this value. Note that HOMER has a list of WTs, but this strategy recommends only this WT according to its value of rated wind speed. The specifications of this WT are shown in Table 3.2. MATLAB program is used to represent GE1.5sle-77 WT characteristics referring to the system of equations (1.12) for WT output power. Fig. 3.7 shows the output power characteristics of the GE1.5sle-77 WT.

Table 3.2 Specifications of GE1.5sle-77 WT

Parameter	Value
Model	GE1.5sle-77
Rated output	1.5 MW
Rated wind speed	14 m/s
Rotor diameter	77 m
Cut-in wind speed	3.5 m/s
Cut-out wind speed	25 m/s
Hub height	77 m

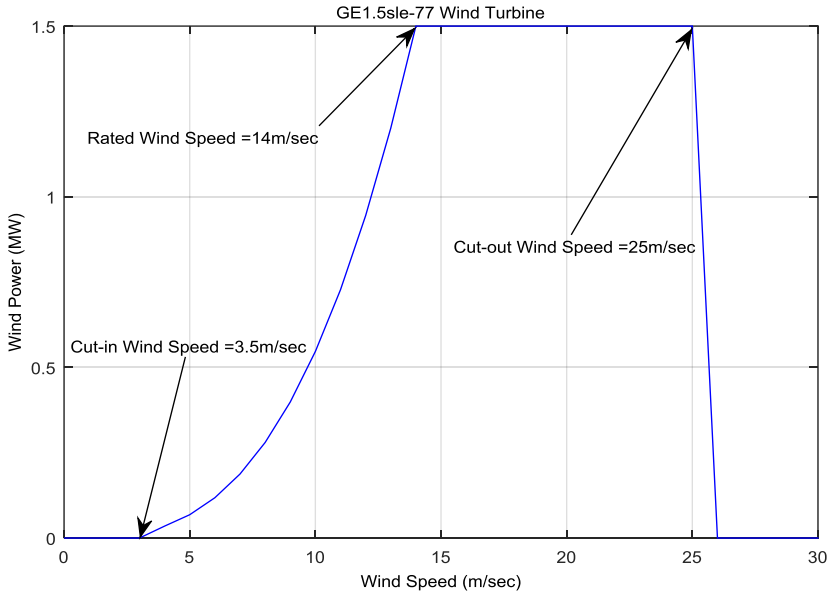

Fig. 3.7 Output power characteristics of the GE1.5sle-77 wind turbine

Most PV modules behave similarly, since there is a common standard, a 1 kW modules from one manufacturer will, for example, output the same power as a 1 kW modules from another manufacturer under the same irradiance. The size, shape, and specific technologies may differ, but these things may not matter for the PV model. Note that, HOMER recommends Polycrystalline PV Panels. Because they have an acceptable efficiency (13%-17%) and affordable cost [56]. The specifications of the selected PV panel (See Table 1.2) are measured under STC as shown in Table 3.3.

Table 3.3 STC parameters

Parameter	Value
Irradiance	1000 W/m²
Spectrum	AM 1.5
Cell temperature	25°C

3.1.3 Estimated cost & life time for each element

The cost of the SPDCS on-grid hybrid wind-PV system includes capital cost (CC), operation & maintenance cost (OMC), and replacement cost (RC). Note that, CC is considered as the component cost plus the installation cost. Furthermore, OMC costs of the PV module has the HOMER default value, and in case of WT, OMC cost is taken as 1% of the CC. Moreover, the Jordanian grid purchase price, and the grid sell back rate price are inserted to the grid (See Table 3.4). Moreover, RC will be zero since the component life time for PV module and converter are the same as project life time. In addition, there will be a RC equal to CC in case of WT that has a life time less than the project life time.

Table 3.4 Estimated cost and life time for components of single point connection

	PV Module	WT	Converter
CC	2475 $/kW [57, 58]	2098$/kW	300
OMC	10$/year	20.98$/kW/yr	0
RC	0	2098$/kW	0
Grid Purchase Price	0.134 $/kWh		
Grid Sell Back Price	0.11143 $/kWh		
Life Time	25 years	20 years	25 years
Project Life Time	25 years		

3.1.4 Sizing of system elements

3.1.4.1 First method using Matlab

This method is applied under the assumption of satisfying Ibrahimyya load with only GE1.5sle-77 wind farm as well as CS6X-310 PV array. A Matlab model has been built to study the sensitivity on the COE over the whole range of wind or PV sharing percent. Three signals were built in Matlab Simulink: Load in kW, single WT output power (P_{SWT}) in kW and global solar radiation (GR) in kW/m^2. See Fig. 3.8, Fig. 3.9 and Fig. 3.10 respectively.

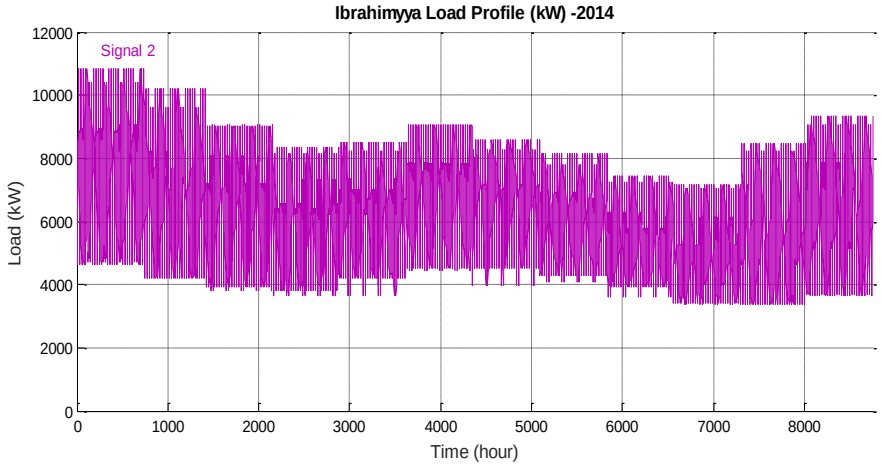

Fig. 3.8 Ibrahimyya load profile

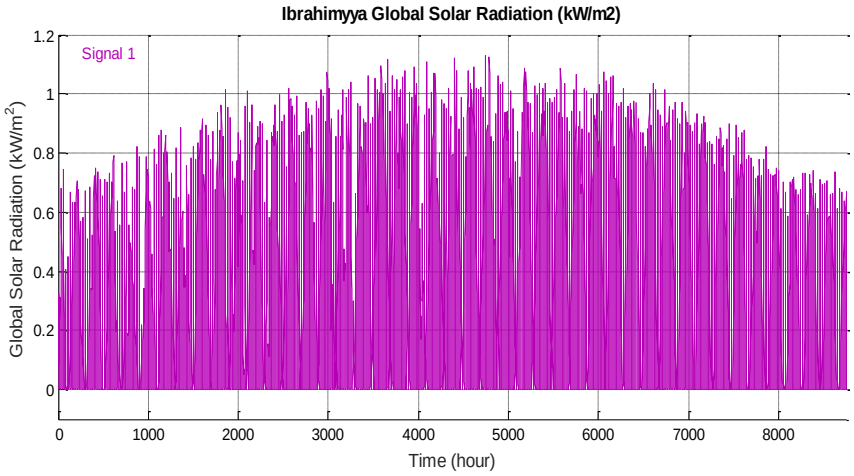

Fig. 3.9 Ibrahimyya global radiation

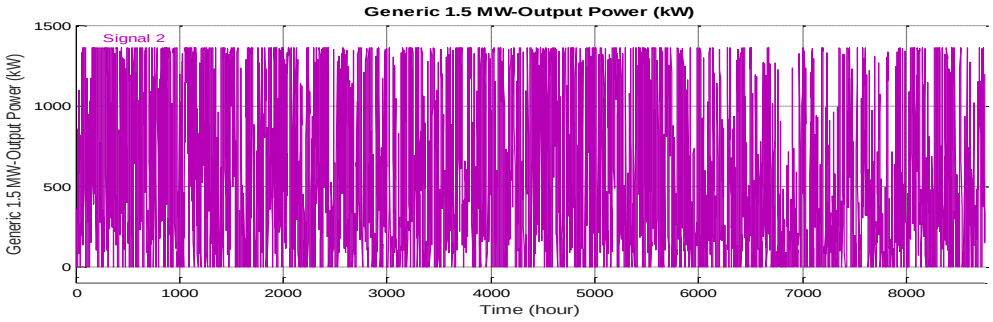

Fig. 3.10 GE1.5sle-77 output power

Equations 3.3, 3.4 and 3.5 have been implemented in Matlab Simulink to size the system elements, i.e. to find the number of WTs (N_{WT}) and the number of PV panels (N_{PV}) taking in to account both wind sharing percent (W_{SP}) and PV sharing percent (S_{SP}). Matlab sizing model has been run to calculate the sizing information for all possible sharing percent. Then, HOMER calculates the COE as shown in Table 3.5.

$$Load\ Energy\ (LE) = \int_{1h}^{8760h} Load\ \ dt \tag{3.3}$$

$$N_{WT} = \frac{LE \times W_{SP}}{\int P_{SWT}} \tag{3.4}$$

$$N_{PV} = \frac{LE \times S_{SP}}{\int GR \times \eta \times A_{VP}} \tag{3.5}$$

Table 3.5 Sizing results for the 1st method

S_{SP}	W_{SP}	N_{PV}	PV array Size (kW)	N_{WT}	COE ($/kWh)
0	1	0	0	11.02	0.083
0.1	0.9	8028.04	2488.692	9.92	0.082
0.2	0.8	16056.08	4977.385	8.82	0.082
0.3	0.7	24084.12	7466.077	7.72	0.082
0.4	0.6	32112.16	9954.77	6.61	0.086
0.5	0.5	40140.2	12443.46	5.51	0.091
0.6	0.4	48168.24	14932.15	4.41	0.099
0.7	0.3	56196.28	17420.85	3.31	0.107
0.8	0.2	64224.33	19909.54	2.20	0.115
0.9	0.1	72252.37	22398.23	1.10	0.124
1	0	80280.41	24886.93	0	0.133

Where: (N_{WT}) is the number of WTs, (N_{PV}) is the number of PV panels, (W_{SP}) is the wind sharing percent, (S_{SP}) is the PV sharing percent, and COE is the cost of energy to the customer. This method shows as the PV sharing increases and the wind sharing decreases, the COE increases. This means that it is expected that penetrating more wind to the hybrid system will make it more feasible. This result will be proved in the HOMER sizing method that is used to find the global solution.

3.1.4.2 Second method using HOMER

HOMER is used for sizing as well as to make an economic study. Since it is a wind-PV grid connected system. It is expected that Ibrahimyya load will be satisfied by wind, PV energy and grid purchases. In order to size this system, an appropriate range has been spread out in the HOMER search space for each component. Refining the search space based on the winner. Running the simulation with no sensitivity inputs shows the optimal size system that has the lowest NPC and 64.56% renewable fraction in Table 3.6.

Table 3.6 Optimal size system main screen HOMER results

Architecture			
# of GE1500 wind turbines	PV array size (kW)	Converter Size (kW)	Grid Purchase Capacity (kW)
8	930	930	12000
Cost			
COE ($/kWh)	NPC ($)	Operating Cost ($)	Initial Capital ($)
0.0817	65,069,349	2,886,295	27,756,750

Table 3.6 shows that HOMER calculates the global sizing solution which has 8 WTs, and 3 PV panels after running a large number of iterations and arranging with respect to the minimum NPC. Table 3.7 shows the only PV panel's configuration with 23% renewable fraction. Also, Table 3.8 shows the case for only wind turbine's configuration with 60% renewable fraction.

Table 3.7 Only PV panels/grid system main screen HOMER results

Architecture			
# of GE1500 wind turbines	PV array size (kW)	Converter Size (kW)	Grid Purchase Capacity (kW)
0	4960	4650	12000
Cost			
COE ($/kWh)	NPC ($)	Operating Cost ($)	Initial Capital ($)
0.123	87,128,488	5,682,258	13,671,000

Table 3.8 Only WTs/grid system main screen HOMER results

Architecture			
# of GE1500 wind turbines	PV array size (kW)	Converter Size (kW)	Grid Purchase Capacity (kW)
8	0	0	12000
Cost			
COE ($/kWh)	NPC ($)	Operating Cost ($)	Initial Capital ($)
0.0822	65,125,284	3,090,252	25,176,000

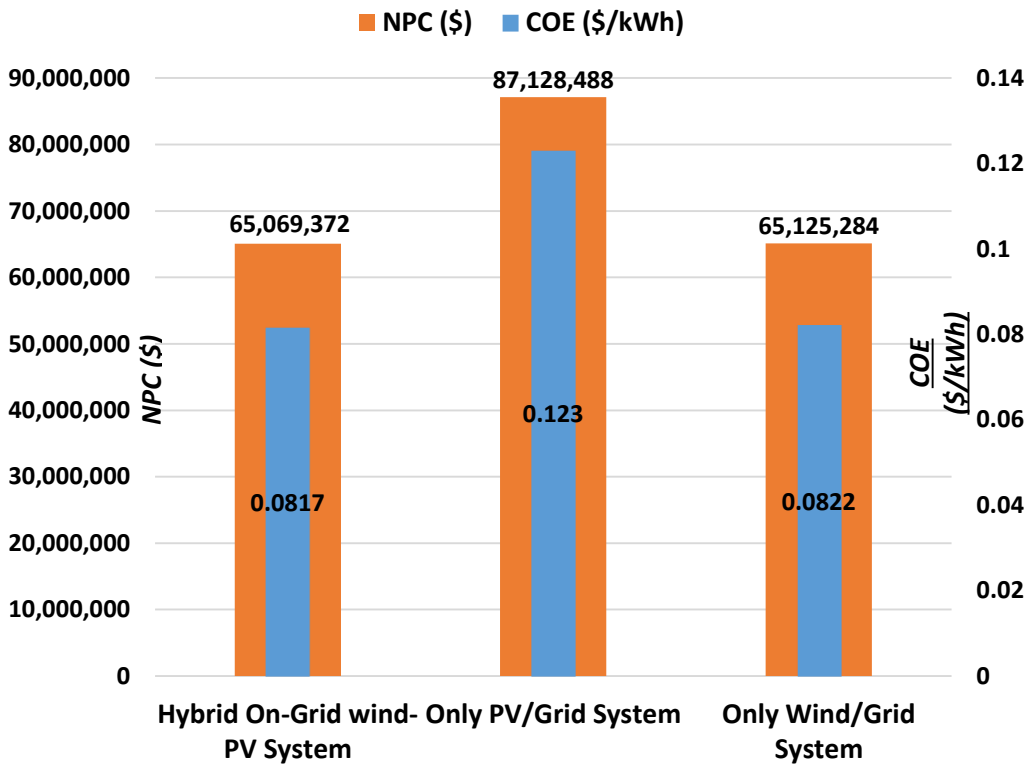

Fig. 3.11 Hybrid wind/PV system compared with other configurations

Fig. 3.11 shows that the hybrid system is more economic compared with the wind/grid and PV/grid connected configurations. This is because the hybrid wind/PV system COE is 0.608% and 33.577% less than the COE of Wind and PV systems respectively. Moreover, the hybrid wind/PV system NPC is 0.086% and 25.318% less than the NPC of Wind and PV systems respectively.

3.1.5 Detailed results of the HOMER optimal system

In this section, detailed results will be explained for the global solution shown in Table 3.6.

3.1.5.1 Discounted cash flow

Table 3.9 is obtained by referring all nominal cost values to the present (year 0) using the discount factor (DF) that proves the time value of the money as shown in

Equation 3.6. So, for real interest rate of 5.88%, the DF refers each value to the present for each year.

Table 3.9 Discounted cash flow

	PV	Wind	Grid	Converter	System
CC ($)	2,301,750	25,176,000	0	279,000	27,756,750
RC ($)	0	8,026,285	0	0	8,026,285
OMC ($)	120,226	3,254,630	30,434,782	0	33,809,640
SC ($)	0	-4,523,326	0	0	-4,523,326
Total Cost ($)	2,421,976	31,933,589	30,434,782	279,000	65,069,349

$$DF = \frac{1}{(1+i)^N} \tag{3.6}$$

The total NPC is computed after summing up all the discounted values. Capital recovery factor (CRF) of 7.73% (i=*5.88%*, N=25years, See Equation 3.7) is multiplied with the NPC (65,069,349$) to get the total annualized cost (TAC) that is an equal incurred annual payments which is used to calculate the COE (0.0817 $/kWh) by dividing TAC to the total energy served to the load.

$$CRF = \frac{i(1+i)^N}{(1+i)^N-1} \tag{3.7}$$

3.1.5.2 Production and consumption of electrical energy

Table 3.10 and Table 3.11 show the annual production and consumption of electric energy. For each time step (one hour by default) in the year, HOMER does an energy balance calculation, i.e. to compare between the amounts of demanded energy required by the load to the amounts of energy that the system can supply. After that, HOMER will calculate the energy flow from, or to each component in the system.

Table 3.10 Production elements

Component	Production(kWh/yr)	Fraction (%)
PV	2,672,088	4.09
WT	39,480,132	60.47
Grid Purchases	23,141,308	35.44
Total	65,293,528	100

Table 3.11 Consumption elements

Load	Consumption(kWh/yr)	Fraction (%)
AC primary load	54,849,616	89.1
Grid Sales	6,726,758	10.9
Total	61,576,376	100

The AC primarily load of Ibrahimyya is covered by the wind farm (WFP) of (Eight GE1.5sle-77 Wind turbines) which constitutes (60.47%) of the total production and the PV array (Three CS6X-310 PV panels) which constitutes (4.09%) of the total production. The renewable fraction is (64.56%), the remaining of (35.44 %) is the grid purchases. Moreover, the excess renewable energy generated which was higher than the demand was sold back to the grid which constitutes (10.9%) of the total energy consumption. Moreover, Fig. 3.12 shows that January has the highest share of wind power production (5.74MW), as was expected in Fig. 3.3 which shows that January has the highest monthly average wind speed of 8.57m/sec.

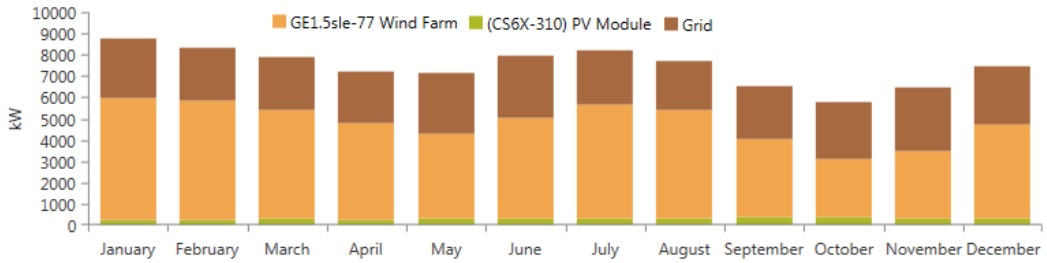

Fig. 3.12 Monthly average electrical production

3.1.5.3 Output of GE1.5sle wind farm & CS6X PV array

Table 3.12 shows the technical output values of the wind farm. It shows the rated capacity (12MW) of 8 GE1.5sle-77 wind turbines. Wind farm penetration (WP) (71.98%), and COE (0.0625$/kWh) are calculated using Equation 3.8 & 3.9.

$$WP = \frac{Mean\ Output\ (wind)}{Average\ load\ demand}\% \tag{3.8}$$

$$COE(wind) = \frac{CRF \times NPC(wind)}{WFP} \tag{3.9}$$

Table 3.12 GE1.5sle-77 wind farm output

Quantity	Value	Units
Total rated capacity	12000	kW
Mean output	4507	kW
Mean daily energy output	108164.75	kWh/d
Capacity factor	37.56	%
Total production	39480132	kWh/yr
Minimum output	0.00	kW
Maximum output	10889	kW
Wind penetration	71.98	%
Hours of operation	7136	hrs/yr
Levelized cost	0.0625	$/kWh

Where WFP is the total wind farm production shown in Table 3.12. Furthermore, Table 3.13 shows the technical output values of the PV array. It shows the rated capacity (0.93MW) of 3 CS6X-310 PV modules. The PV array penetration (4.87%), and the COE (0.07$/kWh) are calculated using Equation 3.8 &3.9 but for PV instead of wind.

Wind penetration is higher than PV penetration. This is due to the availability of wind throughout the whole day as shown in Table 3.12, that the WT produces power for the whole year as the x-axis shows in Fig. 3.13 between 0 and 10.89MW.

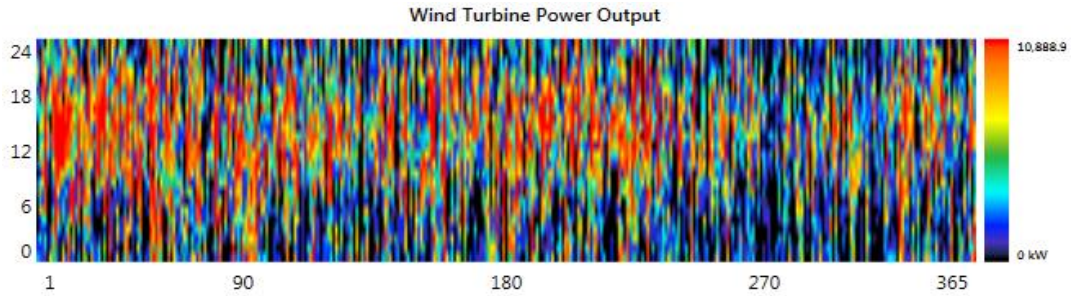

Fig. 3.13 GE1.5sle-77 wind farm output

Table 3.13 CS6X-310 PV array output

Quantity	Value	Units
Rated capacity	930	kW
Mean output	305	kW
Mean daily energy output	7320.80	kWh/d
Capacity factor	32.80	%
Total production	2672088	kWh/yr
Minimum output	0.00	kW
Maximum output	1044.98	kW
PV penetration	4.87	%
Hours of operation	4358	hrs/yr
Levelized cost	0.070	$/kWh

Whereas the sun is not available for about two-third of the whole day as shown in Fig.3.14. Table 3.13 shows that the PV array produces power for 4358 hours, and the range of PV power between zero and 1.04MW. Table 3.12 shows the hours of operation of wind farm is 7840 hour/year, which is greater than hours of operation of the PV array.

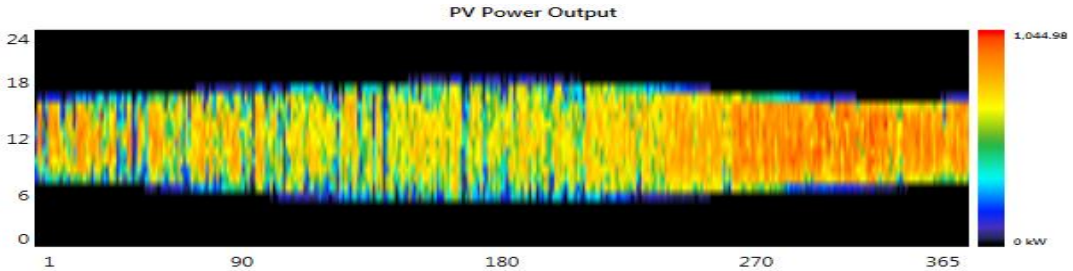

Fig. 3.14 CS6X-310 PV array output

The PV array generation may have a value greater than the rated capacity of 930kW depending on the solar irradiation. For instance, Table 3.13 shows a maximum output of 1045kW. PV panels are generally rated (capacity or kWp) for 1kW/m² solar irradiation. Certain conditions can cause irradiance conditions higher than the STC. The reason behind this phenomenon is that the power a PV module generates in real conditions can exceed the nominal power when the solar radiation exceeds 1kW/m² [59].

3.1.6 Sensitivity analysis

Most of the renewable energy projects include many parameters that are sensitive and vary with time. So, it is very important to repeat the optimization process and simulation for each sensitivity variable in order to evaluate the robustness of the feasibility study, and to know which variable has the highest impact on the results [37].

3.1.6.1 Interest and inflation rates

Changing wind speed as well as interest rate in order to see the optimal system type (OST) with lowest net present cost. Fig. 3.15 shows for a value of wind speed greater than 8.8 m/sec the OST is the wind grid connected system regardless to the value of interest rate.

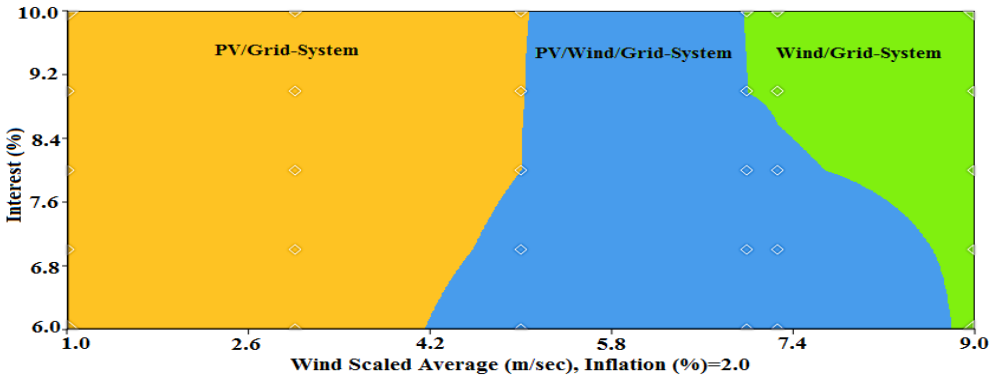

Fig. 3.15 Sensitivity of the interest rate on the OST

Also, Fig. 3.15 shows for a value of wind speed less than 4.14 m/sec the OST is the PV-grid system regardless to the value of interest rate. But, for a value of wind speed between 5 m/sec and 6.98 m/sec the OST is the HWPVG system. Moreover, Fig. 3.15 shows that as the interest rate decreases between 4.14 m/sec and 5 m/sec the OST tends to be HWPVG system. Also, it shows that as the interest rate decreases between 6.98 m/sec and 8.8 m/sec the OST tends to be HWPVG system.

As the inflation rate increases, the real interest rate decreases. So, it is expected to see an opposite behavior for the OST shown in Fig. 3.16. Similar behavior of Fig. 3.15 appears in Fig. 3.16 for cases unaffected by the inflation rate. For example, for a value of wind speed greater than 8.8 m/sec the OST is the wind grid connected system regardless to the value of inflation rate. Also, it shows for a value of wind speed less than 4.14 m/sec the OST is the PV-grid system regardless to the value of inflation rate. For a value of wind speed between 5 m/sec and 6.98 m/sec the OST is the HWPVG system. The opposite behavior appears between 4.14 m/sec and 5 m/sec in Fig. 3.16 As the inflation rate decreases the OST tends to be not HWPVG system. Also, Fig. 3.16 shows that as the inflation rate decreases between 6.98 m/sec and 8.8 m/sec the OST tends to be not HWPVG system.

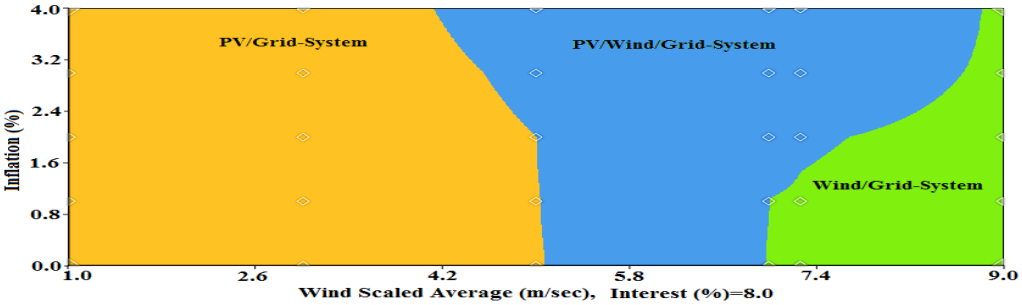

Fig. 3.16 Sensitivity of the inflation rate on the OST

3.1.6.2 Exponent of wind power law

Let's assume the wind speed S_o measured by anemometer at height H_o, then the speed at WT hub height is calculated using Equation 3.10. Empirical studies shows that 0.14 or (1/7) exponent value best fits most sites [60].

$$S = S_o \left(\frac{H}{H_o}\right)^{\alpha} \tag{3.10}$$

The sensitivity for wind power law exponent will be studied in three cases by changing the hub height (H) with respect to the anemometer height of 50 m as the data were measured. First, when the rotor of the WT is placed below the anemometer. Fig. 3.17 shows that wind farm energy output decreases, and COE increases.

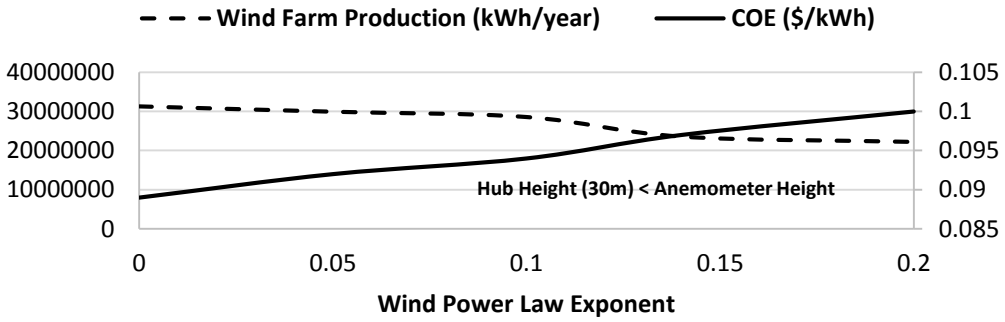

Fig. 3.17 Sensitivity of α if the rotor is below the anemometer

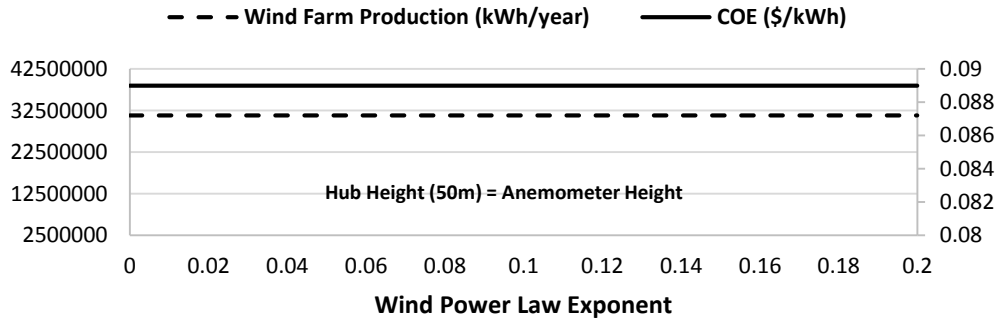

Fig. 3.18 Sensitivity of α if the rotor is at the anemometer

Second, when the rotor of the WT is placed at the anemometer. Fig. 3.18 shows that wind farm energy output and COE have constants of 31,302,498 kWh and 0.089 $/kWh. Finally, when the rotor of the WT is placed above the anemometer. Fig. 3.19 shows that wind farm energy output increases, and COE decreases.

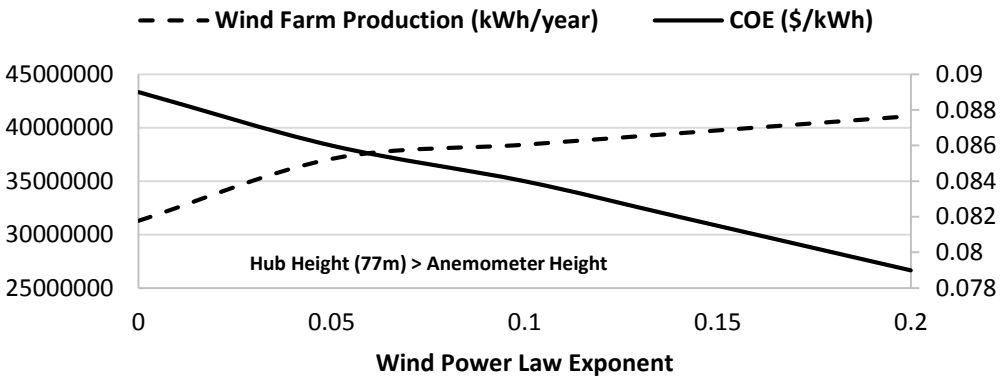

Fig. 3.19 Sensitivity of α if the rotor is above the anemometer

As a result, in the WT selection process, it is better to exclude all WTs with hub height less than or equal the anemometer height. Reviewing the hub heights, for each WT in the HOMER list, shows that GE-1.5 MW WT is the only one which has a height greater than the anemometer height. This result is the same as the outcome of turbine selection method based on the rated wind speed, which recommends the same wind turbine.

3.1.6.3 Average daily load demand

Another parameter that changes with time is the load. Since this study has been performed based on Ibrahimyya load demand in 2014. As can be foreseen that the load will definitely increase significantly. So, it is very important to study the sensitivity on the load variation, and see the effect on the COE and the total NPC as well as the PV and

wind's allocation. At this point, a 6% cumulative growth variation has been assumed for 8 years starting in 2014. Table 3.1 shows the annual average daily energy demand in 2014 of 150,271.608 kWh/d. Table 3.14 shows that as the annual average daily energy load increases, the HWPVG system size increases, which means that the wind and PV's allocation will be modified as shown in Table 3.14. On the other hand, Fig. 3.20 shows a resulting increased variation of 0.006$/kWh for the COE, and 36,449,332$ for the NPC.

Table 3.14 PV and wind's allocation with load sensitivity variation

Annual Average daily Energy Load (kWh/day)	# of GE1500 wind turbines	PV array size (kW)
150271.608	8	930
159287.904	9	0
168845.179	9	310
178975.889	9	1240
189714.443	10	310
201097.309	10	930
213163.148	11	310
225952.937	12	930

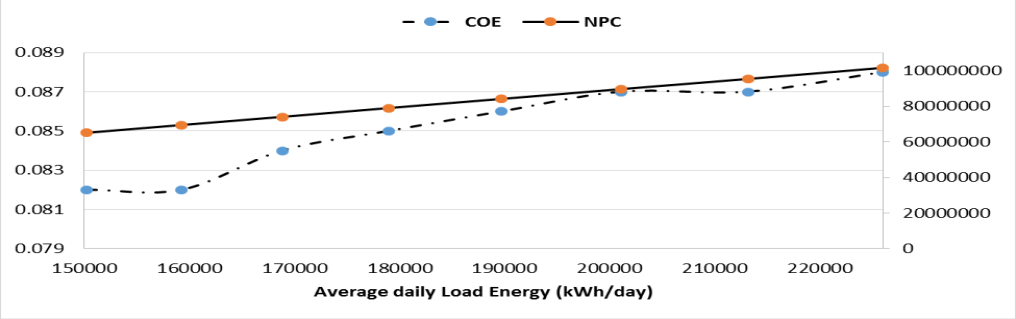

Fig. 3.20 Sensitivity of load demand variation on COE & NPC

3.1.6.4 Oil price

The COE to a grid connected customer is very sensitive to the cost of oil. Logically, if the cost of oil increases then the COE to the customer should be increased. So, a crucial

point in the grid connected renewable energy systems is to study the sensitivity of the fuel prices. In HOMER, you can consider the effect of fuel price by its relation to the grid power price, and perform the sensitivity analysis. Taking five real values of 60, 69, 80, 100 and 120 $/barrel of the oil price and the corresponding utility power price of 0.121, 0.134, 0.151, 0.172 and 0.201 $/kWh [61]. Afterwards, running the simulation to see the effect on COE, NPC, energy purchased and sold to the grid. Fig. 3.21 shows a resulting variation of 0.024$/kWh for the COE, and 21,496,864$ for the NPC.

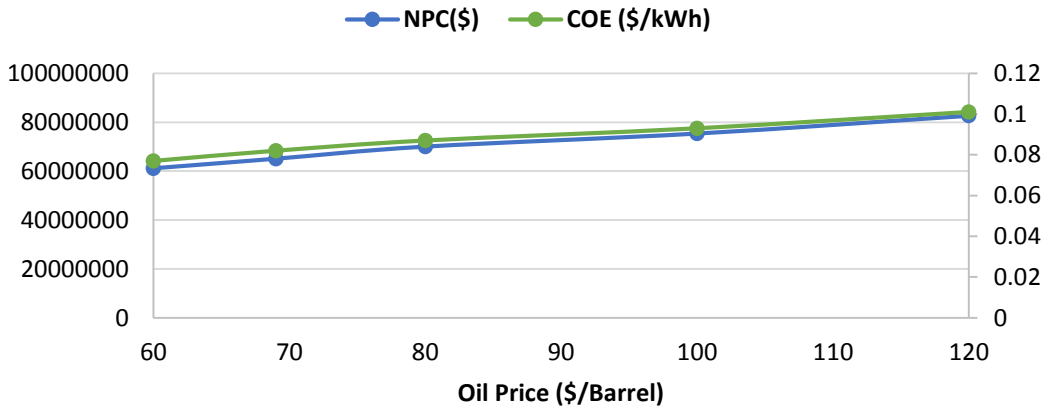

Fig. 3.21 Sensitivity of oil price on COE & NPC

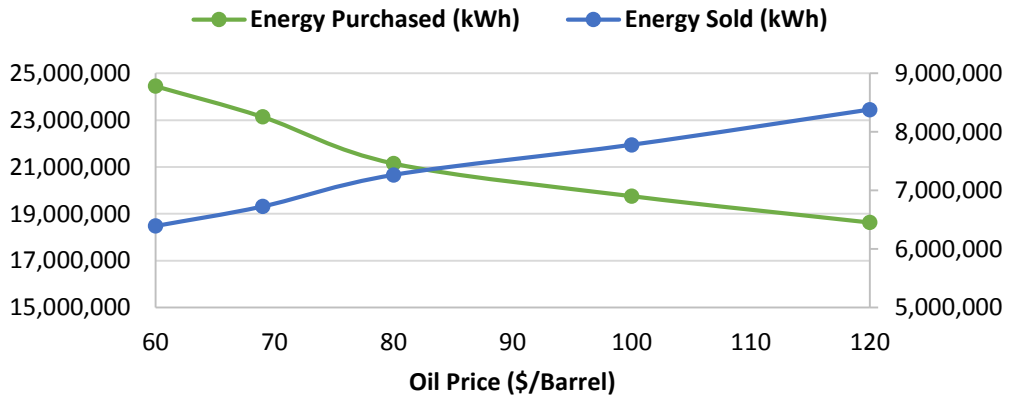

Fig. 3.22 Sensitivity of oil price on energy purchased & sold to grid

Fig. 3.22 shows when the oil prices increase in the given range, the energy purchased from the grid decreases by 23.81%. Also, energy sold to the grid increases by 31.04%. Fig. 3.22 proves the feasibility to purchase less and sell more, when the oil price goes up.

3.1.6.5 Natural gas price

Around 30 explosions of the Egyptian gas pipeline, which was the main source to supply Jordan with natural gas (NG), happened after the Egyptian revolution started in January 2011. The Jordanian government is looking to other NG producing counties. Negotiations have been started with Qatar and many other countries worldwide.

Recently, a two year long term contract has been signed by the Jordanian government in 2015 to import NG from numerous countries for a price around 7.25$ per million British Thermal Unit (MBTUs). During this contract there will be a floating steamship carrying around 160,000 m^3 of liquefied natural gas (LNG). This amount is equivalent to 96 million m^3 once converted into NG. Currently, this amount is capable to cover Jordan load demand needs for approximately 10 days. Afterwards, the steamship will be refilled with LNG. Note that, the utility power price is around 0.1171$/kWh when NG is included in production. In order to compare this price on the sensitivity of oil price in $/barrel, a unit conversion has been performed to convert MBTU to barrel of oil equivalent (BOE). 1MBTU energy unit is equivalent to 0.18014BOE [62]. This means that the equivalent price of NG is 40.25$/BOE. Afterwards, we can add this single data point to the sensitivity analysis graphs on oil price referring to Fig. 3.21 and Fig. 3.22.

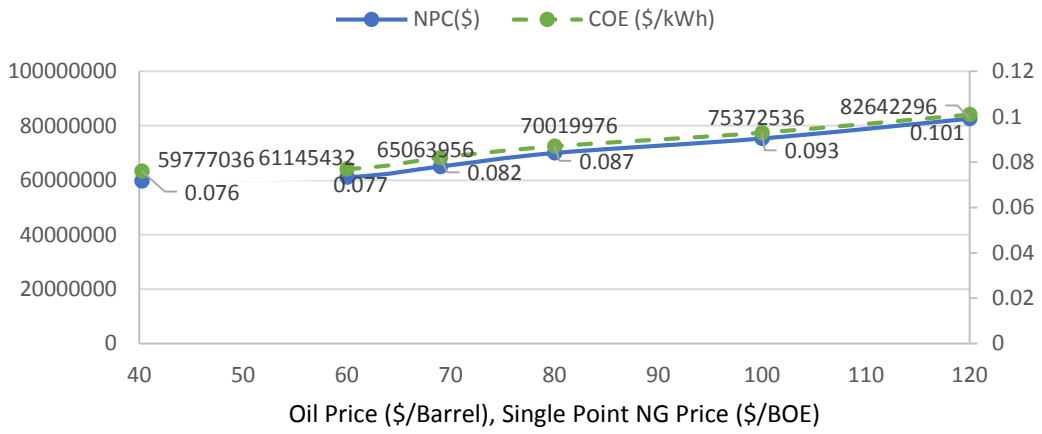

Fig. 3.23 Sensitivity of NG on the COE & NPC

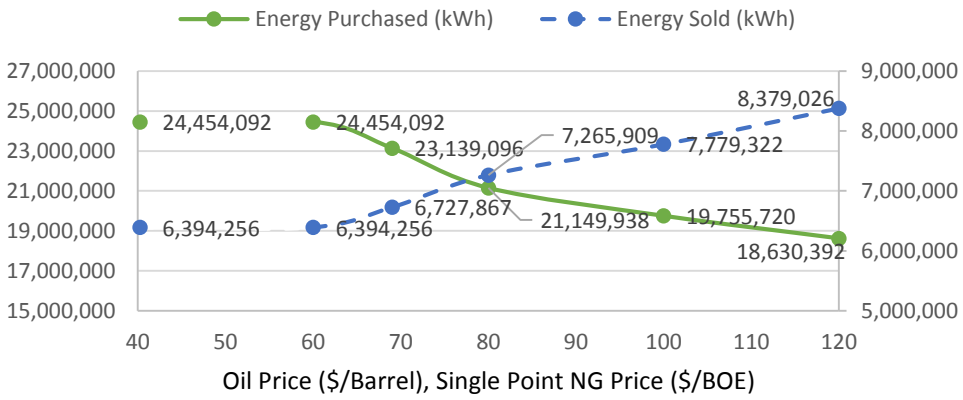

Fig. 3.24 Sensitivity of NG on energy purchased & sold to grid

Fig. 3.23 shows that in case of NG is used for production, the COE and the NPC will be less than all cases when the oil is used. Regarding purchasing energy from the grid, and selling energy to the grid. It is expected when using the NG, to purchase more and sell less. But, Fig. 3.24 shows that the use of NG with 40.25$/BOE is equivalent to the use of oil with cost of 60 $/barrel. This is due to the fixed limits considered of 100% of the peak load for the purchase capacity from the grid, and 25% of the peak load for the selling capacity to the grid.

3.2 Summary

For simplicity in this dissertation, this section investigates a single point renewable connection to the utility grid of Jordan. This is considered as an important step to understand all the concepts behind the multi-point grid connection problem whose solutions are the ultimate goal out from this research project. Therefore, in this section an economic study is performed for connecting a wind-PV hybrid system into the existing Jordanian power system. Ibrahimyya, a city in Jordan, is selected from the SPCDS as an interesting location to apply wind-PV hybrid system. The HWPVG system over 25 years life time is feasible, since the COE is 0.0817$/kWh which is a feasible and competitive price compared to other techno-economical researches and to the Jordanian utilities. Two methods are presented to size the system elements. The 1st one is used to study the sensitivity on the COE over the whole range of wind or PV sharing percents. It shows that penetrating more wind to the hybrid system will make it more feasible. The 2nd sizing method is performed to have an optimal size components of 8 wind turbines, and 3 PV panels. A sensitivity analysis to test the robustness of the designed system is implemented on the interest and inflation rates, wind power law exponent, the annual average daily energy load, the oil price and the natural gas price. In addition, the feasibility is proved by purchasing less and selling more, when the oil price goes upward. Also, when NG is used for production, the COE and the NPC will be less than all cases when the oil is used. At this point, all the aspects behind the multi-point problem have been clarified thru the single point problem discussed in details in this section. So, solution of the multi-point problem will be started from Section 4 by collecting and tailoring the multi-point needed data.

4. MULTI-POINT GRID CONNECTION DATA ACQUISITION AND PREPARATION

In this section, the data needed to solve the multi-point connection problem, will be updated and presented in details. This includes the Jordan hourly load profile in 2014, hourly recent values of wind speed, hourly recent values of solar radiation and the system components' costs.

4.1 Jordan hourly load profile in 2014

The Jordanian load profile in 2014 shown in Fig. 4.1 is obtained from the National Control Center (NCC) of the National Electric Power Company (NEPCO) which is responsible for transmission of electrical power in Jordan. Note that, the load data is gained using the supervisory control and data Acquisition (SCADA) system every 60 minutes a day for the whole year of 2014. Thereby, the number of data entries are found to be 8760 using the counting function in Microsoft Excel.

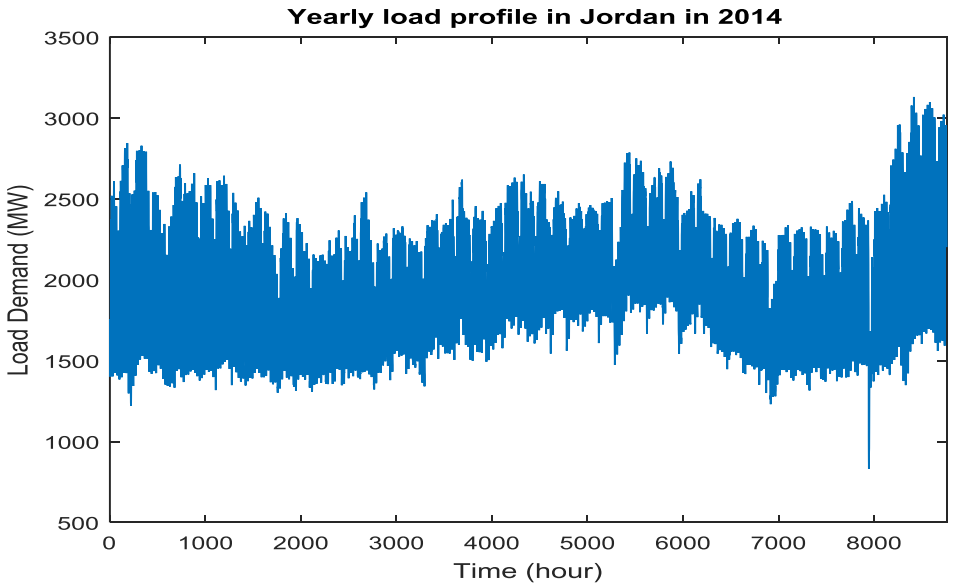

Fig. 4.1. Yearly load profile in Jordan in 2014

Building Fig 4.1. shows that the peak and average values of load demand in Jordan are 3129.95 MW and 2027.74 MW respectively. Load factor is defined as the ratio of average to maximum load for some specified period [63]. So, the load factor for the year of 2014 is calculated to be 64.785% which means that 64.785% of load demand hourly values is around the peak value as can be noticed from Fig 4.1.

4.1.1 Average daily load profile in Jordan in 2014

Moreover, Fig 4.2 shows the average daily load demand in Jordan in 2014. It is clear that load is varying, being maximum with two peaks at 1 P.M and 8 p.m, and minimum at 5 a.m. Also, it shows that the demand during hours of darkness is 1.5 times the demand during dawn hours. The transition from relatively lower loads to higher loads in the morning is called the "morning ramp" [64].

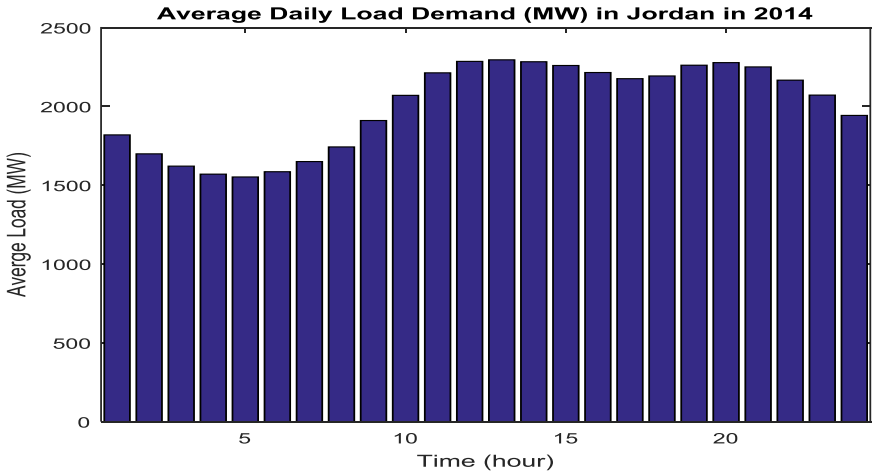

Fig. 4.2. Average daily load demand in Jordan in 2014

Fig. 4.2 shows a distinct morning ramp in load starting at 5:00 a.m. responding to such load changes often requires using units that can start up quickly [64]. The reason for the 1st peak is that most institutions, factories,…etc are in working hours around noon, and

the reason for the 2nd peak is that most citizens in home using their electrical appliances and most lights are turning on. During these peak periods, usually in the early evening, operators need more generating capacity which may include more costly peaking units [64].

4.1.2 Seasonal load profile in Jordan in 2014

Fig. 4.3 shows the seasonal monthly load profile in Jordan in 2014, which includes minimum, maximum and average monthly load. It can be noticed a high maximum value during summer season because of the cooling load mainly in August (2.786 GW) when a large amount of refrigeration is required.

In December and January, the maximum load is 3.13 GW and 2.845 GW respectively. There is an increase in load due to demand in heating and the use of AC air conditioning during winter season.

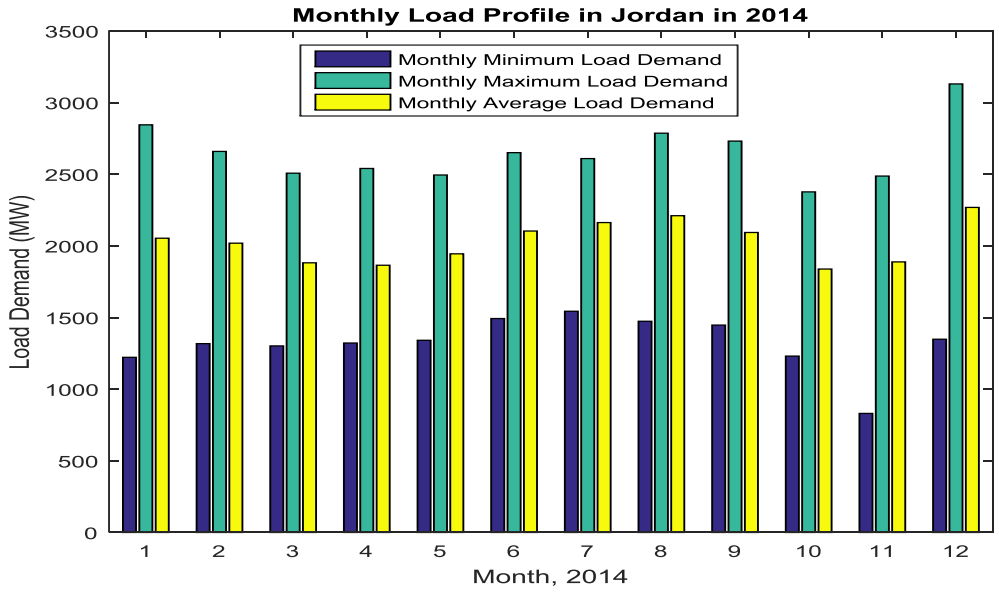

Fig. 4.3 Monthly load profile in Jordan in 2014

4.2 Load in workweek and weekend days in Jordan in 2014

Table 4.1 and Table 4.2 show two types of data set each with 288 entries, which are load of weekdays and load of weekends. Note that, in Jordan and most of the Arab countries the situation is different. The workweek (See Table 4.1) in Jordan starts from Sunday through Thursday, and the weekend days (See Table 4.2) are Fridays and Saturdays.

Table 4.1 Monthly average weekdays load in GW for Jordan in 2014

Hour	Month											
	Jan	Feb	Mar	Apr	May	Jun	Jul	Aug	Sep	Oct	Nov	Dec
0	1.769	1.716	1.605	1.606	1.741	1.925	2.195	2.183	1.890	1.618	1.593	1.869
1	1.597	1.559	1.481	1.491	1.644	1.815	2.092	2.079	1.787	1.517	1.494	1.696
2	1.485	1.474	1.416	1.425	1.574	1.734	2.015	1.990	1.728	1.460	1.426	1.599
3	1.419	1.424	1.377	1.401	1.550	1.716	1.973	1.921	1.686	1.426	1.397	1.554
4	1.410	1.423	1.388	1.435	1.548	1.689	1.835	1.876	1.693	1.429	1.404	1.577
5	1.486	1.544	1.503	1.490	1.498	1.613	1.712	1.786	1.713	1.487	1.503	1.691
6	1.638	1.798	1.637	1.588	1.584	1.672	1.719	1.763	1.735	1.534	1.609	1.844
7	1.713	1.816	1.714	1.712	1.735	1.853	1.815	1.882	1.875	1.664	1.699	1.968
8	1.922	1.974	1.879	1.880	1.921	2.042	1.956	2.034	2.061	1.807	1.841	2.174
9	2.118	2.114	2.006	2.000	2.048	2.186	2.095	2.166	2.176	1.914	1.973	2.381
10	2.287	2.239	2.099	2.088	2.140	2.305	2.208	2.286	2.261	2.002	2.065	2.541
11	2.381	2.297	2.126	2.123	2.193	2.343	2.283	2.355	2.315	2.047	2.097	2.632
12	2.391	2.296	2.113	2.113	2.192	2.346	2.317	2.392	2.317	2.029	2.082	2.634
13	2.359	2.276	2.082	2.098	2.193	2.354	2.345	2.420	2.329	2.028	2.076	2.612
14	2.314	2.256	2.053	2.076	2.182	2.356	2.340	2.433	2.331	2.014	2.067	2.593
15	2.274	2.201	2.003	2.013	2.134	2.321	2.314	2.415	2.292	1.976	2.016	2.564
16	2.236	2.161	1.962	1.972	2.084	2.271	2.287	2.376	2.233	1.934	1.985	2.677
17	2.379	2.180	1.934	1.933	2.032	2.203	2.228	2.311	2.160	1.986	2.225	2.817
18	2.512	2.462	2.165	1.986	2.012	2.129	2.156	2.264	2.310	2.197	2.233	3.130
19	2.419	2.392	2.207	2.210	2.223	2.278	2.211	2.441	2.354	2.121	2.153	2.647
20	2.337	2.301	2.134	2.131	2.184	2.320	2.361	2.438	2.273	2.035	2.118	2.581
21	2.276	2.243	2.041	2.008	2.088	2.246	2.354	2.372	2.190	1.989	2.037	2.483
22	2.158	2.112	1.938	1.818	1.996	2.140	2.297	2.322	2.115	1.871	1.911	2.303
23	1.989	1.935	1.779	1.787	1.895	2.075	2.255	2.253	2.007	1.750	1.764	2.094

Table 4.2 Monthly average weekends load in GW for Jordan in 2014

Hour	Month											
	Jan	Feb	Mar	Apr	May	Jun	Jul	Aug	Sep	Oct	Nov	Dec
0	1.776	1.733	1.613	1.610	1.746	1.951	2.241	2.168	1.902	1.638	1.650	1.827
1	1.611	1.564	1.497	1.486	1.648	1.836	2.133	2.069	1.806	1.536	1.542	1.659
2	1.487	1.476	1.426	1.434	1.577	1.770	2.035	1.973	1.736	1.478	1.484	1.579
3	1.426	1.431	1.399	1.410	1.569	1.750	1.995	1.921	1.713	1.449	1.447	1.542
4	1.429	1.438	1.418	1.462	1.569	1.731	1.868	1.867	1.707	1.458	1.460	1.566
5	1.508	1.584	1.568	1.526	1.540	1.658	1.756	1.771	1.746	1.518	1.582	1.738
6	1.699	1.922	1.826	1.693	1.654	1.729	1.766	1.779	1.819	1.591	1.786	1.952
7	1.822	1.953	1.874	1.792	1.829	1.957	1.884	1.942	1.970	1.725	1.874	2.112
8	2.064	2.092	2.012	1.945	2.029	2.180	2.073	2.117	2.158	1.867	1.997	2.254
9	2.251	2.198	2.076	2.039	2.123	2.320	2.236	2.272	2.259	1.955	2.059	2.379
10	2.391	2.248	2.132	2.100	2.222	2.423	2.360	2.382	2.336	2.034	2.122	2.507
11	2.463	2.284	2.148	2.129	2.248	2.469	2.417	2.451	2.367	2.061	2.137	2.581
12	2.474	2.275	2.139	2.127	2.251	2.477	2.462	2.502	2.380	2.070	2.143	2.608
13	2.441	2.267	2.164	2.159	2.277	2.499	2.490	2.516	2.419	2.073	2.167	2.620
14	2.383	2.264	2.168	2.154	2.271	2.486	2.468	2.531	2.427	2.079	2.184	2.627
15	2.329	2.219	2.122	2.094	2.206	2.436	2.423	2.507	2.369	2.041	2.141	2.611
16	2.302	2.188	2.065	2.046	2.145	2.372	2.368	2.438	2.289	1.988	2.105	2.694
17	2.466	2.199	2.038	2.013	2.094	2.297	2.310	2.374	2.222	2.043	2.340	2.842
18	2.608	2.531	2.274	2.037	2.049	2.201	2.206	2.300	2.367	2.268	2.338	2.780
19	2.516	2.473	2.324	2.246	2.257	2.339	2.263	2.476	2.406	2.178	2.247	3.025
20	2.423	2.386	2.236	2.164	2.204	2.373	2.413	2.473	2.318	2.111	2.197	2.642
21	2.350	2.283	2.114	2.026	2.093	2.284	2.407	2.406	2.203	2.047	2.096	2.538
22	2.220	2.148	1.985	1.922	1.987	2.157	2.347	2.355	2.127	1.925	1.941	2.327
23	2.025	1.926	1.808	1.769	1.871	2.076	2.293	2.287	2.007	1.792	1.779	2.078

4.3 Multi-point grid connection data (MPGCD)

The monthly averages wind speed and solar irradiation data for the MPGCD for the candidate cities in Jordan are obtained from the Energy Center (EC) which is located in the Jordanian Royal Scientific Society (JRSS). The EC provides the Latitude & Longitude and the altitude above sea level (a.s.l) for each candidate city as shown in Table 4.3. The first reason to select those MPGCD for six cities in Jordan is that either they have

a good infrastructure to build wind farms, or having high average annual wind speeds in excess of 6-7 m/s; some more limited areas have an average wind speed above 7 m/s according to the wind atlas of Jordan [65].

Table 4.3 Coordinates and site altitude for each candidate site in Jordan

	Coordinates	Site altitude a.s.l (m)
Ramtha-JUST	E 35.98500°, N 32.47890°	591
UmEjmal-LH	E 36.40417°, N 32.33150°	750
Ibrahimyya	E35.82970°, N 32.43645°	1021
Alreesha2-LH	E 39.01161°, N 32.57046°	876
Maan-LH	E 35.68627°, N 30.26091°	1196
Aqaba5	E 35.04615°, N 29.66323°	139

Another reason to select those MPGCD that they are blessed with an abundance of solar energy, which is evident from the annual daily average solar irradiance (average insolation intensity on a horizontal surface) ranges between 4-7 $kWh/m^2/day$ which is one of the highest in the world. This corresponds to a total annual of 1400-2300 kWh/m^2. The average sunshine duration is more than 300 days per year [66].

4.4 Wind speeds

Fig. 4.4 shows that Aqaba5, Ibrahimyya and Alreesha2-L and have exceptional annual wind speed values of 7.33 m/sec, 7.02 m/sec and 7.17 m/sec respectively. Note that, the wind speeds have been measured for each candidate city for a period between five to ten years, see Table 4.4. Note that, those values are measured at various heights. Thereby, the wind speed power law, with an assumed exponent value of 0.14, is used to tailor the new data at the same height of 50 m. Moreover, Fig. 4.4 shows the annual average wind speed in m/sec for those sites.

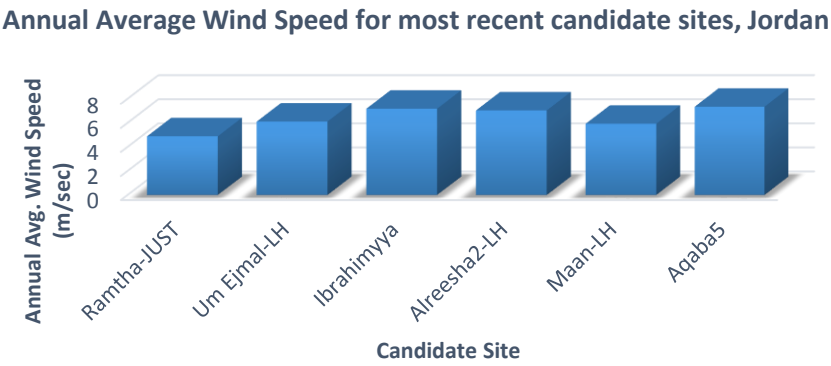

Fig. 4.4 Annual wind speed for most recent candidate sites in Jordan

Table 4.4 Wind speed in m/sec for the candidate sites in Jordan

	Ramtha-JUST	Um Ejmal-LH	Ibrahimyya	Alreesha2-LH	Maan-LH	Aqaba5	Mean
Jan.	4.77	6.12	7.64	7.17	5.48	4.99	6.03
Feb.	5.11	6.46	8.08	8.00	6.90	5.83	6.73
Mar.	4.98	6.32	7.86	7.74	6.35	7.36	6.77
Apr.	4.69	6.01	7.83	7.68	6.13	7.83	6.70
May	4.99	5.96	6.61	6.86	6.23	7.59	6.37
Jun.	5.50	6.48	7.49	7.01	6.83	8.30	6.94
Jul.	5.75	6.82	7.91	6.68	7.01	7.71	6.98
Aug.	5.43	6.67	7.69	6.30	6.37	8.65	6.85
Sep.	4.73	5.98	6.46	6.76	5.70	9.01	6.44
Oct.	4.05	5.45	5.59	6.82	4.91	8.46	5.88
Nov.	3.92	5.47	5.83	6.38	4.21	6.22	5.34
Dec.	4.60	5.46	7.08	6.93	4.91	6.03	5.83

In the multi-point connection problem, the hourly wind speed values for all those MPGCD candidate cities will be considered and used in the mathematical modeling as shown in Section 5. However the wind speed average value for the six candidate sites will be used to investigate the PDF behavior for the wind speed data, see the last column in Table 4.4. Furthermore, Fig. 4.5 shows the monthly average wind speed after averaging

the candidate cities. Note that, the annual average wind speed, as an average of cities, is approximately equal 6.4m/sec which is held in a class that is typically needed to economically generate power [67].

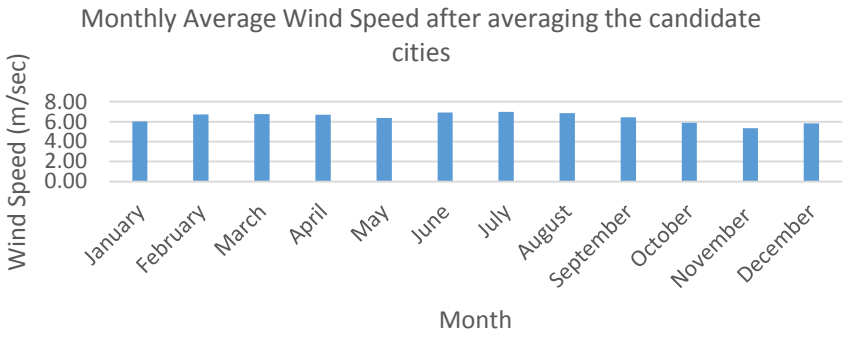

Fig. 4.5 Monthly average wind speed after averaging the MPGCD in Jordan

4.5 Wind speeds probability distribution frequency (PDF) curve

PDF curve (See Fig. 4.6) is used to model the wind speed frequency distribution over one year. At this point, a Histogram curve for the wind speed time series data has been built using Microsoft Excel.

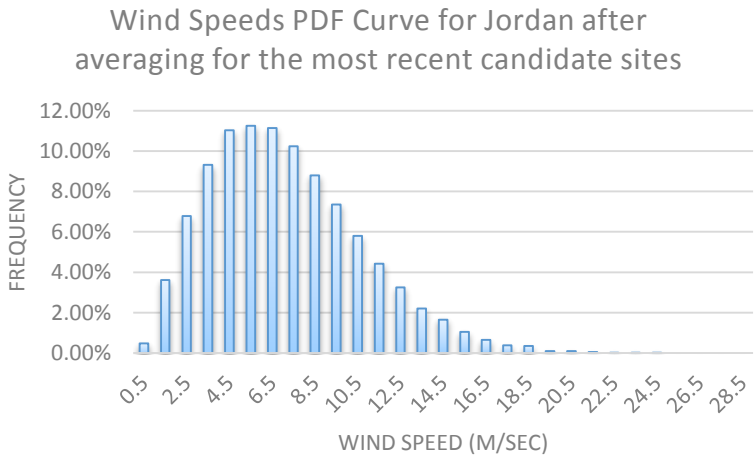

Fig. 4.6 Histogram PDF curve for the wind speed time series data

Fig. 4.6 shows the percentage frequency for each value of wind speed after averaging the MPGCD candidate cities. Moreover, if you multiply the y-axis of Fig. 4.6 by 8760, you will get the hourly distribution for the whole year after averaging the candidate cities, See Fig. 4.7.

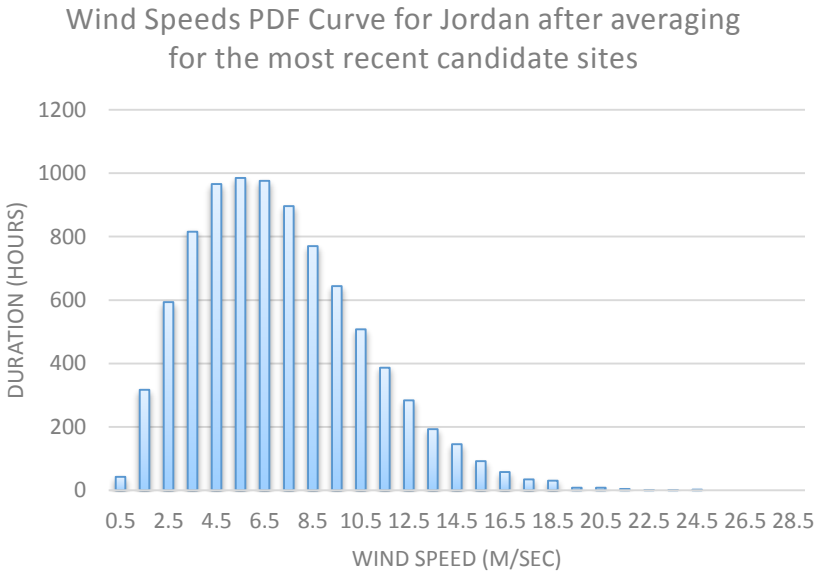

Fig. 4.7 Histogram PDF hourly curve for the wind speed time series data

Building the histograms in Fig. 4.6 and 4.7 shows that the annual frequency (or period) for zero wind speed is 0% (or 0 hours). This means that the wind speed is hourly available during the whole year. At this point, let's see the frequency for the values above or equal the cut-in wind speed. For instance, let's take the GE-1.5sle WT model which has a 3.5m/sec cut-in and 25 m/sec cut-out wind speeds. For this range of useful wind speeds, the histograms built in Fig. 4.6 and 4.7 show a frequency of 89.12% (or 7808 hours). In other words, the availability of useful wind speed resource is 89.12%. This will make the wind farm produces power for 7808 hour during the whole year.

4.6 Solar radiation

Solar energy is one of the environmentally sustainable resources to produce electrical power using PV arrays. The main input for PV energy is the solar radiation. Note that, the reader should be familiar with various solar terms. Irradiance or insolation are measured in kW/m^2. Whereas, radiation or irradiation are measured in kWh/ m^2[68]. The monthly average solar insolation data for most recent candidate sites in Jordan are obtained from Photovoltaic Geographical Information System (PVGIS) which develops a solar radiation database as a solar energy resource. In addition, PVGIS helps researchers evaluate the electricity generation from PV systems in various continents such as: Europe, Africa, and Asia. Note that, PV GIS is used by the Energy Center (EC) which is located in the Jordanian Royal Scientific Society (JRSS). EC is responsible to make renewable energy assessment in Jordan. Fig. 4.8 shows that all the candidate sites have annual irradiation above 5 kWh/m^2/day.

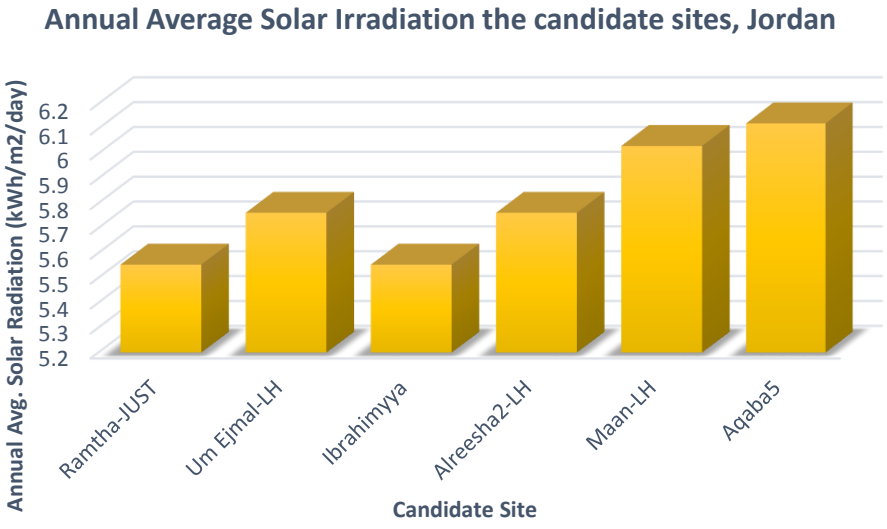

Fig. 4.8 Annual average solar irradiation for the MPGCD in Jordan

Afterwards, each location coordinates are inserted to PVGIS in order to get the solar irradiation data for each candidate site. Note that, PVGIS provides a map-based inventory of solar energy resource and assessment of the electricity generation from photovoltaic systems, see Table 4.5 and Fig. 4.8.

Table 4.5. Monthly average irradiation in kWh/m^2/day for the MPGCD in Jordan

	Ramtha-JUST	Um Ejmal-LH	Ibrahimyya	Alreesha2-LH	Maan-LH	Aqaba5	Mean
Jan.	2.87	3.21	2.87	3.21	3.60	3.69	3.24
Feb.	3.56	4.04	3.56	4.04	4.53	4.66	4.07
Mar.	5.23	5.69	5.23	5.69	6.22	6.42	5.75
Apr.	6.14	6.51	6.14	6.51	6.82	7.00	6.52
May	7.41	7.32	7.41	7.32	7.59	7.72	7.46
Jun.	8.34	8.40	8.34	8.40	8.40	8.36	8.37
Jul.	8.14	8.17	8.14	8.17	8.17	8.14	8.16
Aug.	7.46	7.51	7.46	7.51	7.59	7.58	7.52
Sep.	6.23	6.46	6.23	6.46	6.60	6.61	6.43
Oct.	4.87	5.11	4.87	5.11	5.43	5.56	5.16
Nov.	3.56	3.69	3.56	3.69	4.02	4.23	3.79
Dec.	2.83	3.03	2.83	3.03	3.40	3.49	3.10

As a matter of fact, Jordan is located within the most favorable solar belt worldwide where locations are highly recommended for solar applications, with average solar radiation ranging between 5 and 7 kWh/m^2/day. This belt extends between latitudes 15°N, and 35°N [69].

In the multi-point connection problem, the hourly solar insolation values for all those recent candidate cities will be considered and used in the mathematical modeling as shown in Section 5. However, the solar radiation average value for the six candidate sites

will be used to investigate the PDF behavior for the irradiation data, see the last column in Table 4.5. Moreover, Fig. 4.9 shows the monthly average radiation after averaging the MPGCD in Jordan.

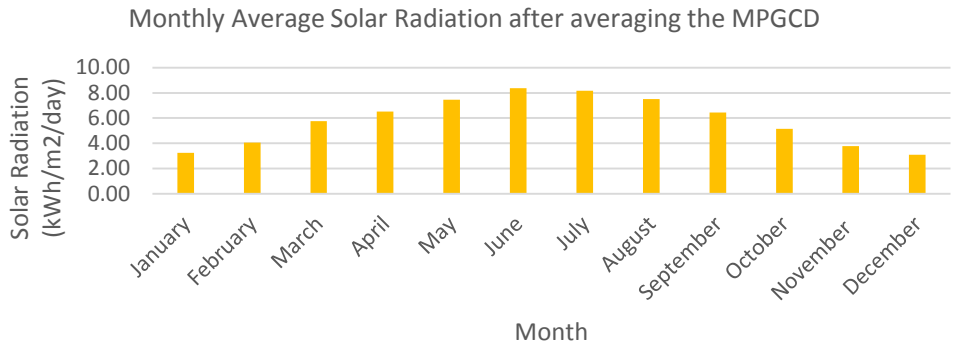

Fig. 4.9 Monthly average solar radiation after averaging the MPGCD in Jordan

Fig. 4.9 shows that the annual average solar radiation after averaging the MPGCD is approximately equal 5.8 kWh/m^2/day. Note that, the hourly solar irradiance in kW/m^2 is also available for each city in Table 4.5.

4.7 Solar insolation probability distribution frequency (PDF) curve

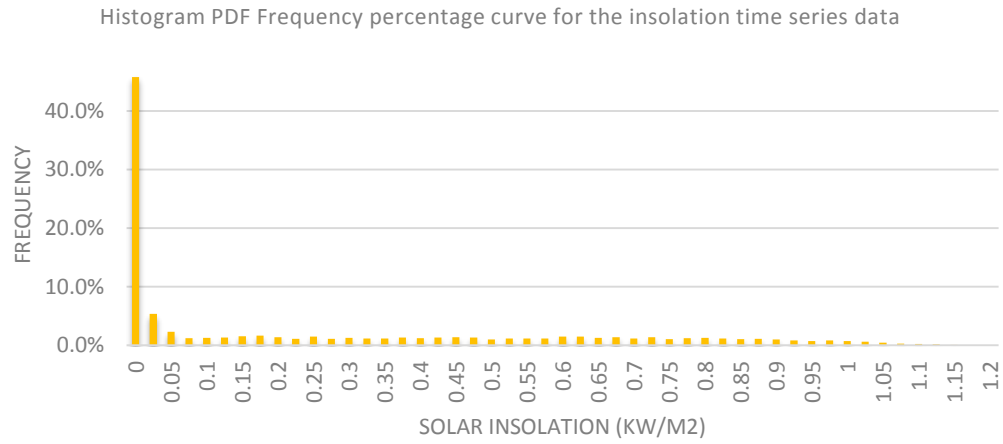

Fig. 4.10 Insolation PDF after averaging the MPGCD in Jordan

PDF curve is used here to model the solar insolation frequency distribution over one year. Note that, the average irradiance value for those 8760 values is 241.563 W/m^2 which is assumed to be the annual average solar irradiance value after averaging the MPGCD candidate cities. At this point, a Histogram curve for the solar insolation time series data has been built using Microsoft Excel. Fig. 4.10 shows the percentage frequency for each value of solar irradiance after averaging the MPGCD candidate cities. Moreover, if you multiply the y-axis of Fig. 4.10 by 8760 hour, you will get the hourly distribution for the whole year, see Fig. 4.11. Building the histograms in Fig. 4.10 and 4.11 shows that the annual frequency (or period) for zero insolation is 45.7991% (or 4012 hours). Also, the total annual frequency (or period) for non-zero insolation is 54.2009% (or 4748 hours). This is because the sun is only shinning during daytime for around 8 hours a day, so there will be no irradiance for around 16 hours a day.

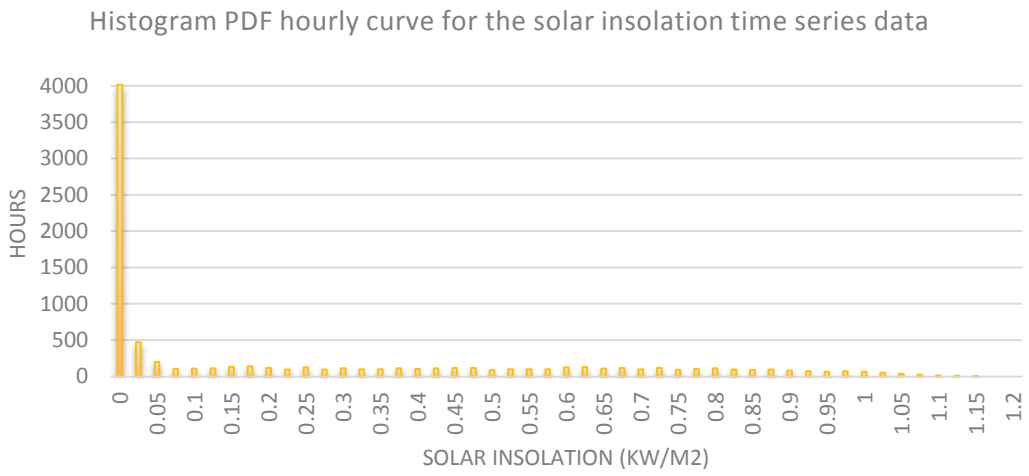

Fig. 4.11 Hourly insolation after averaging the MPGCD in Jordan

4.8 Multi-point system component costs

Cost Engineering is a technical major which includes cost analysis for engineering projects using scientific and engineering methods. This major is considered as a crucial investigation before the application of any project. This is because the accuracy of these results may have big differences, which therefore will affect decisions made by companies and institutions. Thereby, the goal for engineers is to design an optimal system with minimum cost. In this dissertation the cost of wind and PV systems includes Capital Cost (CC), Operation & Maintenance Cost (OMC), and Replacement Cost (RC). Also, the Salvage Cost (SC) that is related to the RC.

4.8.1 Current market price of the renewable components

Note that, the CC is considered as the component cost plus the installation cost. In case of WTs, *the average installed capital cost for WTs is considered as 2098$/kW* of wind power capacity. Note that, this cost includes the costs of WTs, and towers taking into account transportation and installation, balance of unit wiring and salaries for design engineers and financing. Moreover, this cost includes any facility required to develop or construct the WT [70]. Furthermore, note that the converter cost is included in the CC of the WT [70, 71].

Regarding, PV modules the CC is taken as the PV module cost plus the installation costs. Note that the module cost is taken as an average value from the CivicSolar, which is an innovative solar distributor partnering with installers and developers throughout North America. CivicSolar helps solar PV companies make a real time business decision based on efficient price reports. In this study, the average cost value of PV modules is

1270$/kW [72]. In addition, the PV total installation cost for large-scale projects, in 2014, is estimated to be 1500 $/kW in the Middle East [73]. Thereby, *the overall CC for PV is considered as 2770$/kW*. In addition, note that the converter cost is included in the capital cost of the PV panel [71], see Table 4.6.

Table 4.6 Hybrid wind/PV system component costs MPGCD in Jordan

Component	*Value*
Project Life Time	25 years
PV	
CC	2770$/kW
RC	0$/kW
OMC	10 $/kW/year
Life Time	25 years
WT	
CC	2098$/kW
RC	2098$/kW
OMC	20.98$/kW/year
Life Time	20 years
Converter	
CC	Included in PV& WT CC
RC	300 $/kW
OMC	Included in PV& WT OMC
Life Time	15 years

The OMC costs of the PV module has the HOMER default value of 10$/kW/year. Furthermore, the OMC of the WT is taken as 1% of the CC [74]. Note that, the OMC costs of the converter of the WT and converter of the PV panel have been assumed to be included in the OMC costs of the WT as well as the PV panel respectively. Moreover, the RC will be the same as the CC if the project life time is only greater than the component life time. Otherwise it will have a zero value, see Table 4.6.

4.8.2 Current price of dealing with the grid in Jordan

The Jordanian Energy & Minerals Regulatory Commission (ERC) is a governmental body that possesses a legal personality with financial and administrative independence and is considered the legal successor of the Electricity Regulatory Commission [75]. Moreover, ERC provides numerous information related to the upcoming renewable energy projects that are connected to the transmission or distribution systems. For instance, for distribution systems, ERC determines the maximum sale capacity to the AC utility grid, sale price per kWh. For the transmission and distribution systems, it determines the maximum purchase capacity from the AC grid and purchase price per kWh [76]. In this dissertation, a renewable grid connected system will be designed in each candidate city to meet the national load in Jordan. If the hybrid system is connected to the grid, it is required to insert the grid power price which is the utility power price plus the utility passing cost for the energy purchased from the grid when the designed system cannot satisfy the load. Also, in case of small-scale on-grid systems, it is required to insert the sellback rate for additional energy after satisfying the load as shown in Table 4.7. Note that, the currency conversion is based on (1$=0.7JD).

In our multi-point connection problem, we will no longer need the data in Table 4.7, because in our design, the system will not be able to sell any energy back to the grid. Because without renewables the grid is equal to the national load demand. So, once the renewable systems are connected to the grid, they will not be able to sell back anymore. ERC determines the passing cost for the renewables connected to the transmission system to feed a user connected to the distribution system. In our multi-point connection problem,

the price to be added to the purchased from the AC grid is 0.01643$/kWh. Referring to the Jordanian ERC website, for any user, having a renewable energy system connected to the transmission or distribution system, the cost of passing energy is shown in Table 4.8.

Table 4.7 Sale price to the AC grid in Jordan

Renewable Energy Resources Connected to the distribution system	Sale Price ($/kWh)
Solar Energy	0.17143
Hybrid Resources	0.13571
Other Resources	0.12143

Table 4.8 Passing cost with the AC grid in Jordan

Renewable Energy Connection Type	Passing Cost ($/kWh)
Connection to the transmission system to feed a user connected to the transmission system.	0.00643
Connection to the distribution system to feed a user connected to the distribution system.	0.01
Connection to the transmission system to feed a user connected to the distribution system.	0.01643

Table 4.9 Grid cost for renewable hybrid resources

Grid Energy Price	Utility Power Price + Passing Cost = 0.124+0.01643 = 0.14043 $/kWh
Sellback $/kWh	0.0 $/kWh

At this point, all the data needed are available. So, in Section 5 the multi-point individual system components will be mathematically modeled. Each model will be coded on the way to build a new planetary optimization design tool to solve the multi-point connection problem.

5. MATHEMATICAL MODELING, INVESTIGATION AND A DEVELOPED OPTIMIZATION DESIGN TOOL [*]

Three papers in [77-79] have been accepted out of our work in this section. Two of them are forwarded to be reviewed by the IEEE transactions on Industry Applications Society.

After the investigation of the single point connection, it has been concluded that HOMER is a single site simulation tool, and it can't be used to solve our actual problem of multi-point connection to the national grid. Right now, the challenge is to satisfy the national load for the entire country of Jordan (as a case validation) by renewable energy systems installed only in the six MPGCD candidate sites in Jordan. In this section, each component in the multi-point grid connection problem will be mathematically modeled. In addition, each model will be coded on the way to build a planetary optimization design tool to solve real-world sustainable power system multi-connection problems.

Modeling is a cost-efficient tool used to represent the real-world components communicated with each other and test many design conditions. Since it is hard and expensive to replicate the real-world implementation especially for large scale renewable energy utility projects of high initial capital costs. Thereby, a mathematical modeling has been developed for each component in our system. First, WT has been modeled by taking a closer look to many parameters such as air density. Then the impact of WT modeling

[*] Part of this section is reprinted with permission from Hussein M. K. Al-Masri and M. Ehsani, "Impact of Wind Turbine Modeling on a Hybrid Renewable Energy System," IEEE Industry Applications Society Annual Meeting, October, 2016, © 2016 IEEE and Hussein M. K. Al-Masri and M. Ehsani, "Accurate Wind Turbine Annual Energy Computation by Advanced Modeling," IEEE Industry Applications Society Annual Meeting, October, 2016, © 2016 IEEE and Hussein M. K. Al-Masri and M. Ehsani, "Impact of Wind Turbine Modeling on a Renewable Energy System," North American Power Symposium (NAPS), September, 2016, © 2016 IEEE.

has been investigated for a hybrid and a wind energy on-grid systems. Second, PV modeling has been done as long as the solar incident insolation is available. Third, the utility grid model has been done after getting needed data such as the utility purchased price. Fourth, the minimum required rectangular footprint has been modeled for the wind farm and PV array. Fifth, various system performance indicators have been modeled such as the ASCE, LCOE, SC, RC, AEI, LOA and RP. In our problem, the ASCE is considered as the single FOM of optimization problem. Then, a MFOM problem has been optimized which includes LCOE, AEI, ASCE and RP. The optimization process will be discussed in details in the next two chapters. Note that, the optimization design tool has been built by coding each model mentioned earlier. This design tool will be able to find the optimal feasible solution in case of multi-potential cities and satisfying the national load for a country including all candidate cities mentioned in Section 4 (See Fig. 4.1, Fig. 4.4 and Fig. 4.8).

In this section, a new design tool has been built. Actually, the problem is to satisfy the load demand for a country by installing wind farms and PV arrays only in those cities of high potential of both wind speed and solar radiation. Since in any country around the world, some cities or locations (not all) are of high potential of renewable energy natural resources. The goal for this tool is to find the optimal and feasible renewable system configuration for each candidate city in this problem. As a matter of fact, no design tool, used in the literature, can find the solution for such an important problem. Thereby, it is very important to build a design tool like this, which will help many researchers, companies and countries take decisions to apply techno-economic and feasible renewable

energy projects in multi-sites and one load problem. In order to foresee the hybrid system performance, individual components should be mathematically modeled.

5.1 Accurate WT annual energy computation by advanced modeling

The power-speed curve depends on either manufacturer data or more detailed data about the models. The only part that needs to be fitted and modeled is the one between the cut-in and rated wind speed. In [60, 80] the authors used detailed models. These types of models require additional measurements other than those available from the manufacturer. Some models use a cubic polynomial with all coefficient can be extracted from the manufacturer datasheet [81]. Sometimes a quadratic with only one coefficient [82], and the simplest model is the linear function [83].

Wind energy can be calculated by the integration of the power-speed curve (linear, quadratic or cubic models) [84]. In this section, we will discuss the models used in the literature regarding modeling of the WT in the wind speed range between the cut-in and rated wind speed values. In all these models there is a zero output power before the cut-in and after the cut-out wind speed values. Also, a constant output power between the rated and the cut out wind speed values.

5.1.1 Linear model

A simplified model has been used in [83] to simulate the output power of the WT as Equation 5.1 shows.

$$P_w(v) = P_R \frac{v - v_{ci}}{v_{rated} - v_{ci}}, \qquad v_{ci} \le v \le v_{rated} \tag{5.1}$$

Where: v_{ci} is the cut-in wind speed value, v_{rated} is the rated wind speed value, and P_R is the rated output power.

5.1.2 Quadratic model

An approximated quadratic equation has been used in [82] to model the output power of the WT as Equation 5.2 shows.

$$P_w(v) = P_R \frac{v^2 - v_{ci}^2}{v_{rated}^2 - v_{ci}^2}, \qquad v_{ci} \le v \le v_{rated} \tag{5.2}$$

5.1.3 1st Cubic model

A typical WT characteristic equation has been used in [81] to calculate the output power of the WT as Equation 5.3 shows.

$$P_w(v) = av^3 - bP_R, \qquad v_{ci} \le v \le v_{rated} \tag{5.3}$$

Where: $a = \frac{P_R}{v_{rated}^3 - v_{ci}^3}$, $b = \frac{v_{ci}^3}{v_{rated}^3 - v_{ci}^3}$

5.1.4 2nd cubic model

The 2nd cubic model is investigated in details in this dissertation and considered as an Improved Cubic Model (ICM) of the WT. Equation 5.4 shows the WT power captured by the blades (shaft power), and then it can be converted into mechanical power [85].

$$P_{WT} = \begin{cases} 0 & , \quad v < v_{cut_{in}} \\ \frac{1}{2}\rho A_{WT} v^3 Cp & , \quad v_{cut_{in}} \le v \le v_{rated} \\ P_{rated} & , \quad v_{rated} \le v \le v_{cut_{out}} \\ 0 & , \quad v > v_{cut_{out}} \end{cases} \tag{5.4}$$

Where: ρ is the air density in kg/m^3, A_{WT} is the swept area in m^2, $v_{rated}, v_{cut_{in}}$, $v_{cut_{out}}$ are the rated, cut-in and cut-out wind speed values respectively, Cp is the power coefficient and P_{rated} is the rated power of the WT.

5.1.4.1 Air density modeling

Three points of interests are worthy to mention here regarding Equation 5.4. *First*, the air density: In most literature WT related studies, the default density value is the one at sea level, which is 1.225 kg/m^3. However, air density plays an important role in extracting the wind energy, even if it is not directly mentioned in many literature papers. Because it is linearly proportional with the available wind power. It can be included to the calculations by simply taking its average over a year. Manufacturers provide their performance curves for air density at sea level, but the real value depends on climate conditions such as air pressure, temperature, humidity and it depends also on the elevation above sea level (a.s.l). Performance curves for different air densities are shown in Fig. 5.1. It shows that as the air density decreases, the area of the output power of the WT decreases, and this will affect the total EEPY from a single WT as well as the whole wind farm.

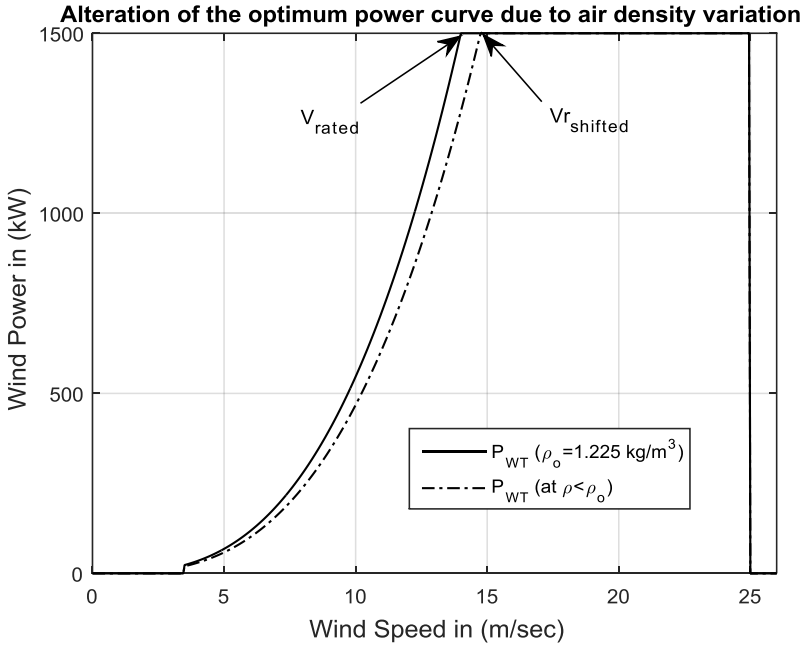

Fig. 5.1 Alteration of the optimum power curve due to air density variation

Some authors approximate air density by a linear relationship [86], exponential relationship [87], or estimated for a specific region which requires various site measurements [88]. In [89], it has been proved that the density reduction causes a shift in the rated velocity toward higher values. But, the rotor will deliver the maximum power for pitch regulated WTs. This will reduce the area of the wind power curve, and hence the EEPY will be reduced, see Fig. 5.1 below.

Most wind farms are practically designed at locations a.s.l. An investigation is performed in this section to compute the actual value of air density at any elevation a.sl. In this dissertation, the air density has been computed and modelled in five ways using the ICM.

5.A. ρ as a function of the elevation a.s.l

According to the International Civil Aviation Organization (ICAO) standard which says that the temperature at sea level is 15°C or 288K [90]. Equation 5.5 will be used to compute the temperature in Kelvin at any height in meter.

$$T = T_o - LH \tag{5.5}$$

Where: T_o is the temperature at sea level in Kelvin (288K). Also, T is the temperature (in Kelvin) at the altitude above sea level H (m). L is the temperature lapse rate (0.0065 °C/m) [91, 92].

At this point, in order to calculate the air density, we need to compute the air pressure (Pa) using Equation 5.6.

$$P = P_o \left(1 - \frac{LH}{T_o}\right)^{\frac{gM}{RL}} \tag{5.6}$$

Where: P_o is the standard pressure at sea level, 101325.0 (Pa). g is the acceleration due to gravity (9.80665 m/sec^2). M is the molecular weight of dry air (0.0289644 kg/mol). R is the ideal gas constant (8.31432 N·m /(mol·K)). The air density is described by Equation 5.7 and the ideal gas law in Equation 5.8.

$$\rho = \frac{PM}{1000RT} \tag{5.7}$$

$$\frac{\rho}{\rho_o} = \frac{P}{P_o} \times \frac{T_o}{T} \tag{5.8}$$

In order to gain the equation of air density (kg/m^3) as a function of the height H (m), Equation 5.9 below is gained by substituting the above equations (5.5, 5.6, 5.7 and 5.8) with each other. Where: ρ_o is the air density at sea level (1.225kg/m^3).

$$\rho = \rho_o \times \left(1 - \frac{LH}{T_o}\right)^{\frac{gM}{RL}} \times \frac{T_o}{T_o - LH} \tag{5.9}$$

5.B. ρ as a function of pressure and the elevation

In this model, Equation 5.9 can be modified by substituting Equation 5.6 as shown in Equation 5.10 below. Note that, the constant values and units as shown before in section 5.A.

$$\rho = \rho_o \times \frac{P}{P_o} \times \frac{T_o}{T_o - LH} \tag{5.10}$$

5.C. ρ as a function of temperature and the elevation

In this model, Equation 5.9 can be modified by substituting Equation 5.5 as shown in Equation 5.11 below. Note that, the constant values and units as shown before in section 5.A.

$$\rho = \rho_o \times \left(1 - \frac{LH}{T_o}\right)^{\frac{gM}{RL}} \times \frac{T_o}{T} \tag{5.11}$$

5.D. ρ as another function of temperature and the elevation

In [87, 93] the authors mentioned another equation to calculate the air density, which can be adjusted for elevation and temperature as Equation 5.12 shows.

$$\rho = \frac{P_o}{K_g T} e^{-\frac{gH}{K_g T}} \tag{5.12}$$

Where: K_g is the specific gas constant for air (287 J/kg K) [87], and g is the acceleration due to gravity ($9.81\ m/sec^2$) [87].

5.E. ρ as a function of temperature, pressure and humidity

In [94], the authors mentioned an approximate (Equation 5.13) to determine the air density as a function of pressure, temperature and relative humidity (RH). Note that, increasing the relative humidity makes the air less dense [92].

$$\rho = \frac{0.348444p - (0.00252t - 0.020582) \times RH}{t + 273.15} \tag{5.13}$$

Where: p is the atmospheric pressure in hPa, (1 hPa = 100 Pa). t is the temperature (°C). RH is the relative humidity in % [94].

Our design tool includes codes described by the flow chart in in Appendix C. They are used to insert the data needed (WT types and data resources of wind speed, ambient temperature and some constant parameters needed to compute the EEPY from the wind farm. So, various constant parameters needed to compute the EEPY from a WT such as the wind speed, anemometer height (50m), altitude of the candidate sites considered, wind power law exponent (1/7). In sum, Appendix C shows how to compute the wind energy, and account for these 4 methods.

5.1.4.2 Wind power coefficient

In order to find the shaft power from a WT, the power in wind should be multiplied by the power coefficient (*Cp*), which is defined as the ratio of the shaft power produced by WT to the total Power available in the wind. Simply, *Cp* is the ratio of the turbine power to the wind power. The maximum value of *Cp* is the Betz limit. Albert Betz was a German physicist who calculated that no WT could convert more than 59.3% of the kinetic energy of the wind into mechanical energy turning a rotor [55]. In [95], it has been mentioned that *Cp* has a constant maximum value when the wind speed ranges between the cut-in and rated wind speed value as shown in Fig. 5.2.

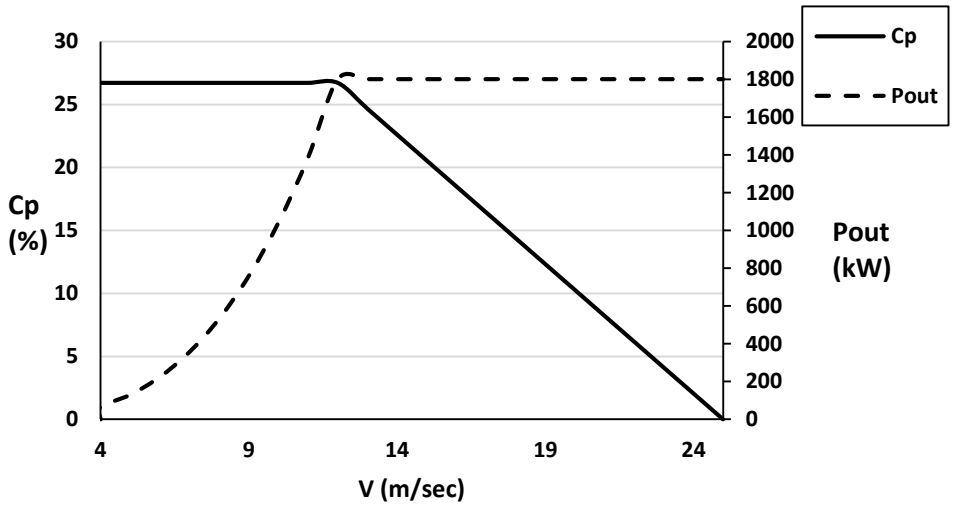

Fig. 5.2 Power coefficient & WT output power curve

Thereby, the maximum power coefficient value has been computed in this range using the rated values of both WT power and wind speed. Fig. 5.2 shows that the power coefficient Cp has a constant maximum value equals to 26.73% for V90-1.8MW WT with specifications shown in Table 5.1.

5.1.4.3 WT hub height

The available measured wind data are not given exactly at the hub height. The higher the turbine, the more wind speed. The relationship that describes the wind speed at a specific higher height is called the wind power law [60, 83] as Equation 5.14 shows.

$$v = v_a \left(\frac{H_{WT}}{H_a}\right)^{\alpha} \tag{5.14}$$

Where: v is the wind speed (in m/s) at the WT hub height H_{WT}; v_a is the wind speed (in m/s) measured by the anemometer at H_a height,; and the exponent α is the wind speed power law coefficient. The value of this coefficient varies from less than (0.10) for very flat land, water or ice to more than (0.25) for heavily forested landscapes. The one-seventh power law (1/7) is a good reference number for relatively flat surfaces such as the open terrain of grasslands away from tall trees or buildings [48].

The wind energy from each WT is computed using Equation 5.15. Note that, the time step depends on the data when they were measured.

$$E_{out_{wind}} = P_{out_{wind}} \times Time\ Step \tag{5.15}$$

In the final analysis, the model of the WT and the amount of the wind EEPY are affected by two scenarios: the accuracy of the WT model, and the accuracy of air density modeling.

5.1.5 Investigation of WT modeling

This scenario includes three simplified or straightforward WT models: Linear model, the Quadratic model, and the 1st cubic model. The WT power is a function of only the wind speed. To make a comparison, the WT output characteristics for these three

models have been plotted for two WTs (See Table 5.1 for their specifications). V90-1.8MW Vestas Dane WT will be installed in Maan-LH candidate site which has 1196m height a.s.l. Also, GE-1.5sle WT will be installed in Ibrahimyya city with 1021 m height a.s.l. Fig. 5.3 and Fig. 5.4 shows the output characteristics for these two WTs modeled three times.

Table 5.1 Specifications considered for two WTs

Parameter	Value	
Model	V90-1.8MW	GE-1.5sle
Rated output	1800 kW	1500 kW
Rated wind speed	12 m/s	14 m/s
Rotor diameter	90 m	90 m
Cut-in wind speed	4 m/s	3.5 m/s
Cut-out wind speed	25 m/s	25 m/s
Hub height	95 m	80 m

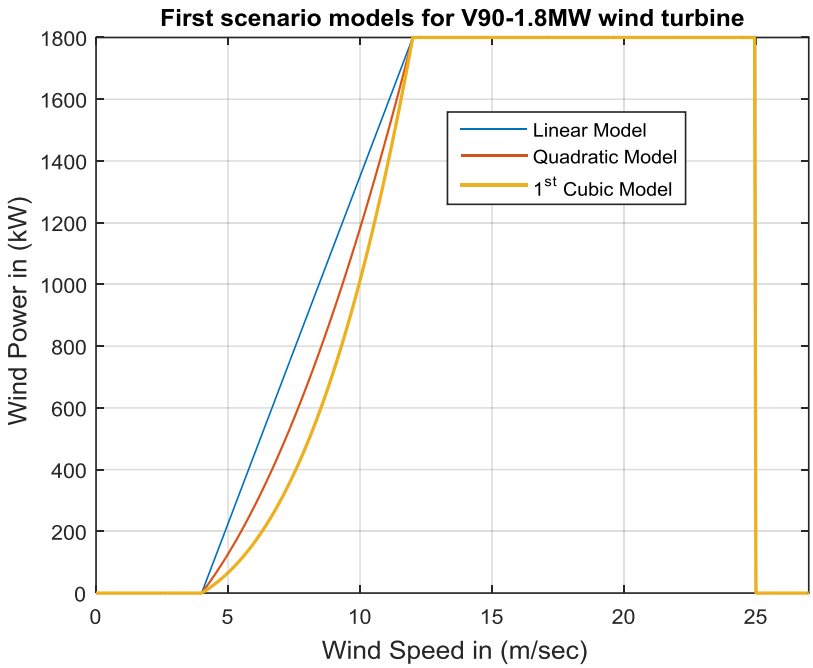

Fig. 5.3 Simplified models for a single V90-1.8MW WT installed in Maan-LH site

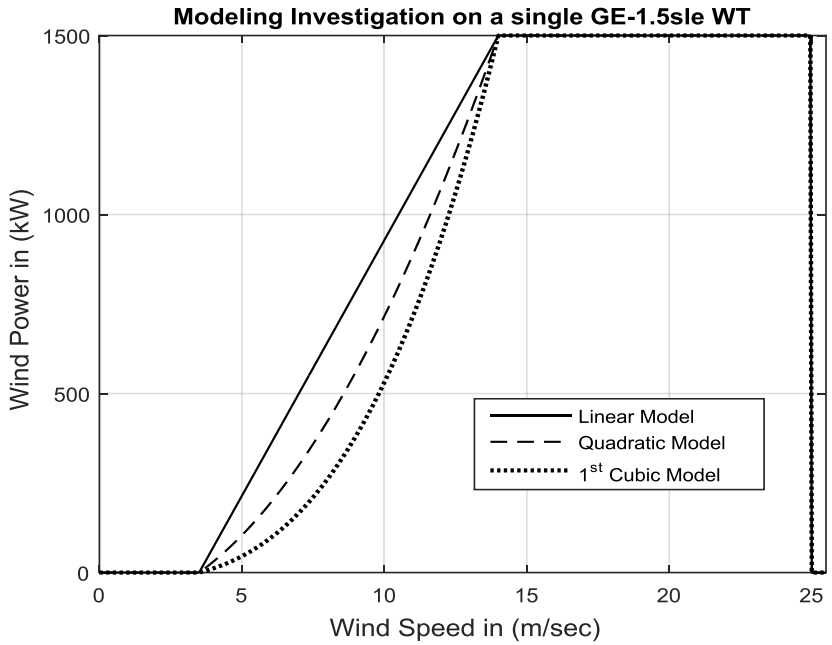

Fig. 5.4 Simplified models for a single GE-1.5sle WT installed in Ibrahimyya city

As you can see that selecting the WT model type in the first scenario will definitely affect the area of the output power of the WT, and this will affect the total wind EEPY from a single WT as well as the whole wind farm for the two cases visualized in Fig. 5.3 and Fig. 5.4.

Table 5.2 EEPY from a single WT unit in Maan-LH and Ibrahimyya cities

WT Model Type	Wind Energy GWh/year		% Energy Decrease from *the 1st cubic model*	
	V90-1.8MW	GE-1.5sle	V90-1.8MW	GE-1.5sle
Linear Model	5.3127	5.2155	30.8563	36.5468
Quadratic Model	4.4051	4.1242	16.6103	19.7566
1st Cubic Model	3.6734	3.3094	0	0

The air density has not been included in the first three methods (Linear Model, Quadratic Model and 1st Cubic Model shown in Table 5.2), which is not correct in most

practical cases. Note that, 1st cubic model is the best to take as a comparison reference, since it is the highest order. Respectively, for the V90-1.8MW and GE-1.5sle WTs: Table 5.2 shows that the EEPY decreases by 30.8563%, 36.5468% and 16.6103%, 19.7566 for the Linear and quadratic models respectively. As a results, the WT has to be modeled very accurate by taking other parameter into account such as the air density.

5.1.6 Investigation of air density modeling

The conditions when the WT is installed in real-world are different than the manufacturers test conditions. At this point, we will test the effect of elevation a.s.l on the WT output power curve and the EEPY from a single WT installed in Ibrahimmya city. Also, the effect of climate parameters will be studied. Note that, these parameters have impact on the WT output power curve as well as the accuracy of air density modeling referring to the ICM built using Equation 5.4. These parameters will be considered to design the wind farm shown in Fig. 1.3 in addition to the wind speed of Maan-LH and Ibrahimyya cities as well as the power coefficient of the two WTs shown in Table 5.2.

5.1.6.1 Effect of city elevation (a.s.l)

The five methods to calculate the air density will be considered and compared in our design tool described by the flow chart in Appendix B. Table 5.3 and Fig. 5.5 below show the candidate cities arranged in ascending order depending on their elevation, and the corresponding air density calculated using Equation 5.9. As the city elevation (a.s.l) increases the values of air density decreases. Let's take the V90-1.8MW WT for instance. This will reduce the area of WT characteristic as shown in Fig. 5.5, which corresponds to a reduction in the wind EEPY.

Table 5.3 Relationship between city elevation and the air density

	Site altitude a.s.l (m)	Air density (kg/m^3)
Aqaba5	139	1.2087
Ramtha-JUST	591	1.1570
UmEjmal-LH	750	1.1392
Alreesha2-LH	876	1.1252
Ibrahimyya	1021	1.1093
Maan-LH	1196	1.0903

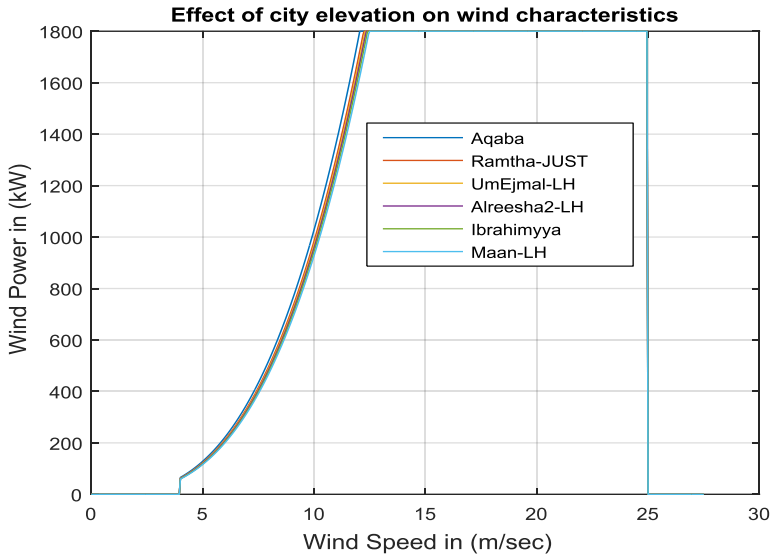

Fig. 5.5 Effect of elevation on V90-1.8MW WT 2nd cubic model characteristics

In the ICM, the actual air density is modeled in five ways. For example, it is computed to be 1.0903 kg/m^3 at 1196m using Equation 5.9 (See Appendix B) and the corresponding wind EEPY is 3.6442 GWh as shown in Fig. 5.6, which is the characteristics for V90-1.8MW turbine installed in Maan-LH site using the ICM. Also, the value of the air density has been considered at sea level, and the corresponding EEPY is 3.9712 GWh. Fig. 5.6 shows the density reduction causes a shift in the rated velocity toward higher values. This leads to 8.23% wind energy reduction.

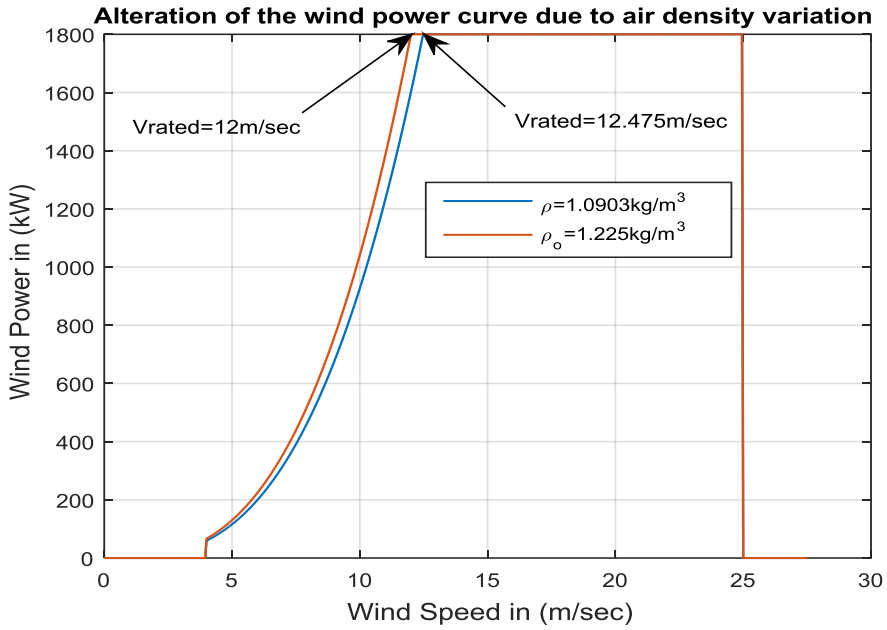

Fig. 5.6 Alteration of the WT power curve due to air density variation

In order to take another case, the EEPY from a single GE1.5sle turbine installed in Ibrahimyya city at its actual elevation (1021 m a.s.l) will be calculated referring to Equation 5.16 derived from Equation 5.4, Equation 5.5 and Equation 5.12 in a case, and at sea level in a second case.

$$P_{WT} = \frac{P_o A v^3 Cp}{2K_g(T_o - LH)} e^{-\frac{gH}{K_g(T_o - LH)}}, \quad v_{ci} < v < v_{rated} \tag{5.16}$$

The air density at the altitude of Ibrahimyya city is computed to be 1.1084 kg/m^3 at 1021m. The corresponding wind EEPY is 3.1873 GWh. This case will be compared to another case when the value of the air density has been assumed to be the one at sea level, where the corresponding wind EEPY is 3.4333 GWh. Fig. 5.7 shows the characteristics for a single GE-1.5sle turbine installed in Ibrahimyya city using the ICM at sea level and at 1021 m (a.s.l). Note that, as the air density is reduced from the value at sea level (1.225

kg/m^3, which is the default value assumed in many literature studies) to the value of (1.1084 kg/m^3) at Ibrahimyya height a.s.l. Fig. 5.7 shows that the rated wind speed is shifted to the right toward higher value of 14.6 m/sec. This causes a 7.1651% reduction in the wind EEPY for only a single WT unit.

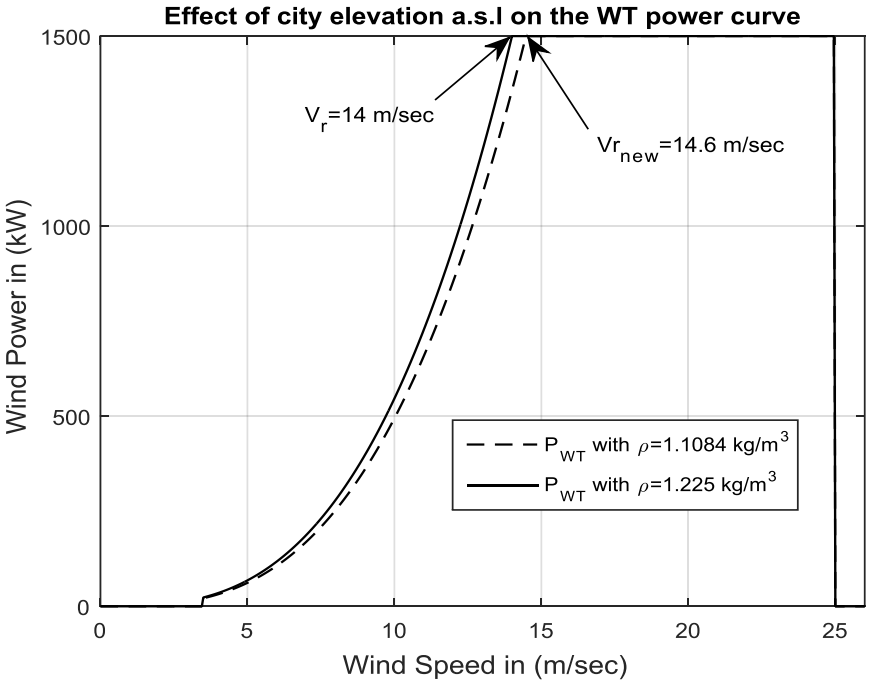

Fig. 5.7 Effect of the city elevation on the WT power curve

The air density slightly affects the WT output power as shown in Fig. 5.7. Its effect on the WT output power is not clear as that of the wind speed, because the dynamic range of the air density is usually small and the WT power is proportional to the cubic value of wind speed [96]. However, the air density influences greatly the EEPY of a WT. There is a percentage error in the estimation of the wind EEPY compared with the actual model at the elevation a.s.l model in Fig. 5.7. This error will be reflected on the cost of the renewable energy system.

5.1.6.2 Effect of temperature variation

Table 5.4 shows the climate effect in terms of the air density model types used in the ICM. Note that, the EEPY is computed at the minimum and maximum temperatures in Jordan which includes Maan-LH location with 1196m height a.s.l. Fig. 5.8 shows that increasing the temperatures from 8.18°C to 26.72°C causes 4.7623% reduction in the wind EEPY. Note that, this percentage is only for a single WT, which means that for a large wind farm, it is very crucial to take the effect of air density into consideration. Note that, the ICM is the one practically, and has acceptable results among other models.

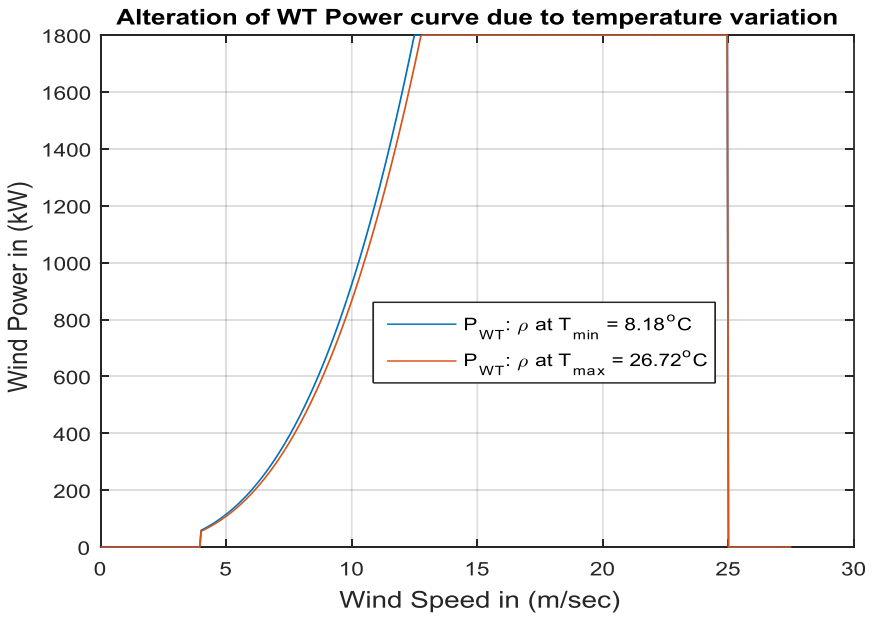

Fig. 5.8 Alteration of WT Power curve due to temperature variation

Table 5.4 Wind energy from a single V90-1.8MW in Maan-LH, at $\boldsymbol{T_{min}} = 8.18°C$, at $\boldsymbol{T_{max}} = 26.72°C$, model C

Air density model	Air density		Annual Wind Energy (GWh)		% Energy Decrease
	At T_{min}	At T_{max}	At T_{min}	At T_{max}	
WT ICM Model C	1.0866	1.0194	3.6348	3.4617	4.7623

Taking GE-1.5sle WT installed in Ibrahimyya as another test case. The hourly temperature values show that maximum temperature value is 26.72°C. So, in the design tool; we include the effect of temperature as discussed before using the ICM with Equation 5.16. Fig. 5.9. Table 5.5 shows that as the temperature increases to the maximum value in Ibrahimyya city, the value of the air density becomes 1.0484 kg/m^3. Comparing with the reference case (of the air density at sea level). This effect causes a reduction of 11.02% in the wind EEPY from a single GE-1.5sle turbine installed in Ibrahimmya city. So, this error percentage in the EEPY will have a considerable impact on the cost of a large-scale wind farm connected to the utility grid. Moreover, an alteration of the WT power curve shown in Fig. 5.9 since the rated wind speed is shifted to the right to 14.75 m/sec.

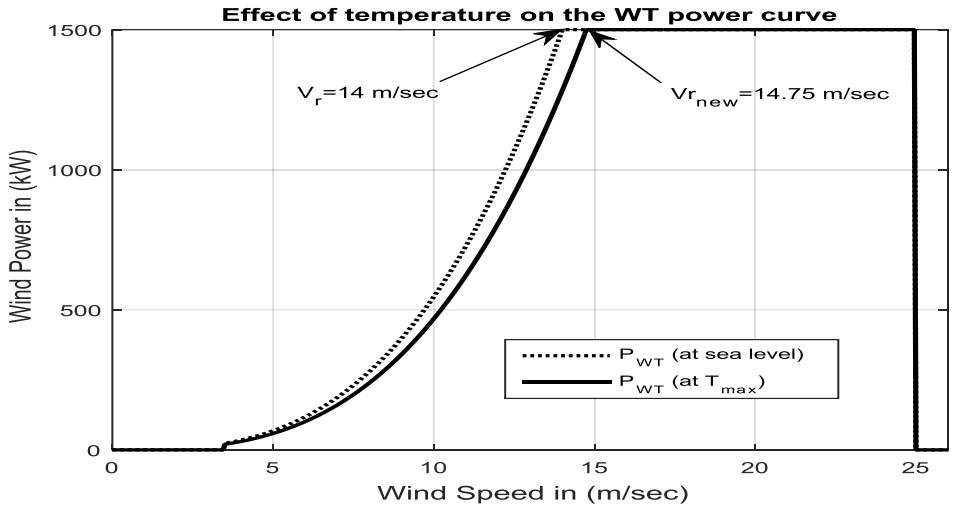

Fig. 5.9 Effect of temperature on the WT power curve

Table 5.5 Temperature effect on a single GE1.5sle installed in Ibrahimyya

Air density (kg/m^3)	At 15°C	1.225
	At T_{max}	1.0484
Annual Wind Energy (GWh)	At 15°C	3.4333
	At T_{max}	3.0549
% Energy Decrease		11.02

From the aforementioned two cases WTs, it can be concluded that ICM is the most accurate one, since it is able to show real effects once the WT is installed in real life. This is crucial to consider, because the conditions when the WT is installed in real-world are different than the manufacturers test conditions.

The effects of modeling the WT or modeling the air density is small on the instantaneous power which may not matter. But, the accurate modeling of the WT has a big difference that should be considered on the wind EEPY. The impact of WT modeling will be investigated in details for a hybrid wind-PV system as well as wind renewable system in Section 5.2 and Section 5.3 respectively.

In reality, the simplified or straightforward three WT models will show deficit in the EEPY which will have to be covered by the conventional power plants of the on-grid system which are more costly than the renewables. Actually, this has the effect of replacing the conventional utility grid and therefore precisely modeling the real-world WT reduce the dependence on the conventional fuel resources.

5.1.7 Investigation of 10 WTs

At this point, Table 5.6 shows a list of ten WTs selected from the main WTs manufacturer of large utility scale systems worldwide [97]. So, these WTs have been considered in our design tool in order to compute the % energy decrease (reference model vs. actual model), then make a comparison to help select the WT to be considered in our multi-point connection problem.

Table 5.6 Ten large-scale WTs

Manufacturer, Country	WT Model	V_{ci} (m/s)	V_r (m/s)	V_{co} (m/s)	$P_{r_{WT}}$ (MW)	D_R (m)	H_h (m)
General Electric, USA	GE-1.5sle	3.5	14	25	1.50	77	65
Vestas, Denmark	V90-1.8MW	4	12	25	1.80	90	95
Enercon, Germany	E-82	2	12.5	34	2.00	82	98
Suzlon, India	S88 - 2.1 MW	4	14	25	2.10	88	100
Nordex, Germany	N-117-gamma	3	12	20	2.40	116.8	120
Gamesa, Spain	G80-2MW	3.5	12	24	2.00	80	78
Mitsubishi, Jaban	MWT-S2000	2.5	13	24	2.00	75	60
Jaban Steel Work, Jaban	J82-2.0	3.5	13	25	2.00	83.3	70
Ecotècnia, Spain	Ecotècnia 74 1.67	3	13	25	1.67	74	70
Repower, Germany	REpower 92-2.05 MW	3	12.5	24	2.05	92.5	100

Where: $P_{r_{WT}}$ is the rated power in W, V_{ci} is the cut-in wind speed in m/sec, V_r is the rated wind speed in m/sec, V_{co} is the cut-out wind speed in m/sec, H_h is the hub height in m and D_R is the rotor diameter in m.

Table 5.7 shows the EEPY from a single WT taking into account the ICM model applied at sea level and using Equation 5.9 for all WTs in Table 5.6. Also, Table 5.7 shows the new value of rated wind speed (See Fig. 5.10), the wind EEPY from a single WT applied in Maan-LH location, and the percentage decrease due to air density variation.

Table 5.7 Alteration of WT curve of all model types
due to ρ variation using model A

WT Type	$\rho_o = 1.225 kg/m^3$ At sea level		$\rho = 1.0903 kg/m^3$ at 1196m		% Energy Decrease
	EEPY (GWh)	V_r (m/sec)	EEPY (GWh)	$V_{r_{new}}$ (m/sec)	
GE-1.5sle	2.0129	14	1.8155	14.5542	9.81
V90-1.8MW	3.9712	12	3.6442	12.4750	8.23
E-82	4.1288	12.5	3.7743	12.9948	8.59
S88 - 2.1 MW	3.2865	14	2.9770	14.5542	9.42
N-117-gamma	5.7272	12	5.2676	12.4750	8.02
G80-2MW	4.1696	12	3.8154	12.4750	8.49
MWT-S2000	3.1754	13	2.8762	13.5146	9.42
J82-2.0	3.3311	13	3.0228	13.5146	9.26
Ecotècnia 74 1.67	2.7940	13	2.5353	13.5146	9.26
REpower 92-2.05 MW	4.2430	12.5	3.8798	12.9948	8.56

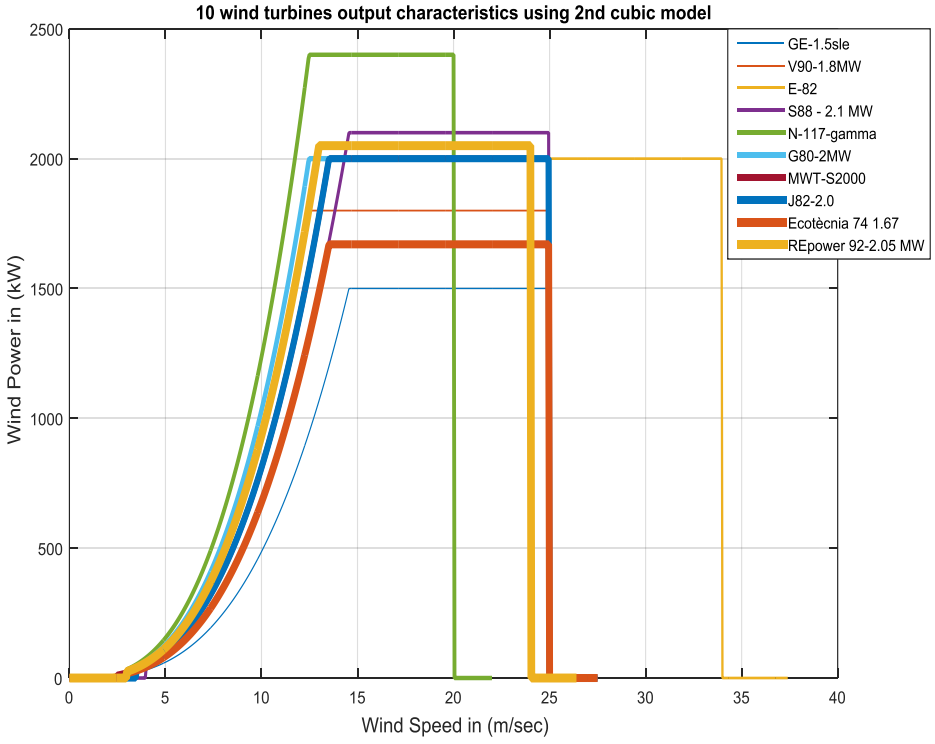

Fig. 5.10 Ten WTs output characteristics using the ICM

Table 5.7 shows the percentage energy decrease is approximately the same between the ten WTs. The difference in percentages is between 0% to 1.79% compared to the highest annual energy percentage decrease. This means that wide variation of WTs manufacturers is not that significant, and any large utility scale WT can be selected as long as we compare the percentage of energy reduction between different manufacturers.

5.1.8 Section summary

In Section 5.1, we have tested the WT modeling as well as air density modeling for two large scale WT units: V90-1.8MW and GE-1.5sle WT. Here in the summary we will talk only about GE-1.5sle WT. It is shown that the model of the WT and the amount of the EEPY obtained are mainly affected by two scenarios: In the accuracy of the WT model, it has been proved for a single GE-1.5sle unit that percentage energy difference from the 1st cubic model is 36.5468% and 19.7566% for the linear and quadratic models, respectively. So, the WT has to be modeled very accurately by taking other parameters into account such as the air density. Studying the accuracy of air density modeling, for a single GE-1.5sle unit installed in Ibrahimyya, shows that the city elevation causes a reduction of 7.1651% compared with the case a.s.l. Furthermore, increasing the temperatures from the one at sea level (15^{o}C) to the maximum value for Ibrahimyya causes 11.02% reduction in EEPY for a single GE-1.5sle WT unit. Moreover, if we compare the percentage of energy reduction between different manufacturers, wide variation of WTs manufacturers is not that important and any large utility scale WT can be selected. Selecting either WT or air density model cause percentage differences in the wind EEPY, which are expected to affect the system component sizing.

Finally, it has been noticed that the effect of selecting the WT model or the air density model has a small effect on the instantaneous power which may not matter, and not that significant. But, they have a considerable difference and effect on the wind EEPY that has an effect on sizing the system as well as replacing the conventional utility grid. This will minimize dependence on the fuel. Thereby, the WT has to be modeled precisely.

5.2 Impact of WT modeling on a hybrid renewable energy system

In this section, we concentrate on the impact of WT modeling on a hybrid wind PV energy system using the WT mathematical models explained in details in Section 5.1. As a matter of fact, most WT manufacturers do not provide all the information needed to get an accurate model for the WT. Actually, most of the literature studies on renewable energy consider a simple output WT characteristic, with manufacturers only given data approximately the same as the ones indicated in Fig. 1.22, without taking into account many parameters that considerably alter the WT power curve. Note that, those parameters have an influence on the installed WT power curve, and affect the EEPY and thereby sizing of the entire system which is expected to satisfy a given load profile. Accurate or appropriate sizing is a critical objective for the electrical system operation as well as the economic aspects of the designed project due to the very high cost of investments [98]. So, accurate mathematical models for the individual system components have to be employed in order to obtain proper sizing results [99].

At this point, the impact of the WT modeling on the hybrid system shown in Fig. 1.3 will be investigated. Ibrahimmya, a city in Jordan, is taken here as a case study with its updated load profile data shown in Fig. 5.11.

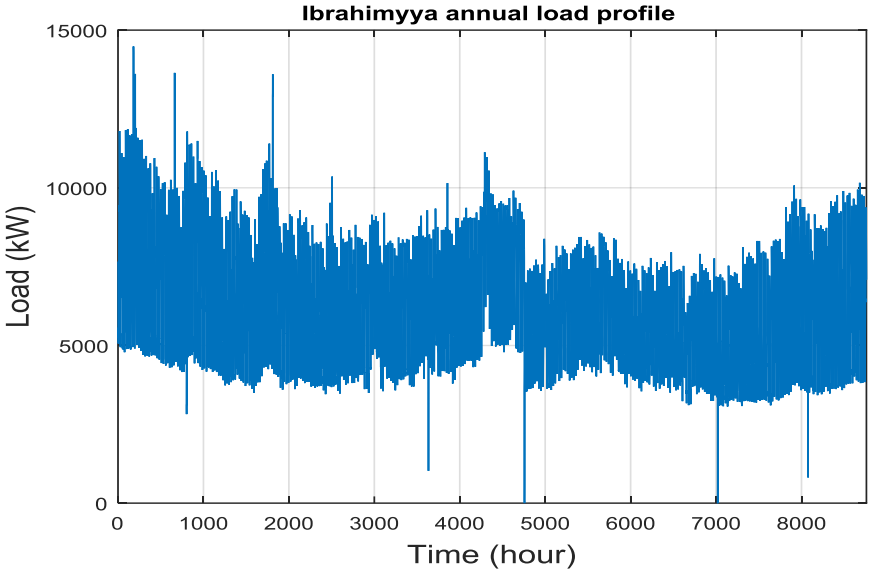

Fig. 5.11 Ibrahimyya load yearly profile in 2015

Thereby, all of the proposed models discussed before will be applied and tested for each WT unit, in the WT farm shown in Fig. 1.3. It is expected that energy difference will affect the size of the wind farm which will be reflected on the size of the entire system, and hence the cost will be changing. This helps in monitoring the WT performance, and sizing of the wind farm, which will significantly affect the EEPY, sizing and the system cost in terms of the NPC as well as the COE. HOMER will be used here in this section, because it is able to solve a single point grid connection problem.

5.2.1 Investigation of the linear model

In this model, each WT in the wind farm shown in Fig. 1.3 is modeled with the linear solid curve shown in Fig 5.4. HOMER shows that the optimal configuration is a wind only grid connected with 68.17% renewable fraction (RF) rather than a hybrid system, and the main screen results are shown in Table 5.8. In HOMER economic point of view, there is no need to use a PV array as well as a converter when using the linear

WT model. Table 5.8 is obtained by building a discounted cash flow that refers all nominal cost values to the present using a discount factor (DF) explained in [50]. Note that, the DF is calculated for 5.88% real interest rate, and each year of the 25 years project life time. The COE (0.0791 $/kWh) is computed by dividing the TAC to the total energy served to Ibrahimyya load shown in Fig. 5.11.

Table 5.8 Optimal size system results for a WT modeled using the linear model

Architecture			
# of WTs	PV array size (kW)	Converter Size (kW)	Annual Energy Grid Purchases (kWh)
10	/	/	19,804,874
Cost			
COE ($/kWh)	NPC ($)	Operating Cost ($)	Initial Capital ($)
0.0791	63,661,020	2,490,117	31,470,000

5.2.2 Investigation of the quadratic model

In this model, each WT in the wind farm shown in Fig. 1.3 is modeled with the dashed curve shown in Fig 5.4. HOMER shows that the optimal configuration is a hybrid wind-PV system with 61.09% RF, and the main screen results are shown in Table 5.9.

Table 5.9 Optimal size system results for a WT modeled using the quadratic model

Architecture			
# of WTs	PV array size (kW)	Converter Size (kW)	Annual Energy Grid Purchases (kWh)
7	4,960	4,340	23,301,602
Cost			
COE ($/kWh)	NPC ($)	Operating Cost ($)	Initial Capital ($)
0.0972	75,298,420	3,070,306	35,607,000

5.2.3 Investigation of the 1st cubic model

Each WT in the wind farm shown in Fig. 1.3 is modeled with the cubic dotted curve shown in Fig 5.4. HOMER shows that the optimal configuration is a hybrid wind-PV system with 48.06% RF, and the main screen results are shown in Table 5.10.

Table 5.10 Optimal size system results for a WT modeled using the 1st cubic model

Architecture			
# of wind turbines	PV array size (kW)	Converter Size (kW)	Annual Energy Grid Purchases (kWh)
5	4,960	4,340	29,762,044
Cost			
COE ($/kWh)	NPC ($)	Operating Cost ($)	Initial Capital ($)
0.1109	82,211,740	4,091,949	29,313,000

5.2.4 Discussion on the simplified WT models

Table 5.8, Table 5.9 and Table 5.10 show that the COE as well as the NPC decrease as the WT model changes from the highest order cubic model toward the linear model. Note that, Table 5.2 shows that the wind EEPY increases from the cubic model passing through the quadratic model toward the linear model. Respectively, Table 5.10, Table 5.9 and Table 5.8 show that the system tends to increase the number of WTs size as a result of the EEPY error estimations calculated before. Referring to the highest order cubic model in Equation 5.3, the COE, the NPC decreased by 12.35%, 8.41% for the quadratic model, and 28.67%, 22.56% for the linear model respectively. Note that, the simplified WT models will not deliver the EEPY theoretically computed because no real parameters have been considered. This will definitely not give the precise sizing solution of the

renewable system, which thereby results a wrong estimate for the project investment. Therefore, the WT has to be modeled very accurate by taking many parameters into account such as the air density.

5.2.5 Impact of air density modeling on a hybrid renewable system

As the ICM shows that the air density affects the output WT power. Thus, the wind EEPY will be considerably affected. In this section, the impact of the air density will be tested by considering the parameters of elevation a.s.l in a case referring to Equation 5.16, and the temperature parameter referring to Equation 5.4 & Equation 5.12 in another case. These two cases will be compared to a reference case when the air density is at sea level as what is assumed in most of the literature studies as shown in [100, 101] for example. So, the design tool will be integrated to HOMER program in order to add and compare the impact of each of these models. Let's see the effect of the air density as the reference case, i.e. when ρ is equal to 1.225 kg/m^3. So, each WT in the wind farm shown in Fig. 1.3 is modeled with the ICM solid curve shown in Fig 5.7. HOMER shows that the optimal configuration is a hybrid wind-PV system with 48.99% RF, and the main screen results are shown in Table 5.11.

Table 5.11 Optimal size system results for a WT modeled at sea level

Architecture			
# of WTs	PV array size (kW)	Converter Size (kW)	Annual Energy Grid Purchases (kWh)
5	4,960	4,340	29,252,304
Cost			
COE ($/kWh)	NPC ($)	Operating Cost ($)	Initial Capital ($)
0.1095	81,259,360	4,018,279	29,313,000

5.2.5.1 Investigation of city elevation

Each WT in the wind farm shown in Fig. 1.3 is modeled with the ICM dashed curve shown in Fig 5.7. HOMER shows that the optimal configuration is a hybrid wind-PV system with 47.41% RF, and the main screen results are shown in Table 5.12. Table 5.12 shows that the size of the hybrid system remains the same with no need to increase the size of the renewable components for economic feasibility and availability purposes. The annual energy purchased from the grid increases by 2.6307%. Fig. 5.12 shows monthly and yearly difference of the energy purchased from the grid referred to the reference model at sea level. The annual energy difference from the grid is 769548 kWh. Nevertheless, note that the reference system, if it is applied in real world, will not be able to maintain the same theoretical energy difference for each month shown in Fig. 5.12. This is because the reference model doesn't consider the real value of elevation a.s.l for Ibrahimyya city.

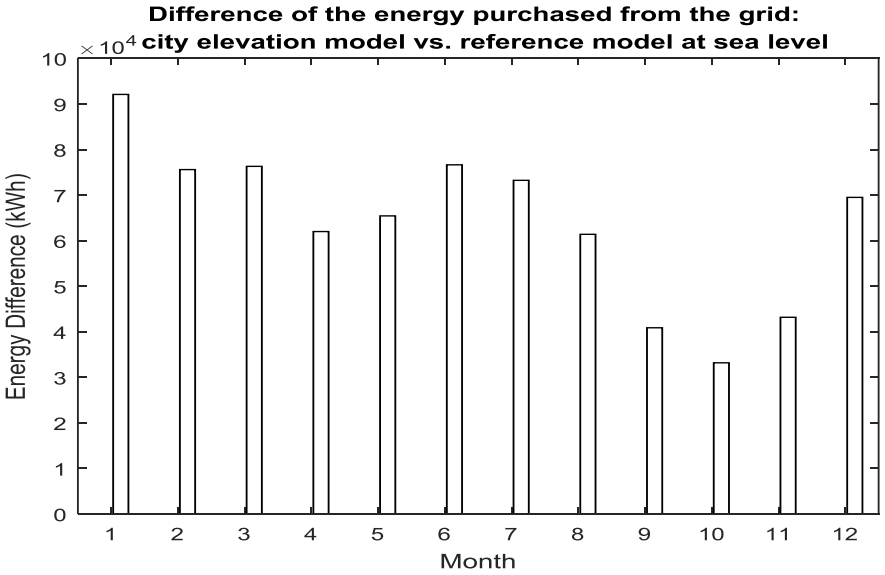

Fig. 5.12 Energy purchased difference from the grid for the elevation model

Table 5.12 Optimal size system for a WT modeled using Equation 5.4 & Equation 5.16

Architecture			
# of WTs	PV array size (kW)	Converter Size (kW)	Annual Energy Grid Purchases (kWh)
5	4,960	4,340	30,021,852
Cost			
COE ($/kWh)	NPC ($)	Operating Cost ($)	Initial Capital ($)
0.1124	82,981,340	4,151,481	29,313,000

The GOC is increased by 3.31%. It is defined as the annualized cost of buying electrical energy from the grid. The estimated COE and the NPC of the reference model in Table 5.11 are 2.158%, 2.075% less than the ones of the actual model in Table 5.12. These error cost estimations of the simplified WT model (with ρ=1.225 kg/m^3) results in sizing and operation inaccuracies for the entire system. In reality, the reference model will not be able to deliver the EEPY theoretically designed. The EEPY deficit will be substituted by the conventional power plants of the on-grid system which are more expensive than renewables. This will definitely affect the decision of the project investments. So, other parameters have to be considered such as the air temperature.

5.2.5.2 Investigation of temperature model

Table 5.13 Optimal size system for a WT modeled using equation 5.4 & equation 5.12

Architecture			
# of WTs	PV array size (kW)	Converter Size (kW)	Annual Energy Grid Purchases (kWh)
5	4,960	4,340	30,440,770
Cost			
COE ($/kWh)	NPC ($)	Operating Cost ($)	Initial Capital ($)
0.1139	83,910,230	4,223,335	29,313,000

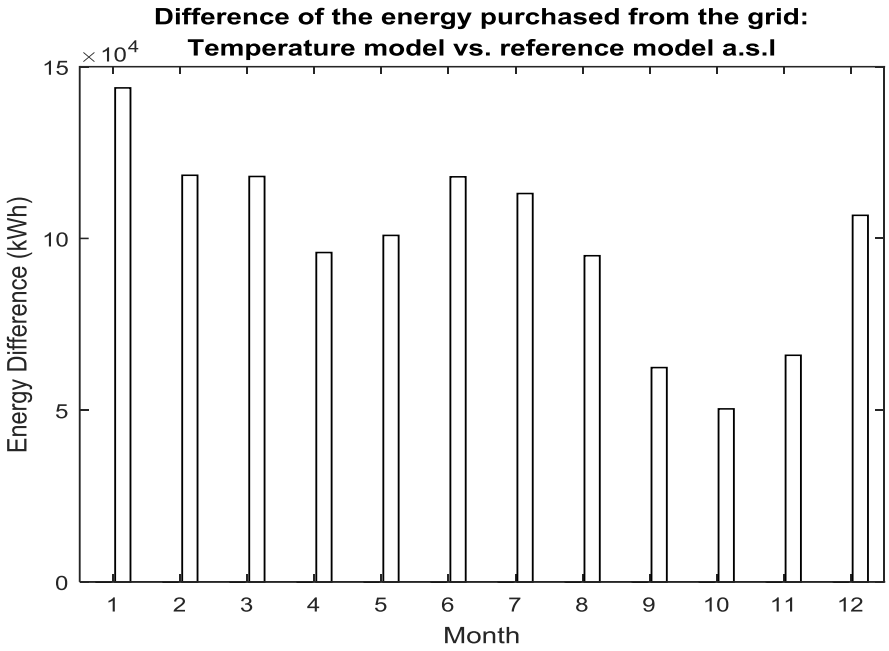

Fig. 5.13 Energy purchased difference from the grid for the temperature model

In this model, each WT in the wind farm shown in Fig. 1.3 is modeled with the improved solid cubic curve shown in Fig 5.9. HOMER shows that the optimal configuration is a hybrid wind-PV system with 46.54% RF.

Table 5.13 shows that the size of the hybrid system doesn't change. The grid energy purchases per year increases by 4.0628%. Fig. 5.13 shows monthly and yearly differences of the energy purchased from the grid for the temperature model referred to the reference model at sea level. The annual grid energy purchase difference is 1,188,466 kWh, which will not be maintained in the real operation since the real temperature is not considered in the reference model. Due to the availability of renewable energy resources and economic purposes, the winning configuration in HOMER purchases from the grid without changing the size of the hybrid renewable energy system as compared with the reference case. Note, that the GOC purchases are increased by 5.10%. Furthermore, Table

5.8 shows that the estimated COE, the NPC is less by 3.863%, 3.159% the actual ones in Table 5.13.

5.2.5.3 An ICM vs. a simple linear model

Let's compare the ICM in section 5.2.5.2 as a reference to the simple linear model in section 5.2.1. For a single unit comparison, the percentage decrease is 41.4265%, which is reflected on the system level shown in Fig. 1.3 that has been changed from a hybrid wind-PV configuration to a wind only configuration. The estimated COE and the NPC of the linear model in Table 5.8 are 30.55%, 24.13% less than the ones of the improved model in Table 5.13.

In other words, the linear WT model and the other simple models, without considering real parameter, have errors estimated in both cost as well as the EEPY and energy purchased compared the configuration designed at the actual value of air density at Ibrahimyya city elevation a.s.l as well as its actual maximum temperature. In other words, in order to solve a real problem, the real values for parameters affecting the WT have to be considered in modeling. Since in reality, the simple WT models show a deficit in delivering energy, and this shortfall of the EEPY will be substituted by the conventional power plants of the on-grid system, which are more costly than the renewables, and thereby has an effect of replacing the conventional utility grid and hence minimize the dependence on the fuel. So, the WT has to be modeled accurately.

5.2.5.4 Section summary

Section 5.2 investigates the impact of the WT modeling on a hybrid wind-PV system installed in a city in Jordan. A closer look is taken at the parameters affecting the

output power to accurately model the system. This helps in monitoring the WT performance, sizing of the wind farm and the entire hybrid system, which will definitely affect the EEPY from a single WT as well as the whole farm. Also, the cost of the hybrid system such as the NPC and the COE will be affected. Six WT models are added to Hybrid Optimization Multiple Energy Resources software in order to see the sizing and cost effects of the new system. A step-by-step analysis and design of each proposed WT model and its effects on the hybrid system are presented. Results show that as the WT simple models change from the cubic, quadratic, toward the linear one, the resulting system has a significant percentage error in the estimation of the cost as well as EEPY. In fact, the difference in the EEPY has to be replaced by the conventional power plants of the on-grid system, which are more costly than the renewables. Also, the number of WTs increases at the system level till it becomes a wind only configuration in the linear model. But, this is at the penalty of the Imprecise sizing solution, which leads to wrong estimates for the project investment. Therefore, the WT has to be modeled accurately by considering many parameters such as the air density, e.g., geographic elevation. The results show that the WT model designed at sea level shows error estimates in both EEPY and the system cost from the one designed at actual temperature or elevation above sea level (a.s.l).

The simple WT models will not deliver the EEPY theoretically computed. This energy deficit will be substituted by the more expensive on-grid conventional power plant fuel energy. In other words, in order to solve a real problem, the real values for parameters affecting the WT model have to be considered. The same procedure can be applied in other locations around the world.

5.3 Impact of WT modeling on a wind energy system

In order to investigate the WT modeling using the models discussed in Section 5.1, Ibrahimmya, is taken again here as a case study with the same load demand given in Fig. 5.11. In this section, we have only a wind only grid connected system as shown in Fig. 5.14 below. In light of the straightforward models and the ICM mentioned in section 5.1, their impacts will be examined here on the wind farm on a system level described in Fig. 5.14.

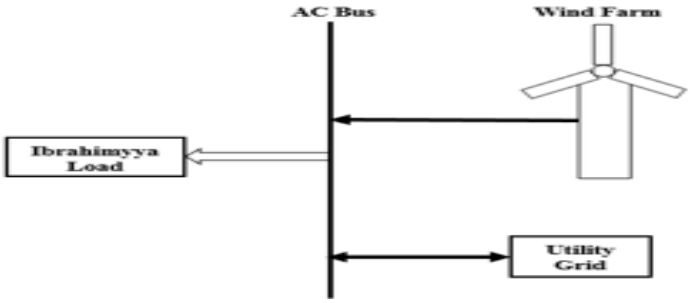

Fig. 5.14 Wind on-grid energy system

5.3.1 Impact of straightforward WT models on a system level

5.3.1.1 Impact of the WT linear model on a system level

The linear solid curve in Fig. 5.4 is employed here to model each WT in the wind farm of Fig. 5.14. HOMER shows that the optimal configuration is an on-grid wind energy system with 68.17% RF, and HOMER main screen results are shown in Table 5.14.

Table 5.14 System results for the linear modeled wind farm

Architecture	# of WTs	10
	Grid Purchases (kWh)	19,804,874
Cost	COE ($/kWh)	0.0791
	NPC ($)	63,661,020
	Operating Cost ($)	2,490,117
	Initial Capital ($)	31,470,000

5.3.1.2 Impact of the WT quadratic model on a system level

The quadratic dashed curve in Fig. 5.4 is used here to model each WT in the wind farm of Fig. 5.14. HOMER shows that the optimal configuration is an on-grid wind energy system with 53.37% RF, and HOMER main screen results are shown in Table 5.15.

Table 5.15 System results for the quadratic modeled wind farm

Architecture	# of WTs	9
	Grid Purchases (kWh)	27,631,836
Cost	COE ($/kWh)	0.1010
	NPC ($)	77,457,750
	Operating Cost ($)	3,800,788
	Initial Capital ($)	28,323,000

5.3.1.3 Impact of the WT straightforward cubic model on a system level

The cubic dotted curve in Fig. 5.4 is employed here for each WT in the wind farm of Fig. 5.14 HOMER shows that the optimal configuration is an on-grid wind energy system with 36.96% RF, and HOMER main screen results are shown in Table 5.16.

Table 5.16 System results for the straightforward cubic modeled wind farm

Architecture	# of WTs	7
	Grid Purchases (kWh)	35,875,560
Cost	COE ($/kWh)	0.1184
	NPC ($)	87,134,160
	Operating Cost ($)	5,036,170
	Initial Capital ($)	22,029,000

5.3.1.4 Discussion on the accuracy of the straightforward WT models

As the WT model changes from the simple cubic model to the quadratic model toward the linear model; the COE as well as the NPC decrease as shown in Table 5.16,

Table 5.15 and Table 5.14 respectively. This is because the wind EEPY increases in the same order for a single WT unit as shown in Table 5.2. As a result, this is reflected here in the system level which tends to increase the number of WTs as consequences of the EEPY error estimations calculated before. The COE, the NPC decreased by 14.696%, 11.105% for the quadratic model, and 33.193%, 26.939% for the linear model respectively. Increasing the number of WTs can be noticed by firstly increasing the initial capital cost (ICC). ICC is defined as is the total installed cost of the component at the onset of the project. Secondly, the reduction of the GOC. GOC is the cost of buying energy from the grid per year. The ICC is increased by 28.571%, 42.857 for the quadratic and the linear models respectively. Whereas, the GOC is decreased by 24.530%, 50.555% for the quadratic as well as the linear models respectively. Note that, the straightforward WT models will not deliver the EEPY theoretically calculated because no real parameters have been considered. Thus, many parameters should be considered such as the air density.

5.3.2 Impact of air density modeling on a wind system

The impact of the air density are examined by testing the elevation a.s.l (Equation 5.16) in a case, and the temperature (Equation 5.17) in another case.

$$P_{WT} = \frac{P_o A v^3 Cp}{2K_g T} e^{-\frac{gH}{RT}}, \quad v_{ci} < v < v_{rated} \tag{5.17}$$

Those two cases will be compared to the reference case when the air density is assumed to be at sea level as what is considered in most of the literature studies as shown in [101] for example. So, this ICM, built in our design tool, is added to HOMER to economically compare it with the reference model as well as the straightforward models.

At the outset, let's see the effects of the reference case, i.e. when ρ is equal to 1.225 kg/m^3. So, each WT in the wind farm shown in Fig. 5.14 is modeled with the solid cubic model displayed in Fig 5.7. HOMER shows that the optimal configuration is an on grid wind energy system with 38.33% renewable fraction, and the main screen results are shown in Table 5.17.

Table 5.17 Wind only system results for a WT modeled at sea level

Architecture	# of WTs	7
	Grid Purchases (kWh)	35,108,672
Cost	COE ($/kWh)	0.1165
	NPC ($)	85,779,190
	Operating Cost ($)	4,931,357
	Initial Capital ($)	22,029,000

5.3.2.1 Impacts of elevation a.s.l on a system level

In this model, each WT in the wind farm shown in Fig. 5.14 is modeled with the ICM dashed curve shown in Fig 5.7, i.e. when the air density get reduced due to Ibrahimyya city elevation a.s.l. HOMER shows that the optimal configuration is a grid connected wind energy system with 35.87% renewable fraction, and the main screen results are shown in Table 5.18.

Table 5.18 Wind only system results for a WT ICM a.s.l

Architecture	# of wind turbines	7
	Grid Purchases (kWh)	36,310,800
Cost	COE ($/kWh)	0.1206
	NPC ($)	88,304,940
	Operating Cost ($)	5,126,734
	Initial Capital ($)	22,029,000

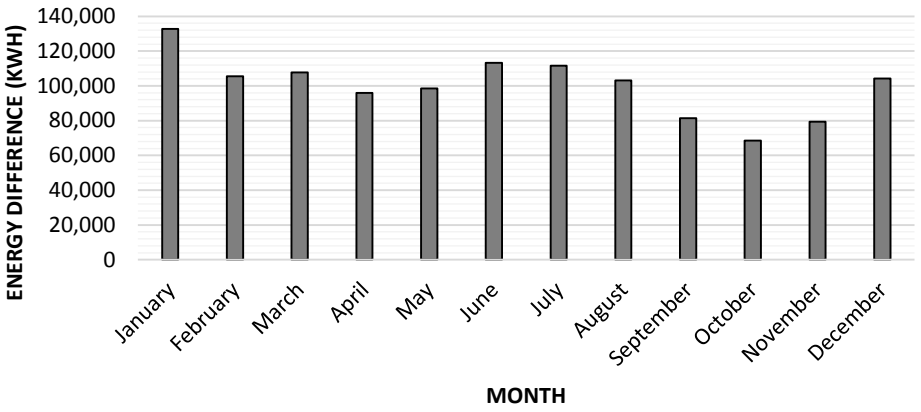

Fig. 5.15 Grid energy purchased difference: city elevation vs. reference models

Table 5.18 shows that the number of WTs remains the system compared with the reference case in Table 5.17 for economic and availability purposes. Fig. 5.15 shows the monthly difference of the energy purchased from the grid referred to the reference model at sea level. The grid energy purchased per year increases by 3.4240%. The annual energy purchase difference is 769,548 kWh, which is the sum for all values in Fig. 5.15. Furthermore, the GOC is increased by 3.9619%, which is the annualized cost of buying electrical energy from the grid. Therewith, the reference system, if it is practically applied, will not be able to maintain the same theoretical energy monthly differences in Fig. 5.15. This is due to ignoring the effect of the real city elevation a.s.l on the air density. If the reference model is employed to model the wind farm in Fig.5.14, the estimated COE, and the NPC in Table 5.17 are 3.3997%, 2.8603% less than that in Table 5.18 respectively. This error estimations of reference WT model (with ρ=1.225 kg/m^3) results in imprecise sizing solutions and operation of the entire system. In fact, the reference model will not be able to deliver the EEPY theoretically designed. The EEPY deficit will be substituted

by the conventional power plants of the on-grid system which are more costly than the wind renewable energy system. This will absolutely affect the decision regarding the project investments. Subsequently, other parameters have to be considered such as the air temperature.

5.3.2.2 Impacts of air temperature on a system level

In this model, each WT in the wind farm shown in Fig. 5.14 is modeled with the solid ICM shown in Fig 5.9. HOMER shows that the optimal configuration is an on-grid wind energy system with 34.52% renewable fraction, and the main screen results are shown in Table 5.19, which shows that the number of WTs don't change from the reference case.

Table 5.19 Wind only system results for a WT ICM at T_{max}

Architecture	# of wind turbines	7
	Grid Purchases (kWh)	36,976,888
Cost	COE ($/kWh)	0.1227
	NPC ($)	89,665,060
	Operating Cost ($)	5,231,946
	Initial Capital ($)	22,029,000

The grid energy purchases per year increases by 5.3212%. Fig. 5.16 shows the monthly difference of the energy purchased from the grid for the temperature model referred to the reference model at sea level.

The GOC purchases are increased by 6.095%. Moreover, Table 5.17 shows that the COE, the NPC 5.0530%, 4.3338% are respectively lower comparing with Table 5.19. The grid energy purchase difference per year is 1,868,216 kWh which will not be

preserved in the real operation since the real temperature is not taken into account in the reference model.

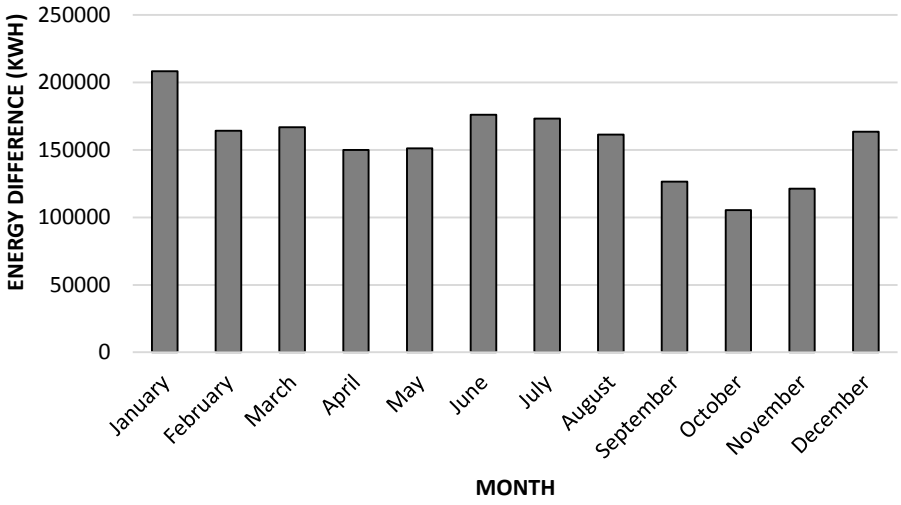

Fig. 5.16 Grid energy purchased difference: Temperature vs. reference models

5.3.2.3 An ICM compared with a linear straightforward model

At this point, the proposed ICM is compared as a reference to the straightforward linear model. For a single WT unit comparison, the percentage error energy is 41.4265%, which is reflected on the system level shown in Fig. 5.14.The estimated COE and the NPC of the linear model in Table 5.14 are 35.53%, 29.00% less than the ones of the ICM in Table 5.19. Strictly speaking, the straight forward models don't consider real parameters, which result in errors estimated in both cost as well as the EEPY and energy purchased compared with the configuration designed at the real value of air density at Ibrahimyya city elevation a.s.l and its real maximum temperature. In other words, in order to solve a real problem, the real values for parameters affecting the WT have to be practically modeled. In fact, the simple WT models show a deficit in delivering energy, and this

shortfall of the EEPY will be replaced by the conventional power plants of the on-grid system, which are more costly than the wind energy, and thus has an effect of replacing the conventional utility grid and hence minimize the dependence on the fuel. In other words, in order to solve a real-world problem, the real values for parameters affecting the WT have to be precisely considered in modeling of the WT.

5.3.2.4 Section summary

This section investigates the influence of the WT modeling on an on-grid wind energy system installed in Ibrahimyya, a city in Jordan. A closer look is taken at parameters affecting the output power for correctly modeling the system. This helps in monitoring the turbine performance, sizing of the wind farm and the entire system, which significantly affect the EEPY from the WTs and the entire system. The NPC, GOC and the COE are affected. As the WT model changes from the linear to quadratic and on to the cubic model the system has progressively more percentage error in the estimation of the cost as well as EEPY, which cannot be neglected. In fact, the EEPY difference has to be supplied by the conventional generation of the utility grid, which is more expensive than wind energy. However, this is the result of imprecise sizing solutions, which result in error estimates for the project investment. So, an ICM is suggested to model the WT precisely by considering more parameters such as the air density. The WT model designed at sea level, shows error estimates in cost and EEPY compared with the ICM. This paper investigates the effects of elevation a.s.l and temperature to model the WT in addition to wind speed and WT power coefficient. Therefore, the simplified WT models will not deliver the EEPY that is theoretically possible. The theoretical reduction in the GOC for

the simplified models will be a practical increase in the real world conditions. This means that the more costly utility conventional fuel plants will have to replace this energy deficit. In other words, to solve a real-world problem, the real values for parameters affecting the WT model must be considered. This same procedure can be applied in any location worldwide.

5.4 Modeling of the PV module

There are many methods to compute the energy of PV systems. In fact, they are much more sophisticated than those of wind systems. Few methods are based on full circuit-based models. Introduction of new equations that require additional measurements, fill factor with datasheet parameters, which requires less data measurements. These are fundamentally the same even if they appear different [83, 102, 103]. Based on the data of global solar radiation incident on the surface of the PV array in kW/m^2 that have been gained for each candidate city in Section 4, the applicable way found to compute the output PV power is by Equation 5.18 [104].

$$Pout_{PV} = Prated_{PV} * \frac{G_I}{Radiation_{STC}} * [1 + (T_C - T_{STC}) \times TC_p] \quad (5.18)$$

Where: G_I is the global solar radiation incident on the surface of the PV array in kW/m^2, TC_p is the maximum power temperature coefficient (given in most PV module datasheets), and T_c is the module cell temperature. Note that, the required data are the temperature, irradiance, and power at STC, i.e. $T_{ambient}$, G_I and $Prated_{PV}$ in Equation 5.18 & Equation 5.19. The PV system is generally rated at STC conditions (25 ℃ and 1000 W/m^2). Note that, the ratio of $\left(\frac{G_I}{Radiation_{STC}}\right)$ is called normalized de-rated radiation.

Practically, the operating conditions may be different, i.e. the temperature could be higher as well as the insolation could be lower. In this case, it is very important to know the PV system operating cell temperature, in order to compute the actual output from the PV system. Furthermore, Nominal operating cell temperature (T_{NOCT}) is defined at specific condition such as: insolation of 800 W/m^2, air temperature of 20℃, and wind velocity of 1 m/sec. Experimentally, it is found that the best formula describes the PV cell temperature (T_c) estimated in Equation 5.19 [105, 106].

$$T_C = T_{ambient} + (T_{NOCT} - 20) \times \frac{G_I}{800} \tag{5.19}$$

Where: $T_{ambient}$ is the ambient temperature in℃.

5.4.1 Incident radiation, temperature & PV output energy in Ma'an

Fig. 5.17 shows the hourly global incident radiation (G_I) in Maan-LH. Also, Fig. 5.18 shows the hourly basis average temperature in Jordan which are taken from NASA Surface meteorology and Solar Energy [107] as recommended by the EC.

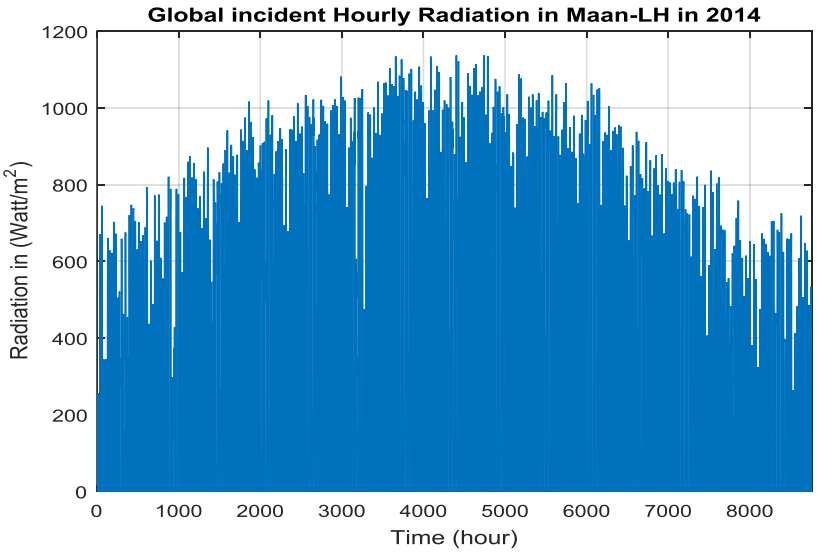

Fig. 5.17 Global hourly incident radiation in Maan-LH

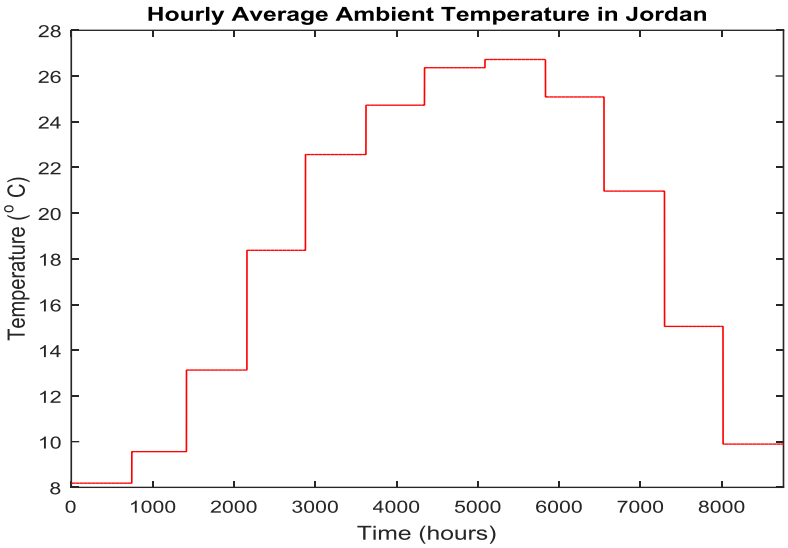

Fig. 5.18 Global hourly basis average temperature in Jordan

Let's take (VBHN240SA11) monocrystalline PV Panel as a case validation with characteristics shown in Table 5.20.

Table 5.20 Specifications considered for (VBHN240SA11) PV panel

$P_{nominal}$ (W)	V_{oc} (V)	I_{sc} (A)	V_{mp} (V)	I_{mp} (A)	TC_p (%/°C)	T_{NOCT} (°C)	η (%)	FF (%)
240	52.4	5.85	43.7	5.51	-0.3	48.3	21.6	78.55

At this point, the part of our design tool described by the flow chart in Appendix D to compute the PV module temperature using equation 5.19. Furthermore, Appendix D shows that the DC output power from a single PV module has been computed using equation 5.18. Appendix D shows the data needed (PV module types and data resources of global incident radiation, ambient temperature and some constant parameters needed to calculate the energy from the PV array. Another input to this file is the inverter efficiency. The inverter efficiency varies in the literature. Typical values are 95.5–98% [108], 92%

[83, 109], but they were not mentioned any details such as whether these are the claimed numbers by the manufacturers or the practical ones. In [110], the inverter efficiency is found to be 86.3% for insolation at sea level, and 81.6% for 1529 kWh/ m^2 radiation level at the site tested. A more recent study, however, also tested practical efficiencies for inverter found that it is around 92% at low irradiance, and it is around 94% at higher irradiance [111]. Thus, in sight of these reviewed papers, it appears that 95% is a very realistic choice to be considered in our multi-point grid connection problem which will affect the solar energy extracted from the PV module.

The inverter efficiency (η_{inv}) should be multiplied by the DC output power of the PV panel, i.e. with η_{inv} =95%. The energy output from (VBHN240SA11) PV module is computed using Equation 5.20 (See Fig. 5.19). The one-hour time step is the time when the incident radiation values were measured.

$$E_{out_{PV}} = Pout_{PV} \times \eta_{inv} \times Time\ Step \tag{5.20}$$

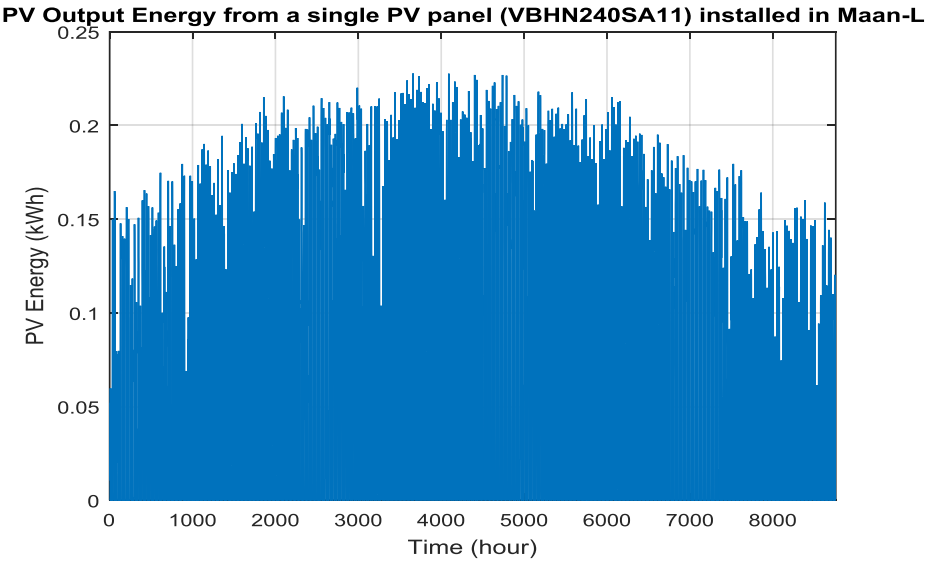

Fig. 5.19 PV output energy from a single PV panel installed in Maan-LH

Fig. 5.19 shows that PV energy is higher in summer than winter. This is because the radiation is higher in the summer and lower in the winter as noticed in Fig. 5.17.

5.4.2 Investigation of 10 PVs

At this point, a list of ten PV modules in Table 5.21 has been considered [72] in order to let our design tool finds the best PV panel to consider in our multi-point connection problem.

Table 5.21 Ten PVs

Manufacturer Part #	$P_{r_{PV}}$ (W)	TC_p (%/°C)	T_{NOCT} (°C)	L_{PV} (m)	W_{PV} (m)	V_{mp} (V)	I_{mp} (A)	V_{oc} (V)	I_{sc} (A)
CS6X-310P	310	-0.43	45	1.954	0.982	36.4	8.52	44.9	9.08
SW 290	290	-0.41	46	1.675	1.001	31.4	9.33	39.9	9.97
Q.PRO BFR-G3 260	260	-0.42	45	1.67	1	30.78	8.53	38.18	9.09
SNPM-GxB-300	300	-0.28	46	1.663	0.99	34.5	8.7	44.9	9.3
VBHN240SA11	240	-0.3	48.3	1.58	0.798	43.7	5.51	52.4	5.85
OPT275-60-4-100	270	-0.42	46	1.652	0.982	31.2	8.68	38.5	9.15
JKM310P-72	310	-0.41	45	1.956	0.992	37	8.38	45.9	8.96
ET-P660260WBAC	260	-0.44	45.3	1.64	0.992	31.48	8.26	38.09	8.84
CS6P-265P	265	-0.43	45	1.638	0.982	30.6	8.66	37.7	9.23
LG315N1C-G4	315	-0.38	46	1.64	1	33.2	9.5	40.6	10.02

Where P_{rPV} is the rated power of the PV module in Watt, TC_p is the temperature coefficient of the maximum power in %/°C, T_{NOCT} is the nominal operating cell temperature in °C, L_{PV} is the length of the PV panel in meter, W_{PV} is the width of the PV panel in meter, V_{mp} is the voltage at maximum power point in V, I_{mp} is the current at maximum power point in A, V_{oc} is the open circuit voltage in V and I_{sc} is the short circuit current in A. Moreover, Table 5.22 shows the EEPY from a single PV module, and the fill factor (FF) shown in Equation 5.21. FF is the ratio of maximum power from the PV cell to the product of open circuit voltage and short circuit current. The FF measures the quality

of the PV module, and helps select the suitable PV panel of high FF value available in the market [112].

$$FF = \frac{V_{mp} I_{mp}}{V_{oc} I_{sc}} \tag{5.21}$$

Table 5.22 EEPY and the FF from a single PV model

PV panel Model	EEPY (kWh)	FF(%)
CS6X-310P	603.1675	76.07
SW 290	564.1182	73.64
Q.PRO BFR-G3 260	506.7621	76.65
SNPM-GxB-300	597.4543	71.88
VBHN240SA11	473.3330	78.55
OPT275-60-4-100	524.2523	76.88
JKM310P-72	605.2653	75.39
ET-P660260WBAC	504.3972	77.22
CS6P-265P	515.6109	76.15
LG315N1C-G4	616.1132	77.53

The (VBHN240SA11) PV module will be considered in finding the solution of the multi-point connection problem in this dissertation, because it has the highest FF (78.55%) compared with other types shown in Table 5.21. Table 5.23 shows results of a single (VBHN240SA11) PV panel installed in each candidate city such as: Annual global radiation and the PV EEPY.

Table 5.23 Results of a single (VBHN240SA11) PV module installed in each site

	Annual global radiation (kWh/m^2/day)	EEPY (kWh)
Ramtha-JUST	5.55	436.2410
Ibrahimyya	5.55	436.2410
UmEjmal-LH	5.76	452.4668
Alreesha2-LH	5.76	452.4668
Maan-LH	6.03	473.3330
Aqaba5	6.12	480.3399

5.5 Utility grid model

The annual system cost of energy (ASCE) is the cost of energy produced by the entire system including the renewable system as well as the utility grid. The ASCE component has been modeled in our design tool following the algorithm shown in Appendix E. Two cases are considered. In the demand satisfied case, the renewable on-grid system, there will be no energy sold back to the grid. Because, the utility grid without renewables is equal to the national load demand. In the demand unsatisfied case, the priority is for renewables to satisfy the national load with LCOE energy price. Then, the energy deficit is substituted by the grid with the utility purchased energy price given in Table 4.9. Moreover, the utility grid purchases have been modeled following the algorithm in Appendix F. In order to test the grid model, trial and error are considered here to have a sense on the ASCE values. Because, the optimal solutions will be discussed and explained later on in Section 7. Table 5.24 shows trial and error results for only WTs test.

Table 5.24 Trial and error grid model results for only WTs (GE-1.5sle) test

# of WT units	ASCE ($/kWh)
1	0.1404
10	0.1404
100	0.1397
1000	0.1332
5000	0.0555

Table 5.24 shows that as the number of WTs increases, the ASCE decreases. When the number of WT units is either 1 or 10, the ASCE is the same as the purchased price (0.1404$/kWh) from the grid. Because the number of WT units are negligible to

have an effect on the ASCE. After that, the ASCE starts decreasing because of the increase in the WTs share of low cost value.

Considering the same number of WT units in case of number of PVs. Table 5.25 shows that the ASCE is the same as the grid purchased price (0.1404$/kWh) from the grid. Because the number of PV modules are negligible to have an effect on the ASCE. So, the PV modules number is taken as a multiple of thousands to affect the ASCE, which increases at a very large number of PV panels for example.

Table 5.25 Trial and error grid model results for only PVs (VBHN240SA11) test

PVs number	ASCE ($/kWh)
1	0.1404
10	0.1404
100	0.1404
1000	0.1404
5000	0.1404
1×10^4	0.1404
10×10^4	0.1404
100×10^4	0.1406
1000×10^4	0.1414

As a results, the trial and errors test of the renewable units on the ASCE shows that the wind energy is expected to have a higher share than the PV energy once the optimal feasible solution is optimized and found in Section 7.

5.6 Footprint of renewable energy generation

Google Earth [113] and Wikimapia [114] websites are used to find, then compute the geographical available and appropriate area in each city from the candidate cities in Jordan that is neither habited and planted, See Table 5.26. This area value for each city

which can't be exceeded once the optimized WTs and PVs are filled in a reasonable order for each city.

Table 5.26 Geographical available area for the candidate cities in Jordan

Candidate Cities	Geographical Available Area (km^2)
Ramtha-JUST	28.3148
UmEjmal-LH	7.3338
Ibrahimyya	3.7637
Alreesha2-LH	470.2879
Maan-LH	83.16
Aqaba5	67.3257

5.6.1 Footprint of wind farm

To compute the area of the entire wind farm, it is very important to specify the clearance spacing between the WTs within the row to be from 3 to 4 times the rotor diameter (RD), and the spacing between the rows of the wind farm to be 10 times (RD) [115]. Fig. 5.20 shows the typical layout of the wind farm as well as each spacing assumed. Each spacing is an important input that is used to mitigate the turbulence due to the rotation of the blades.

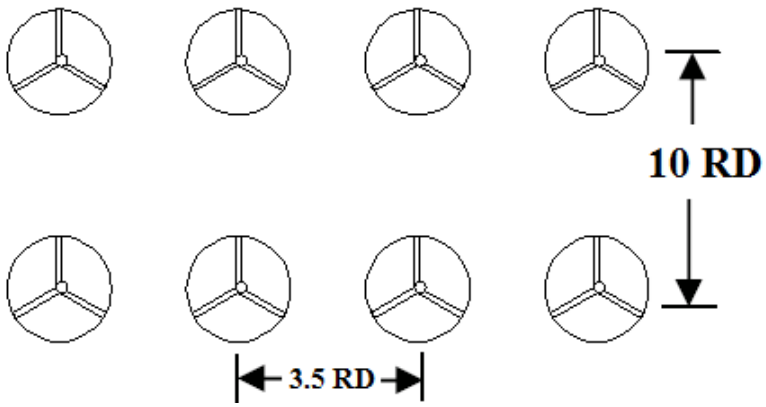

Fig. 5.20 Typical layout spacing of a wind farm

Referring to Fig. 5.20, Equation 5.22 can be applied to compute the minimum area of the wind farm following the flow chart algorithm shown in Appendix G. Where: N_{WT} is the number of WT units and N_{rows} is the number of rows in a rectangular wind farm (i.e. Fig.5.20 shows two rows and four columns).

$$A_{wind\ farm} = RD^2\left[35N_{WT} - 31.5\frac{N_{WT}}{N_{rows}} - 25N_{rows} + 22.5\right] \quad (5.22)$$

5.6.2 Footprint of PV array

Many considerations are considered when calculating the PV array area. For instance, a minimum spacing (d_{min}) between the PV panels should be adhered in order to prevent self-shading [116] as shown in Fig. 5.21. The PV array should be installed at no self-shading on the shortest day of the year. In the Northern hemisphere, December 21st (Winter Solstice) at 12 PM is the time at when the Sun has the minimum elevation angle (α_{min}). At this point, d_{min} should be maintained between PV rows in order to prevent self-shading between PV modules in different rows. So, d_{min} can be calculated using Equation 5.23 for a minimum solar altitude angle (See Equation 5.24 for α_{min} [116]), and PV module tilt angle (β).

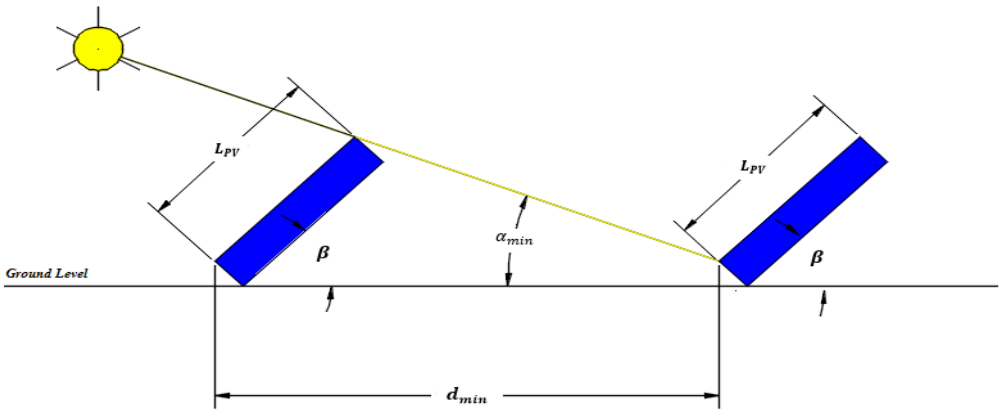

Fig. 5.21 Typical layout spacing of a PV array

$$d_{min} = L_{PV} \frac{\sin(\alpha_{min}+\beta)}{\sin(\alpha_{min})} \quad (5.23)$$

$$\alpha_{min} = 66.6° - \emptyset \quad (5.24)$$

Where $\emptyset$ is the latitude of the location being considered in December 21st at noon. This spacing (d_{min}) is an important value that should be considered to prevent PV modules to shade each other.

Fig. 5.21 is used to compute the area of the whole PV array ($A_{PV\ array}$) as shown in Equation 5.25 following the flow chart algorithm shown in Appendix H.

$$A_{PV\ array} = [(N_{rows} - 1)\, d_{min} + L_{PV}\ cos\beta] \times \frac{W_{PV} N_{PV}}{N_{rows}} \quad (5.25)$$

Where: N_{rows} is the number of rows in the PV array rectangular area ($N_{rows} = 2$ in Fig. 5.21) and N_{PV} is the number of PV panels in the whole PV array.

5.7 System performance indicators

The proper sizing of the components is the key factor to the feasibility of the multi-points grid connection system in order to find the best optimal configuration. The FOM must be clearly defined in terms of the optimization or decision variables. The constraints which govern the FOM should also be clearly defined in terms of the optimization or decision variables. In this case, the system components can be technically sized [1].

There are various system performance indicators, which can evaluate the renewable energy systems in terms of economic feasibility and environmental issues.

5.7.1 The ASCE & the LCOE

The Annual System Cost of Energy (ASCE) is the cost of energy produced by the on-grid renewable energy system as shown in Equation 5.26. Appendix E shows the

algorithm used to compute the ASCE. As a matter of fact, the ASCE is our single FOM that will be optimized using the GA in Section 7.

$$ASCE = \frac{Annal\ System\ Cost\ (\$)}{Total\ Energy\ served\ to\ the\ national\ load\ (kWh)} \tag{5.26}$$

Another system performance indicator is the Levelized Cost of Energy (LCOE) described in Equation 5.27. It is the cost of energy produced by renewables.

$$LCOE = \frac{TAC\ (\$)}{Energy\ Production\ (kWh)} \tag{5.27}$$

LCOE is defined as the total annualized cost (TAC) of the energy produced by the renewable energy components. The TAC in Equation 5.28 is the annualized value of the total net present cost (TNPC). So, a series of future payments are discounted to the present to reflect the time value of the money. TNPC is the present value of all costs incur during the project life time (such as: CC, OMC, RC) minus the salvage costs (SC). Note that, these calculations are performed annually.

$$TAC = CRF(t_{Project}, i) \times Total_{NPC} \tag{5.28}$$

Where CRF in Equation 5.29 is Capital Recovery Factor that is used to calculate the present value of an annuity that are series of equal annual cash flows [117].

$$CRF(i, N) = \frac{\mathrm{i}(1+\mathrm{i})^{\mathrm{N}}}{(1+\mathrm{i})^{\mathrm{N}}-1} \tag{5.29}$$

Where: N is the project life time. Note that, many finance rates are used in economic calculations. The nominal interest rate (i'), which is the percentage that the lender puts on the borrower when lending the money. The escalation rate is used to represent the rise in the prices for specific goods or commodities, and this rate is not commonly used if the problem is generally solved and not specific. The inflation (f),

which is used to represent the rise in the prices for goods or commodities in general. The real interest rate (i) includes both nominal interest rate (i') as well as the inflation rate (f). Approximately, the real interest rate (i) is estimated by Equation 5.30, and exactly given by Fisher equation [118, 119] as shown in Equation 5.31.

$$i \cong i' - f \tag{5.30}$$

$$i = \frac{i'-f}{1+f} \tag{5.31}$$

Where i' is the nominal interest rate (the rate at which you could borrow money), f is the inflation rate. Usually, i' is greater than f when the lender agrees to give the the money to the borrower. For example *(TAC, CRF)*: If a loan of 1000$ is taken from the bank to be paid in 5 years, with a real interest rate of 7%. Then, CRF is calculated to be 0.2439 using Equation 5.29. This means 5 yearly payments of a TAC of 243.9$ (CRF*Present Value=0.2349*1000) should be paid to meet the present value of 1000$ taken from the bank.

As we all know that the renewable energy projects are designed for a specific period of time ends in the future. Note that, the time value of money will differ at the end of that project, which could be less or more than the money value at the beginning of the project. But, as we all know that the design decision should be made before the real implementation of the system. So, a method called discounted cash flow (DCF) is used to compute the cost of renewable energy technologies which includes some parameters such as the CRF and the discount factor in order to take into account the time value of the money [120].

For example (Time value of Money, Present Value): For an interest rate of 6%. If you have the option to receive 1000$ in 12 years, or 400$ right now. Which option you will choose, and why? Since, we live in the present, let's calculate the present value (PV) for a future or final value (FV) of 1000$ paid in 12 years using Equation 5.32.

$$PV = \frac{FV}{(1+i)^N} \tag{5.32}$$

In this case the present value is 496.97$. Thereby, it is better to wait till getting 1000$ which is worthy more than the first option of 400$. At this point, we can determine a factor which proves that a dollar now is worthy more than a dollar in the future. It is the discount factor (DF) which is defined using Equation 5.33 in terms of the interest rate and the time.

$$DF = \frac{1}{(1+i)^N} \tag{5.33}$$

For the same example above, DF=0.497 → 1000$ in year 12 is equivalent to 497$ (DF*Future Value) in year 0. In other words, 497$ right now is worth 1000$ in 12 years. This is a demonstration of the time value of money that a dollar now is worthy more than a dollar twelve years in the future. At this point, let's see some practical examples to clarify these concepts.

5.7.2 Salvage & replacement costs

The salvage value is the cost of any component in the multi-point connection system at the end of the project lifetime. The cost of each component in the system is assumed to be linearly depreciated. In other words, the salvage cost (SC) has a direct relationship to the replacement cost (RC) as well as to the remaining life time of the

component with respect to its manufacturer life time. There are three steps to calculate the SC. First, you need to calculate how many times (n) does the component (WT, PV or converter) has been replaced with respect to the project life time, see Equation 5.34.

$$n = \frac{t_{project}}{t_{component}} \tag{5.34}$$

Then, calculating the remaining time of the component by multiplying the ceiling value of (n) with the component life time. Afterwards, you need to subtract this value from the project life time in order to know the remaining time of the component before or after the end the project lifetime as shown in Equation 5.35. So, the SC is calculated using Equation 5.36, which can be simplified to Equation 5.37 which will be used in the part of our design tool updated in Appendix J.

$$t_{remaining} = ceiling[n] \times t_{component} - t_{project} \tag{5.35}$$

$$SC = \frac{RC(Ceiling[n] \times t_{component} - t_{project})}{t_{component}} \tag{5.36}$$

$$SC = RC(ceiling[n] - n) \tag{5.37}$$

5.7.3 Clarification example

At this point, let's use Microsoft Excel to construct the nominal and discounted cash flows. Then, calculate the total net present cost for many cases. For example, let's take V90-1.8MW wind turbine with a CC of $3,776,400 calculated based on the assumed ratio of 2098$/kW, a lifetime of 20 years, and an OMC of $ 37,764 per year. What is the TAC over a 25-year project lifetime at nominal interest rate of 8% and inflation rate of 2%?

5.7.3.1 1st case: Single WT /ignoring SC & RC

For simplicity, in this case let's ignore the RC and SC for the clarification example in Section 5.7.3. i is calculated using Equation 5.31 to be 5.88%. The CRF over 25 years with an annual real interest rate of 5.88% is calculated using Equation 5.29 to be 7.73%. As we know that the TAC is the annualized value of the total NPC. So, to find the NPC, we need to calculate the DCF by referring the nominal cash flow (NCF) to the present (year 0). The NCF and the DCF over the 25-year project life time are shown in Table 5.27, Fig. 5.22 and Fig. 5.23.

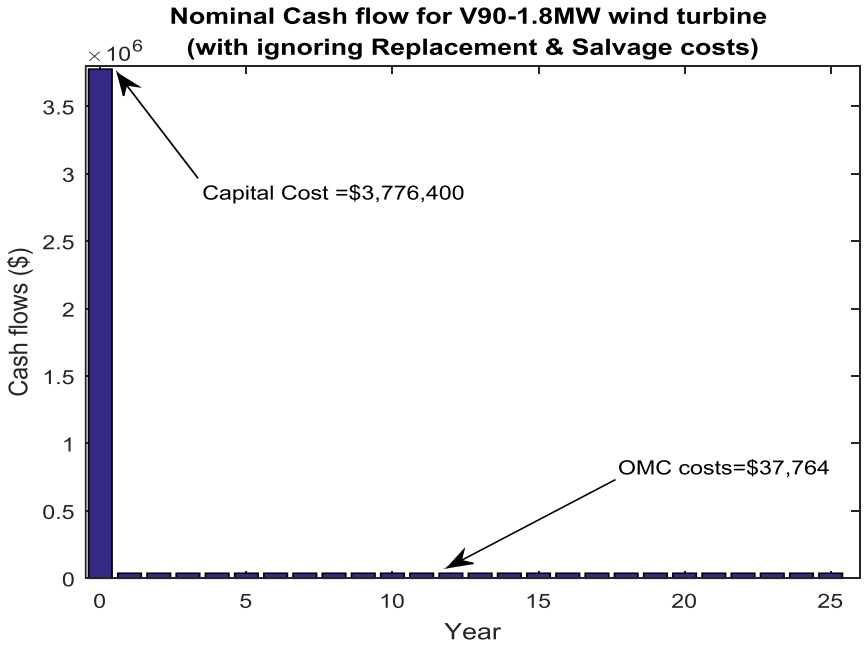

Fig. 5.22 NCF for V90-1.8MW WT with ignoring RC & SC

Note the time value of money in Fig. 5.22. For example, the OMC which will be paid in 25 years is worthy less at the present as shown in Fig. 5.23. In other words, the NCF is called the future cash flow, and the DCF can be called the present cash flow. At

this point, a part of our design tool, described by the flow chart in Appendix I, has been written to implement the LCOE function for given types of WT as well as PV module. Running this part of our design tool shows that the total NPC is (4.265435524728e+06$), which is the same as what we got in Table 5.26.

Table 5.27 NCF & DCF for a single V90-1.8MW WT during the project life time

Year	Discount Factor	Cost Type	NCF (FV at each year)	DCF (PV at each year)
0	1	CC ($)	3776400	3776400
1	0.944444444	OMC ($/year)	37764	35666
2	0.891975309		37764	33684.56
3	0.842421125		37764	31813.19
4	0.795619951		37764	30045.79
5	0.751418843		37764	28376.58
6	0.709673352		37764	26800.1
7	0.670247054		37764	25311.21
8	0.633011107		37764	23905.03
9	0.597843823		37764	22576.97
10	0.564630277		37764	21322.7
11	0.533261929		37764	20138.1
12	0.503636266		37764	19019.32
13	0.475656473		37764	17962.69
14	0.449231114		37764	16964.76
15	0.42427383		37764	16022.28
16	0.400703061		37764	15132.15
17	0.37844178		37764	14291.48
18	0.357417237		37764	13497.5
19	0.337560724		37764	12747.64
20	0.31880735		37764	12039.44
21	0.301095831		37764	11370.58
22	0.284368285		37764	10738.88
23	0.268570046		37764	10142.28
24	0.253649488		37764	9578.819
25	0.23955785		37764	9046.663
Total NPC ($)				4264594.735

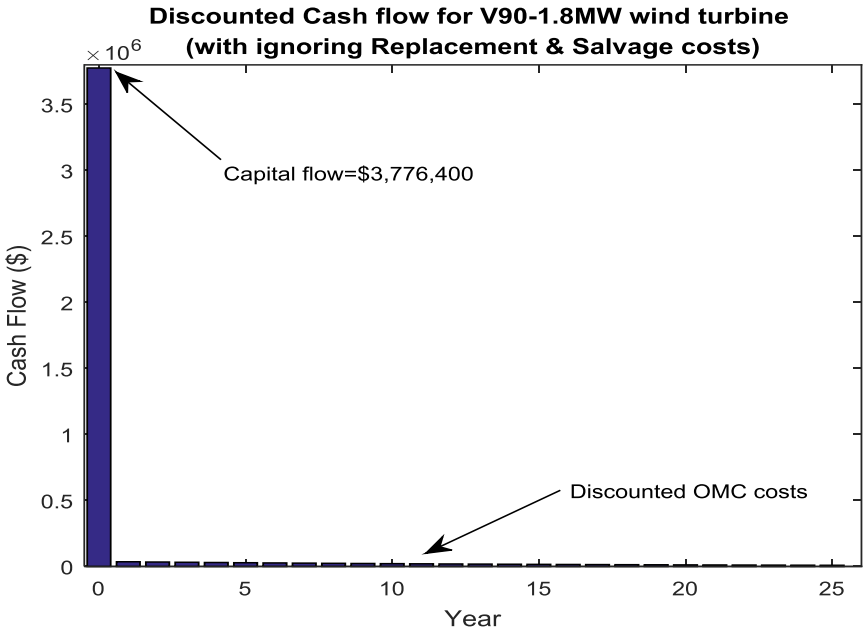

Fig. 5.23 DCF for V90-1.8MW WT with ignoring RC & SC

5.7.3.2 2nd case: Single WT/including SC & RC

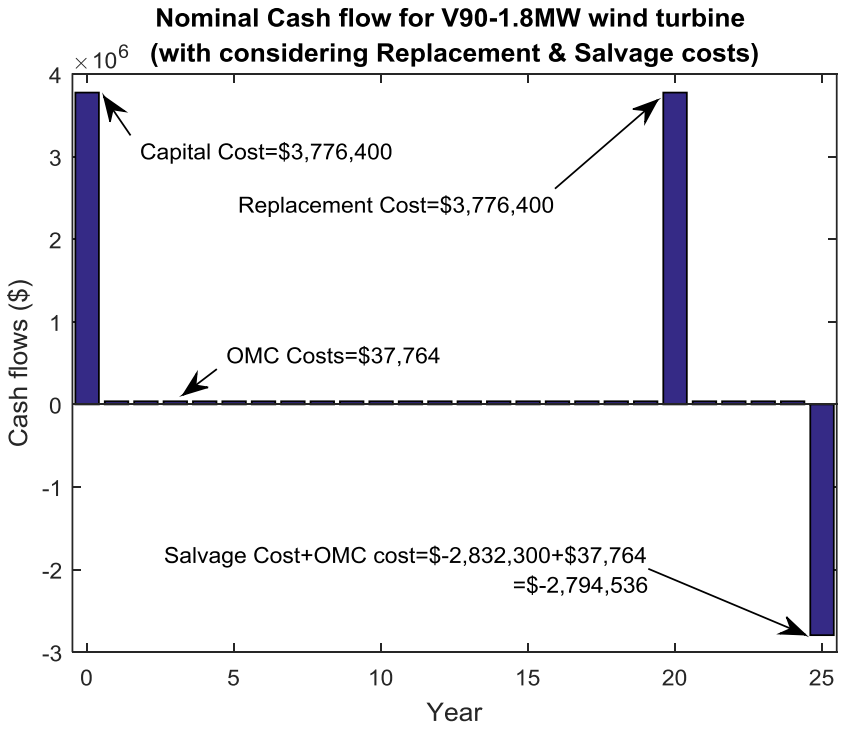

Fig. 5.24 NCF for V90-1.8MW WT with including SC & RC

Table 5.28 NCF for a single V90-1.8MW WT during the project lifetime

Nominal Cash Flows					
Year	Capital Cost ($)	Replacement Cost ($)	Salvage Cost ($)	OMC Cost ($)	Total Cost ($)
0	3,776,400				3,776,400
1				37,764	37,764
2				37,764	37,764
3				37,764	37,764
4				37,764	37,764
5				37,764	37,764
6				37,764	37,764
7				37,764	37,764
8				37,764	37,764
9				37,764	37,764
10				37,764	37,764
11				37,764	37,764
12				37,764	37,764
13				37,764	37,764
14				37,764	37,764
15				37,764	37,764
16				37,764	37,764
17				37,764	37,764
18				37,764	37,764
19				37,764	37,764
20		3776400			3,776,400
21				37,764	37,764
22				37,764	37,764
23				37,764	37,764
24				37,764	37,764
25			-2,832,300	37,764	-2,794,536

Right now, let's repeat the same example in Section 5.7.3, but with taking into account the RC and SC of the same WT. In this case, the NCF and DCF will be modified as shown in Table 5.28. SC is calculated using Equation 5.37 to be $2,832,300 for a RC that is equal to the CC of $3,776,400. But, since the SC is a revenue, it has been assigned a negative value in order to distinguish between the positive values of other payments. Note that, there will be no OMC costs at the CC as well as at the RC. The NCF is described

by Table 5.27 and Fig. 5.24. The DCF is described by Table 5.29 and Fig. 5.25. At this point, running the part of our design tool written to implement the LCOE function for a V90-1.8MW turbine shows that the total NPC is (4.778e+06$), which is the same as what we got in Table 5.29.

Table 5.29 DCF for a single V90-1.8MW WT during the project life time

Discounted Cash Flows						
Year	Discount Factor	Capital	Replacement	Salvage	O&M	Total
0	1	3,776,400				3776400
1	0.944444444				35666	35666
2	0.891975309				33685	33685
3	0.842421125				31813	31813
4	0.795619951				30046	30046
5	0.751418843				28377	28377
6	0.709673352				26800	26800
7	0.670247054				25311	25311
8	0.633011107				23905	23905
9	0.597843823				22577	22577
10	0.564630277				21323	21323
11	0.533261929				20138	20138
12	0.503636266				19019	19019
13	0.475656473				17963	17963
14	0.449231114				16965	16965
15	0.42427383				16022	16022
16	0.400703061				15132	15132
17	0.37844178				14292	14291
18	0.357417237				13498	13498
19	0.337560724				12748	12748
20	0.31880735		1203944			1203944
21	0.301095831				11371	11371
22	0.284368285				10739	10739
23	0.268570046				10142	10142
24	0.253649488				9579	9579
25	0.23955785			-678500	9047	-669453
Total NPC						4,778,001

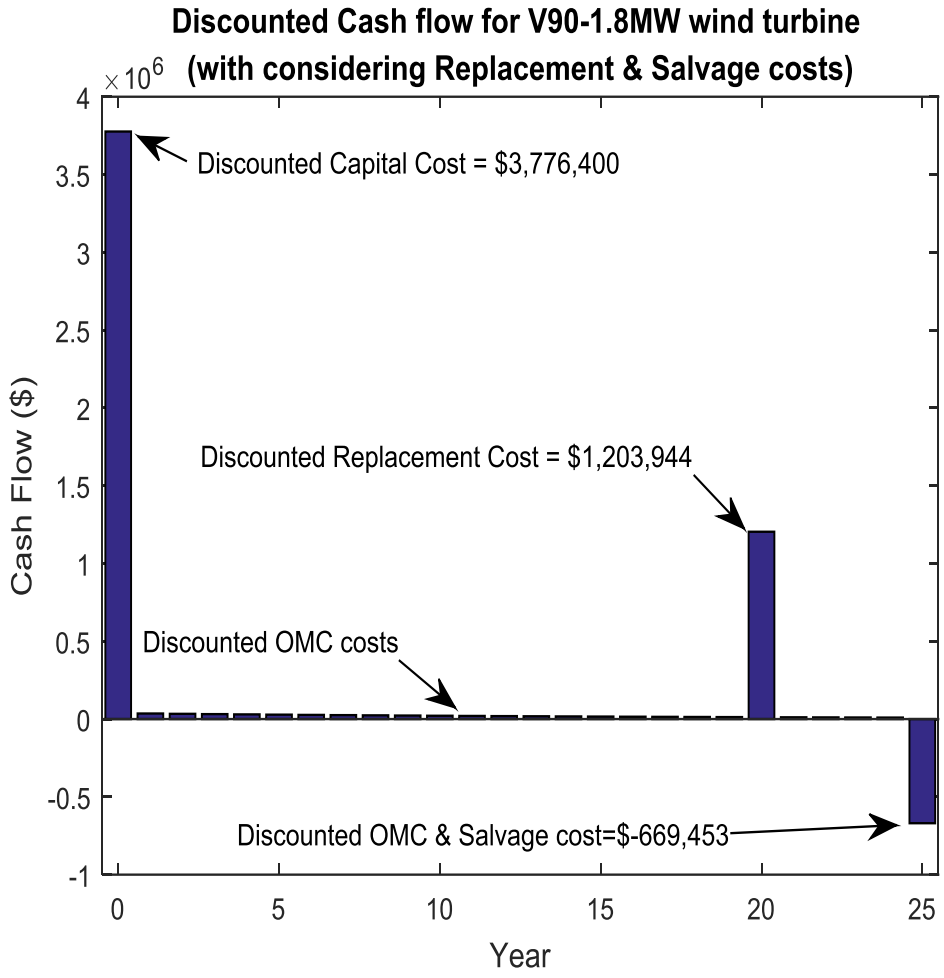

Fig. 5.25 DCF for V90-1.8MW WT with including SC & RC

5.7.3.3 3rd case: System/single unit each/including SC&RC

Right now, let's repeat the same example in Section 5.7.3, but with taking into account the RC & SC. After making sure that our design tool is working properly, let's repeat the same procedure for the whole system which includes a single "V90-1.8MW" turbine and its converter, a single "SW 290" PV panel with its converter. The NCF and the DCF flows are shown in Fig. 5.26 and Fig. 5.27 respectively. It is found that the total NPC is (4.9650e+06$) for the cost values in Fig. 27.

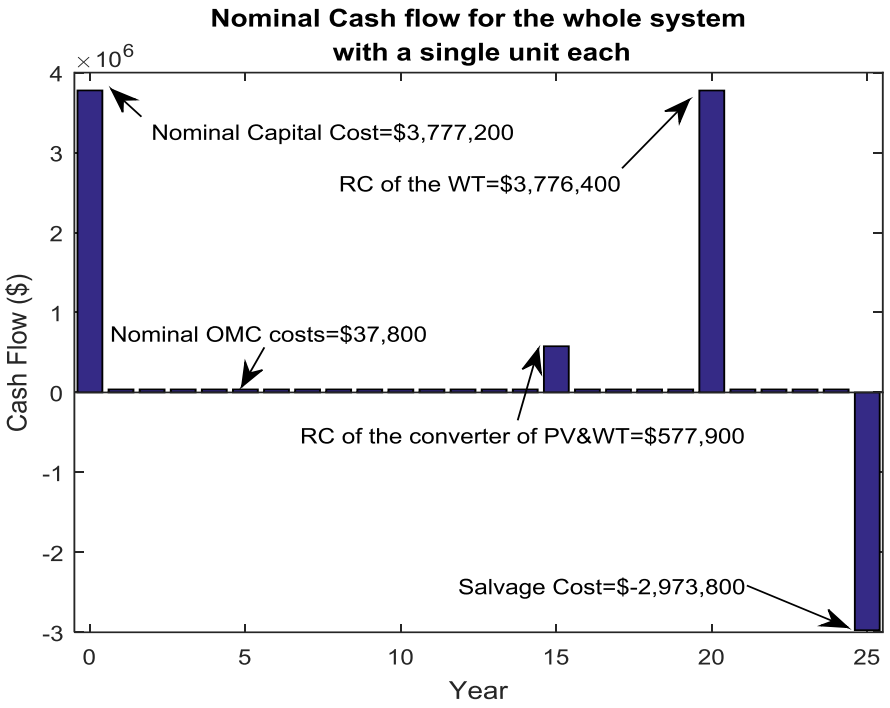

Fig. 5.26 NCF for the entire system with a single unit each

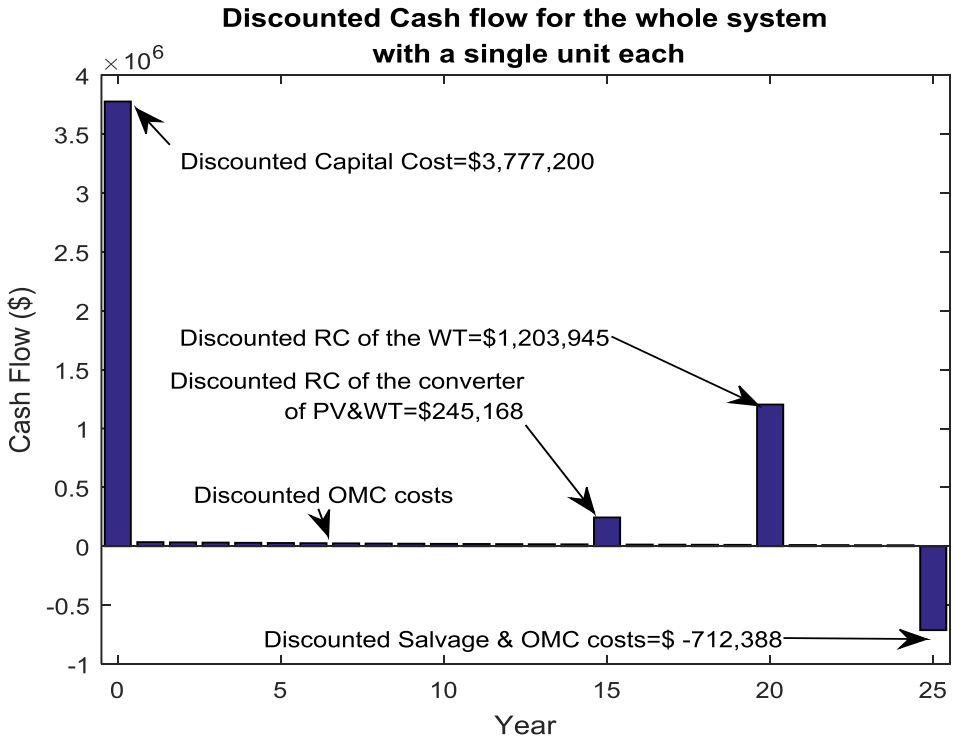

Fig. 5.27 DCF for the entire system with a single unit each

5.7.4 Annual CO_2 emission indicator (AEI)

Again, as mentioned before in Section 1.3 that the Carbon dioxide (CO_2) causes the major detrimental impact on the environmental system. Fig. 1.5 shows that the CO_2 impact constitutes 76% of the global GHG compared with the other greenhouse gases. So, in this dissertation, the annual CO_2 emission indicator (AEI) is modeled in our design tool to indicate the quantity of CO_2 thrown into the atmosphere per year. It is the result of each unit of electricity purchased from the utility grid in case if the renewable energy system is not able to satisfy the national load demand. In other word, the AEI is computed by multiplying the CO_2 Emission Factor (EF in $kgCO_2/kWh$) by the total energy purchased from the grid (E_{grid}) per year as shown in Equation 5.38. The algorithm to compute the annual energy purchased is explained in Appendix F. So, the AEI is measured in MegatonneCO_2/year in this dissertation. In case of Jordan as a validation case, the EF is 0.580548 $kgCO_2/kWh$ in Jordan in 2009, after reviewing many emission reports and standards in [121-123].

$$AEI = EF \times E_{grid} \tag{5.38}$$

5.7.5 Level of autonomy (LOA)

The Level of autonomy (LOA) is defined as the fraction of time when the load is met [1, 124] by the renewable energy system. It is mathematically described by equation 5.39.

$$LOA = 1 - \frac{T_{ns}}{T_{total}} \tag{5.39}$$

Where: T_{ns} is the time in hour when the load has not been satisfied and T_{total} is the total time in hour, i.e. 8760 hour in our case.

Many results come out after testing the LOA for many cases. First, when we have a single unit hybrid system (i.e only one WT (V90-1.8MW) and one PV panel (SW-290W). The LOA is zero, and it is expected since the Jordan hourly load values are much higher than the size of single units' hybrid system. Second, the number of WTs shows a quite effect on the value of the LOA rather the number of PV panels. This was expected since the WT size is in MW scale and the PV panel size is in Watt scale. Third, adding different sizes by trial and error for only WT in a case and only PV in another case. So, randomly increasing the WT number shows a zero LOA values, till the number of WTs reach 733 which shows the first non-zero LOA value of 0.0114%. Doing the same for the PV shows that the first non-zero value of the LOA of 0.0114% happens when the number of PV panels is 6.99×10^{6}. This means that 733 WTs (V90-1.8MW) is equivalent to approximately 7 million PV panels (SW-290W) in terms of the LOA comparison. Fourth, the complementary nature has been verified when testing the LOA of a wind only system. The LOA has a constant a value of 74.2808% for equal or greater that a number of WT of 46546 units. It was concluded that the LOA can only be above 74.2808% by adding PV panels. However, It may be not appropriate for the LOA to be applied for Jordan problem. LOA is good to apply as a FOM for cases like Germany who will be 100% renewable in 2050.

So, LOA is not suitable to apply for cases like Jordan. Because the FOM in our problem is the ASCE not LOA. Also, LOA may not be suitable to use as constraint too in cases like Jordan. Since in Jordan case, we don't care about the availability of the renewables, but we do care about the ASCE.

5.7.6 Renewable penetration (RP)

The RP in Equation 5.40 is the fraction of the renewable energy produced (E_{ren}) to the total energy produced (E_{tot}).

$$RP = \frac{E_{ren}}{E_{tot}} \tag{5.40}$$

RP is modeled in our dissertation to express the amount of the produced renewable energy as explained in Appendix K. It will be used in Section 7 as a FOM in a MFOM optimization problem to see various trade-off relationships with other FOMs such as the LCOE and the AEI. In other words, it can be called an environmental impact indicator. In our problem, the E_{ren} is produced by the wind and PV energies in kWh. The E_{tot} is the total energy in kWh produced by the renewables as well as the utility grid.

The flow chart algorithm in Appendix K shows that RP is to be computed for two cases of the load demand. First, when the demand is satisfied when there is only a renewable generation with no grid share. Second, when the demand is unsatisfied when there is a renewable generation plus a grid energy purchases equals the demand energy minus the renewable generation.

In order to test the *RP* model, trial and error is considered here for the time being here to have a sense on the *RP* range values. So, trial and error results shows that the RP ranges between 0% (for very small number of renewable units) to 100% (for very large number of renewable units).

6. OVERVIEW OF GENETIC ALGORITHMS

In 1975, John Holland (February 2nd, 1929 – August 9th, 2015) presented the genetic algorithm (GA) to describe the biological evolution and to give theoretical framework to be adapted under GA [125]. GA is one of the artificial intelligence techniques (AIT) that is recommended to converge toward the optimal solution in case of complex real-world problems. In the GA, each solution represents a chromosome in the natural evolution [126]. GA is known as one of the most popular non-gradient AIT, when the gradient information are not available, or in case of Multi-Figure of Merit (MFOM) or multi-modal problems.

6.1 Motivations of the AIT to optimize hybrid renewable systems

Most of the literature studies, to solve MFOM hybrid renewable system problems, have some drawbacks. First, they did not precisely model system components, which will have a big difference in the energy extracted per year (EEPY) from a single unit as well as the entire system size. Second, some papers suggest changing linearly the decision variables to have suboptimal solution, but this will take long time and effort and may result in falling in one of the local minima solutions. Designing the hybrid renewable systems becomes more complex because of the following challenges [1]:

1- Non-linear characteristic of the system components.

2- Stochastic availability of the renewable energy resources (i.e. solar and wind).

3- Increasing the number of the design constraints.

4- Increasing the number of the optimization or decision variables.

Many of the methods used in the literature are based on enumeration iterative methods which may not guarantee the convergence toward the global solution. On the other hand, AIT optimization based approaches were rarely used due to the difficulty to construct the algorithm to solve the problem [20]. However, AIT optimization is recommended to solve renewable energy problems, because the global solution is guaranteed in most cases.

6.2 The GA operators for a single FOM

Initially, one population of "chromosomes" (bits or strings of 0's and 1's) is randomly selected and tested in using the FOM. Each chromosome consists of "genes" (or bits). Afterwards, the natural genetics−inspired operators of (selection, crossover, mutation) are applied to get new solutions.

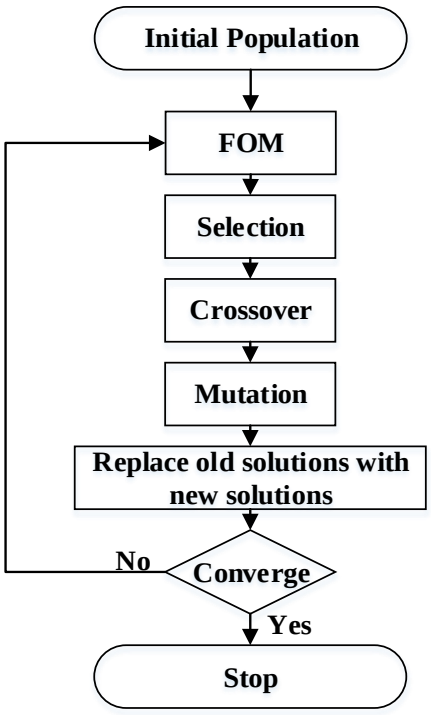

Fig. 6.1 GA operators for a single FOM

Fig. 6.1 shows the flowchart for the GA operators in order to converge to the optimal solution [126]. In the selection operator, chromosomes are selected from the population according to their FOM to be parents (old solution) to crossover and then produce more offsprings (New solutions). Crossover exchanges subparts of two single chromosomes, and it is classified into many types such as single point crossover and two point crossover. In the mutation, two numbers are selected and exchanged. Mutation in GA is an important operator, since it helps get the global solution, and not falling in one of the local solutions [127].

6.3 Non-dominated sorting genetic algorithm (NSGA)

The presence of MFOM problems includes a set of optimal results called Pareto frontier optimal solutions [128]. Remember that, the GA is generally robust and effective when the global solution is difficult to find. Non-dominated Sorting Genetic Algorithm (NSGA) is one of the methods used to solve such a problem. Note that, in the MFOM there will be a set of equally feasible solutions represented by the Pareto frontier. Whereas, in case of single FOM optimization problem, we have only one single feasible solution.

Fig. 6.2 shows the flowchart for the NSGA operators in order to solve a MFOM multi-point connection problem. NSGA starts optimizing by randomly generating an initial population. Then, NSGA will discover the trade-off solutions come out for the MFOM multi-connection problem. At this point, the distance crowding is computed. It is defined as the distance between two adjacent solutions on each side of this solution [129]. Moreover, these non-dominant Pareto fronts are sorted from the highest rank FOM to the lowest rank FOM [130]. Thereafter, the GA operators (Selection, Crossover, and

Mutation) are applied to get new set of solutions added to the old one making a new magnified generation. Afterwards, a Pareto non-dominance check for this generation provides and export the set of solutions called non-dominant or trade-off solutions based on the Pareto fraction. Note that, the Pareto fraction controls the elitism in the NSGA [131]. In the final set, there is no solution is strictly better than any other solution.

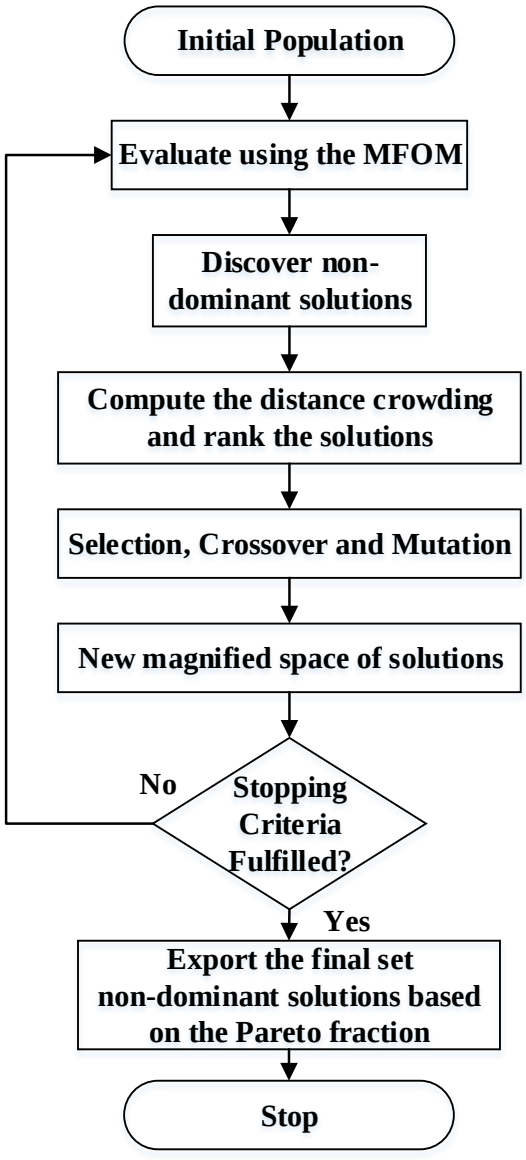

Fig. 6.2 NSGA operators for a MFOM

7. PERFORMANCE RESULTS AND DISCUSSION

In this section the results obtained for the multipoint grid connection are presented and discussed. All of the results presented are based on the mathematical models, GA and the NSGA discussed in Sections 5 and 6 respectively.

7.1 Introduction & tailoring needed information

In this section, the results for the problem of the multi-point connection of a renewable power system to the utility grid of Jordan are presented. This has been done by the development of optimization criteria and design tool by applying the GA and NSGA artificial intelligence techniques to find the optimal, feasible and environmental solutions of our multi-point-connection problem. This tool is applied to the country of Jordan for case validation. However, this design tool will be versatile enough for application to any renewable power system for any utility gird anywhere in the world. The multi-point connection is considered here because we need to install wind farms and PV arrays in each candidate city in Jordan as shown in Fig. 7.1 and Table 7.1. The EC provides the elevation a.s.l for each candidate city as shown in Table 4.3 in Section 4. However, the geographical available area for each city is required in order to install wind farms and/or PV arrays. Therefore, Google Earth [113] and Wikimapia [114] are used to find, then compute the geographical available and appropriate area in each city that is neither inhabited nor planted. Renewable units filling order has to be done, because we have a multi-point connection to satisfy the national load of Jordan. Renewable units' allocation idea comes and implemented based on the highest value of wind or PV potential in each city. Afterwards, all the candidate cites can be arranged, with their corresponding needed

information, based on the highest EEPY. At this point, the EEPY from a single unit installed in each city, is computed for a single WT as well as a single PV panel installed in each candidate city as shown in Table 7.2.

Fig. 7.1 Wind & PV candidate cities in Jordan [132]

Table 7.1 Multi-point connection candidate cities information needed

Candidate Cities	Elevation a.s.l (m)	Geographical Available Area Cap (km^2)	Annual average radiation in 2015 ($kWh/m^2/day$)	Annual Wind Speed in 2015 (m/sec)
Ramtha-JUST	591	28.3148	5.5533	4.88
UmEjmal-LH	750	7.3338	5.7617	6.10
Ibrahimyya	1021	3.7637	5.5533	7.17
Alreesha2-LH	876	470.2879	5.7617	7.03
Maan-LH	1196	83.16	6.0308	5.92
Aqaba5	139	67.3257	6.1217	7.33

Table 7.2 EEPY per unit ("GE-1.5sle" WT & "VBHN240SA11" PV module) installed in each candidate city

Candidate City	WT EEPY (GWh)	PV EEPY (kWh)
Ramtha-JUST	2.2990	436.2410
UmEjmal-LH	4.0687	452.4668
Ibrahimyya	5.4995	436.2410
Alreesha2-LH	5.3680	452.4668
Maan-LH	3.6442	473.3330
Aqaba5	5.9665	480.3399

7.2 Filling order of the candidate cities

The GA operators in Fig. 6.1 are applied in our designed tool to optimize the number of renewables to satisfy the national load of Jordan. As mentioned earlier, that we need to have a criteria for the filling order of renewable optimized number of units in order to be allocated in each city. Therefore, the candidate cities have been arranged with respect to the EEPY for wind in a case as shown in Table 7.3 and with respect to the solar potential in another case as shown in Table 7.4. Optimizing the renewable wind and PV energy systems using the GA and NSGA has been done based on the algorithms described in Fig. 6.1 and Fig. 6.2 respectively.

Table 7.3 Arranging MPGCD cities based on the highest wind EEPY

Arranged Candidate Cities	Arranged Elevation a.s.l (m)	Arranged Area Cap (km^2)	Arranged EEPY for one WT unit (GWh)	Arranged Annual Wind Speed (m/sec)
Aqaba5	139	67.3257	5.9665	7.33
Ibrahimyya	1021	3.7637	5.4995	7.17
Alreesha2-LH	876	470.2879	5.3680	7.03
UmEjmal-LH	750	7.3338	4.0687	6.10
Maan-LH	1196	83.16	3.6442	5.92
Ramtha-JUST	591	28.3148	2.2990	4.88

Table 7.4 Arranging MPGCD cities based on the highest solar EEPY

Arranged Candidate Cities	Arranged Elevation a.s.l (m)	Arranged Area Cap (km^2)	Arranged EEPY for one PV unit (kWh)	Annual average radiation ($kWh/m^2/day$)
Aqaba5	139	67.3257	480.3399	6.1217
Maan-LH	1196	83.16	473.3330	6.0308
UmEjmal-LH	750	7.3338	452.4668	5.7617
Alreesha2-LH	876	470.2879	452.4668	5.7617
Ramtha-JUST	591	28.3148	436.2410	5.5533
Ibrahimyya	1021	3.7637	436.2410	5.5533

7.3 Single FOM solution to satisfy the national load

The design tool has been run for more than a day to optimize the ASCE as our FOM. Fig. 7.2 shows how the GA looks for the optimal solution staring by figuring out some candidate solutions and then select the optimal one which is the best fitness feasible value.

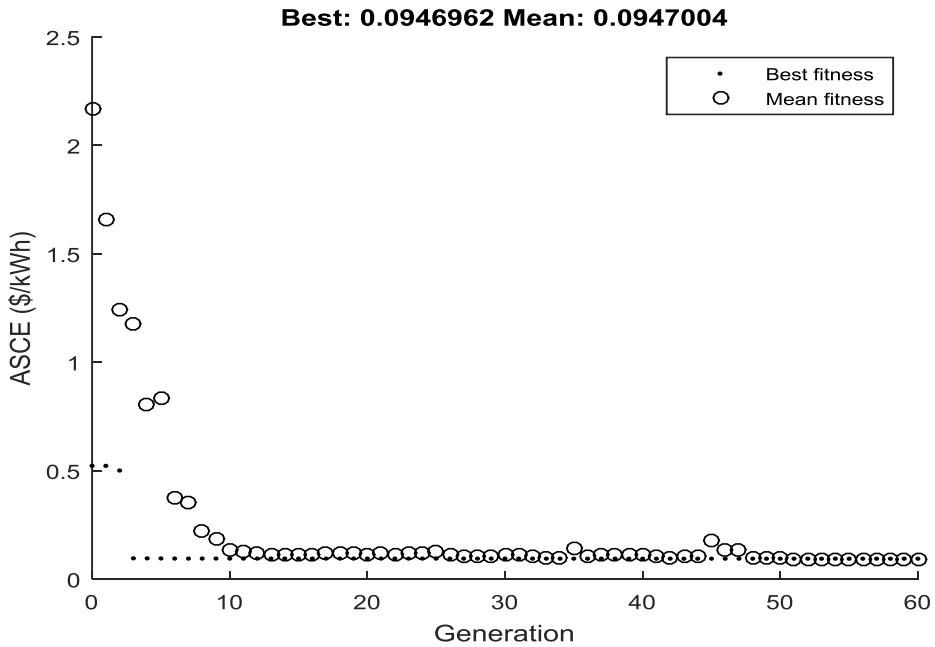

Fig. 7.2 GA optimization of ASCE as the FOM

Note that, for each generation there is two values: best fitness (dots in Fig. 7.2) and mean fitness (circles in Fig. 7.2). Fig. 7.2 shows how the optimizing process converges. The best FOM dot values of the last few generations become inside the mean circle values. In this case, the GA optimizes the annual system cost of energy (ASCE) as our FOM with a value of 0.0946962$/kWh which is 32.57% less than the Jordan utility grid purchased price. This is an excellent indication about the feasibility of this system if it is adopted and practically implemented. Furthermore, Fig. 7.3 shows the genealogy of GA children individuals, which depicts the children of mutation, crossover and elitism for sixty generation each with two-hundred populations.

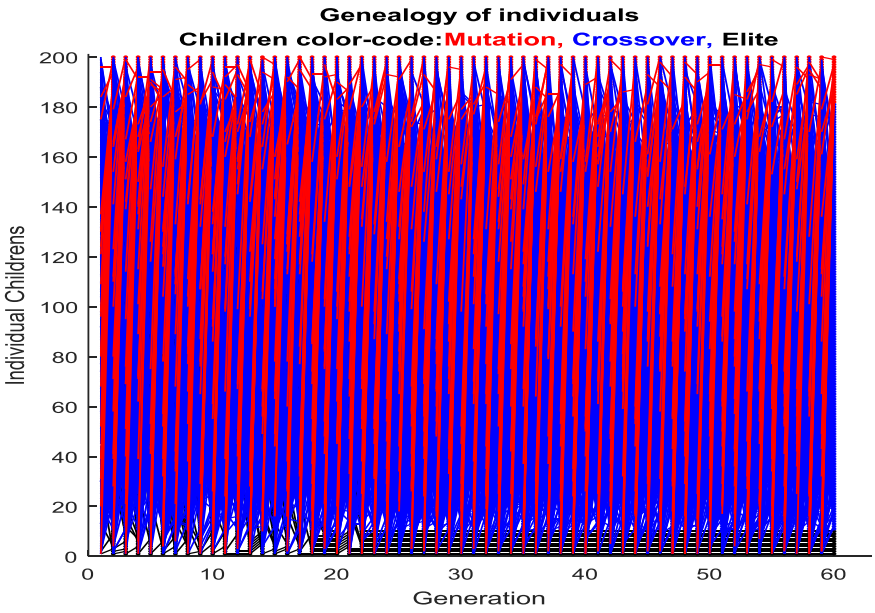

Fig. 7.3 Genealogy of individual children

To satisfy the national load of Jordan, the number of renewable units' decision variables are optimized to be 2079 for WTs and 129,362 for PVs. The specifications of the selected WT and PV module are shown in Table 7.5 and 7.6 respectively.

Table 7.5 Specifications for the selected WT for the multi-point investigation

Parameter	Value
Model	GE-1.5sle
Rated output	1.5 MW
Rated wind speed	14 m/s
Rotor diameter	77 m
Cut-in wind speed	3.5 m/s
Cut-out wind speed	25 m/s
Hub height	65 m

Table 7.6 Specifications for the selected PV Panel of (VBHN240SA11) model for the multi-point investigation

Manufacturer Part #	$P_{r_{PV}}$ (Watt)	TC_p (%/°C)	T_{NOCT} (°C)	L_{PV} (m)	W_{PV} (m)	V_{mp} (V)	I_{mp} (A)	V_{oc} (V)	I_{sc} (A)
VBHN240SA11	240	-0.3	48.3	1.58	0.798	43.7	5.51	52.4	5.85

It can be noticed that the optimized system to satisfy the national load of Jordan is a hybrid wind/PV/grid configuration with information shown in Table 7.7 and Fig. 7.4. In other words, it is a hybrid renewable configuration if there is a single site that can accommodate the optimized decision variables for the number of renewable units' mentioned earlier.

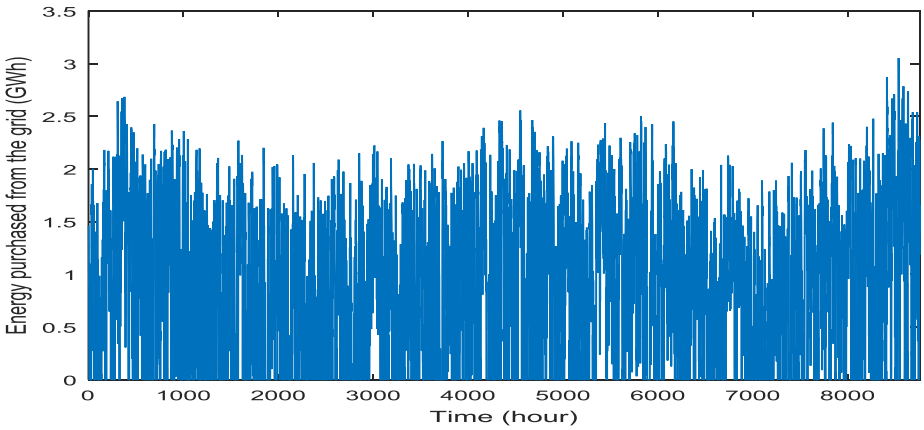

Fig. 7.4 Instantaneous energy purchased from grid

Table 7.7 The optimized hybrid wind/PV system to satisfy the national load of Jordan

LCOE in $/kWh	0.058212
TNPC in billion $	8.713857
RP in %	59.49817
CO_2 Emissions (Megatonne/year)	4.576

The Global Carbon Atlas in [133] shows that the CO_2 Emissions in Jordan in 2014 is 23Mt CO_2 for a total number of population of 7,416,083. Therefore, our designed system will reduce the carbon emissions by 80.13% as shown in Table 7.7. This is another excellent indication for the environmental benefit comes out after solving the multi-point connection problem in Jordan. The minimum areas required to accommodate the optimized value of WT and PV units have been computed to be 301.6853 km^2 and 196,158.1 m^2 respectively. These need more than a single city (See Table 7.1) to be installed. This means that different renewable configurations are expected for each city based on their potential of renewable energy resources.

7.4 Multi-Point solutions using the GA & NSGA

The optimized number of renewable units', to satisfy the national load of Jordan, have been allocated for each candidate city from the MPGCD. Table 7.8 shows that the hybrid wind/PV is the optimal and the feasible configuration in Aqaba5 site. Moreover, the wind only configuration is the best to be installed in Ibrahimyya as well as Alreesha2 sites. Further, the PV only configuration is the optimal configuration to be installed in MaanLH site. Whereas there is no need to install renewables in Ramtha-JUST and UmEjmal-LH for the current national load in Jordan.

Table 7.8 OST for each location in the multi-point connection

Candidate Cities	On-Grid System Type
Aqaba5	Hybrid Wind/PV
Ibrahimyya	Wind Only
Alreesha2-LH	Wind Only
Maan-LH	PV only
UmEjmal-LH	No need for renewables for the current national load
Ramtha-JUST	

In the future it can be foreseen that the load will be definitely increased. So, it is expected that those unused cities (Ramtha-JUST and UmEjmal-LH) will have a WT and PV shares to satisfy the national load. Moreover, the GA specifies the WT sharing percents as six decision variables for each candidate city as in Table 7.9 which are used to compute the dedicated WT area for each candidate city. Table 7.9 and Table 7.10 show that the dedicated area of WTs or PVs are less than the geographical available area cap shown in Table 7.3 and Table 7.4 as was expected. Afterwards, the PV sharing percents are computed as the complement of the WT ones for each candidate city as shown in Table 7.10 which are used to compute the dedicated PV area for each city.

Table 7.9. Optimized WT value of:
Sharing percent, dedicated and occupied area for each candidate city

WT Arranged Candidate Cities	Optimized WT sharing percent (%)	Dedicated WTs area (km^2)	Number of WTs	Occupied WTs area (km^2)
Aqaba5	99.86	67.2348	590	67.1756
Ibrahimyya	99.55	3.7468	34	3.7175
Alreesha2-LH	82.11	386.1555	1455	211.0428
UmEjmal-LH	75.70	5.5519	0	0
Maan-LH	34.06	28.3231	0	0
Ramtha-JUST	34.74	9.8370	0	0

Table 7.10 Optimized PV value of:
Sharing percent, dedicated and occupied area for each candidate city

PV Arranged Candidate Cities	PV sharing percent (%)	Dedicated PVs area (km^2)	Number of PVs	Occupied PVs area (km^2)
Aqaba5	0.14	0.09094	59696	0.09087
Maan-LH	65.94	54.83686	69666	0.10529
UmEjmal-LH	24.30	1.78187	0	0
Alreesha2-LH	17.89	84.13237	0	0
Ramtha-JUST	65.26	18.47781	0	0
Ibrahimyya	0.45	0.01693	0	0

Furthermore, Table 7.9 shows that the occupied area is less than the dedicated area in each candidate city for either WTs or PVs. In other words, the WT ratio of the occupied to the dedicated area for Aqaba5, Ibrahimyya and Alreesha2-LH cities are 99.91%, 99.22% and 54.65% respectively. Moreover, Table 7.10 shows that the PV ratio of the occupied to the dedicated area for Aqaba5 and Maan-LH cities are 99.93% and 0.192% respectively.

7.5 Discussion on the GA single FOM solutions

There are many points can be discussed regarding the single FOM solutions mentioned earlier. First, Table 7.8, Table 7.9 and Table 7.10 show that the cities of Aqaba5, Ibrahimyya and Alreesha2-LH are enough to install the optimized number of WTs of 2079 units. In addition, Aqaba5 and Maan-LH sites are sufficient to install the optimized number of PVs of 129,362 units.

Second, the number of WTs and PVs for each city are computed by allocating the 2079 WT and 129,362 PV after optimizing the ASCE single FOM using the GA to share in satisfying the national load of Jordan. This has been done by filling each city up to the

dedicated area cap limit shown in Table 7.9 and Table 7.10 starting from the city with the highest EEPY. Afterwards, the last column of Table 7.9 and Table 7.10 show the occupied WT and PV areas respectively, which have been computed by finding the rectangular wind farm configuration, which has the minimum geographical area.

Last, as was expected when the data were collected that the cities with high potential of wind or PV energy will have the highest area share as shown in Table 7.9 and Table 7.10. This has been proved after optimizing the ASCE single FOM for the hybrid system using the GA.

For instance, Aqaba5 has the highest annual wind speed of 7.33 m/sec as well as the highest wind EEPY of 5.9665GWh for a single unit (See Table 7.3 and Table 7.4). Further, Aqaba5 has the highest annual radiation of 6.1217 kWh/m^2/day, and the corresponding highest solar EEPY of 480.3399 kWh for a single unit. These expectations are enhanced for Aqaba5 which got the highest area share as wells as the first choice in the filling order of renewable energy units.

7.6 MFOM solutions using the NSGA

It is not possible to simultaneously have a single solution for a MFOM optimization problem. Thereby, an algorithm is needed to give alternative solutions or what is called Pareto frontier [134]. Actually, our design tool has been built to have the ability to optimize a single FOM in a case, as well as to be able to find multiple Pareto-optimal solutions in another case for a MFOM problem. As illustrated in Section 6 that in the MFOMs optimizations there will be a set of equally feasible and optimal solutions represented by the Pareto frontier. This means that one FOM will be minimized while

maximizing the other. In other words, a set of non-dominant competing solutions is obtained where a trade-off relationship governs the behavior of the FOMs. A project management plan can be technically constructed after optimizing MFOMs problem. This will definitely help decision makers and engineers take the right choice based on their specific interests. In this section, MFOM competitive solutions are obtained using the NSGA.

7.6.1 Results – 2D Pareto Frontier

7.6.1.1 Pareto Points – CO_2 emissions vs. ASCE

Recall that the ASCE has been optimized in Section 7.3 as a single FOM with a value of 0.0946962 $/kWh as shown in Fig. 7.2. Note that, this value of ASCE is the first point to the left side of the Pareto points shown in Fig. 7.5.

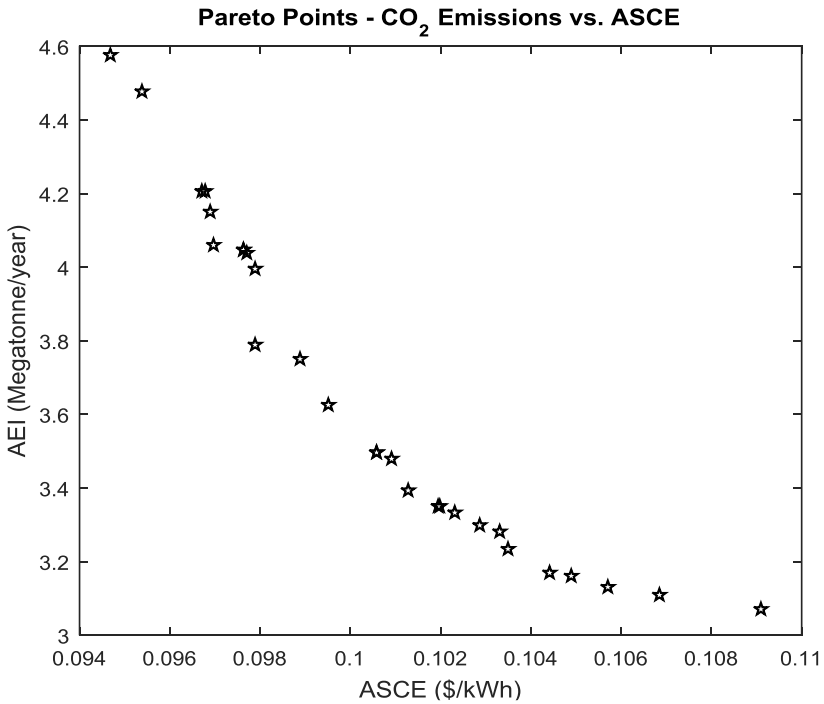

Fig. 7.5 Pareto Points – CO_2 emissions vs. ASCE

The ASCE and the CO_2 Emissions (AEI) are optimized here together as a MFOM problem using the NSGA. Fig. 7.5 describes the trade-off relationship between the ASCE and the AEI. This means that increasing the ASCE will gradually decrease the AEI values. Comparing the first and the final point of the Pareto points shows that decreasing the AEI with a 32.91% is at the expense of the ASCE which has been increased by 15.21%.

7.6.1.2 Pareto Points – CO_2 emissions vs. LCOE

Furthermore, Fig. 7.6 shows another trade-off relationship represented by the Pareto points for the LCOE and the AEI. Note that, these Pareto points start with the LCOE value optimized before (0.058212 $/kWh). Moving from the left to the right side of Fig. 7.6, i.e from the first to the final point of the Pareto points will minimize the AEI by 34.46%, whereas the LCOE will be maximized by 66.73%.

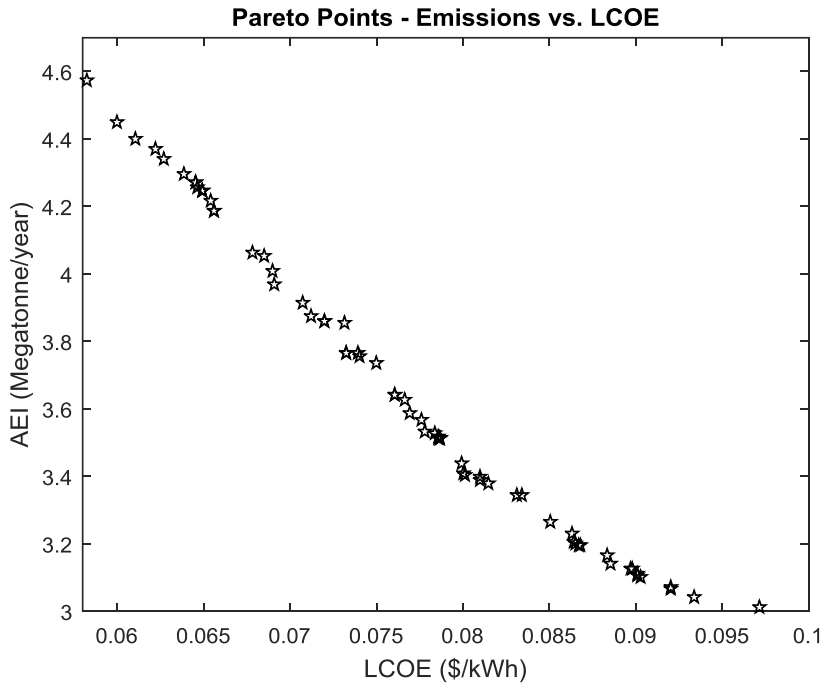

Fig. 7.6 Pareto Points – CO_2 emissions vs. LCOE

7.6.1.3 Pareto Points – CO_2 emissions vs. RP

Moreover, Fig. 7.7 shows another set of tradeoff solutions for the AEI and the RP optimized as a MFOM using the NSGA. The RP at the end of the Pareto points is increased around (14.90) times the RP at the first Pareto point. The corresponding reduction of the AEI is 68.26%. This will offer different design alternatives for the decision makers based on specific preferences in their energy plan investment. As can be noticed in these Pareto points that penetrating more renewables will rapidly reduce the CO_2 Emissions. This is an indication of the important environmental benefits that renewable energy technologies can provide. In this case, it can be foreseen that the very low-carbon energy production can be achieved in the near future.

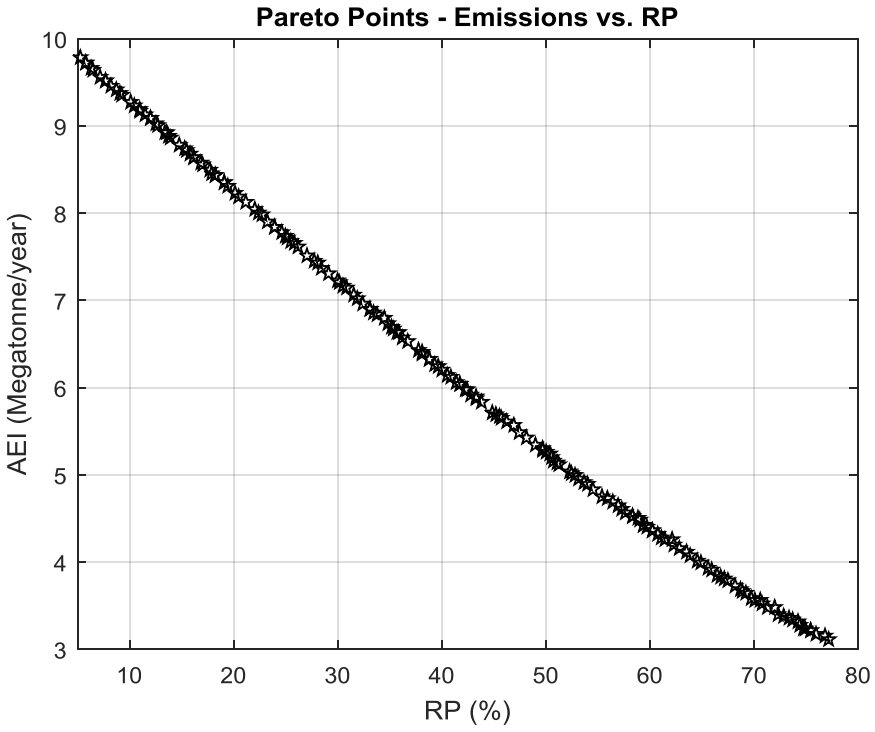

Fig. 7.7 Pareto Points – CO_2 emissions vs. RP

7.6.1.4 Sweet spot selection procedure

The developed sweet spot selection (triple-S) procedure will definitely help the decisions maker to take an excellent solution for the two FOMs problems. In order to take an acceptable point as a solution to two FOMs in Fig. 7.5 we will use the (Triple-S) procedure. Triple-S procedure can only be used with a 2D Pareto points by employing two functions. This helps find the Sweet Spot as shown in Fig. 7.8.

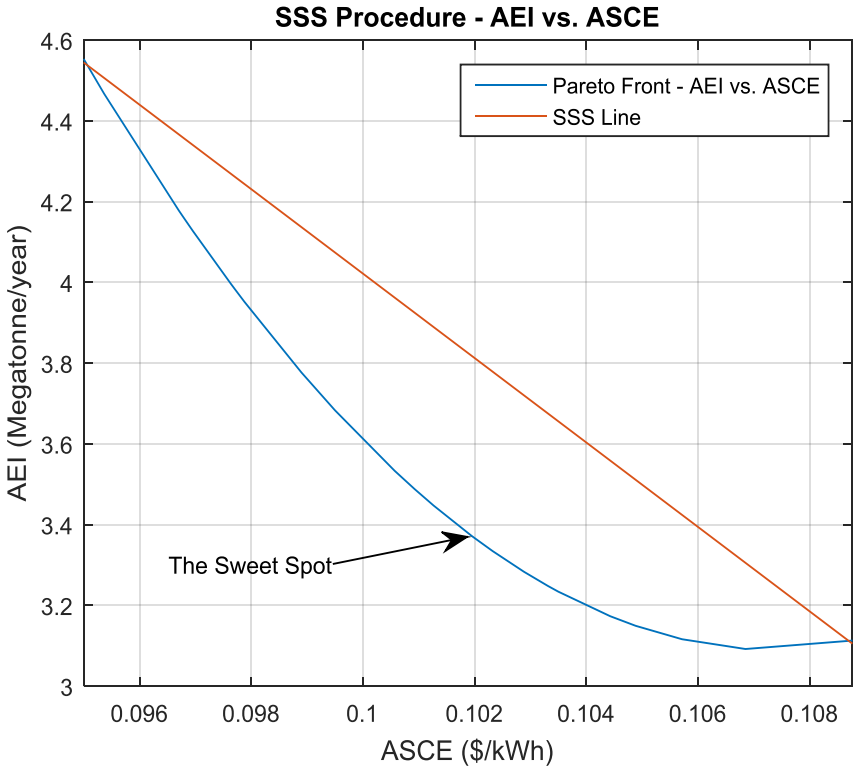

Fig. 7.8 Triple-S procedure for the Pareto Front of Fig. 7.5

First, you need to find the linear triple-S curve function which extends from the first to the last point of the Pareto points shown in Fig. 7.5. Then, the Pareto front will be found for the actual NSGA optimized Pareto points shown in Fig. 7.5. Afterwards, an

iterative technique is applied to find the largest deviation between those two functions. For instance, the acceptable point for the two FOMs shown in Fig. 7.8 has been computed using the triple-S procedure to be 3.3762 Megatonne/year for the CO_2 Emissions, and 0.1019 $/kWh for the ASCE.

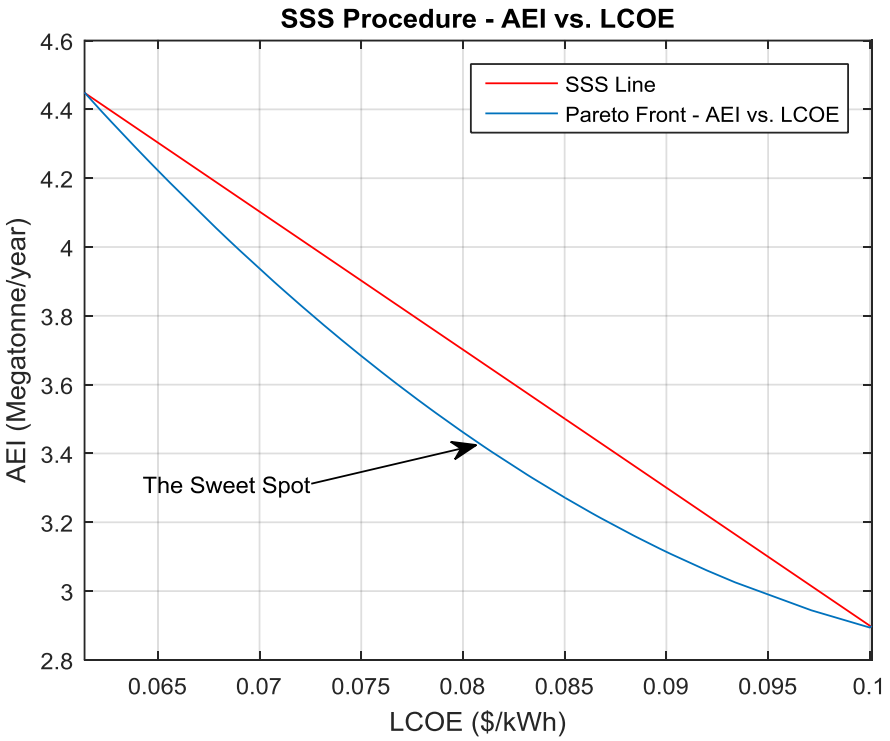

Fig. 7.9 Triple-S procedure for the Pareto Front of Fig. 7.6

Further, if you apply the same triple-S procedure for the Pareto points in Fig. 7.6, you will get the solution of 0.0808$/kWh for the LCOE, and 3.4288 Megatonne/year for the CO_2 Emissions as shown in Fig. 7.9. Moreover, the application of the triple-S procedure for the Pareto points in Fig. 6.7 will help get an acceptable solution for the CO_2 Emissions (6.0994 Megatonne/year) and the RP (41.0803%). This Sweet Spot is shown in Fig. 7.10. In all of these three cases, triple-S procedure helps find a solution that is

accepted environmentally and economically. This will help many investor take the right decision in their renewable energy project plans.

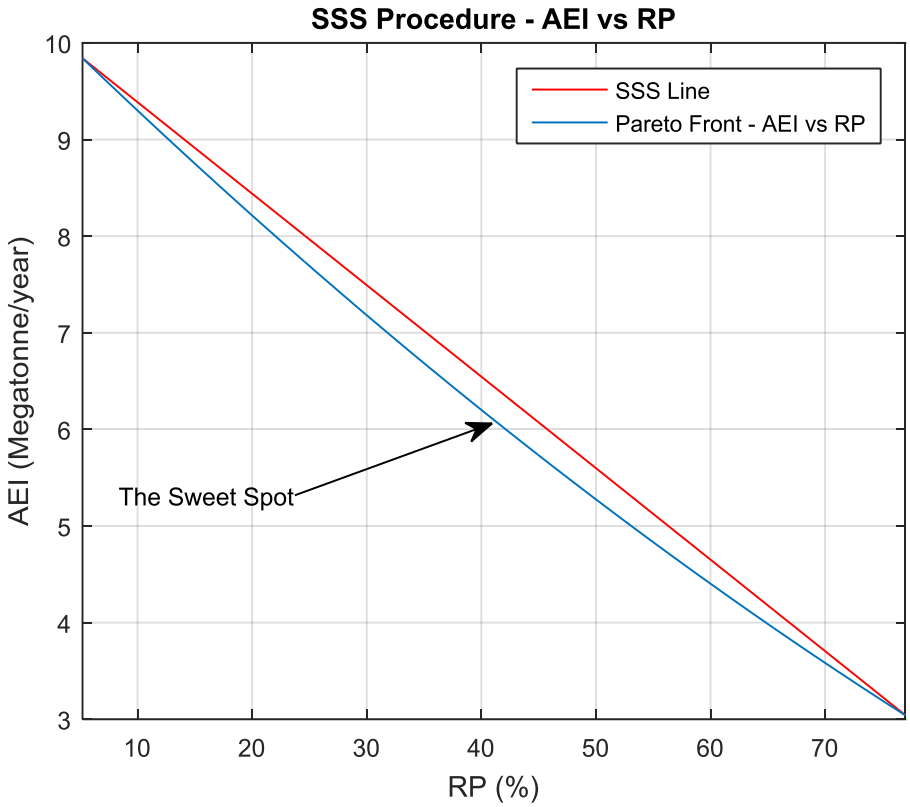

Fig. 7.10 Triple-S procedure for the Pareto Front of Fig. 7.7

7.6.2 Results – 3D Pareto Frontier

It is very interesting to deal with three dimensions (3D) Pareto frontier which include three FOMs. This has the advantage to visualize the behavior of the complete Pareto non-dominated solutions optimal set in the 3D space. Fig. 7.11 shows a 3D Pareto front for RP, LCOE and AEI FOMs.

Note that, in the low penetration region the CO_2 Emissions is very high, because most of the energy to satisfy the national load comes for the conventional utility grid

regardless of the value of the LCOE that is the price of energy produced by renewables. Furthermore, as the RP increases the CO_2 Emissions is gradually decreases (as what is obtained in Fig. 7.7). In addition, as the RP becomes higher, the LCOE starts affecting the 3D surface. So to the right of Fig. 7.11, as the LCOE increases the CO_2 Emission will be gradually reduced as what we got in Fig. 7.6.

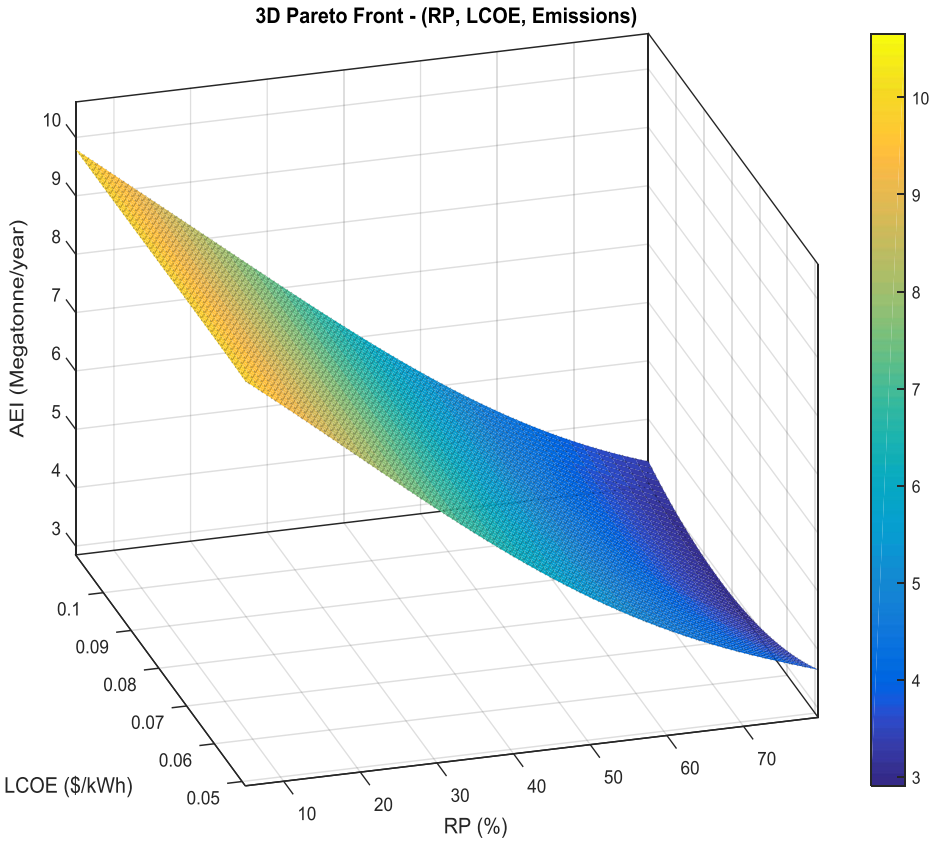

Fig. 7.11 Pareto Front – (RP, LCOE, CO_2 emissions)

8. CONCLUSIONS AND FUTURE WORKS

8.1 Conclusions

The ideas that we discussed in this dissertation are based on the fact that there is plenty of fossil fuels for hundreds of years. Worldwide, the urgency of sustainable energy comes from global warming or greenhouse effects, and equitable access to energy for all humanity. The developing world is the sector that will dominate the growth of greenhouse gas emissions in the coming decades. The developed world should provide technologies for the developing world (90%) that are green and are appropriate for their development, which is the key to reduce carbon emissions, rather than making the developed world clean (10% solution).

The main objective in this dissertation is to meet a country national load by considering multiple connections to the national grid at different geographical locations of high potential of wind and/or solar resources. This has been accomplished by building a new optimization design tool which is based on the GA to solve a single FOM, and a NSGA to solve MFOM problems. This design tool computes the number of WTs, number of PVs and the sharing percent of wind or PV in each promising city. This design tool has the capability to determine the renewable system configuration in each city, and if any of the MPGCD candidate cites is needed or not to satisfy a current national load.

At the outset, the single point connection was investigated for simplicity and to understand all the aspects behind the multi-point connection problem. HOMER can't solve our actual problem to satisfy the national load demand for a country by installing wind farms and/or PV arrays only in those cities of high potential of wind speed and/or solar

radiation. Thereby, a new optimization design tool has been built in this dissertation after mathematically modeling each component of the hybrid on grid renewable system.

The WT has been precisely modeled by taking many parameters into account such as air density. Then, the impact of WT modeling has been investigated for a hybrid and a wind energy on-grid systems. The PV panel is modeled with the available input of PV incident irradiation. Also, the utility grid is modeled with many available inputs such as the utility purchased price. Moreover, the minimum required rectangular geographic area is modeled for the wind farm and PV array. In addition, numerous system performance indicators are modeled such as the ASCE, LCOE, TNPC, AEI, LOA and RP. In our multi-point connection problem, the ASCE is considered as a single FOM and the others as indicators.

This design tool is applied to the country of Jordan as a case validation. The GA optimizes the ASCE as the FOM to be 0.0946962$/kWh. It is 32.57% less than the utility grid purchased price. This is an excellent results to indicate the feasibility of the optimized system to satisfy the national load. Moreover, the LCOE, TNPC, RP and AEI are 0.058212 $/kWh, 8.713857 billion$, 59.49817% and 4.576 Megatonne/year respectively. Results show that the hybrid wind/PV is the optimal and the feasible configuration in Aqaba5 site. Moreover, the wind only configuration is the best to be installed in Ibrahimyya as well as Alreesha2 cities. Further, the PV only configuration is the optimal configuration to be installed in MaanLH site. There is no need to install renewables in Ramtha-JUST and UmEjmal-LH for the current national load of Jordan. In the multi-point, the NSGA is used to solve MFOM problems of AEI vs. ASCE, AEI vs. LCOE, AEI vs. RP and AEI vs.

LCOE vs RP. The results out of these MFOM problem are either 2D or 3D Pareto frontier that are used to have many alternative solutions selected based on preferences of the decision makers. The triple-S procedure is developed to help select the sweet spot in the two FOMs problems. This helps get environmental and feasible solution recommended for investors who are looking to have a single point solution out of a two FOMs problem.

Note that, this design tool will be versatile enough for application to any hybrid renewable power system for any utility gird anywhere in the world. This tool will then be made available on the internet as a public service of Texas A&M University Renewable Energy Program at the Power Electronics and Motor Drives Laboratory of the Department of Electrical and Computer Engineering.

8.2 Future works

This project will be extended in the future, by employing similar studies to investigate other possible potential locations worldwide. Furthermore, other hybrid systems are available other than wind/PV systems. It is interesting to investigate other possibilities and compare results.

For instance, Panama is rich in water resources. Approximately, half of Panama's electrical energy comes from hydro-generation. So, it is very interesting to hybridize hydro with wind power generation. This helps decrease Panama's dependence on fossil fuel. This also reduces the emissions of the GHG in Panama.

REFERENCES

[1] R. Luna-Rubio, M. Trejo-Perea, D. Vargas-Vázquez, and G. J. Ríos-Moreno, "Optimal sizing of renewable hybrids energy systems: A review of methodologies," *Solar Energy*, vol. 86, pp. 1077-1088, 4// 2012.

[2] B. Petroleum, "BP Statistical Review of World Energy 2015," ed: London, 2015.

[3] B. K. Bose, "Global Warming: Energy, Environmental Pollution, and the Impact of Power Electronics," *Industrial Electronics Magazine, IEEE*, vol. 4, pp. 6-17, 2010.

[4] V. Nelson, *Wind energy: renewable energy and the environment*: CRC press, 2013.

[5] G. L. Johnson, *Wind energy systems*: Gary L. Johnson, 2006.

[6] J. Peinke, P. Schaumann, and S. Barth, *Wind energy : proceedings of the Euromech colloquium*: Berlin : Springer, [2007], 2007.

[7] G. W. E. Council, "Global wind statistics 2015," *Report. Brussels, Belgium: GWEC*, 2015.

[8] M. E. Mackay, *Solar Energy : An Introduction*. Oxford, GB: Oxford University Press, 2015.

[9] BP. (1/31/2016). *Solar power generating capacity*. Available: http://goo.gl/8y71pN

[10] U.S. Energy Information Administration. (1/31/2016). Available: http://goo.gl/soGmyv

[11] E. Takle and R. Shaw, "Complimentary nature of wind and solar energy at a continental mid-latitude station," *International Journal of Energy Research*, vol. 3, pp. 103-112, 1979.

[12] C. Yaow-Ming, C. Chung-Sheng, and W. Hsu-Chin, "Grid-connected hybrid PV/wind power generation system with improved DC bus voltage regulation strategy," in *Applied Power Electronics Conference and Exposition, 2006. APEC '06. Twenty-First Annual IEEE*, 2006, p. 7 pp.

[13] Wikipedia. *Energy in Jordan*. Available: https://en.wikipedia.org/wiki/Energy_in_Jordan

[14] S. Sinha and S. S. Chandel, "Review of software tools for hybrid renewable energy systems," *Renewable and Sustainable Energy Reviews,* vol. 32, pp. 192-205, 4// 2014.

[15] M. A. M. Ramli, A. Hiendro, K. Sedraoui, and S. Twaha, "Optimal sizing of grid-connected photovoltaic energy system in Saudi Arabia," *Renewable Energy,* vol. 75, pp. 489-495, 3// 2015.

[16] M. Ehsani and H. Al-Masri, "Engineering and Socio-Economic Aspects of Sustainable Energy," presented at the IEEE Global Humanitarian Technology Conference (GHTC), Seattle, Washington USA, 2016.

[17] R. A. Muller, *Energy for future presidents: the science behind the headlines*: WW Norton & Company, 2012.

[18] (04/11/2016). *Adoption Of The Paris Agreement*. Available: https://goo.gl/rM6ghl

[19] (01/21/2016). *Kyoto Protocol*. Available: http://www.kyotoprotocol.com/

[20] Y.-Y. Hong and R.-C. Lian, "Optimal sizing of hybrid wind/PV/diesel generation in a stand-alone power system using Markov-based genetic algorithm," *Power Delivery, IEEE Transactions on,* vol. 27, pp. 640-647, 2012.

[21] (EPA). (02/01/2016). *Global Greenhouse Gas Emissions Data*. Available: http://goo.gl/SYIJ5F

[22] L. Bayon, J. Grau, M. Ruiz, and P. Suarez, "Optimization of SO2 and NO x Emissions in Thermal Plants," *Journal of mathematical chemistry,* vol. 40, pp. 29-41, 2006.

[23] L. Wang and C. Singh, "Multicriteria design of hybrid power generation systems based on a modified particle swarm optimization algorithm," *Energy Conversion, IEEE Transactions on,* vol. 24, pp. 163-172, 2009.

[24] G. Boyle, *Renewable Energy: Power for a Sustainable*: Oxford University Press, USA, 1996, 1996.

[25] H. Al-Masri, F. Alhuwaishel, F. Alismail, S. Sabeeh, and H. Kanakri, "Investigation of MPPT for PV applications by mathematical model," in *Environment and Electrical Engineering (EEEIC), 2015 IEEE 15th International Conference on*, 2015, pp. 1800-1805.

[26] H. M. Al-Masri, A. Abu-Errub, W. R. Ayyad, and M. Ehsani, "On the PV module characteristics," in *2016 International Symposium on Power Electronics, Electrical Drives, Automation and Motion (SPEEDAM)*, 2016, pp. 901-905.

[27] N. Pandiarajan and R. Muthu, "Mathematical modeling of photovoltaic module with Simulink," in *Electrical Energy Systems (ICEES), 2011 1st International Conference on*, 2011, pp. 258-263.

[28] PV Education. (02/24/2015). Available: http://pveducation.org/pvcdrom/pn-junction/diode-equation

[29] S. Kurtz, K. Whitfield, D. Miller, J. Joyce, J. Wohlgemuth, M. Kempe, *et al.*, "Evaluation of high-temperature exposure of rack-mounted photovoltaic modules," in *Photovoltaic Specialists Conference (PVSC), 2009 34th IEEE*, 2009, pp. 002399-002404.

[30] (02/25/2015). *Effect of Temperature*. Available: http://bit.ly/1eJz683

[31] (02/25/2015). *Effect of Light Intensity*. Available: https://goo.gl/prlf7l

[32] A. M. Al-Ashwal and I. S. Moghram, "Proportion assessment of combined PV-wind generating systems," *Renewable Energy*, vol. 10, pp. 43-51, 1// 1997.

[33] I. M. C. Navigant Consulting, "Relative Merits of Distributed vs. Central Photovoltaic (PV) Generation Prepared.," California Energy Commission Renewable Energy Program., Boston, Massachusetts, April 7, 2004

[34] A. Sanz, I. Vidaurrazaga, A. Pereda, R. Alonso, E. Roman, and V. Martinez, "Centralized vs distributed (power optimizer) PV system architecture field test results under mismatched operating conditions," in *Photovoltaic Specialists Conference (PVSC), 2011 37th IEEE*, 2011, pp. 002435-002440.

[35] B. E. Türkay and A. Y. Telli, "Economic analysis of standalone and grid connected hybrid energy systems," *Renewable Energy*, vol. 36, pp. 1931-1943, 7// 2011.

[36] S. Rehman, M. Mahbub Alam, J. P. Meyer, and L. M. Al-Hadhrami, "Feasibility study of a wind–pv–diesel hybrid power system for a village," *Renewable Energy*, vol. 38, pp. 258-268, 2// 2012.

[37] T. Ma, H. Yang, and L. Lu, "A feasibility study of a stand-alone hybrid solar–wind–battery system for a remote island," *Applied Energy*, vol. 121, pp. 149-158, 5/15/ 2014.

[38] A. Helal, R. El-Mohr, and H. Eldosouki, "Optimal design of hybrid renewable energy system for electrification of a remote village in Egypt," in *Communications, Computing and Control Applications (CCCA), 2012 2nd International Conference on*, 2012, pp. 1-6.

[39] HOMER Energy Support. (01/29/2015). *Clearness index in HOMER*. Available: https://goo.gl/OjEeFD

[40] (01/29/2015). Available: http://solarexpert.com/2013/03/21/central-inverter-vs-micro-inverters/

[41] (01/29/2015). *Grid Emission Factor (GEF)* Available: https://goo.gl/zhTtVx

[42] S. Rehman, I. M. El-Amin, F. Ahmad, S. M. Shaahid, A. M. Al-Shehri, J. M. Bakhashwain, *et al.*, "Feasibility study of hybrid retrofits to an isolated off-grid diesel power plant," *Renewable and Sustainable Energy Reviews*, vol. 11, pp. 635-653, 5// 2007.

[43] Y. M. Atwa and E. F. El-Saadany, "Optimal Allocation of ESS in Distribution Systems With a High Penetration of Wind Energy," *IEEE Transactions on Power Systems*, vol. 25, pp. 1815-1822, 2010.

[44] H. Al-Masri and M. Ehsani, "Feasibility investigation of a hybrid on-grid wind photovoltaic retrofitting system," in *Industry Applications Society Annual Meeting, 2015 IEEE*, 2015, pp. 1-7.

[45] A. Kusiak and W. Li, "Virtual Models for Prediction of Wind Turbine Parameters," *IEEE Transactions on Energy Conversion*, vol. 25, pp. 245-252, 2010.

[46] A. Kusiak, Z. Zhang, and M. Li, "Optimization of Wind Turbine Performance With Data-Driven Models," *IEEE Transactions on Sustainable Energy*, vol. 1, pp. 66-76, 2010.

[47] T. Senjyu, D. Hayashi, N. Urasaki, and T. Funabashi, "Optimum configuration for renewable generating systems in residence using genetic algorithm," *Energy Conversion, IEEE Transactions on*, vol. 21, pp. 459-466, 2006.

[48] H. Yang, W. Zhou, L. Lu, and Z. Fang, "Optimal sizing method for stand-alone hybrid solar–wind system with LPSP technology by using genetic algorithm," *Solar Energy*, vol. 82, pp. 354-367, 4// 2008.

[49] E. Koutroulis, D. Kolokotsa, A. Potirakis, and K. Kalaitzakis, "Methodology for optimal sizing of stand-alone photovoltaic/wind-generator systems using genetic algorithms," *Solar energy*, vol. 80, pp. 1072-1088, 2006.

[50] H. M. Al-Masri and M. Ehsani, "Feasibility Investigation of a Hybrid On-Grid Wind Photovoltaic Retrofitting System," *IEEE Transactions on Industry Applications*, vol. 52, pp. 1979-1988, 2016.

[51] HOMER Energy. (12/8/2015). Available: http://www.homerenergy.com/

[52] OpenEI Wiki. (12/8/2015). Available: http://en.openei.org/wiki/HOMER

[53] A. Walker, *Solar Energy : Technologies and Project Delivery for Buildings*: John Wiley & Sons, August 2013.

[54] L. N. Ibrahim Nassar, Barakat Hasaneen, Ahmed Elbendary, Abdelrahman Atallah Saleh, "A Novel Method of Optimization and Matching Generation of Photovoltaic Modules and Wind Turbines Models using Matlab," *International Journal of Scientific & Engineering Research*, vol. 5, 2014.

[55] S. Shokrzadeh, M. J. Jozani, and E. Bibeau, "Wind Turbine Power Curve Modeling Using Advanced Parametric and Nonparametric Methods," *Sustainable Energy, IEEE Transactions on,* vol. 5, pp. 1262-1269, 2014.

[56] A. Shah. (06/21/2015). *Types of Solar Panels*
Available: http://goo.gl/JUZvBf

[57] (06/22/205). *PVinsights Website*. Available: http://goo.gl/1Syqnp

[58] (06/22/2015). *Solar power to shine through in the Middle East in 2015*.
Available: http://goo.gl/6Anfqd

[59] (11/5/2015). *Nominal power (photovoltaic)*. Available:
https://en.wikipedia.org/wiki/Nominal_power_(photovoltaic)

[60] S. Diaf, D. Diaf, M. Belhamel, M. Haddadi, and A. Louche, "A methodology for optimal sizing of autonomous hybrid PV/wind system," *Energy Policy,* vol. 35, pp. 5708-5718, 11// 2007.

[61] NEPCO, "National Electric Power Company Annual Report," Jordan, 2014.

[62] (12/21/2015). *Convert million btu to barrels of oil equivalent*. Available:
https://www.unitjuggler.com/convert-energy-from-MMBtu-to-boe.html

[63] G. P. Watkins, *A Third Factor in the Variation of Productivity: The Load Factor* vol. 5: American Economic Association, 1915.

[64] U.S. Energy Information Administration. (12/12/2015). *Demand for electricity changes through the day*. Available: https://goo.gl/y5DZ7e

[65] (12/21/2015). *Wind Energy in Jordan*. Available:
http://www.wecsp.org.jo/content/wind-energy-jordan

[66] (12/12/2013). *Solar Energy in Jordan* Available:
http://www.wecsp.org.jo/content/csp-energy-jordan

[67] N. P. Tao Xie, Andrew Fischer Lees, Eve Ewing, "Wind Energy: A Thorough Examination of Economic Viability," University of Chicago2008.

[68] S. A. Kalogirou, *Solar energy engineering: processes and systems*: Academic Press, 2013.

[69] (07/31/2016). *Worldwide Solar Belts*. Available: http://goo.gl/IyfpSm

[70] M. Giberson, "Assessing Wind Power Cost Estimates," Texas Tech UniversityOctober 2013.

[71] X. Lin, R. Xinbo, M. Chengxiong, Z. Buhan, and L. Yi, "An Improved Optimal Sizing Method for Wind-Solar-Battery Hybrid Power System," *Sustainable Energy, IEEE Transactions on,* vol. 4, pp. 774-785, 2013.

[72] (12/13/2013). *CivicSolar*. Available: http://www.civicsolar.com/

[73] (12/13/2015). *Solar power to shine through in the Middle East in 2015* Available: http://goo.gl/6Anfqd

[74] A. Duffy, *Renewable Energy and Energy Efficiency : Assessment of Projects and Policies*: Wiley, April 2015.

[75] (12/13/2015). *Energy Regulatory Commission (ERC) in Jordan*. Available: https://goo.gl/L5ChLT

[76] (12/13/2015). *Energy Regulatory Commission (ERC) in Jordan/Renewable Energy Passing Costs.* Available: https://goo.gl/2zkvto

[77] H. M. K. Al-Masri and M. Ehsani, "Accurate Wind Turbine Annual Energy Computation by Advanced Modeling," in *the Proceedings of the IEEE Industry Applications Society Annual Meeting*, Portland, USA, 2016.

[78] H. M. K. Al-Masri and M. Ehsani, "Impact of Wind Turbine Modeling on a Hybrid Renewable Energy System," in *the Proceedings of the IEEE Industry Applications Society Annual Meeting*, Portland, USA, 2016.

[79] H. M. K. Al-Masri and M. Ehsani, "Impact of Wind Turbine Modeling on a Renewable Energy System," in *the Proceedings of the IEEE North American Power Symposium (NAPS)*, Denver, USA, 2016.

[80] T.-J. Chang, Y.-T. Wu, H.-Y. Hsu, C.-R. Chu, and C.-M. Liao, "Assessment of wind characteristics and wind turbine characteristics in Taiwan," *Renewable Energy*, vol. 28, pp. 851-871, 5// 2003.

[81] M. K. Deshmukh and S. S. Deshmukh, "Modeling of hybrid renewable energy systems," *Renewable and Sustainable Energy Reviews*, vol. 12, pp. 235-249, 1// 2008.

[82] S. Diaf, G. Notton, M. Belhamel, M. Haddadi, and A. Louche, "Design and techno-economical optimization for hybrid PV/wind system under various meteorological conditions," *Applied Energy*, vol. 85, pp. 968-987, 10// 2008.

[83] H. Yang, L. Lu, and W. Zhou, "A novel optimization sizing model for hybrid solar-wind power generation system," *Solar Energy*, vol. 81, pp. 76-84, 1// 2007.

[84] S. A. Papathanassiou and N. G. Boulaxis, "Power limitations and energy yield evaluation for wind farms operating in island systems," *Renewable Energy*, vol. 31, pp. 457-479, 4// 2006.

[85] Y. L. Bin Wu, Navid Zargari, Samir Kouro, *Power Conversion and Control of Wind Energy Systems*: Wiley-IEEE Press, August 2011.

[86] G. Gualtieri and S. Secci, "Wind shear coefficients, roughness length and energy yield over coastal locations in Southern Italy," *Renewable Energy*, vol. 36, pp. 1081-1094, 3// 2011.

[87] M. H. Albadi, E. F. El-Saadany, and H. A. Albadi, "Wind to power a new city in Oman," *Energy*, vol. 34, pp. 1579-1586, 10// 2009.

[88] M. C. Mabel and E. Fernandez, "Estimation of Energy Yield From Wind Farms Using Artificial Neural Networks," *Energy Conversion, IEEE Transactions on*, vol. 24, pp. 459-464, 2009.

[89] L. Battisti, *Wind turbines in cold climates : icing impacts and mitigation systems*: Cham ; New York : Springer, 2015.

[90] (12/15/2015). *International Standard Atmosphere*. Available: http://en.wikipedia.org/wiki/International_Standard_Atmosphere

[91] (12/15/2015). *Atmospheric pressure*. Available: https://en.wikipedia.org/wiki/Atmospheric_pressure

[92] (12/15/2015). *Density of air*. Available: https://en.wikipedia.org/wiki/Density_of_air

[93] T. Ackermann, *Wind Power in Power Systems, 2nd Edition*, May 2012.

[94] (12/15/2015). *Air Buoyancy*. Available: http://metrology.burtini.ca/grav_air.html

[95] M. R. Patel, *Wind and solar power systems : design, analysis, and operation*: Boca Raton, FL : Taylor & Francis, 2006.

[96] S. Li, D. C. Wunsch, E. O'Hair, and M. G. Giesselmann, "Comparative analysis of regression and artificial neural network models for wind turbine power curve estimation," *Journal of Solar Energy Engineering,* vol. 123, pp. 327-332, 2001.

[97] M. Ragheb, "Modern Wind Generators," 02/28/2014.

[98] M. Korpaas, A. T. Holen, and R. Hildrum, "Operation and sizing of energy storage for wind power plants in a market system," *International Journal of Electrical Power & Energy Systems,* vol. 25, pp. 599-606, 10// 2003.

[99] D. Ipsakis, S. Voutetakis, P. Seferlis, F. Stergiopoulos, and C. Elmasides, "Power management strategies for a stand-alone power system using renewable energy sources and hydrogen storage," *International Journal of Hydrogen Energy,* vol. 34, pp. 7081-7095, 8// 2009.

[100] D. B. Nelson, M. H. Nehrir, and C. Wang, "Unit sizing of stand-alone hybrid wind/PV/fuel cell power generation systems," in *Power Engineering Society General Meeting, 2005. IEEE,* 2005, pp. 2116-2122 Vol. 3.

[101] I. Pan and S. Das, "Fractional Order AGC for Distributed Energy Resources Using Robust Optimization," *IEEE Transactions on Smart Grid,* vol. PP, pp. 1-1, 2015.

[102] M. Castañeda, A. Cano, F. Jurado, H. Sánchez, and L. M. Fernández, "Sizing optimization, dynamic modeling and energy management strategies of a stand-alone PV/hydrogen/battery-based hybrid system," *International Journal of Hydrogen Energy,* vol. 38, pp. 3830-3845, 4/1/ 2013.

[103] M. Alsayed, M. Cacciato, G. Scarcella, and G. Scelba, "Multicriteria Optimal Sizing of Photovoltaic-Wind Turbine Grid Connected Systems," *Energy Conversion, IEEE Transactions on,* vol. 28, pp. 370-379, 2013.

[104] M. Thomson and D. G. Infield, "Impact of widespread photovoltaics generation on distribution systems," *Renewable Power Generation, IET,* vol. 1, pp. 33-40, 2007.

[105] M. E. Meral and F. Dinçer, "A review of the factors affecting operation and efficiency of photovoltaic based electricity generation systems," *Renewable and Sustainable Energy Reviews,* vol. 15, pp. 2176-2184, 6// 2011.

[106] E. Skoplaki, A. G. Boudouvis, and J. A. Palyvos, "A simple correlation for the operating temperature of photovoltaic modules of arbitrary mounting," *Solar Energy Materials and Solar Cells,* vol. 92, pp. 1393-1402, 11// 2008.

[107] (12/16/2015). *NASA Surface meteorology and Solar Energy*. Available: https://eosweb.larc.nasa.gov/sse/

[108] E. Ghiani, F. Pilo, and S. Cossu, "Evaluation of photovoltaic installations performances in Sardinia," *Energy Conversion and Management,* vol. 76, pp. 1134-1142, 12// 2013.

[109] E. Kymakis, S. Kalykakis, and T. M. Papazoglou, "Performance analysis of a grid connected photovoltaic park on the island of Crete," *Energy Conversion and Management,* vol. 50, pp. 433-438, 3// 2009.

[110] M. D. R. Rüther, I. Salamoni, P. Knob & U. Bussemas, "Performance of the first grid-connected, BIPV installation in brazil over eight years of continuous operation," presented at the 21st European Photovoltaic Solar Energy Conference, Dresden, Germany, September 2006.

[111] R. Eke and A. Senturk, "Performance comparison of a double-axis sun tracking versus fixed PV system," *Solar Energy,* vol. 86, pp. 2665-2672, 9// 2012.

[112] N. A. Azli, Z. Salam, A. Jusoh, M. Facta, B. C. Lim, and S. Hossain, "Effect of fill factor on the MPPT performance of a grid-connected inverter under Malaysian conditions," in *Power and Energy Conference, 2008. PECon 2008. IEEE 2nd International*, 2008, pp. 460-462.

[113] (05/22/2016). *Google Earth*. Available: https://www.google.com/earth/

[114] (05/22/2016). *Wikimapia - Let's describe the whole world!* Available: http://goo.gl/97aq1b

[115] S. Mathew, *Wind energy: fundamentals, resource analysis and economics* vol. 1: Springer, 2006.

[116] K. Mertens, *Photovoltaics: Fundamentals, Technology and Practice*: John Wiley & Sons, 2013.

[117] A. Roy, S. B. Kedare, and S. Bandyopadhyay, "Optimum sizing of wind-battery systems incorporating resource uncertainty," *Applied Energy,* vol. 87, pp. 2712-2727, 8// 2010.

[118] (12/16/2015). *Real interest rate*. Available: http://en.wikipedia.org/wiki/Real_interest_rate

[119] M.-A. Yazdanpanah, "Modeling and sizing optimization of hybrid photovoltaic/wind power generation system," *Journal of Industrial Engineering International,* Mar 2014.

[120] "Renewable Power Generation Costs in 2014," January 2015.

[121] A. Kuriyama. (2016/03). *List Of Grid Emission Factor*. Available: http://goo.gl/9N2aXZ

[122] M. Brander, A. Sood, C. Wylie, A. Haughton, and J. Lovell, "Technical Paper| Electricity-specific emission factors for grid electricity," *Ecometrica, Emissionfactors. com*, 2011.

[123] W. B. C. f. S. Development and W. R. Institute, "The greenhouse gas protocol: a corporate accounting and reporting standard," World Resources Inst. 2012.

[124] A. N. Celik, "Techno-economic analysis of autonomous PV-wind hybrid energy systems using different sizing methods," *Energy Conversion and Management*, vol. 44, pp. 1951-1968, 7// 2003.

[125] J. H. Holland, *Adaptation in natural and artificial systems: an introductory analysis with applications to biology, control, and artificial intelligence*: MIT press, 1992.

[126] H. Al-Masri and H. Q. Al-Zoubi, "Genetic and Lagrange Relaxation Algorithms for Solving Constrained Economic Dispatch Including Losses," *World Applied Sciences Journal*, vol. 20, pp. 1188-1192, 2012.

[127] M. Mitchell, *An introduction to genetic algorithms*: MIT press, 1998.

[128] K. Deb, A. Pratap, S. Agarwal, and T. Meyarivan, "A fast and elitist multiobjective genetic algorithm: NSGA-II," *Evolutionary Computation, IEEE Transactions on*, vol. 6, pp. 182-197, 2002.

[129] F.-A. Fortin and M. Parizeau, "Revisiting the NSGA-II crowding-distance computation," in *Proceedings of the 15th annual conference on Genetic and evolutionary computation*, 2013, pp. 623-630.

[130] H. Fang, Q. Wang, Y. Tu, and M. Horstemeyer, "An Efficient Non-dominated Sorting Method for Evolutionary Algorithms," *Evolutionary Computation*, vol. 16, pp. 355-384, 2008.

[131] G. Ruhe and Y. Zhang, *Search Based Software Engineering: 5th International Symposium, SSBSE 2013, St. Petersburg, Russia, August 24-26, 2013. Proceedings* vol. 8084: Springer, 2013.

[132] (10/27/2016). Google Earth V 5.0.11733.9347. (May 5, 2009). *Jordan Map*. 31°01'13.07" N and 36°18'30.52" E, Eye alt 504.67 mi. ORION-ME 2016, Basarsoft 2016. Available: https://www.google.com/earth

[133] (08/06/2016). *The Global Carbon Atlas* Available: http://www.globalcarbonatlas.org/?q=en/emissions

[134] K. Deb, S. Agrawal, A. Pratap, and T. Meyarivan, "A fast elitist non-dominated sorting genetic algorithm for multi-objective optimization: NSGA-II," in *International Conference on Parallel Problem Solving From Nature*, 2000, pp. 849-858.

APPENDIX A

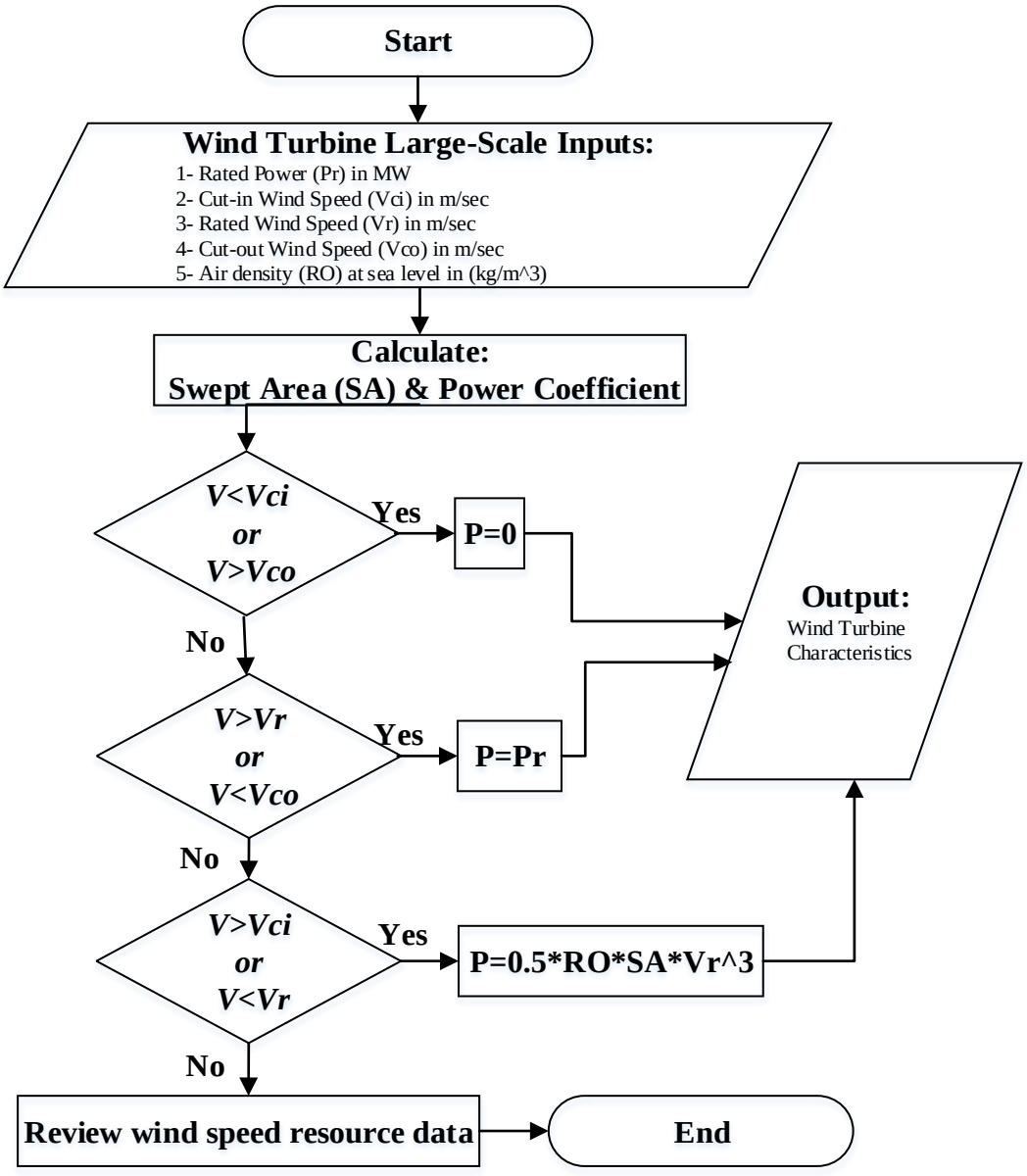

Fig. A. Flow chart to get a simplified characteristic of a wind turbine

APPENDIX B

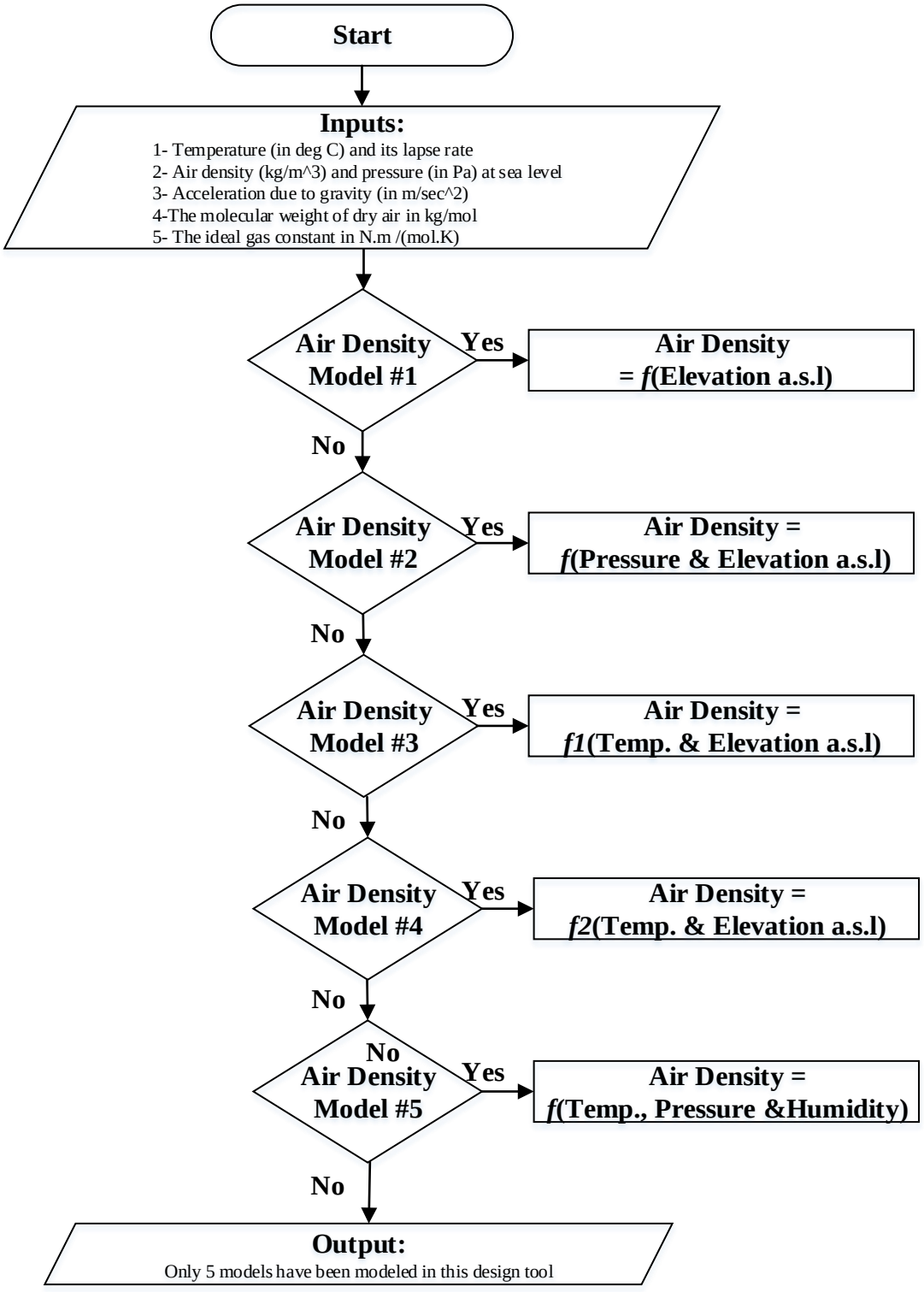

Fig. B. Flow chart presenting 5 models to compute the air density

APPENDIX C

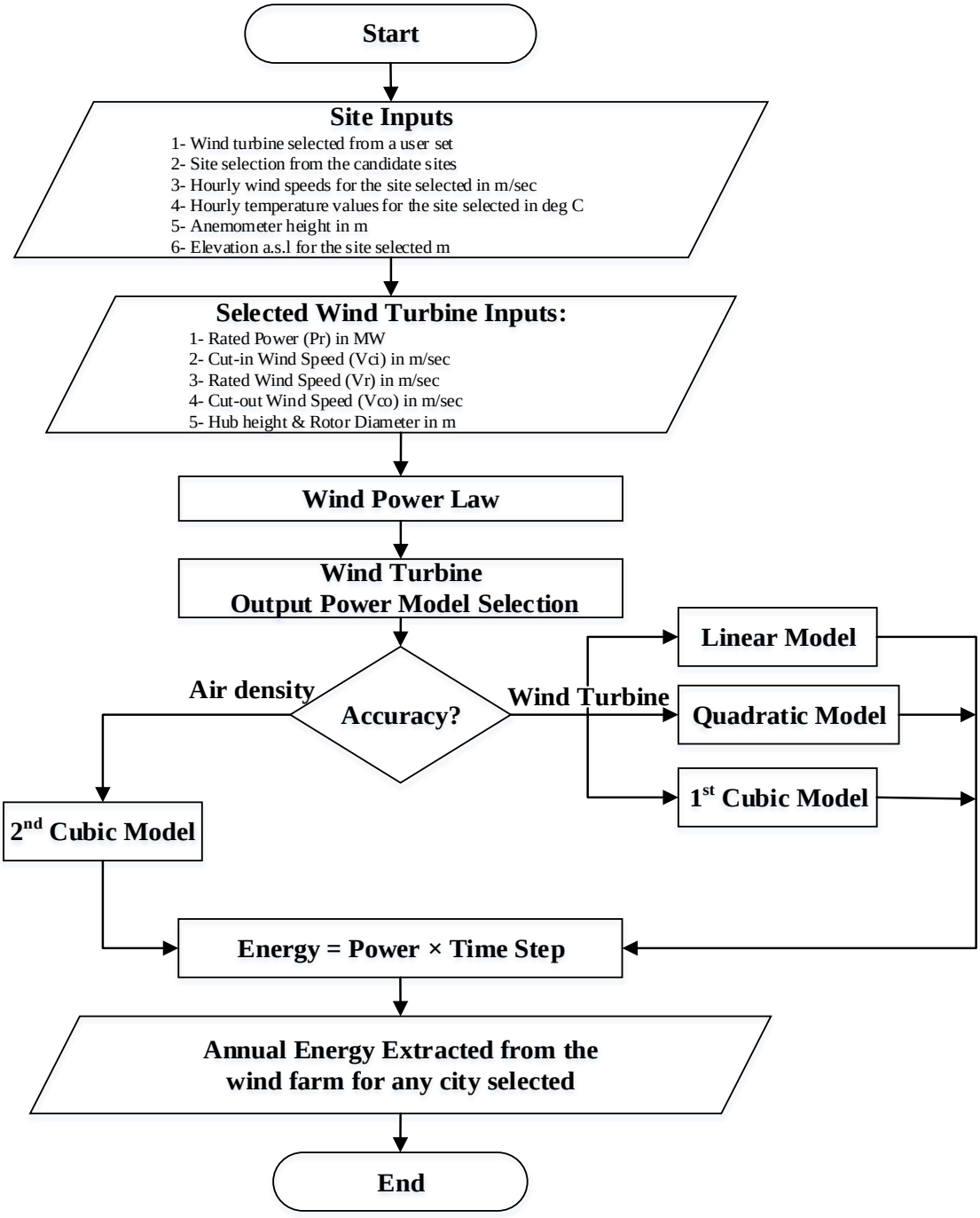

Fig. C. Flow chart to compute wind farm annual energy using 4 models

APPENDIX D

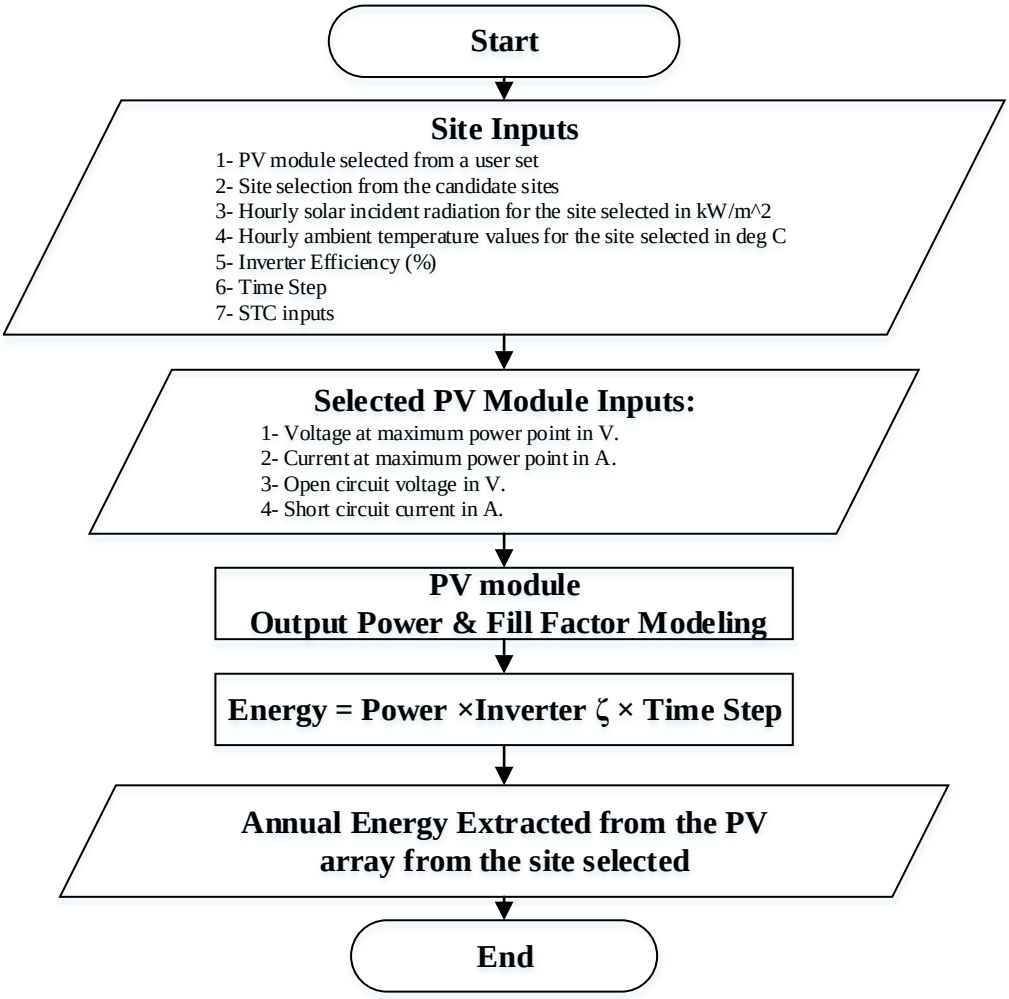

Fig. D. Flow chart to compute PV array annual energy

APPENDIX E

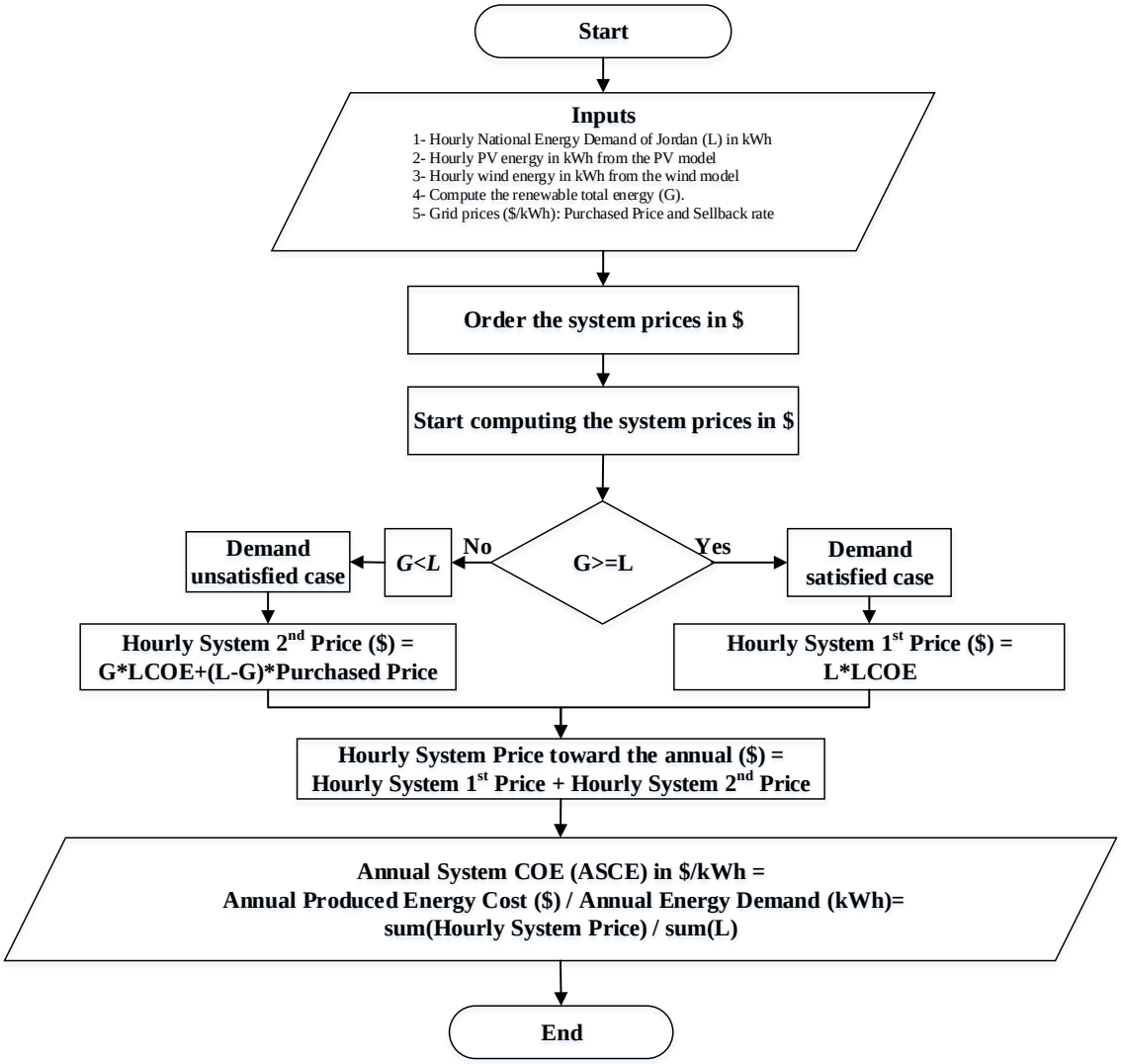

Fig. E. Flow chart to compute the ASCE

APPENDIX F

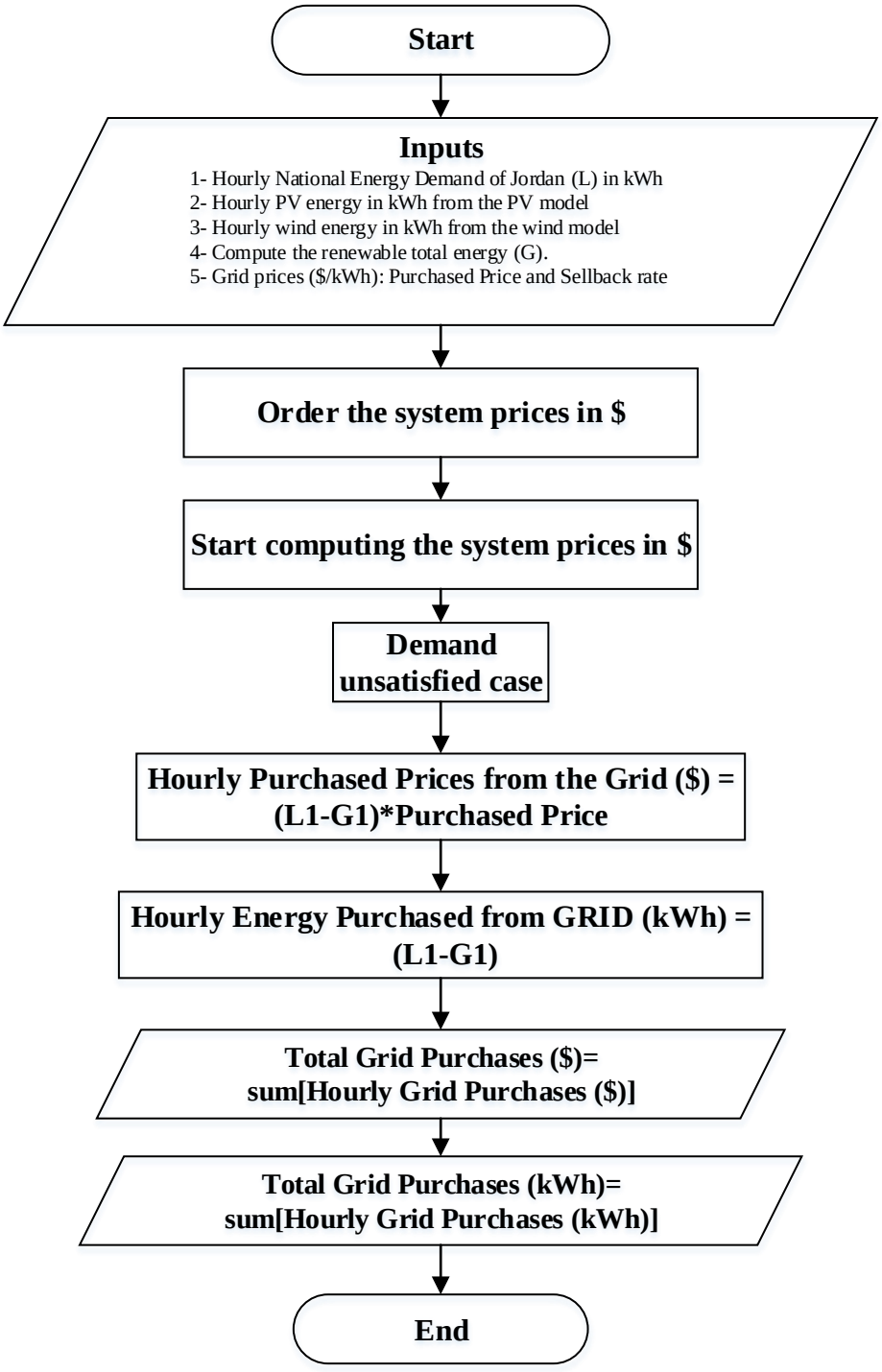

Fig. F. Flow chart to compute the grid purchases in $ & in kWh

APPENDIX G

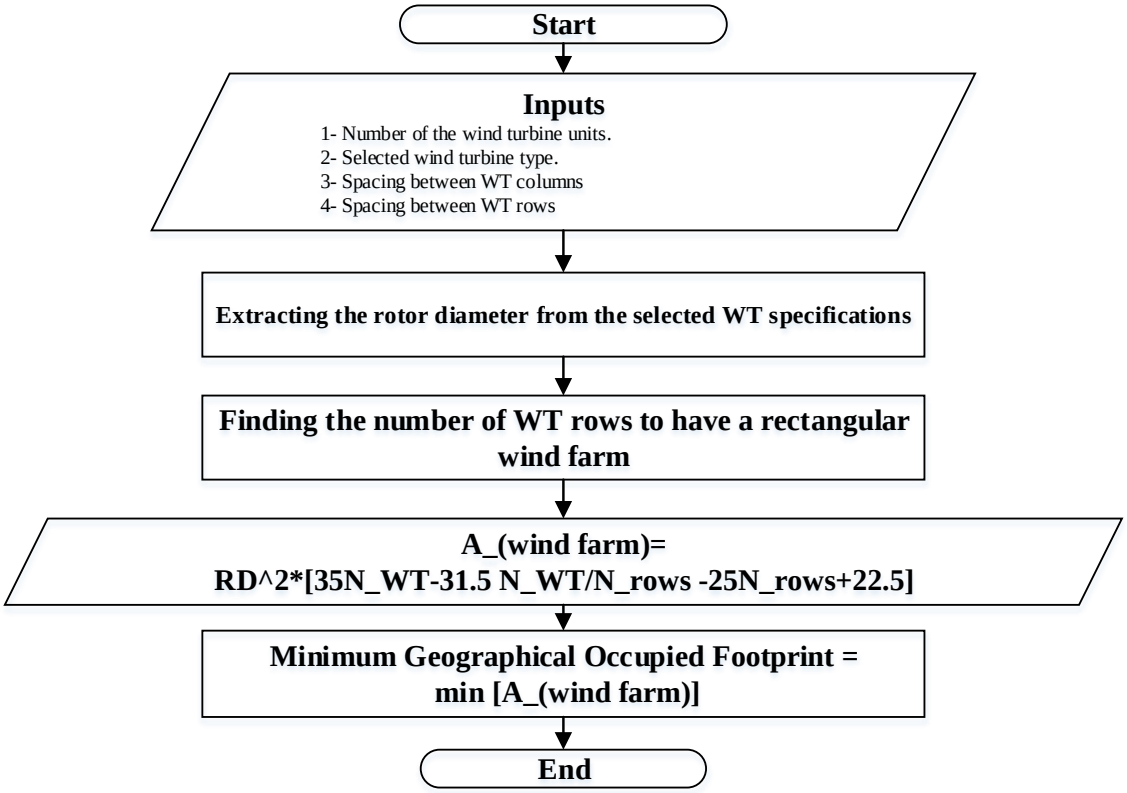

Fig. G. Flow chart to compute the footprint of the wind farm

APPENDIX H

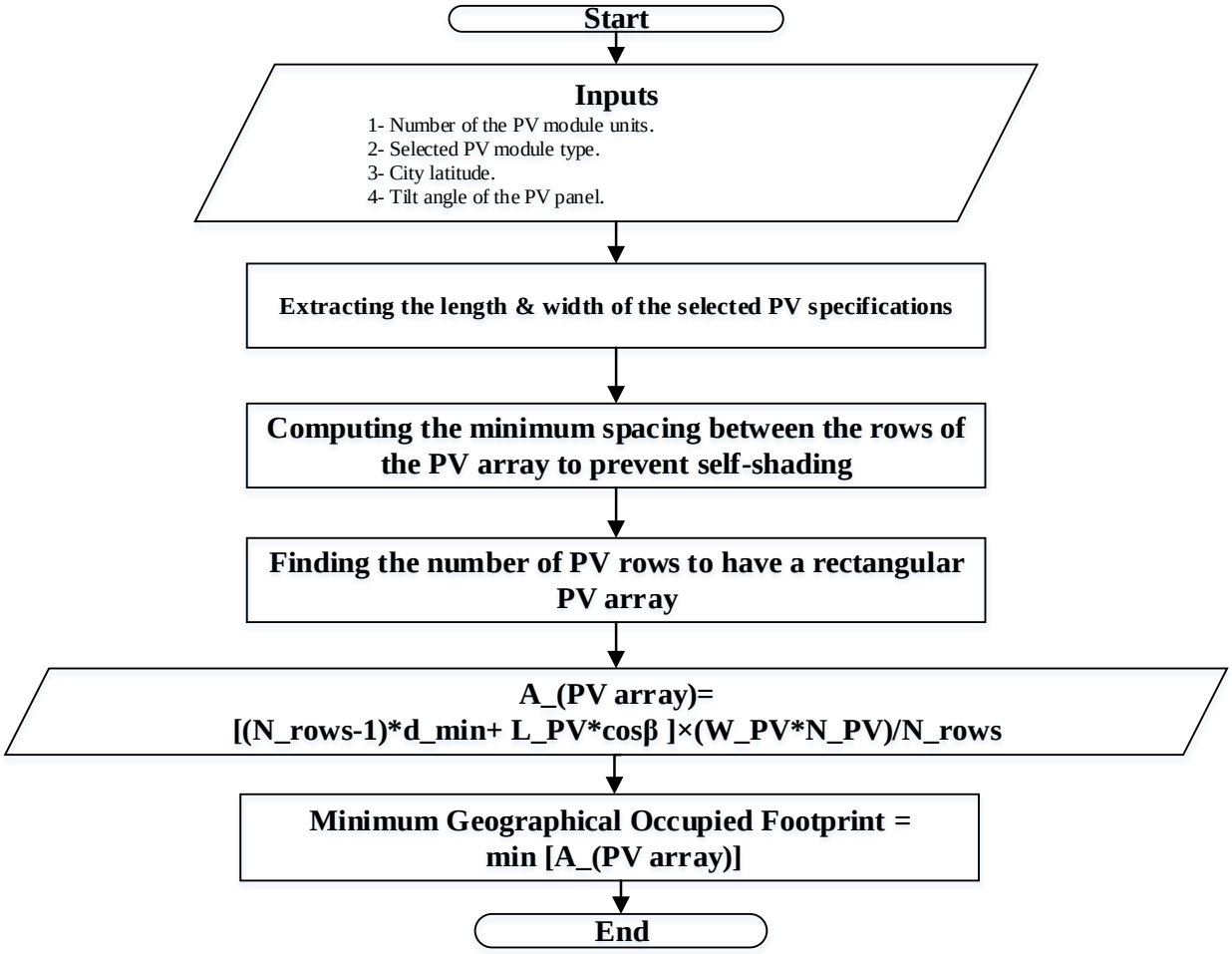

Fig. H. Flow chart to compute the footprint of the PV array

APPENDIX I

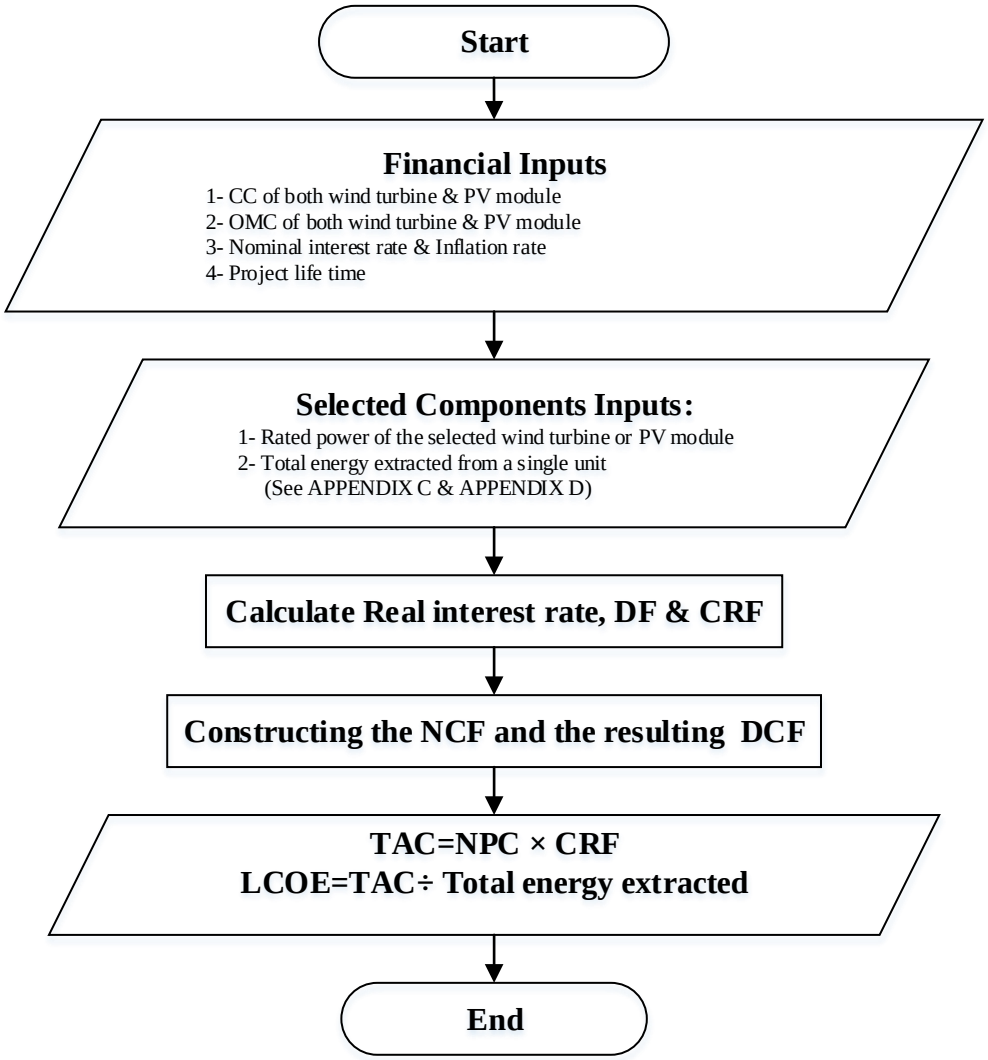

Fig. I. Flow chart to compute LCOE without RC&SC of a single unit

APPENDIX J

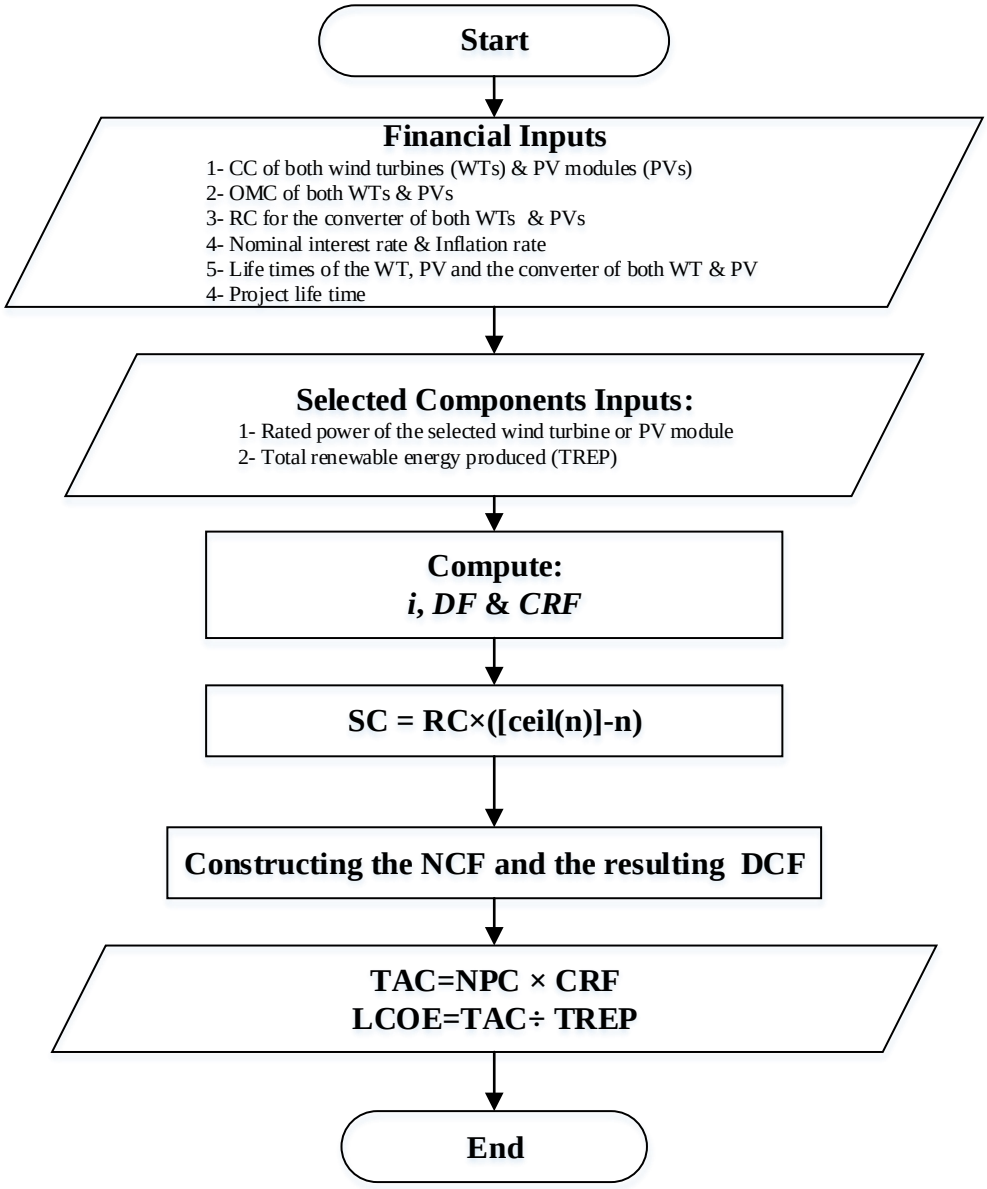

Fig. J. Flow chart to compute LCOE including the RC&SC

APPENDIX K

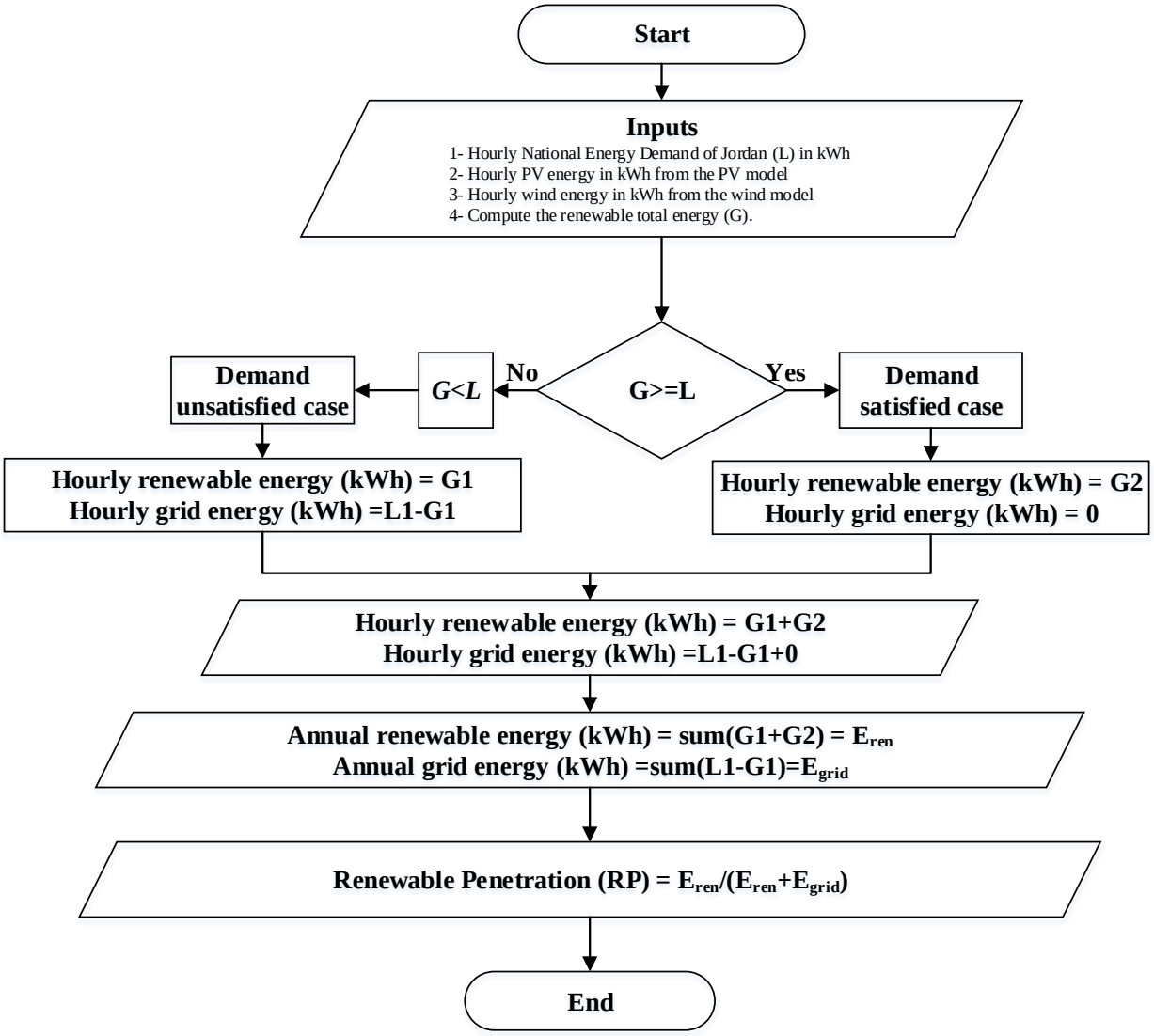

Fig. K. Flow chart to compute the RP in %